The reorganization of model membranes by Gb3-binding lectins and the bacterium Pseudomonas aeruginosa

Taras Sych

UNIVERSITÉ DE STRASBOURG
ALBERT-LUDWIGS
UNIVERSITÄT FREIBURG

ÉCOLE DOCTORALE DES SCIENCES DE LA VIE ET DE LA SANTÉ

LABORATOIRE BIOIMAGERIE ET PATHOLOGIES UMR 7021

BIOSS CENTRE FOR BIOLOGICAL SIGNALING STUDIES

THÈSE

présentée par :

Taras SYCH

soutenue le : **16 juillet 2019**

pour obtenir le grade de : **Docteur de l'université de Strasbourg**

Discipline/ Spécialité : biophysique

Rôles et mécanismes des Lectines à Gb3 et de P. aeruginosa sur la réorganisation de la membrane plasmique

CO-TUTTELLE de THÈSE dirigée par :

M RÖMER Winfried	Professeur, Albert-Ludwigs Universität Freiburg
M MELY Yves	Professeur, université de Strasbourg

RAPPORTEURS :

M HOF Martin	Professeur, J. Heyrovsky Institute of Physical Chemistry, Prague
M HEERKLOTZ Heiko	Professeur, Albert-Ludwigs Universität Freiburg

AUTRES MEMBRES DU JURY :

M Carlos Marques	Docteur, L'Institut Charles Sadron, université de Strasbourg

The reorganization of model membranes by Gb3-binding lectins and the bacterium *P. aeruginosa*

Inaugural Dissertation

for obtaining the doctoral degree

from the Faculty of Biology

of the Albert-Ludwigs-University Freiburg im Breisgau

and the Doctoral School of the Sciences of Life and Health

of the University of Strasbourg

presented by

Taras Sych

born in Ivano-Frankivsk, Ukraine

Freiburg im Breisgau/Strasbourg

June 2019

Prepared at the Institute of Biology II

and BIOSS Centre for Biological Signalling Studies (University of Freiburg)

and Laboratory of Bioimaging and Pathologies (University of Strasbourg)

Joint supervision (co-tutelle) by:

Prof. Winfried Römer

Prof. Yves Mely

Examiners:

Dr. Carlos Marques

Prof. Martin Hof

Prof. Heiko Heerklotz

Date of the oral exam: 16th of July 2019

Acknowledgements

This work was the biggest project I performed in my life so far. I would not be able to accomplish my aims without the help and support of multiple people who made a significant impact on my professional and private life over last years. Here, I am happy to acknowledge all of them.

I would like to thank Prof. Winfried Römer, who in collaboration with Prof. Yves Mely established the project and provided me this wonderful opportunity to perform research in such interesting interdisciplinary domain. Thank you for supervision and guidance, countless big and small discussions, your patience while working on my manuscripts and for being continuous source of inspiration and motivation.

In the group of Prof. Yves Mely I started to work 5 years ago as a master student. The majority of the techniques and methods I use till now I learned during my first couple of months in the laboratory of Bioimaging and Pathologies. In this group, I became fascinated with the field of membrane biophysics which, in a way, determined my further step in research – the phd project. I would like to thank Prof. Yves Mely for guidance and help, for the creation of a very nice working environment in the group and for the possibilities to work on the nice master and phd projects.

I would like to say special thanks to Ludovic Richert, who introduced me to the world of fluorescence microscopy – my favorite set of techniques so far. Under your supervision, I learned all types of microscopy I am using and also the basics of the image processing. Thank you very much for your instructions, advices and help.

Furthermore, I would like to thank other people from the Laboratory of Bioimaging and Pathologies, in particular Guy Dupotail for teaching and lots of help with the adaptation in the laboratory, Andrey Klymchenko for useful technical advises and providing membrane markers for my experiments and Romain Vauchelles for technical help with microscopy and image processing.

I would like to thank others from the LBP, who made my life colorful and exciting, namely: Oleksii, Sasha, Bogdan, Katia, Rajhans, Lesia, Ira, Vasia, Eugen, Nina, Jurii, Pascal, Fred, Galina, Mayeul, Andreas, Kyong, Nicolas, Dorianne, Redwan, Roman, Nazar, Dima, Christian, Mariana and many others who created very nice ambience in the group.

When I only started my second part of the project at the group of Prof. Römer at BIOSS, I had a lot of help from people form “synthetic membranes” subgroup. Thank you all! First of all, I would like to thank Thomas Schubert and Josef Madl. You both did great amount of work before I arrived to the group. I learned a lot from you and I guess that based on your work and together with both of you was the only possible way for my project to succeed. I am grateful to Ramin Omidvar for our joint experiments (when two of us occupied all the devices in the microscopy room), for our discussions and collaboration.

Special thanks to Sarah Villringer for our collaboration but also for the nice example of wise and rational approach to research in general – I learned a lot from you.

I would like to thank Raisa Kociurzynski and Dr. Volker Knecht for supporting our work with molecular dynamic simulations, you provided valuable insights for understanding our systems, I enjoyed our discussions a lot.

I would like to say thanks to the post docs of the group – Julie, Roland and Constanze, it was an honor and pleasure to work and discuss projects with you.

I am grateful to Anne, Marco, Sabrina, Peter, Sahaja, Timo and Alessia. We were not only working together, but also spent a lot of time outside of the lab. Thanks for creating a very nice environment in the group and our countless activities outside – running, bouldering or just evenings at McNamara's Irish pub. Special thanks to Anne, Marco and Sabrina for proofreading my manuscript.

During my phd project I had three students under my supervision. Thank you, Leo, Lukas and Fabian, it was a pleasure to work with you. You produced valuable data and did a good job. Moreover, teaching you I learned a lot myself.

I am very grateful to other people I met at the group of Prof. Römer: Maokai, Valeria, Stefan, Isabel, Thorsten, Lina, Francesca, Levin, Anna-Maria, Anika, Kai, Gilles, Axel, Julia and many others.

I am particularly grateful to my thesis committee, consisting of Dr. Carlos Marques, Prof. Martin Hof and Prof. Heiko Heerklotz who agreed to read and grade this work. Thank you very much for your time and valuable impact.

I am grateful to the IRTG "Soft Matter Science" for the financial and organizational support, in particular – IRTG spokespersons Prof. Jörg Baschnagel and Prof. Günter Reiter. Special thanks to the IRTG administration – Birgitta Zovko, Jana Husse and Melisa Mustafovic – you helped a lot.

I would like to thank my funding agencies – German Research Foundation (DFG), International Graduate Academy (IGA) of the University of Freiburg, Franco-German University and International doctoral program of the European Doctoral College of the University of Strasbourg.

I am very grateful to my former teacher and supervisor, Dr. Sergii Kutovy from the Taras Shevchenko University of Kyiv, you directed my first steps in science, you made a colossal impact on my choice to proceed in research.

I would like to thank my family; in particular my mother Nataliia for the love and support, this project wouldn't be possible without you.

Contents

Abbreviations

Lectins:

LecA	*P. aeruginosa* lectin PAO1L
StxB	B subunit of Shoga toxin from *S. dysenteriae*
CtxB	B subunit of Shoga toxin from *V. cholerae*
RSL	*R. solanacerum* lectin
RPL	Recombinant procariotic lectin α Gal

Bacteria:

PAO1	*P. aeruginosa* strain PAO1 wild type
PAO1 ΔLecA	*P. aeruginosa* strain PAO1 deficient in LecA

Lipids:

GSL	glycosphingolipid
Gb3	globotriaosylceramide
FSL	function-spacer-lipid
GM1	monosialotetrahexosylganglioside
DOPC	1,2-dioleoyl-sn-glycero-3-phosphocholine
SM	sphingomyelin
choleterol	chol

Membrane fluorescent markers:

Bodipy	β-Bodipy FL C12-HPC
Texas Red	Texas Red – DHPE
NR12S	Nile Red 12 S

Fluorescence microscopy techniques:

LSCM	Laser scanning confocal microscopy
TIRFM	Total internal reflectin fluorescence microscopy
HILO	highly inclined and laminated optical sheet microscopy

Summary

Plasma membrane glycosphingolipids (GSLs) are important membrane components involved in cell adhesion, signaling and endocytosis. They consist of a hydrophobic ceramide backbone embedded in the lipid bilayer and a carbohydrate head group exposed to the extracellular environment. GSLs can be highjacked by viruses, bacteria and bacterial products (such as toxins) which recognize their oligosaccharides using special carbohydrate binding proteins (called "lectins"). Lectin-GSL interactions are exploited by pathogens for binding to the membrane surface which can further result in pathogen uptake by the host cell. For instance, the entry of the pathogenic bacterium *Pseudomonas aeruginosa* into a host cell strongly depends on the specific interactions of its surface lectin LecA with the plasma membrane GSL globotriaosylceramide (Gb3). It has recently been shown that LecA-Gb3 interactions can initiate the formation of a so-called "lipid zipper" which leads to the bacterial internalization.

In this work, we investigated the interaction of LecA (coupled to bacteria or purified) with Gb3. Moreover, we compared LecA to another well-known lectin which binds Gb3, the Bsubunit of Shiga toxin from *Shigella dysenteriae* (StxB). We have strong indications that, despite sharing the same receptor, the two lectins behave differently as they induce different signaling events and follow different intracellular trafficking pathways. We hypothesized that these differences can originate already at the plasma membrane and can be explained by the selective binding of LecA and StxB to Gb3 incorporated into membrane nanodomains of different composition and organization.

We reconstituted the binding of lectins to Gb3 in model membranes (giant unilamellar vesicles - GUVs) of different membrane composition and order. We developed a method for quantitative description of lectin binding to GUVs based on the analysis of fluorescence microscopy images. Using this method, we confirmed that StxB prefers more ordered lipid bilayers, whereas LecA is less selective and binds efficiently to membranes of low order as well. Moreover, we studied the lectin binding to synthetic Gb3 species with 24:0 and 24:1 fatty acyl chains as well as to the synthetic construct FSL-Gb3. Using these species, we elucidated the role of the Gb3 molecular structure in the binding of lectins. Remarkably, using the information obtained from our binding studies, we succeeded to recreate the segregation of LecA and StxB in GUVs.

In the second part of the project, we explored the impact of LecA and StxB on membrane organization. Here, we were particularly interested in the rearrangement of ordered nanodomains in the plasma membrane by both lectins. The visualization of such nanodomains in the native plasma membrane is an extremely challenging task, which is why we mimicked them with liquid-ordered (Lo) domains in phase separated supported lipid bilayers (SLBs). We functionalized such lipid bilayers with Gb3 receptor molecules and found that StxB shrinks existing Lo domains and induces the formation of novel Lo domains. This suggests that StxB clusters "stabilize" the existing Lo domains. Moreover, the efficient clustering of Gb3 receptors by StxB induces the formation of new

Lo domains. LecA shows a completely opposite behavior. Applied to SLBs, LecA induces the dissolution of Lo domains, homogenizing the membrane. Finally, *P. aeruginosa* applied to SLBs was found to dissolve Lo domains as well. This dissolution induced by the bacterium was observed for the first time. In summary, we learned/understood/demonstrated/revealed that the LecA-Gb3 interaction is the key to the dissolution of Lo domains by *P. aeruginosa.*

Zusammenfassung

Als wichtige Komponenten der Plasmamembran sind Glykosphingolipide (GSLs) an Zelladhäsion, Signalprozessen und Endozytose beteiligt. Sie bestehen aus einem hydrophoben, in die Lipiddoppelschicht eingebetteten Ceramid-Rückgrat und einer Kohlenhydrat-Kopfgruppe, die zur extrazellulären Umgebung exponiert ist. GSLs können von Viren, Bakterien und bakteriellen Produkten (wie Toxinen) gekapert werden, die deren Oligosaccharide mit Hilfe spezieller zuckerbindender Proteine (genannt „Lektine“) erkennen. Lektin-GSL-Interaktionen werden von Pathogenen zur Bindung an Membranoberflächen genutzt, was auch zur Aufnahme des Pathogens in die Zielzelle führen kann. Beispielsweise hängt der Eintritt des pathogenen Bakteriums *Pseudomonas aeruginosa* in eine Wirtszelle stark von der spezifischen Interaktion seines Oberflächenlektins LecA mit dem Plasmamembran-GSL Globotriaosylceramid (Gb3) ab. Es wurde kürzlich gezeigt, dass LecA-Gb3-Interaktionen die Bildung eines sogenannten „Lipid-Reißverschlusses“ induzieren können, der wiederum die bakterielle Internalisierung ermöglicht.

In der vorliegenden Arbeit untersuchten wie die Interaktionen zwischen LecA (an Bakterien gekoppelt oder aufgereinigt) und Gb3. Darüber hinaus verglichen wir LecA mit einem weiteren bekannten Gb3-bindenden Lektin, der B-Untereinheit des Shiga-Toxins aus *Shigella dysenteriae* (StxB). Vorangegangene Untersuchungen deuteten darauf hin, dass sich die Lektine, obwohl sie den gleichen Rezeptor teilen, verschieden verhalten, da sich induzierte Signale und intrazellulärer Transport unterscheiden. Wir vermuteten, dass diese Differenzen bereits an der Plasmamembran entstehen und durch die selektive Bindung von LecA und StxB and Gb3 in verschiedenen Nanodomänen der Membran mit unterschiedlicher Zusammensetzung und Organisation erklärt werden können.

Wir rekonstituierten die Bindung der Lektine an Gb3 in Modellmembranen (gigantische, unilamellare Vesikel – GUVs) unterschiedlicher Komposition und Ordnung. Wir entwickelten eine Methode zur quantitativen Beschreibung der Lektinbindung and GUVs basierend auf der Analyse von fluoreszenzmikroskopischen Aufnahmen. Mit dieser Methode bestätigten wir, dass StxB stärker geordnete Lipiddoppelschichten bevorzugt, während LecA weniger selektiv ist und Membranen geringer Ordnung ebenfalls effizient bindet. Des Weiteren studierten wir die Lektinbindung an synthetische Gb3-Spezies mit 24:0- und 24:1-Fettsäureketten sowie an das synthetische Konstrukt FSL-Gb3. Mit diesen Spezies klärten wir die Rolle der molekularen Struktur des Gb3 in der Bindung der Lektine auf. Es gelang uns auf Grundlage unserer Bindestudien die Segregation von LecA und StxB in GUVs zu nachzubilden.

Im zweiten Teil des Projektes erkundeten wir die Auswirkung von LecA und StxB auf die Membranorganisation. Hierbei waren wir besonders an der Umgestaltung geordneter Nanodomänen in der Plasmamembran durch die Lektine interessiert. Die Visualisierung solcher Nanodomänen in der nativen Plasmamembran ist eine äußerst

herausfordernde Aufgabe, weshalb wir sie mit flüssig-geordneten (liquid-ordered, Lo-) Domänen in phasenseparierten gestützten Lipiddoppelschichten (supported lipid bilayers, SLBs) nachahmten. Wir funktionalisierten diese Lipidschichten mit Gb3-Rezeptormolekülen und fanden heraus, dass StxB vorliegende Lo-Domänen schrumpfen lässt und die Bildung neuer Lo-Domänen induziert. Das weist darauf hin, dass StxB effizient Gb3 bündelt und den Rezeptor in Lo-Domänen stabilisiert. LecA zeigt ein völlig gegensätzliches Verhalten. Auf SLBs angewendet induziert LecA die Auflösung von Lo-Domänen und homogenisiert die Membran. Abschließend beobachteten wir, dass *P. aeruginosa* ebenfalls die Auflösung von Lo-Domänen in SLBs bewirkt. Diese durch das Bakterium induzierte Auflösung wird mit der vorliegenden Arbeit zum ersten Mal beschrieben. Zusammengefasst haben wir gelernt/verstanden/demonstriert/aufgedeckt, dass die LecA-Gb3-Interaktion den Schlüssel zur Auflösung von Lo-Domänen durch *P. aeruginosa* darstellt.

Résumé

Les glycosphingolipides membranaires plasmatiques (GSL) sont d'importants composants membranaires impliqués dans l'adhésion cellulaire, la signalisation et l'endocytose. Ils se composent d'un squelette en céramide hydrophobe noyé dans la bicouche lipidique et d'un groupe de têtes glucidiques exposées à l'environnement extracellulaire. Les GSL peuvent être détournées par des virus, des bactéries et des produits bactériens (comme les toxines) qui reconnaissent leurs oligosaccharides en utilisant des protéines spéciales de liaison aux glucides (appelées "lectines"). Les interactions Lectine-GSL sont exploitées par les pathogènes pour se lier à la surface de la membrane, ce qui peut entraîner l'absorption de pathogènes par la cellule hôte. Par exemple, l'entrée de la bactérie pathogène P. aeruginosa dans la cellule hôte dépend fortement des interactions spécifiques de sa lectine de surface LecA avec la membrane plasmatique GSL globotriaosylceramide (Gb3). Il a été récemment démontré que les interactions LecA-Gb3 peuvent initier la formation de ce que l'on appelle la "lipid zipper" qui conduit à l'internalisation bactérienne.

Dans ce travail, nous avons étudié l'interaction de LecA (couplé à des bactéries ou purifié) avec Gb3. De plus, nous avons utilisé pour la comparaison une autre lectine bien connue qui se lie au Gb3, la sous-unité B de la toxine Shiga de S. dysenteriae (StxB). Nous avons de fortes indications que malgré le partage du même récepteur, les deux lectines se comportent différemment car elles induisent des événements de signalisation différents et suivent des voies de trafic intracellulaire différentes. Nous avons émis l'hypothèse que ces différences peuvent déjà provenir de la membrane plasmatique et s'expliquer par la liaison sélective de LecA et StxB au Gb3 incorporés dans des nanodomaines membranaires de composition et d'organisation différentes.

Nous avons reconstitué la liaison des lectines au Gb3 dans des membranes modèles (vésicules unilamellaires géantes - GUVs) de composition et d'ordre différents. Nous avons développé une méthode de description quantitative de la liaison de la lectine aux GUVs basée sur l'analyse d'images microscopiques à fluorescence. En utilisant cette méthode, nous avons confirmé que le StxB préfère les bicouches lipidiques plus ordonnées, alors que le LecA est moins sélectif et se lie efficacement aux bicouches lipidiques d'ordre inférieur également. De plus, nous avons étudié la liaison de la lectine aux espèces synthétiques Gb3 à chaînes acyles grasses 24:0 et 24:1 ainsi qu'à la construction synthétique FSL-Gb3. En utilisant ces espèces, nous avons élucidé le rôle de la structure moléculaire du Gb3 dans la liaison des lectines. Notamment, en utilisant les informations obtenues à partir des études des interactions de LecA et StxB avec le Gb3, nous avons réussi à recréer la ségrégation de LecA et StxB dans les GUVs.

Dans la deuxième partie du projet, nous avons exploré l'impact du LecA et du StxB sur l'organisation de la membrane. Ici, nous nous sommes particulièrement intéressés au réarrangement des nanodomaines ordonnés dans la membrane plasmique par les deux lectines. La visualisation de ces nanodomaines dans la membrane plasmique est une

tâche extrêmement difficile, c'est pourquoi nous les avons imités avec des domaines à ordre liquide (Lo) dans des bicouches lipidiques supportées et séparées en phase (SLBs). Nous avons fonctionnalisé ces bicouches lipidiques avec des molécules réceptrices de Gb3. Nous avons constaté que le StxB rétrécit les domaines Lo existants et induit la formation de nouveaux domaines Lo. Cela suggère que les clusters StxB "stabilisent" les domaines Lo existants. De plus, le regroupement efficace des récepteurs Gb3 par StxB induit la formation de nouveaux domaines Lo. LecA montre un comportement complètement opposé. Appliqué aux SLBs, LecA induit la dissolution des domaines Lo, homogénéisant la membrane. Enfin, P. aeruginosa appliqué à SLB dissout également les domaines Lo. Nous avons constaté que l'interaction LecA-Gb3 est le processus clé pour la dissolution des domaines Lo induits par P. aeruginosa. Cette dissolution des domaines Lo dans les SLBs induite par la bactérie a été observée pour la première fois.

I Introduction

1. Structure et fonctions de la membrane plasmique

La membrane plasmique cellulaire (figure 1) est un objet biologique fascinant. Il définit la barrière entre le cytosol et l'environnement extracellulaire, détermine la forme de la cellule et maintient son intégrité. La membrane plasmatique assure l'absorption et la libération de matériaux par la cellule, processus cruciaux pour le métabolisme cellulaire. La transduction du signal et la communication cellule-cellule sont effectuées par divers composants membranaires plasmatiques spécifiques. De plus, la membrane plasmique est un exemple exceptionnel d'auto-assemblage et d'auto-organisation. Il représente une barrière semi-perméable, basée sur une bicouche lipidique avec une grande variété de composants et des propriétés uniques.

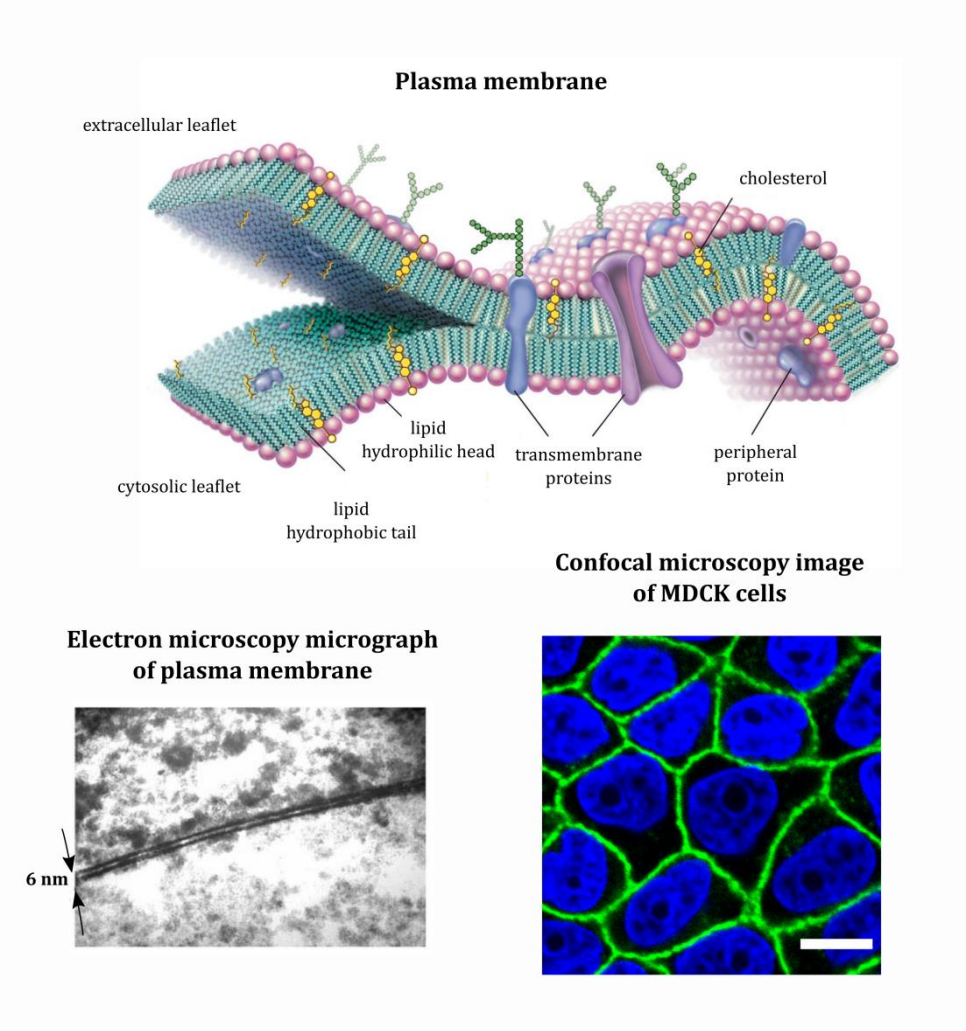

Figure 1 | **Membrane plasmique.** Schéma de la membrane plasmique (Encyclopedia Britannica). Micrographie EM de la membrane plasmique de Chara corallina (Coster, 2003). Image en microscopie confocale de la coupe transversale de cellules MDCK-II: membrane plasmique (myristoyl-LYN-GFP - verte); noyau (DAPI - bleu). Barre d'échelle - 10µm. Image fournie par le Dr. Roland Thuenauer.

1.1. Auto-assemblage des lipides dans l'eau, bicouche lipidique

Les lipides sont parmi les éléments les plus importants de la vie. Ils contribuent au stockage de l'énergie, participent aux événements de signalisation et composent l'épine dorsale de la membrane plasmique. Les lipides membranaires sont des molécules amphiphiles, composées d'un groupe de tête hydrophile et d'une ou plusieurs chaînes acyle grasses hydrophobes. (Israelachvili, 2011; van Meer et al., 2008).

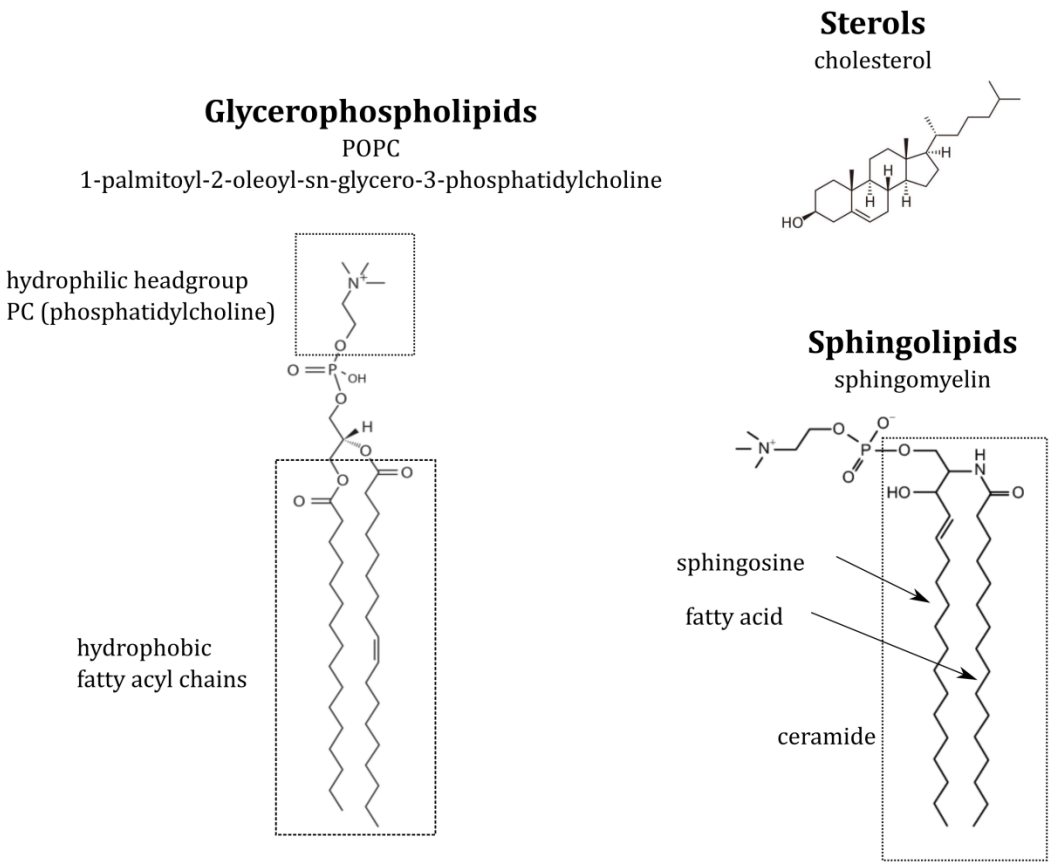

Figure 2 | **Structures chimiques des espèces lipidiques membranaires.** Les glycérophospholipides sont constitués d'un groupe de tête à base de phosphate et d'une ou plusieurs chaînes acyle grasses. Les sphingolipides sont basés sur un squelette en céramide (sphingosine + acide gras). Les stérols sont un sous-groupe de stéroïdes dont la structure centrale est constituée de quatre cycles fusionnés avec un groupe hydroxyle en position 3 du cycle A. Adapté de (Fahy et al., 2005; Jäpelt and Jakobsen, 2013).

Les glycérophospholipides sont la classe de lipides membranaires la plus abondante (van Meer et al., 2008). Ils sont composés d'un acide glycérophosphorique, qui sert de squelette à deux chaînes acyle grasses (partie hydrophobe) et d'un groupe de tête hydrophile (figure 2). Les sphingolipides membranaires, une autre classe importante de lipides membranaires, sont organisés sur la base d'un squelette en céramide, auquel

différents groupes de tête peuvent être attachés (figure 2). Les stérols membranaires, en particulier le cholestérol (figure 2), forment un groupe de petits lipides présents dans les membranes des cellules animales (Maxfield and Tabas, 2005).

Exposés à l'eau, les lipides (ou les molécules amphiphiles similaires en général) y compactent des fractions hydrophobes et mettent leurs groupes de tête hydrophiles en contact avec de l'eau en même temps (Israelachvili et al., 1977; Sych et al., 2018a). Cela conduit à l'assemblage du «noyau hydrophobe», isolé du milieu aqueux. Leur assemblage dépend de la géométrie lipidique, à savoir du volume de la partie non polaire V, de la longueur de la chaîne acyle grasse 1 et de la surface du groupe de tête polaire A. La combinaison de ces trois paramètres définit la géométrie de l'ensemble lipidique dans l'eau (Gennis, 2013; Israelachvili, 2011). Par exemple, le volume V_m d'une micelle sphérique composée de N molécules lipidiques peut être exprimé par:

$$V_m = \frac{4}{3}\pi R^3 = NV$$

où R est le rayon de la micelle. La surface Am d'une telle micelle est:

$$A_m = 4\pi R^2 = NA$$

Par conséquent, le rayon d'une telle micelle sphérique peut être exprimé par:

$$R = \frac{3V_m}{A_m}$$

Pour une micelle sphérique, $R \leq l$, donc:

$$\frac{V_m}{A_m l} \leq \frac{1}{3}$$

Le rapport $V_m / A_m l$ est appelé paramètre de tassement critique et, numériquement, le type d'assemblage lipidique basé sur les paramètres géométriques des molécules lipidiques individuelles. La longueur 1 et le volume v de la partie lipidique hydrophobe peuvent être déterminés par la structure chimique de la chaîne acyle grasse, tandis que la surface spécifique du groupe de tête, a, dépend en outre du contenu ionique de la solution aqueuse (pH, pK) et la charge du groupe de tête (Israelachvili, 2011). Sur la base du paramètre d'emballage critique, les lipides membranaires peuvent être classés en trois groupes principaux (figure 3):

1) Les lipides en forme de cône inversés ($v / la_0 < 1/2$) s'assemblent en micelles avec une surface de courbure positive. Ce groupe comprend principalement des lipides à une seule chaîne acyle grasse, tels que les lysophospholipides. Pour être assemblés dans des micelles sphériques, le paramètre de compression critique des lipides doit être inférieur à $1/3$, tandis que les lipides avec $1/3 < v / la_0 < 1/2$ s'assemblent sous forme de micelles cylindriques (Fan et al., 2016).

2) Les lipides en forme de cônes (v / la_0> 1) s'auto-organisent en micelles hexagonales (phase HII) à courbure négative (en milieu acide). Ce groupe contient des lipides polyinsaturés qui préfèrent être incorporés dans des membranes à courbure négative (Jouhet, 2013).
3) Les lipides en forme de cylindre ($1/2$ <v / la_0 ≤ 1) s'assemblent dans une bicouche lipidique (également appelée «phase lamellaire»). Ce groupe d'espèces lipidiques, représenté par des lipides à deux chaînes d'acyle gras de longueur et de degré de saturation différents, revêt une importance particulière du fait qu'il forme principalement la matrice lipidique de la membrane plasmique. Ils peuvent être assemblés dans les bicouches lipidiques souples de liposomes ($1/2$ <v / la_0 <1) ainsi que dans les bicouches lipidiques planaires (v / la_0 1)(Angelova and Dimitrov; Méléard et al., 2009).

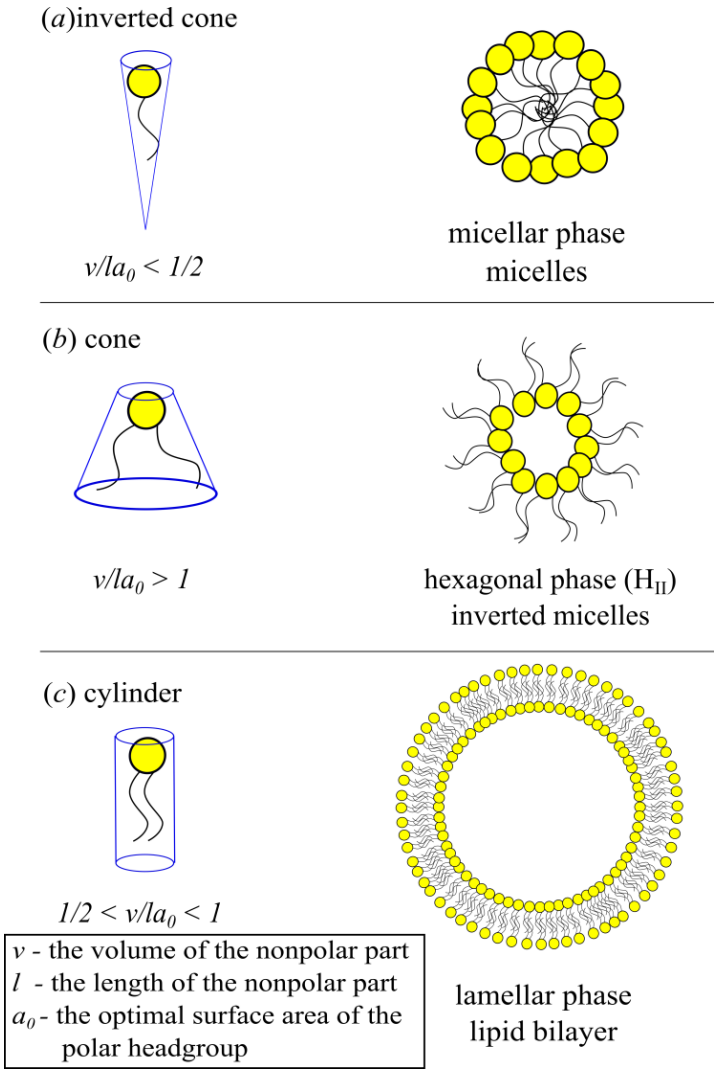

Figure 3 | **Auto-assemblage des lipides dans l'eau.** a) Les lipides en forme de cône inversé s'assemblent dans des micelles en contact avec de l'eau; b) Les lipides en forme de cônes s'assemblent en micelles inversées (phase HII) au contact de l'eau; c) Les lipides de forme cylindrique s'assemblent dans des bicouches lipidiques dans de l'eau. Révisé de (Sych et al., 2018a).

Les lipides membranaires peuvent exister dans divers états de phase lamellaires qui déterminent l'ordre membranaire et la diffusion translationnelle des lipides (Lee, 1977a, 1977b). Les bicouches lipidiques à un composant peuvent subir une transition de phase entre les phases solide et cristalline liquide (Aufderhorst-Roberts et al., 2017; Busto et al., 2014; van Meer et al., 2008). Une phase bicouche lipidique solide se caractérise par une faible mobilité et un compactage élevé de ses composants, tandis que la phase cristalline liquide, au contraire, présente un ordre faible et une mobilité de translation élevée. Une telle phase lipidique faiblement ordonnée et à forte mobilité peut également être appelée phase désordonnée des liquides (Ld). La température de transition de phase (également appelée température de fusion de chaîne) pour les bicouches lipidiques composées d'une seule espèce lipidique dépend de la structure moléculaire des molécules lipidiques, le rôle prédominant étant la longueur et le degré de saturation des chaînes acyle grasses, mais également de la structure du groupe de tête. Pour les phospholipides, cette température peut varier de 70 ° C pour 20: 4 PC (1,2-diarachidonoyl-sn-glycéro-3-phosphatidylcholine) avec des chaînes acyle polyinsaturées à 100 ° C pour DSPE (1,2-distéaroyl-sn- glycéro-3-phosphatidyléthanolamine) avec de longues chaînes acyle saturées (Silvius, 1982). La structure du groupe de tête (figure 4) a également une influence sur la température de transition de phase principale. Par exemple, les lipides PS et PE ont des températures de transition plus élevées que les lipides PC et PG, même s'ils sont tous composés de chaînes acyle grasses identiques.

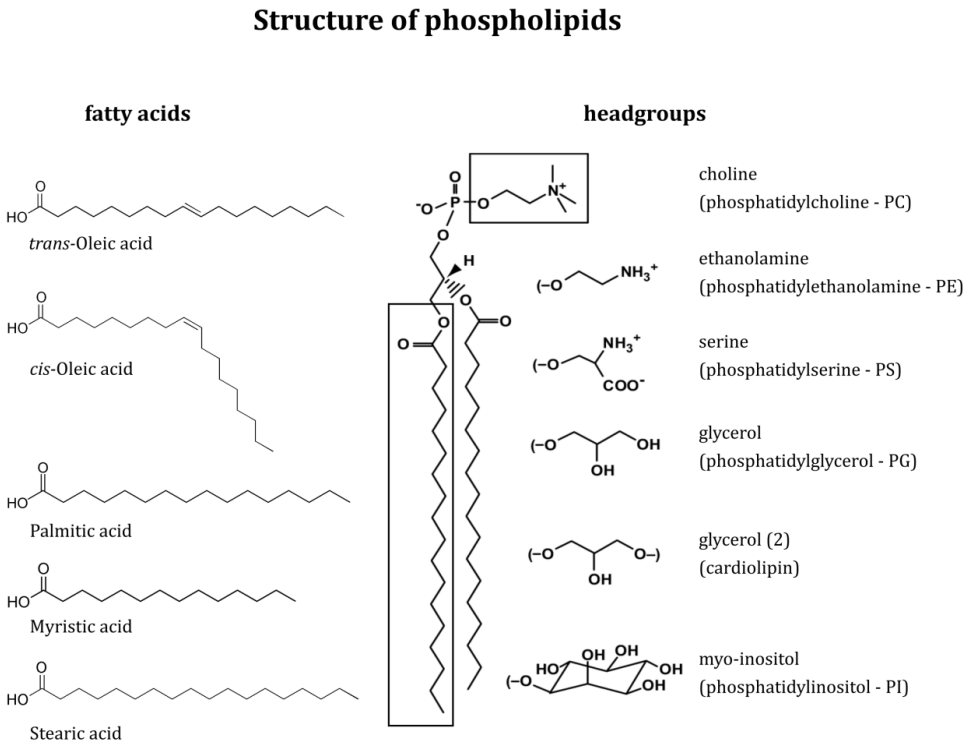

Figure 4 | **Glycérophospholipides.** Différents types de groupes de tête et de structures en chaîne acyle grasse des glycérophospholipides. Révisé de (Aktas et al., 2014).

Les sphingolipides à membrane, en particulier la sphingomyéline (SM), ont tendance à former des bicouches lipidiques en phase solide avec une température de transition de phase de 38 ° C (figure 5). L'introduction de stérols (cholestérol, par exemple) dans les bicouches lipidiques peut avoir un effet intéressant(Gracià et al., 2010; van Meer et al., 2008; Veatch and Keller, 2005). Dans les bicouches lipidiques riches en SM, le cholestérol agit comme un espaceur entre les molécules de SM étroitement emballées et améliore par conséquent la mobilité des lipides dans ces membranes. Comme l'ordre de la membrane reste élevé, ces membranes adoptent un nouvel état de phase lipidique - dit à commande liquide (Lo). Il est à noter qu'en raison de la liaison hydrogène unique entre le SM et le cholestérol, ces deux lipides forment des domaines Lo particulièrement stables. (Quinn and Wolf, 2009). Il est intéressant de noter que l'introduction de cholestérol (cholestérol) dans les bicouches lipidiques de Ld constituées de phospholipides non saturés (par exemple le 1,2-dioléoyl-sn-glycéro-3-phosphocholine (DOPC)) améliore l'ordre de ces membranes et, par conséquent, le DOPC / chol. Les bicouches lipidiques présentent un ordre membranaire supérieur à celui de Ld.

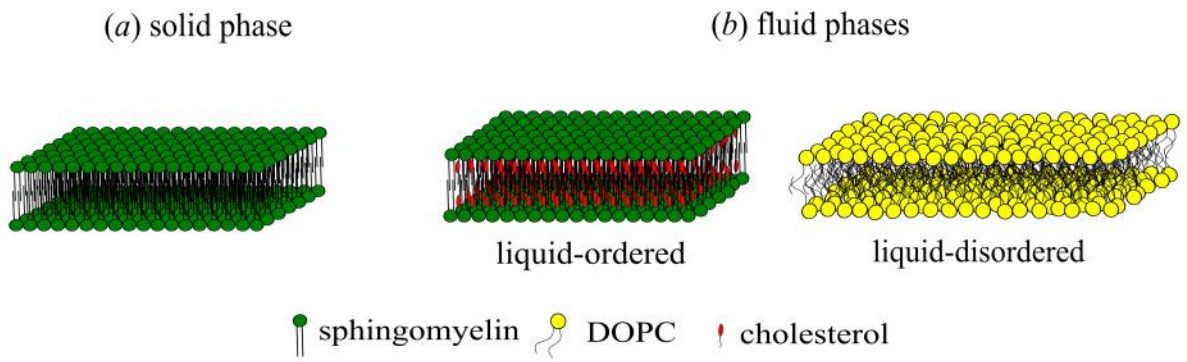

Figure 5 | **Les phases bicouches lipidiques.** Dans un environnement aqueux, les bicouches lipidiques peuvent former des phases de tassement et de mobilité lipidique différents. a) phase solide (ici constituée de SM); b) Phases fluides: ordonnées liquides (ici formées de SM et de chol) et désordonnées liquides (ici formées de DOPC). Révisé de (Sych et al., 2018a).

Des domaines membranaires ségrégés spatialement de différentes phases peuvent coexister dans une bicouche lipidique à plusieurs composants (Almeida, 2011; Bacia et al., 2005). Ce phénomène s'appelle la séparation de phase. Habituellement, il se produit dans les bicouches lipidiques contenant des lipides avec différentes températures de transition de phase principale. Par exemple, la bicouche lipidique à deux composants composée de DOPC (T_m = -17 ° C) et de sphingomyéline (T_m = 38 ° C) présente une séparation de phase aux températures situées entre les transitions de phase principales des deux lipides. (Leonenko et al., 2004). Dans ce cas, il contient des domaines en phase solide enrichis en domaines SM et en phase liquide (Ld) riches en DOPC. Une addition supplémentaire de cholestérol à ces bicouches lipidiques peut convertir les domaines de la phase solide riches en SM en Lo (van Meer et al., 2008). De plus, à des rapports molaires spécifiques SM / DOPC / chol, les trois phases peuvent coexister dans la

bicouche lipidique. (Aufderhorst-Roberts et al., 2017). La séparation de phases est réversible et disparaît en augmentant la température de la bicouche lipidique.

Ce phénomène de séparation de phases a fait l'objet de nombreuses études au cours des trois dernières décennies, à l'aide de diverses techniques, telles que la calorimétrie par titrage isotherme. (Mabrey and Sturtevant, 1976), microscopie à fluorescence (Almeida, 2011; Carravilla et al., 2015), microscopie à force atomique (Mingeot-Leclercq et al., 2008; Yilmaz and Kobayashi, 2015) et simulations de dynamique moléculaire (Koldsø et al., 2014; Wang et al., 2016). Les interactions lipides-lipides contrôlent la formation et la dynamique de tels domaines membranaires, qui revêtent une importance capitale dans les membranes hautement complexes à plusieurs composants des cellules vivantes.

1.2. Organisation lipidique d'ordre supérieur dans la membrane plasmique

Le premier modèle descriptif de la membrane cellulaire a été présenté par Singer et Nicolson en 1972 (Nicolson, 2014; Singer and Nicolson, 1972). Ce modèle indique que tous les composants de la membrane sont intégrés à la matrice bicouche lipidique séparant l'intérieur de la cellule de l'environnement extracellulaire. Selon ce modèle, tous les composants de la membrane (lipides et protéines) sont répartis de manière homogène dans la matrice bicouche lipidique et peuvent diffuser librement dans le plan latéral de la membrane. Ce modèle a été appelé «modèle de mosaïque fluide», car il décrit la membrane plasmique comme un liquide bidimensionnel. Des études ultérieures de la membrane biologique utilisant divers détergents (par exemple Triton X 100) ont montré la séparation du matériau de la membrane en deux fractions principalement: une membrane résistante aux détergents (DRM) et une membrane soluble pour détergents (DSM). Il est intéressant de noter que la fraction DRM s'est révélée être enrichie en sphingolipides à longues chaînes d'acyle gras saturés et en cholestérol, alors que la fraction DSM était enrichie en phospholipides membranaires. Ces résultats suggèrent d'abord l'association du SM et du cholestérol dans la membrane plasmique (Fra et al., 1994; Mahfoud et al., 2009; Seddon et al., 2004). Des études ultérieures sur la composition des feuillets membranaires plasmatiques ont révélé la préférence des lipides SM et PC pour le feuillet membranaire plasmatique externe (extracellulaire), alors que la majorité des lipides chargés négativement (tels que PE et PS), ainsi que PI et PG étaient principalement prédominants. situé dans la notice interne (Devaux, 1991; Devaux and Morris, 2004). Des lipides glycosylés ont été trouvés dans la foliole externe de la membrane plasmique avec des fragments de sucre exposés à l'environnement extracellulaire. (Simons and Van Meer, 1988). Une telle localisation des espèces lipidiques est activement maintenue par la cellule afin de prendre en charge diverses fonctions cellulaires. Par exemple, les espèces de PI, situées dans la feuille de membrane interne, peuvent être phosphorylées trois fois pour former PIP, PIP2 et PIP3, qui revêtent une importance cruciale pour la transduction du signal cellulaire (Yoshida et al.). Le cholestérol est également représenté dans les deux feuillets membranaires

(Rothman and Lenard, 1977). L'hétérogénéité de la membrane plasmique dans le plan latéral a été constatée dans des cellules épithéliales polarisées (Simons and Van Meer, 1988). Les membranes apicales et basolatérales des cellules épithéliales sont séparées par des jonctions serrées. La membrane apicale est enrichie en sphingolipides et en cholestérol, tandis que la membrane basolatérale - en phospholipides (Gerl et al., 2012). Ces deux membranes présentent également un ordre lipidique différent, la membrane apicale étant plus ordonnée. (Ikenouchi et al., 2012). Des domaines membranaires latéraux plus petits ont été découverts pour la première fois sous forme de fosses membranaires plasmatiques d'un diamètre de 60 à 80 nm, appelées cavéoles. (Barnett-Norris et al., 2005; Parton and del Pozo, 2013; Parton and Simons, 2007). Ils sont stables dans le temps et enrichis en sphingolipides et en cholestérol, ce qui suggère un ordre membranaire élevé. Les cavéoles condensent également un grand nombre de composants de la membrane plasmique. Ils sont impliqués dans l'endocytose, la transcytose et la transduction du signal (Collins et al., 2012; Pelkmans and Helenius, 2002; Tuma and Hubbard, 2003). De plus, ils sont considérés comme les réservoirs de la courbure de la membrane plasmique qui aident une cellule à survivre au stress mécanique (Sinha et al., 2011).

Sur la base de ces résultats, Simons et Ikonen ont amélioré le modèle de membrane plasmique en 1997 (figure 6). Ils ont présenté les «radeaux lipidiques», qui correspondent à des plates-formes dynamiques, hautement ordonnées, très bien organisées, enrichies en sphingomyéline, en cholestérol et en protéines membranaires et en glycolipides (Sezgin et al., 2017; Simons and Ikonen, 1997). Contrairement aux cavéoles, les radeaux lipidiques plans sont très dynamiques, ils s'assemblent et se réorganisent très rapidement (Fan et al., 2010). La formation de radeaux lipidiques est une caractéristique unique de la feuille externe de la membrane plasmique. (Meer, 2002). La notice membranaire cytosolique ne contient pas de radeaux lipidiques; cependant, on sait que les amas lipidiques PS et PI dans la foliole interne de la membrane s'interdigitent avec les radeaux lipidiques (Raghupathy et al., 2015).

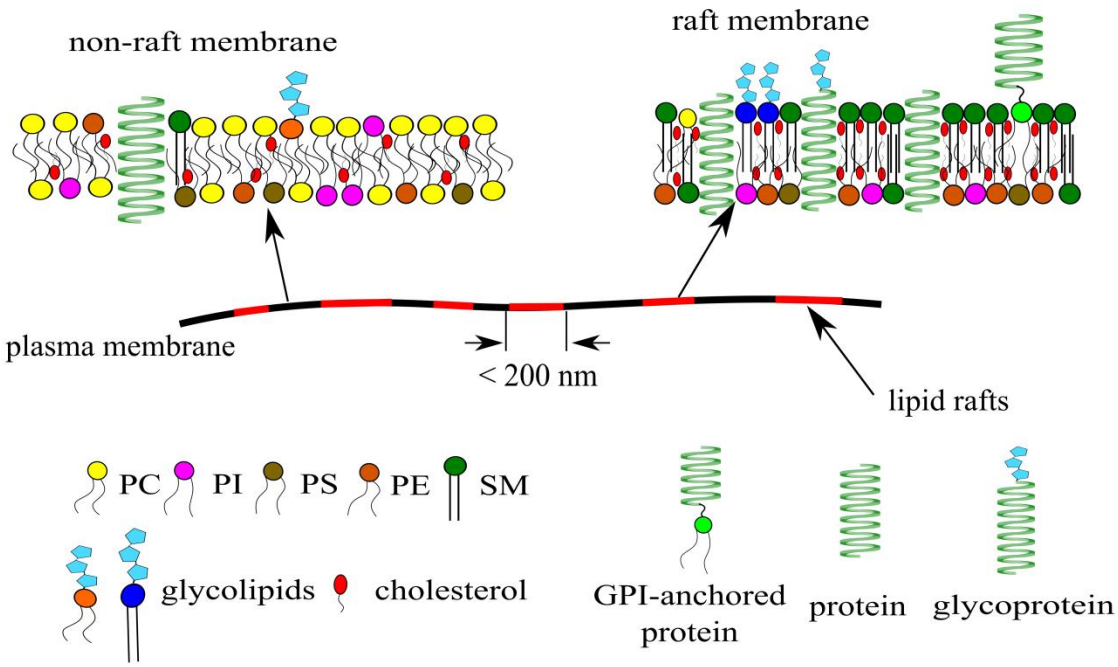

Figure 6 | **Nanodomaines de la membrane plasmique.** La membrane plasmique native contient des nanodomaines lipidiques compactés et hautement ordonnés appelés «radeaux lipidiques». Des radeaux lipidiques se forment dans la feuille externe de la membrane plasmique et sont enrichis en sphingomyéline et en cholestérol. Les radeaux lipidiques s'associent aux glycosphingolipides, aux protéines transmembranaires et ancrées au GPI. La foliole cytosolique de la membrane plasmatique est enrichie en PI, PG, PS et PE, tandis que la foliole externe contient la majorité des lipides SM et PC. Le cholestérol est uniformément distribué entre les monocouches lipidiques. Adapté de (Sych et al., 2018a).

Les radeaux lipidiques peuvent inclure ou exclure des protéines membranaires (Simons and Gerl, 2010; Simons and Toomre, 2000). Ils fournissent la configuration nécessaire au bon fonctionnement des protéines membranaires, notamment dans la signalisation cellulaire. On sait que les protéines à ancrage glycosylphosphatidylinositol (GPI) et d'autres protéines liées à la membrane par des groupes cholestérol ou palmitoyle sont associées aux radeaux lipidiques (Simons and Ikonen, 1997). Les radeaux lipidiques hébergent les hélices a des protéines G, ce qui permet leur implication dans la signalisation par GPCR (Barnett-Norris et al., 2005). En outre, les radeaux lipidiques sont impliqués dans la signalisation du récepteur de l'antigène des lymphocytes T (Owen et al., 2012), ainsi que dans la signalisation de la tyrosine kinase (Simons and Toomre, 2000). Les radeaux lipidiques participent à l'endocytose, au trafic cellulaire et à l'exocytose. Un exemple typique est l'entrée et la libération cellulaires du virus de l'immunodéficience humaine (VIH). L'entrée du VIH dépend du récepteur CD4 de la glycoprotéine cellulaire, connu pour s'associer aux radeaux lipidiques (Carter et al., 2009). Au cours de la libération du virus, la protéine Gag myristoylée du VIH s'accroche à la feuille de membrane plasmatique cytosolique de la cellule hôte et induit le regroupement de radeaux lipidiques dans la feuille de membrane extérieure, ce qui entraîne la formation de particules virales et la formation de bourgeons (Ono and Freed,

2001). En conséquence, l'enveloppe virale est enrichie en sphingomyéline et en cholestérol, qui sont principalement des composants associés aux radeaux lipidiques (Sengupta et al., 2019).

1.3. Composants membranaires glycosylés et radeaux lipidiques, Glycosphingolipides

La surface externe de la membrane plasmique est fonctionnalisée avec une grande variété de molécules différentes qui permettent à la cellule d'interagir avec son environnement. Les lipides et les protéines membranaires peuvent subir des modifications post-traductionnelles, telles que la glycosylation (Ambrosi et al., 2005). De plus, les parties lipidiques ou protéiques de telles molécules glycosylées servent d'ancres bicouches lipidiques pour les glucides, exposés à l'environnement extracellulaire. En particulier, les glycosphingolipides (GSL) présents dans la foliole externe de la membrane (Schnaar et al., 2009), incorporer dans la bicouche lipidique avec la fraction hydrophile de céramide. Les GSL sont définis par les structures des glucides attachés au squelette des céramides. Sur cette base, trois groupes de GSL peuvent être mis en évidence (figure 7):

1) Les gangliosides (Svennerholm, 1964) sont des glycosphingolipides avec des groupes de sucre contenant de l'acide N-acétylneuraminique (NANA, également appelé acide sialique). Ils peuvent également être subdivisés en fonction du nombre (un, deux, trois ou quatre) de fractions acide sialique associées au glucide GSL. Les représentants typiques sont GM1, GD1, GT1, GQ1;
2) Les cerebrosides (Tan and Chen, 2003) sont des glycosphingolipides avec un seul sucre fixé au squelette des céramides (également appelés monoglycosylcéramides). Comme ce sucre peut être du glucose ou du galactose, les deux groupes de cérébrosides sont les glucocérébrosides et les galactocérébrosides;
3) Les globosides (Jones et al., 1997) sont des glycosphingolipides à sucres multiples liés au squelette des céramides. Les représentants typiques sont Gb3 et Gb4.

Les glycanes de surface cellulaire remplissent une grande variété de fonctions (Varki, 2017). Entre autres, les glycanes de surface cellulaire participent à la communication cellule-cellule, à l'adhésion et à la formation du glycocalyx cellulaire (Shurer et al., 2019). Ils participent également à la modulation de l'organisation de la membrane plasmique et de la communication entre feuillets. Ici, en particulier, les GSL à long squelette en céramide permettent une interdigitation efficace (Manna et al., 2017). Les glycanes médient la transduction du signal et l'initiation de la cascade de signaux sur la membrane plasmique. De plus, les glycanes sont utilisés par les

virus et les bactéries afin de permettre une adhésion et une internalisation efficaces dans la cellule hôte.

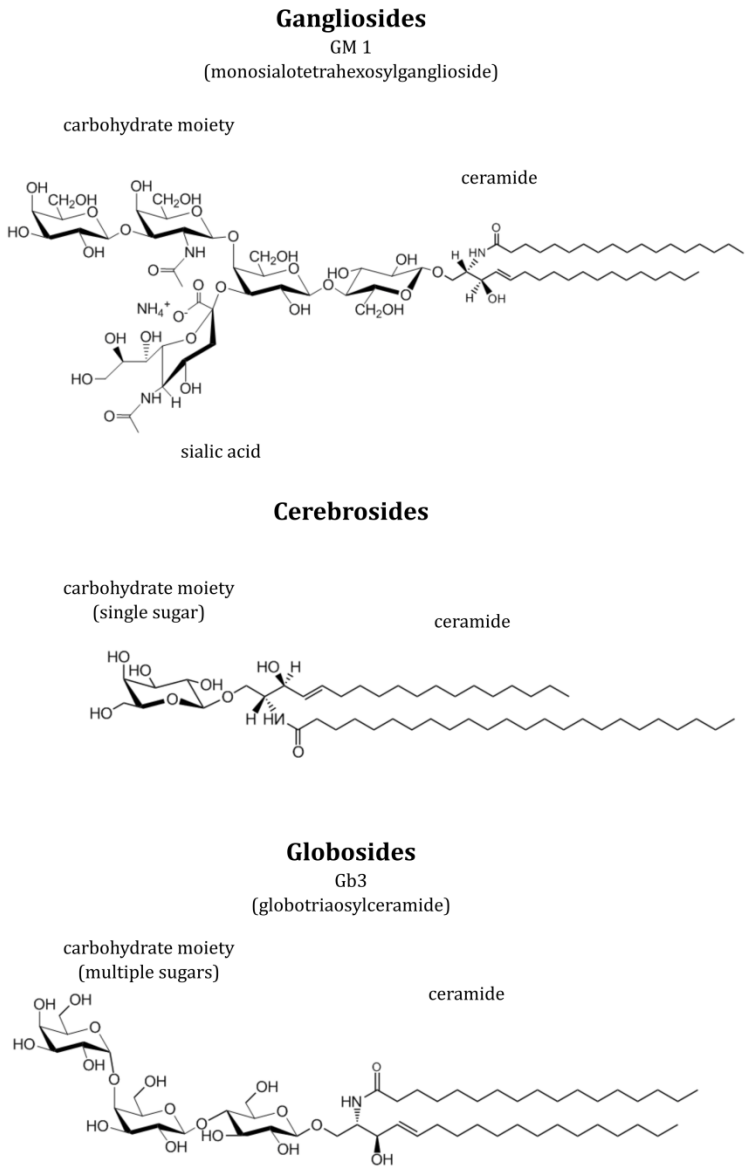

Figure 7 | **Glycosphingolipides.** Structure de trois classes principales de glycosphingolipides. Les structures chimiques sont adaptées de Avanti Polar Lipids.

1.4. Imagerie de la membrane plasmique par microscopie à fluorescence

En biologie cellulaire, la microscopie à fluorescence est une méthode de choix car elle offre la capacité unique de suivre des composants cellulaires spécifiquement marqués et de suivre visuellement leur comportement au cours de processus cellulaires complexes. En particulier, depuis la découverte de la protéine fluorescente verte (GFP), la

microscopie à fluorescence est devenue un outil essentiel pour déchiffrer la localisation et le devenir de la protéine (Tsien, 1998). Les protéines fluorescentes peuvent être utilisées comme marqueurs de protéines en les fusionnant avec la protéine cible au niveau génétique. En outre, la microscopie à fluorescence offre l'opportunité de l'imagerie de cellules vivantes et constitue un outil puissant pour élucider les mécanismes moléculaires au niveau de la membrane plasmique cellulaire. (Kwiatek et al., 2014). La membrane plasmique peut être marquée avec des fluorophores organiques à base de lipides ou lipophiles (Klymchenko and Kreder, 2014). Cependant, ces marqueurs peuvent induire une cytotoxicité par le biais du stress photo-oxydant. En variante, les PF fluorescents peuvent être conjugués à des protéines transmembranaires ou à des protéines ancrées GPI. Cette approche est moins susceptible d'induire une phototoxicité. De plus, il est possible de marquer des composants de la membrane plasmatique (par exemple des espèces lipidiques distinctes ou des protéines membranaires) avec des fluorophores et de suivre leur localisation et leur trafic (Klymchenko and Kreder, 2014; Zhang et al., 2017). La multitude de techniques de microscopie à fluorescence utilisées de nos jours est impressionnante. Pour la visualisation de la membrane plasmique, les approches classiques de la microscopie confocale ou à champ large sont souvent associées à des techniques quantitatives (imagerie de durée de vie en fluorescence, microscopie à corrélation de fluorescence) ou à des techniques de super résolution afin d'améliorer la résolution spatio-temporelle ou d'extraire des informations supplémentaires sur la membrane locale. environnement (Kwiatek et al., 2014; Sezgin et al., 2017). Ici, je passerai brièvement en revue deux techniques de microscopie à fluorescence largement utilisées: la microscopie confocale à balayage laser (LSCM) et la microscopie à fluorescence à réflexion interne totale (TIRFM).

1.4.1. Fluorescence

La fluorescence est un processus d'émission de lumière par une substance initialement excitée par un rayonnement électromagnétique (Lakowicz, 2006). Pour être transféré à l'état excité, un fluorophore doit absorber un quantum de lumière - un photon. L'excitation lumineuse induit la transition d'un électron de l'état fondamental à une orbitale supérieure, amenant la molécule à l'état excité. Par la suite, cette molécule peut revenir à l'état fondamental avec l'émission d'un photon. Habituellement, les processus de lumière d'absorption et d'émission sont affichés à l'aide du diagramme de Jablonski (figure 8A). La transition de la molécule a lieu de l'état 0-singulet (S_0 - état fondamental) au premier état singulet (S_1 - état excité). L'électron revient dans l'état fondamental avec l'émission d'un photon ou de manière non radiative. De plus, un passage intersystème à l'état triplet est possible.

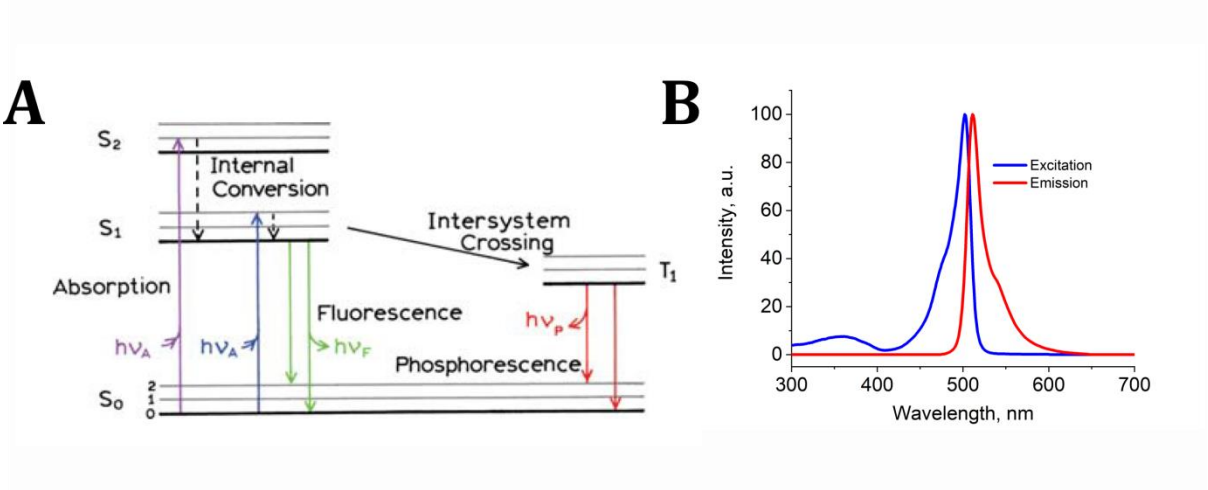

Figure 8 | **Fluorescence.** A) Diagramme de Jablonski (Lakowicz, 2006). Le fluorophore absorbe une quantité de lumière qui entraîne le transfert d'un électron de l'état fondamental (SO) à l'état excité (S1 - flèche bleue ou S2 - flèche violette). Les sous-états vibratoires des états électroniques sont indiqués par des lignes grises. Le processus d'absorption peut transférer un électron à plusieurs états vibratoires de l'état excité. La conversion interne non radiative amène l'électron à l'état vibratoire le plus faible de l'état excité S1. Par la suite, la fluorescence est la transition de l'électron à l'état fondamental SO par l'émission d'un photon. L'électron peut être transféré dans différents états vibratoires de l'état fondamental. Alternativement, un électron peut subir un croisement intersystème vers l'état de triplet excité (T1). B) Spectres d'excitation et d'émission de fluorescence du fluorophore organique Bodipy (Thermo Fisher Scientific).

Les propriétés des fluorophores définissent leurs spectres d'absorption et d'émission. Le spectre d'absorption définit la longueur d'onde de la lumière à utiliser pour exciter le fluorophore. Les spectres d'absorption et d'émission (figure 8B) des fluorophores dépendent souvent des propriétés de l'environnement (polarité du solvant, viscosité, pH, etc.) et peuvent donc être utilisés en tant que capteurs environnementaux. De plus, les phénomènes de fluorescence sont largement utilisés en microscopie pour la localisation des fluorophores.

1.4.2. Microscope confocal à balayage laser

Les lasers fournissent une émission lumineuse intense d'une bande spectrale très mince. Par conséquent, ils sont largement utilisés comme sources d'excitation pour la microscopie à fluorescence. La lumière laser peut être focalisée en un point distinct de l'échantillon avec l'objectif. De plus, la fluorescence induite par la lumière laser peut être collectée et analysée. En analysant l'échantillon point par point, vous pouvez obtenir une image de la tranche de l'échantillon située dans le plan focal de l'objectif, pixel par pixel. Le problème commun de la microscopie est d'établir un rapport signal sur bruit élevé. Une quantité considérable d'arrière-plan provient de la fluorescence en dehors du plan focal de l'objectif. Afin de surmonter ce problème, le signal provenant d'au-delà du plan focal est éliminé par l'introduction d'un trou d'épingle dans le système de microscopie. Cette technique de microscopie s'appelle Microscopie confocale à balayage laser (LSCM, figure 9) (Pawley, 2010). Cela permet non seulement

d'enregistrer l'image d'un plan de l'échantillon, mais également d'obtenir l'image 3D de l'échantillon en l'imaginant image par image. La taille de l'échantillon pouvant être imagée est définie par la distance de travail de l'objectif. Cette technique est également largement utilisée pour l'imagerie de cellules vivantes. Les principales limitations de LSCM proviennent de la limite de diffraction qui définit la résolution optique. Habituellement, les microscopes confocaux sont capables d'imager des objets avec une limite de résolution de 200 nm dans le plan latéral et de 400 à 500 nm dans la direction z. Un autre inconvénient de la microscopie confocale est la vitesse d'acquisition, qui est relativement lente en raison de la nécessité de numériser - 1 à 2 images par seconde pour une image de 1024 × 1024 pixels. Cette fonctionnalité a été partiellement surmontée par le développement et la mise en œuvre de scanners plus rapides (par exemple, le «mode résonant»).

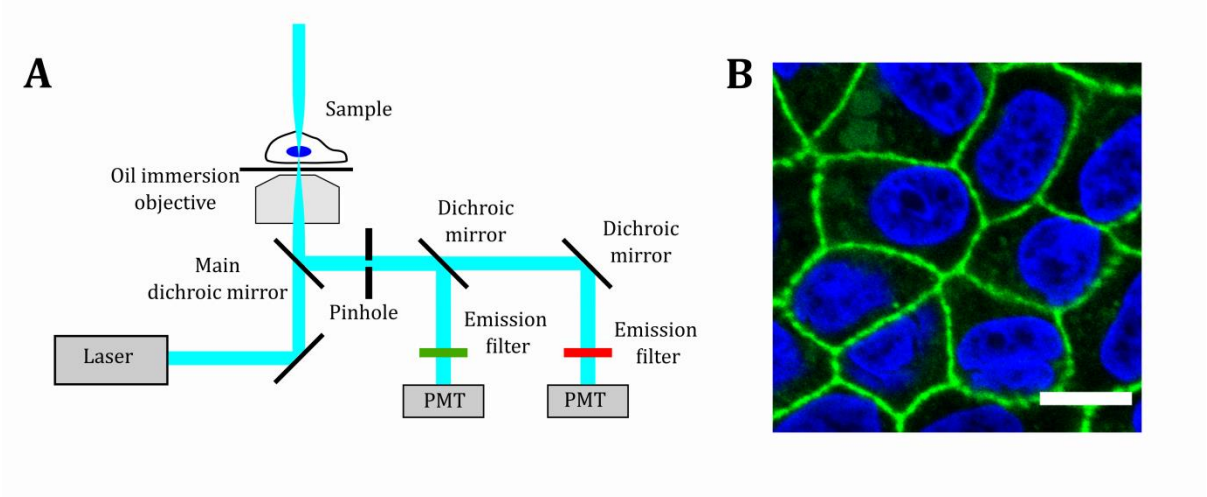

Figure 9 | **Microscopie confocale à balayage laser (LSCM).** A) Schéma d'une configuration de microscopie confocale inversée. La lumière d'excitation laser est focalisée sur le plan focal de l'échantillon. La réflexion laser est coupée avec un miroir dichroïque. La lumière de fluorescence est transmise à travers un filtre d'émission approprié et détectée à l'aide d'un photomultiplicateur. Le balayage permet l'acquisition d'une image pixel par pixel; B) Image de microscopie confocale de la coupe transversale de cellules MDCK-II. La membrane plasmatique (myristoyl-LYN-GFP - verte); noyau (DAPI - bleu). Image fournie par le Dr Roland Thuenauer.

1.4.3. Microscopie à fluorescence à réflexion interne totale

La focalisation du laser sur le plan focal arrière de l'objectif permet l'éclairage de l'échantillon avec le faisceau de lumière laser parallèle. Cela permet une excitation uniforme d'une zone relativement grande à la fois et augmente considérablement la vitesse d'acquisition pour une seule image. La fluorescence est détectée à l'aide d'une caméra (CCD, CMOS, etc.) capable de réaliser un instantané de l'ensemble de la zone d'imagerie. Ce type de microscopie est appelé "champ large" (Axelrod et al., 1983) (figure 10). L'avantage évident est la vitesse d'acquisition des images. Cependant, une excitation de champ large produit une quantité considérable de fluorescence de fond.

Afin d'éliminer le fond de fluorescence, le faisceau d'excitation laser est incliné. Le meilleur rapport signal / bruit de fond est obtenu par microscopie à fluorescence par réflexion interne totale (TIRFM). Ici, le laser est incliné par rapport à l'angle TIR au niveau de l'interface lamelle / échantillon (Axelrod, 2001). Le laser ne peut plus pénétrer dans l'échantillon, mais l'onde évanescente, induite à l'interface verre de protection / échantillon, permet toujours une excitation efficace d'une couche mince de l'échantillon. La principale limite de cette technique est qu'elle ne peut exciter qu'une couche de l'échantillon d'une épaisseur de 100 nm, adjacente au verre de protection. Un bon compromis entre l'élimination du fond et l'épaisseur de la couche d'excitation peut être obtenu en utilisant un éclairage appelé HILO (Tokunaga et al., 2008) - éclairage lamellaire fortement incliné de l'échantillon avec le faisceau laser.

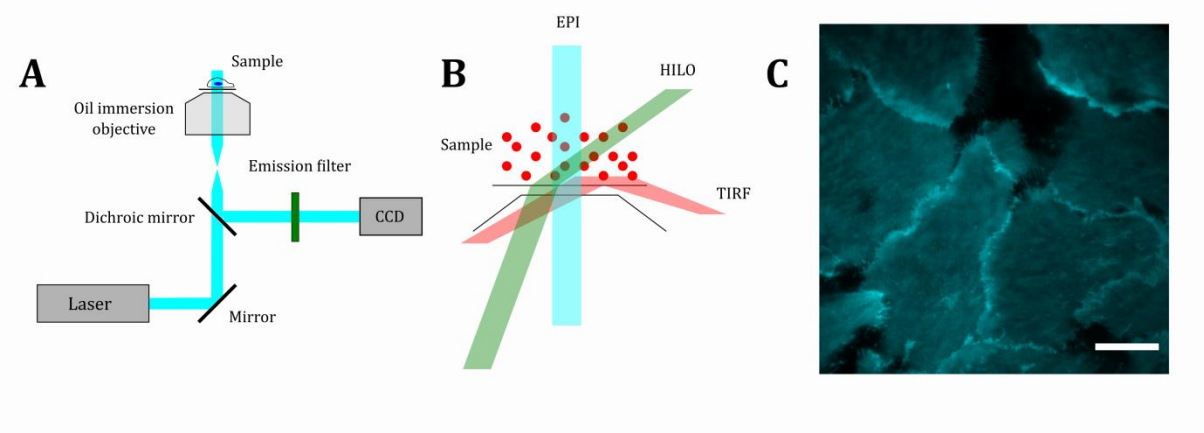

Figure 10 | **Microscopie à excitation large champ.** A) Schéma d'une configuration de microscopie inversée à champ large. La lumière d'excitation laser est focalisée sur le plan focal arrière de l'objectif. L'échantillon est illuminé comme illustré en B. La réflexion du laser est coupée avec un miroir dichroïque. La lumière de fluorescence est transmise à travers un filtre d'émission approprié et détectée à l'aide d'une caméra (dans ce cas, CCD). B) Trois modes d'éclairage de l'échantillon: EPI, HILO et TIRF. C) Image TIRF des membranes plasmiques inférieures de cellules vivantes MDCK-II marquées avec myristoyl-LYN-GFP. Barre d'échelle - 10 µm. Image fournie par Marco Frensch.

Le champ large en mode EPI / TIRFM / HILO est particulièrement efficace pour l'imagerie de cellules vivantes car il permet une acquisition à haute vitesse (des dizaines de millisecondes par image). Le TIRFM est particulièrement utile pour l'imagerie de la membrane plasmique à la surface inférieure des cellules vivantes.

2. Reconstitution de l'organisation de la membrane plasmique dans un système synthétique

L'étude de l'organisation membranaire dans les membranes cellulaires natives est une tâche exigeante (Klymchenko and Kreder, 2014; Kwiatek et al., 2014). Dans les cellules vivantes, les radeaux lipidiques sont très mobiles et de petite taille (Sezgin, 2017). De plus, afin de réaliser tous les différents processus cellulaires, ils assemblent et dissocient en permanence (Fan et al., 2010). Malgré les progrès récents des techniques de microscopie à super-résolution avec une augmentation impressionnante de la

résolution spatiale et temporelle, la visualisation directe des nanodomaines membranaires reste difficile. De plus, l'abondance des composants de la membrane plasmatique limite l'analyse aux lipides et protéines membranaires uniques dans des processus cellulaires spécifiques.

2.1. Membranes modèles

L'organisation membranaire est non seulement maintenue activement par la cellule, mais également par les interactions lipides-lipides et lipides-protéines dans la membrane plasmique (Sprong et al., 2001). Ces interactions peuvent être isolées de la machinerie cellulaire active par reconstitution synthétique en une bicouche lipidique multicomposante composée d'espèces lipidiques et / ou protéiques distinctes (Bacia et al., 2005; Lin and London, 2014). Une telle approche «ascendante» permet un contrôle précis du contenu et de la structure de la membrane artificielle obtenue. Les membranes artificielles peuvent imiter les caractéristiques spécifiques de la membrane plasmique. Ils sont extrêmement utiles pour caractériser l'organisation de la membrane (Dietrich et al., 2001), reconstitution de l'adhésion cellulaire (Villringer et al., 2018) and endocytose (Römer et al., 2007). De nombreux types de membranes modèles ont été développés au cours des quatre dernières décennies. Les vésicules unilamellaires géantes (VUV), qui sont largement utilisées pour la reconstitution synthétique du transport transmembranaire, sont particulièrement intéressantes (Hermann et al., 2014). Alternativement, de grandes plaques planes de bicouche lipidique étalées sur un support solide (Windschiegl et al., 2009), par conséquent, les bicouches lipidiques supportées (SLB) sont utilisées pour étudier l'organisation de la membrane à grande échelle.

2.1.1. Vésicules unilamellaires géantes

Des sphères bicouches lipidiques avec deux surfaces hydrophiles et un noyau hydrophobe entre elles offrent la possibilité de compartimenter de petits volumes de solutions aqueuses et de les isoler de l'extérieur aqueux (Yang et al., 2016). De telles sphères (également appelées liposomes) sont naturellement utilisées par la cellule pour les moyens de transport (endocytose (Pakkanen, 2009), transcytose (Thuenauer et al., 2017), trafic intracellulaire (Sens et al., 2008), exocytose et communication cellule-cellule (Xu et al., 2016). En fait, le cytosol cellulaire est isolé du liquide extracellulaire selon un principe similaire: il est confiné par la barrière bicouche lipidique. Les liposomes peuvent être utilisés pour imiter une telle barrière. Cependant, les liposomes qui se forment spontanément en appliquant une solution aqueuse aux lipides ont normalement une taille beaucoup plus petite (0,1 à 1 μm de diamètre) que les cellules régulières (dizaines de micromètres) (Antonietti and Förster, 2003). De plus, des vésicules dites multilamellaires se forment fréquemment. Pour obtenir des structures unilamellaires, les liposomes doivent être décomposés en vésicules unilamellaires par extrusion ou sonication. Angelova et Dimitrov ont mis au point un protocole permettant

d'obtenir des liposomes unilamellaires à la taille d'une cellule à partir de films lipidiques étalés sur une surface en 1986 (Angelova and Dimitrov). La procédure s'appelle l'électroformation et fournit des bicouches lipidiques sphériques de plusieurs dizaines de centaines de μm de diamètre - vésicules unilamellaires géantes (GUV). Il est important de pouvoir contrôler la formation de GUV avec des espèces distinctes de lipides et de protéines (Dezi et al., 2013; Madl et al., 2017). Ainsi, divers processus cellulaires peuvent être reconstitués à l'aide de GUV. En particulier, les GUV sont des systèmes modèles parfaits pour les études de transport à travers la bicouche lipidique dans le contexte de la formation de pores (Gilbert et al., 2014), absorption et libération cellulaire (Mellander et al., 2014; Römer et al., 2007; Sasai et al., 2010). Les GUV peuvent également être utilisés pour imiter l'adhésion cellulaire (Tareste et al., 2008) et fusion de vésicule (Witkowska et al., 2018). De plus, des composants cytosoliques cellulaires peuvent être ajoutés à la lumière du GUV. Par exemple, un maillage d'actine recréé dans des GUV a permis d'étudier le rôle du cytosquelette dans la déformation de la membrane (Vogel and Schwille, 2012). De plus, l'intérieur des GUV peut être fonctionnalisé avec une machinerie cellulaire reconstituée synthétiquement pour la réplication de l'ADN (Xu et al., 2010). Ces GUV à plusieurs composants peuvent être utilisés pour imiter une variété de processus cellulaires tels que la communication cellule-cellule (Joesaar et al., 2019) et même la division cellulaire (Xu et al., 2010). Globalement, de tels systèmes peuvent être utilisés pour générer des protocellules et des prototissues synthétiques (Gobbo et al., 2018; Omidvar and Römer, 2019; Villringer et al., 2018) afin de recréer les principes de base de la vie.

Les GUV marquées avec des marqueurs lipophiles fluorescents peuvent être visualisées avec les techniques de microscopie conventionnelles, alors que l'imagerie de vésicules plus petites (<200 nm de diamètre) est limitée par la limite de diffraction. Des coupes transversales équatoriales de GUV représentées avec LSCM sont illustrées à la figure 11. De plus, il est possible de visualiser les phases liquides dans les GUV. Sur la figure 11, une VUV est constituée d'une bicouche lipidique séparée en phases. Parce que la phase désordonnée en liquide est plus fluide (moins serrée), le marqueur de fluorescence (HPC-Bodipy) préfère s'associer à cette phase Ld. En conséquence, il semble brillant en comparaison de la phase Lo très compacte qui est dépourvue de marqueur membranaire. Dans cette VUV particulière, la phase Ld est constituée de DOPC et la phase Lo est composée de sphingomyéline et de cholestérol. Une telle hétérogénéité latérale imite l'organisation de la membrane plasmique native à l'échelle microscopique (Dietrich et al., 2001).

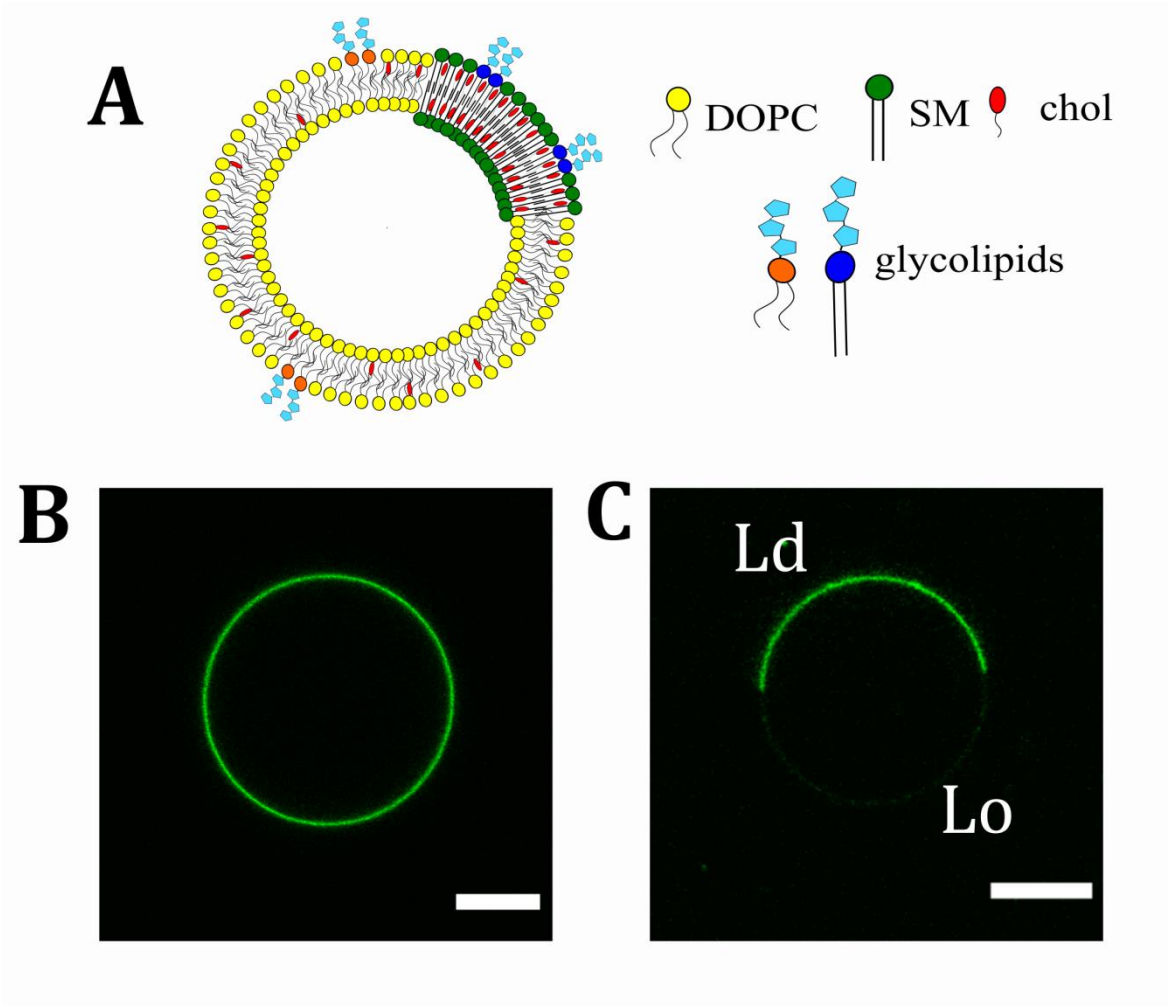

Figure 11 | **Vésicules unilamellaires géantes.** A) Schéma d'une GUV à séparation de phase. B) Image confocale de la section transversale équatoriale d'un GUV homogène composé de DOPC / chol (70/30) marqué avec HPC-Bodipy. C) Image confocale de la coupe transversale équatoriale d'un GUV à séparation de phase composé de DOPC / chol / SM (2/1/2) marqué avec HPC-Bodipy. HPC-Bodipy incorpore de préférence le domaine Ld plus fluide (composé principalement de DOPC), tandis que le domaine Lo (composé principalement de SM et de cholestérol) apparaît sombre. Barres d'échelle - 10 μm. Régime révisé du (Sych et al., 2018a).

2.1.2. Bicouches lipidiques supportées

Le dépôt d'une bicouche lipidique sur un support solide offre la possibilité d'étudier les interactions lipide-lipide à très grande échelle dans d'immenses plaques membranaires planaires. Des bicouches lipidiques supportées peuvent être obtenues par l'application de vésicules unilamellaires sur une surface hydrophile. L'adhésion de la vésicule au support augmente la tension superficielle dans la bicouche lipidique, ce qui entraîne l'explosion de la vésicule et l'étalement de la bicouche lipidique sur le substrat hydrophile (Jing et al., 2014). Normalement, de petites vésicules unilamellaires

fortement incurvées (de diamètre inférieur à 100 nm) sont utilisées pour le dépôt sur le support plan.

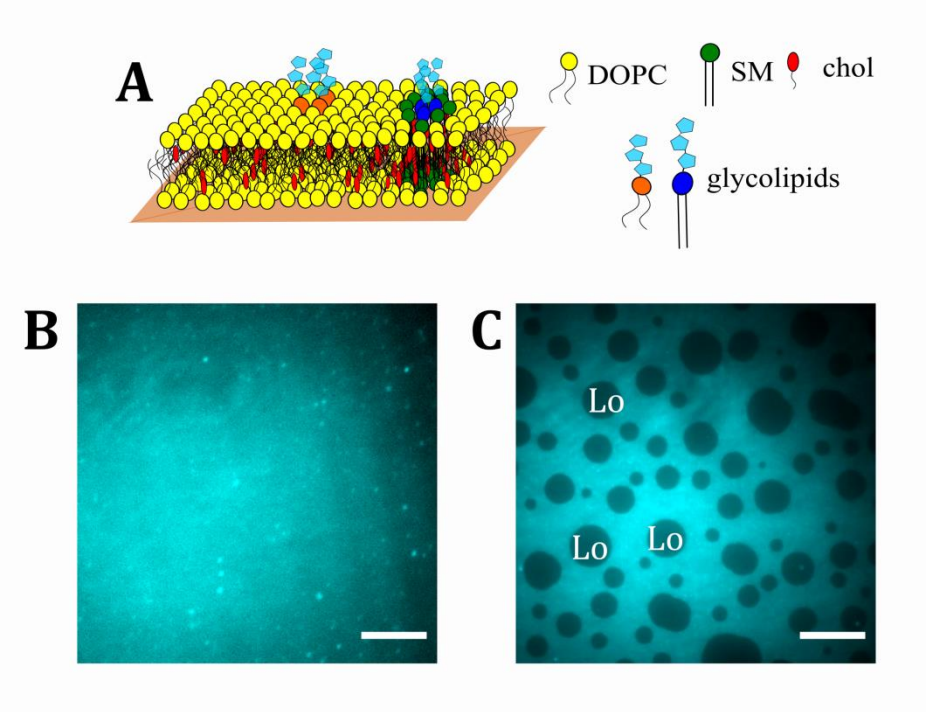

Figure 12 | **Bicouches lipidiques soutenues.** A) Schéma d'un SLB à séparation de phase. B) Image à grand champ (HILO) d'un SLB homogène composé de DOPC / chol (70/30) marqué avec HPC-Bodipy. C) Image à large champ (HILO) d'un SLB à séparation de phases composé de DOPC / chol / SM (2/1/2) marqué avec HPC-Bodipy. Parce que HPC-Bodipy préfère incorporer dans le domaine plus fluide de Ld (composé principalement de DOPC), le domaine Lo (composé principalement de SM et de cholestérol) apparaît sombre. Barres d'échelle - 10 µm. Régime révisé du (Sych et al., 2018a).

Les principales limitations des bicouches lipidiques supportées (SLB) proviennent des interactions de la membrane avec le support. Le choix du support est particulièrement important dans la conception générale des expériences impliquant des SLB. Afin d'étudier les SLB par microscopie à fluorescence, les chercheurs utilisent classiquement un support de verre. Le verre est un matériau amorphe et la surface du verre nécessite un traitement supplémentaire (par exemple, nettoyage à l'acide ou nettoyage au plasma) avant l'application de liposomes (Cremer and Boxer, 1999). De plus, le couplage de la feuille inférieure à la surface du verre est très fort. Il limite presque complètement la diffusion des lipides dans la foliole inférieure (Hennesthal and Steinem, 2000). Une autre solution consiste à utiliser une surface de mica comme support (Glazier and Salaita). Le mica est un minéral de silice naturelle avec une charge de surface et un clivage basal presque parfait. La surface hydrophile en mica permet une adhésion efficace des vésicules lipidiques. Les substrats de mica sont classiquement utilisés comme support bicouche lipidique pour la microscopie à force atomique. Les multicouches épaisses de mica ne sont pas transparentes, ce qui empêche leur application en microscopie à fluorescence pour de telles études SLB. Néanmoins, le

clivage du mica en couches minces permet l'application de certains modes de microscopie à fluorescence (Madl et al., 2017). En outre, malgré le couplage de la foliole bicouche lipidique inférieure sur le support en mica, la mobilité lipidique au niveau de cette foliole inférieure est supérieure à celle sur le support en verre. (Richter and Brisson, 2005). Les autres matériaux solides utilisés pour le support de la bicouche lipidique sont SiO2, Or, TiO2, PDMS, etc. (Tero, 2012). Le support solide empêche l'insertion de protéines transmembranaires et, en outre, aucune étude de déformation membranaire ne peut être réalisée. Afin de remédier à ces inconvénients, les supports à polymère (Kühner et al., 1994) ou bicouches lipidiques planes suspendues dans les pores (Römer and Steinem, 2004) peut être employé.

L'épaisseur de la bicouche lipidique étant d'environ 5 nm, il est possible de l'étudier avec une microscopie à excitation en couche mince, telle que TIRF ou HILO (Figure 12). Ceci fournit un bon contraste d'imagerie associé à une résolution temporelle relativement élevée (due à une acquisition rapide). Les domaines de phase ordonnés et désordonnés dans un liquide reconstitués dans des SLB sont illustrés à la figure 12. De nouveau, les domaines Ld sont enrichis dans le marqueur membranaire (HPC-Bodipy), tandis que les domaines Lo sont appauvris en marqueur membranaire et apparaissent en noir. Les domaines Lo adoptent une forme ronde. en raison de la minimisation de la tension de ligne aux limites des phases liquides.

2.2. Etudes d'ordre membranaire utilisant des sondes membranaires sensibles à l'environnement

L'ordre des membranes est déterminé par l'alignement de la chaîne acyle grasse et le degré de tassement des lipides dans la bicouche lipidique (Almeida, 2011). L'ordre des membranes est essentiel pour la caractérisation de l'organisation et de la composition des membranes locales. Les marqueurs membranaires lipophiles ou les lipides fluorescents (voir le chapitre précédent) indiquent les positions des domaines Ld et Lo dans les membranes modèles. Cependant, cette approche assez simple ne permet pas de résoudre le problème du degré de compression dans les phases Ld ou Lo. Modification de la composition de la chaîne acyle grasse de la sphingomyéline et des lipides de PC, variation du contenu en cholestérol et introduction de glycosphingolipides dans les membranes modèles peuvent modifier de manière significative l'ordre des membranes des phases Ld et Lo (Carravilla et al., 2015; DeWitt and Dunn, 2015). Afin de déchiffrer les modulations fines de l'ordre de la membrane, des techniques plus sensibles doivent être appliquées.

Le degré de tassement de la bicouche lipidique peut être détecté par son niveau d'hydratation (Sanchez et al., 2007). Les molécules d'eau peuvent se localiser dans la bicouche lipidique au niveau des groupes de tête lipidiques. La quantité d'eau dans la bicouche lipidique est modulée par le tassement lipidique - des membranes plus fluides

peuvent contenir de l'eau au niveau des groupes de tête polaires, alors que l'eau est presque complètement exclue des bicouches lipidiques rigides. L'eau est un solvant polaire et le noyau hydrophobe de la membrane est clairement un environnement non polaire. Les spectres de fluorescence de sondes insérées dans un environnement polaire présentent un décalage de leur fluorescence maximale vers de plus grandes longueurs d'onde (Lakowicz, 2006). Ce «décalage vers le rouge» est dû à la relaxation du solvant, due à l'interaction des moments dipolaires du solvant avec le moment dipolaire du fluorophore à l'état excité. En conséquence, une nouvelle population de fluorophores à énergie réduite de l'état excité se forme et émet une lumière de plus grande longueur d'onde. Pour plusieurs molécules fluorescentes, le décalage vers le rouge induit par l'augmentation de la polarité du solvant est radical (Klymchenko and Kreder, 2014). Ces sondes sensibles à l'environnement peuvent être utilisées pour détecter la rigidité de l'environnement de la membrane.

Au cours des dernières décennies, de nombreuses sondes lipohiles sensibles à l'environnement ont été développées et appliquées pour la détection locale de l'ordre et de la rigidité des membranes dans les cellules et les membranes modèles. Dans mon projet, j'ai utilisé le dérivé Nile Red - NR12S (figure 13) développé par Kucherak et al.(Kucherak et al., 2010). Cette sonde a différents spectres de fluorescence dans les domaines de phase Ld (composé de DOPC pur) et Lo (composé de SM / chol 2/1). Le spectre de fluorescence de NR12S dans les membranes Ld pures est décalé vers le rouge (figure 13). Dans les membranes modèles à séparation de phase, le NR12S s'intègre avec succès dans les domaines de phase Lo et Ld. Les GUV et les SLB marqués par NR12S peuvent être imagés davantage dans deux canaux de couleur d'émission distincts. La sélection des canaux de couleur est basée sur les spectres de fluorescence du NR12S - vert (525/50 nm) et rouge (700/75 nm). La microscopie confocale a révélé que, dans le canal de détection vert, les domaines Lo sont plus lumineux que les domaines Ld, tandis que dans le canal de détection rouge, les domaines Ld apparaissent plus lumineux. Sur la base de ces images bicolores, la polarisation générale (GP) de NR12S dans les membranes modèles peut être quantifiée pour chaque pixel de l'image confocale. Les valeurs de GP peuvent varier de -1 à 1. Elle est faible pour le NR12S incorporé dans des domaines de membrane moins ordonnés et augmente en même temps que l'ordre de la membrane. Cette approche peut être utilisée pour cartographier l'ordre des membranes des membranes plasmiques natives et des systèmes membranaires synthétiques.

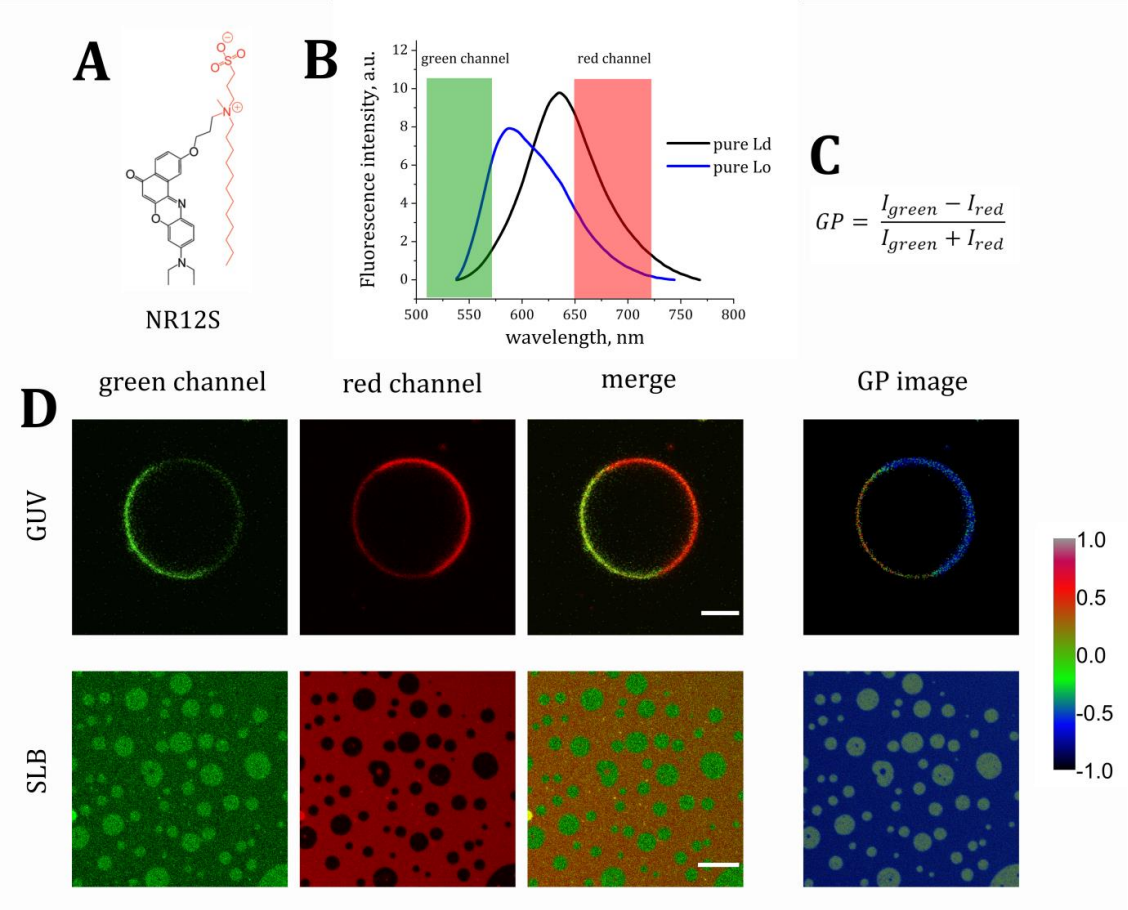

Figure 13 | **Études d'ordre membranaire utilisant NR12S** A) Structure de la sonde NR12S (Kucherak et al., 2010); B) Spectres de fluorescence de NR12S incorporés dans des bicouches lipidiques de Ld (DOPC) et de Lo (SM / chol - 2/1) purs (Kucherak et al., 2010). Les bandes verte et rouge représentent les parties verte et rouge des spectres pris pour le calcul de la polarisation générale (GP); C) Formule pour le calcul du médecin généraliste (Sanchez et al., 2007); D) Imagerie ratiométrique à deux couleurs de GUV et SLB à phases séparées utilisant la microscopie confocale. Les filtres passe-bande pour les canaux de couleur verte et rouge sont sélectionnés comme indiqué en B. L'image GP est reconstruite par application de la formule en C aux canaux de couleur pixel par pixel. Plus le GP est élevé, plus l'ordre des membranes est élevé. Selon la barre de calibration, la valeur GP en Lo est plus élevée. Barres d'échelle - 10 μm.

La séparation de phase dans les membranes modèles a été largement étudiée à l'aide de sondes membranaires sensibles à l'environnement (Almeida et al., 2003; Carravilla et al., 2015; Sanchez et al., 2007; Veatch et Keller, 2005). Souvent, des domaines coexistants ordonnés et désordonnés dans des liquides dans des membranes modèles sont produits en utilisant des compositions ternaires de DOPC, de cholestérol et de SM. L'ordre des membranes dépend des rapports molaires entre les trois lipides. Il est clair que l'augmentation de la teneur en SM et en cholestérol chez les VUG non séparés en phase augmente l'ordre des membranes. En utilisant la sonde écologiquement sensible Laurdan, Carravilla et al. (Carravilla et al., 2015) ont mesuré l'ordre membranaire de différentes compositions ternaires et obtenu le diagramme de phase ternaire pour les GUV composées de DOPC, de SM (extrait d'œufs) et de chol. En outre, ils ont mis en évidence la zone du diagramme de phase (figure 14), où la séparation de phase a lieu à

température ambiante. De plus, l'ordre membranaire des domaines Lo et Ld dans des vésicules à phases séparées à différents rapports a été quantifié. Il est intéressant de noter que l'ordre des membranes des domaines Lo et Ld purs dans les GUV à phases séparées varie selon le rapport entre les lipides. Ces diagrammes de phase ternaires sont extrêmement utiles pour la préparation ultérieure de VUV homogènes ou à séparation de phase avec un ordre de membrane distinct des domaines de phases Ld et Lo.

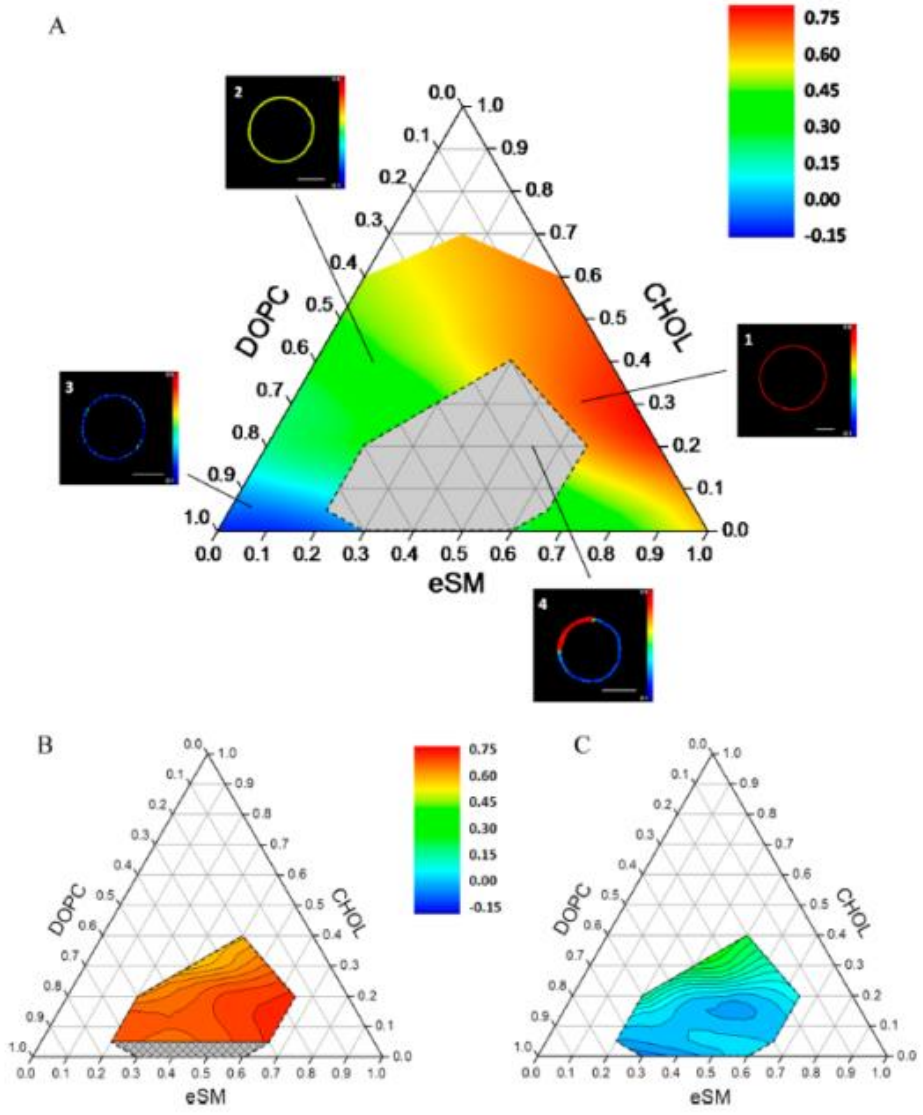

Figure 14 | Diagramme de phase ternaire obtenu par des études d'ordre membranaire avec Laurdan. A) L'ordre des membranes dépend du rapport molaire entre les trois lipides. Le code de couleur illustre la valeur GP des VUC composées de différents rapports molaires DOPC, SM et chol. La zone grise décrit les rapports auxquels se produit la séparation de phase. L'ordre des membranes des domaines Lo et Ld dans les vésicules à phases séparées varie également; B) Ordre membranaire des domaines Lo dans des vésicules à phases séparées à différents rapports molaires de lipides; C) Ordre membranaire des domaines Ld dans des vésicules à phases séparées à différents rapports molaires de lipides; Révisé de (Carravilla et al., 2015).

3. Investigation of the cellular uptake using model membranes

Endocytosis is a mode of active cellular transport of extracellular material into the cell (Doherty and McMahon, 2009). It is involved in cell-cell exchange of substances and mediates the entry of various pathogens. Different cells possess different mechanisms of endocytosis. Phagocytosis (Underhill and Goodridge, 2012) is the uptake of large extracellular particles (cell debris, microorganisms, apoptotic cells etc.) for further decomposition and recycling (Cox et al., 2000). Phagocytosis requires extensive actin rearrangement. Only some cells are equipped with this mechanism (macrophages, monocytes, etc.). Non-phagocytic cells can internalize extracellular material via clathrin-mediated endocytosis (Kaksonen and Roux, 2018) (clathrin assembly on the cytosolic side of the plasma membrane promotes the formation of the endocytic bud), caveolae-mediated endocytosis (highly curved caveolae contain multiple cellular receptors that mediate uptake) or pinocytosis ("cell drinking" – the uptake of small volumes of extracellular fluid, which normally occurs at regions of the plasma membrane where a lot of membrane ruffles are located). The induction of endocytic pathways often requires the activation of distinct plasma membrane receptors (Eierhoff et al., 2012). Glycosylated lipids and proteins, embedded in the plasma membrane are particularly important and abundant class of membrane commponents.

3.1. Lectins and glycosphingolipids as the main players in the uptake initiation

Carbohydrate groups of glycosylated membrane components present an attractive target for extracellular pathogens (viruses, bacteria) and pathogenic products (such as toxins) for specific binding and the subsequent exploitation of the native cellular endocytic pathways (Aigal et al., 2015; Schubert and Römer, 2015). The recognition of the carbohydrates is granted by carbohydrate binding proteins (lectins), that are ubiquitously present in viruses and bacteria (Ambrosi et al., 2005; Lis and Sharon, 1998). Lectins highjack the glycosphingolipids and induce activation of cellular signaling pathways. Moreover, clustering of GSLs induced by lectins can lead to the induction of local asymmetric stress in the lipid bilayer that results in endocytic tubule nucleation (Ewers et al., 2010; Römer et al., 2007). Plasma membrane tubules grow longer and sequester lectins on the negatively bent surface. Finally, an endocytic bud is detached from the plasma membrane and follows intracellular transport pathways (Duncan and Richardson, 2012).

3.1.1. Toxins/lectins act as clustering devices and generate membrane deformation

Over the past decade, clustering of glycosphingolipids was shown to be a decisive event in internalization of lectins (Aigal et al., 2015). Despite the obvious involvement of cellular cytosolic components, such as clathrin and actin, the plasma membrane deformation relies on asymmetric stress induced by the specific multivalent binding of

lectins to the plasma membrane surface (Pezeshkian et al., 2016). For example, the galactose-specific B subunit of Shiga toxin (StxB, expressed by *S. desynteriae* or *E. coli* (Sandvig, 2001)) is known to follow the clathrin-dependent endocytic pathway (Johannes and Römer, 2010). However, it was shown by Römer et al. (2007) thatalternative uptake strategies take place when the cytosolic endocytic machinery is inhibited or absent (figure 15). StxB recognizes the α-1-4-galactose of the GSL globotriaosylceramide (Gb3) and induces membrane deformation. Remarkably, the uptake of StxB was reconstituted synthetically in GUVs. These model membranes were constructed using the minimal set of lipids for lipid bilayer formation – DOPC, chol and 5 mol % of Gb3 receptor. StxB bound to Gb3, formed aggregates and induced membrane tubular invaginations, evenin such a minimalistic system. As suggested by theoretical models, the formation of lectin aggregates on the membrane surface is necessary for the membrane deformation (Johannes et al., 2014; Pezeshkian et al., 2016). In order to compensate for the bending rigidity of the lipid bilayer, such aggregates must grow until the tubule is nucleated. The origin force for the lectin aggregation is yet unclear, however, Pezeshkian et al. proposed an interesting model based on their molecular dynamic simulation studies (Pezeshkian et al., 2017).

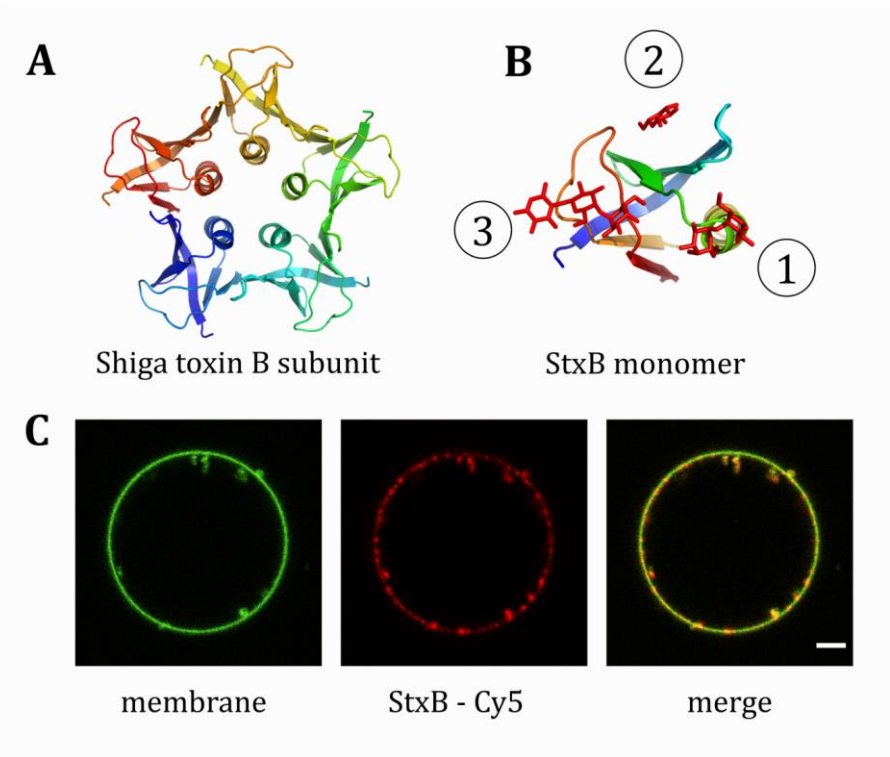

Figure 15| **Shiga toxin induces tubular invaginations in GUVs** A) The ribbon diagram of pentameric Shiga toxin B subunit (StxB); B) The ribbon diagram of StxB monomer with indicated binding sites; C) StxB induces tubular invaginations in GUVs composed of DOPC/chol/Gb3 (65/30/5) labeled with HPC-Bodipy. StxB clusters on the outer leaflet of the GUV membrane and induces tubules. Tubules are enriched in StxB. Scale bar – 10 μm.

They suggest that the aggregation of lectins is driven by the fluctuation forces of the membrane, the analogue of the Casimir effect. At once, StxB can bind up to 15 Gb3 molecules. Such a multivalent interaction grants an efficient clustering of Gb3, which is necessary for the induction of asymmetric stress and tubule nucleation. The role of the specific binding sites in the uptake initialization was explored using site-directed mutagenesis. It was shown that the depletion of the binding sites 3 or 2 (figure 15) decreases the binding affinity of StxB to Gb3, whereas the deletion of the binding site 1 does not (Soltyk et al., 2002). Remarkably, deletion of the binding site 1 prevents StxB from efficient clustering and tubule formation (Römer et al., 2007). This suggests a crucial importance of this particular binding site for Gb3 clustering by StxB. Similar studies were performed for the fucose-specific *Ralstonia solanacerum* lectin (RSL). This protein is a trimer with two binding sites per monomer (Arnaud et al., 2013). It is also known to induce membrane invaginations in GUVs spiked with fucosylated lipids. Studies employing the modification of the lectin valence via site-directed mutagenesis or (Arnaud et al., 2013) or production of neolectins with engineered binding sites based on RSL (Arnaud et al., 2014) showed very clearly the implication of the distinct binding sites in the tubule nucleation. Remarkably, the neolectins where the two closest binding sites were present, showed almost the same efficiency in tubule formation as its natural hexavalent analogue. Other divalent or even trivalent lectins displayed a significantly reduced tubule formation. All these studies show the particular importance of lectin geometry and valence for endocytic tubule formation.

3.1.2. Lectin-induced lipid sorting and membrane reorganization

Apart from membrane deformation, lectins are also known to induce lipid sorting in GSL-containing membranes (Windschiegl et al., 2009). Clearly, curvature-driven lipid sorting occurs during various cellular processes, including uptake and release (Callan-Jones et al., 2011). As indicated by Pinot et al. (2014) the polyunsaturated phospholipids are abundantly implicated in the local membrane tubule or bud formation. They can adapt their configuration (mainly via the cis-trans isomerization of the unsaturated fatty acyl chains) in order to fit the curved profile of the plasma membrane in endocytic or exocytic buds. Furthermore, based on their molecular geometry (cone, cylinder, inverted cone), lipids prefer surfaces of their native curvature (Roux et al., 2005). This effect was extensively studied in asymmetric model membranes; however, a significant curvature-driven sorting based solely on lipid geometry could not even be observed even in highly curved lipid bilayers (Callan-Jones et al., 2011). Nevertheless, this effect is possible in presence of membrane-bound proteins (e.g. lectins). Interesting studies of lipid sorting in model membranes were performed by pulling a tether from GUV membranes using optical tweezers and micropipette aspiration. With this technique, Sorre et al. (2009) demonstrated that curved and non-curved membranes differ in their lipid composition. Again, unsaturated lipids (DHPE-Texas Red) were found to associate with the highly curved membrane. Furthermore, Sorre et al. spiked the GUV with the ganglioside GM1 and applied the B

subunit of Cholera toxin (CtxB) to the membrane. It was found that such CtxB–Gm1 interaction even amplified the sorting of unsaturated DHPE molecules to the highly curved tether. The composition of the lipid bilayer played a very important role in this phenomenon. Significant sorting could occur only in GUVs with a lipid composition in close the phase demixing point (e.g. DOPC/chol/SM – 1/1/1). Lectin-induced lipid sorting in non-curved planar lipid bilayers has similar features. It was shown that applying CtxB or StxB to a lipid bilayer composed of a ternary mixture near the demixing point can induce phase separation (Safouane et al., 2010). Such an effect, of course, requires efficient binding of the lectins to their membrane receptors has toin the GUV. Subsequently, these lectins induce phase separation and localize at the newly formed Lo domains. The distinct lipid composition of the membrane tubules formed by lectins is still an open question (Safouane et al., 2010; Sorre et al., 2009). On one hand, highly curved membrane surfaces clearly attract unsaturated lipids, on the other hand lectins are bound to glycosphingolipids that associate with the saturated sphingolipids and cholesterol. All in all, the resulting composition of the endocytic tubule is determined by the interplay between the attraction of unsaturated lipids and the sequestering of lectins associated to saturated sphingolipids.

3.1.3. The role of GSL fatty acyl chain structure in lectin binding and internalization

The GSLs are usually categorized by its carbohydrate moiety. However, the ceramides of GSLs with identical sugars can contain fatty acids of various lengths and saturation degrees. For example, the Gb3 naturally occurs in various isoforms (figure 16). The ratio between the content of the isoforms depends on the cell from which the mixture was extracted (Shin et al., 2018).

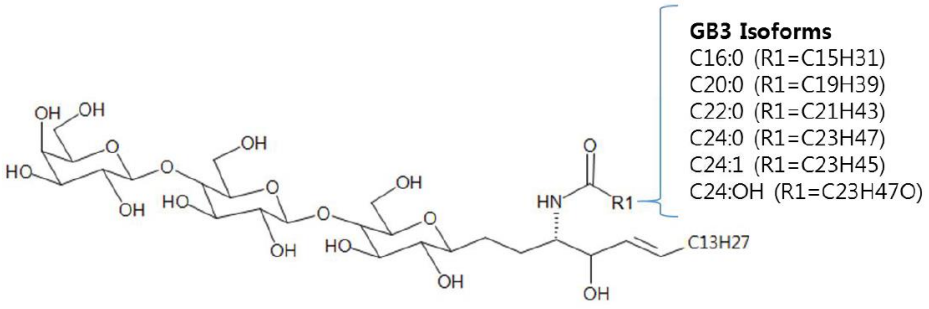

Figure 16| **Glycosphingolipid globotriaosylceramide.** Gb3 is defined by its carbohydrates (galactosylα1-4galactosylβ1-4glucosyl). However, different Gb3 species (isoforms) can vary in their fatty acids of the ceramide backbone. Revised from (Shin et al., 2018).

The structure of the lipid anchor (as well as the local lipid bilayer composition) moderates the exposure of the sugar group to the extracellular space, which in turn can prevent glycan recognition by a lectinlectins if the distinct position of the sugar group is unfavorable (Lingwood et al., 2011). Consequently, altering the fatty acyl chain can inhibit the binding, clustering and formation of tubular invaginations by lectins. Schütte

et al. (2015) studied the Gb3 C24:1 OH species in the context of StxB uptake in giant unilamellar vesicles. They spiked GUVs with Gb3 molecules with either natural (Gb3-*R*) or unnatural (Gb3-*S*) configuration of the hydroxyl group. Both species showed similar high nanomolar affinity to StxB. However, StxB induced tubular invagination twice less efficient in GUVs spiked with Gb3-*R* in comparison to Gb3-*S*. Remarkably, such minor modification of the fatty acyl chain significantly altered the behavior of Gb3 in the lipid bilayer.

In their further work, Schütte et al. studied the organization of supported lipid bilayers that contained 5 mol % of Gb3 species with either a C24:0 or a C24:1 fatty acyl chains (Schütte et al., 2014). In phase separated (Lo and Ld) supported lipid bilayers, Gb3 with the C24:1 fatty acid induced the formation of a phase domain of intermediate order, which they called liquid-intermediate phase (Li). In SLB spiked with Gb3 C24:0 such an effect was not observed. StxB applied to the supported lipid bilayer, in both cases successfully recognized Lo phase domains, whereas Ld and Li domains were not recognized by the toxin. These domains may be either depleted of sufficient amounts of Gb3 molecules, or the Gb3 molecules incorporated into these domains cannot be recognized due to an altered exposure of the sugar groups to the aqueous solution.

In the context of intracellular trafficking of the cholera toxin from *V. cholerae* (Ctx), Chinnapen et al. (2012) studied the cellular sorting of isoforms of the gangliosides GM1. They found that during the uptake and trafficking of Ctx only the GM1 molecules with unsaturated fatty acyl chains (16:1) are successfully transported to the trans-Golgi network and endoplasmic reticulum, whereas the GM1 with saturated fatty acyl chains.

GSLs are important molecules for plasma membrane interleaflet communication and signaling (Manna et al., 2017). The binding of lectins to GSLs at the plasma membrane can induce a signaling cascade required for triggering a certain cellular process (e.g. lectin internalization). Interestingly, lectins specific to the same glycans can induce different signaling events. For example, the α-galactose specific lectin StxB from *S. dysenteriae* and LecA from *P. aeruginosa* target the same GSL globotriaoylceramide (Gb3), but they induce different signaling events (Zheng et al., 2017). These differences may originate from a selective recognition of the Gb3 trisaccharide exposed in functional membrane domains of distinct composition (Lingwood et al., 2011). The collective behavior of membrane lipids alters the exposure of the carbohydrate headgroup to the extracellular space. In turn, StxB and LecA can have preferences for Gb3 receptor molecules with differently oriented the head groups of the Gb3 receptor molecules.

All these fascinating findings emphasize crucial importance of the fatty acyl chain of glycosphingolipids for lectin binding, induction of membrane reorganization and deformation and, subsequently, intracellular trafficking of lectins.

3.2. Lectin-GSL interactions in viral and bacterial uptake

Lectin–glycan interactions are abundantly exploited byhuman pathogens like viruses and bacteria (Eierhoff et al., 2012). Bacteria produce lectins in order to target host cell glycans for different purposes. Shiga (Johannes and Römer, 2010) and cholera toxins (Haan and Hirst, 2004), introduced above, are secreted by their bacteria and exert their cellular toxicity after their uptake. Lectins can also assist bacteria in targeting cell surface glycans for the means of adhesion to the host cell (Cossart, 2004). Many non-invasive bacteria adhere to cell and form biofilms, which is oftenlectin-mediated (Johansson et al., 2008; Kadam et al., 2011). Furthermore, bacteria can stimulate a targeted cell to polymerize actin intracellularly and engulf the extracellular bacterium(Pizarro-Cerdá and Cossart, 2006). Unlike bacteria, viruses require the cellular machinery for proliferation (Eierhoff et al., 2012). Some viruses express lectins on their surfaces in order to recognize host cell surface glycans (Carter et al., 2009; Ewers et al., 2010; Rydell et al., 2013). The interaction facilitates the viral uptake and further trafficking to the correct cellular compartment, where the viral genetic material can be integrated into the cellular DNA.

3.2.1. Glycan-mediated uptake of viruses

Numerous viruses are functionalized withlectins in order to recognize cell surface glycans (Eierhoff et al., 2012). Enveloped viruses like HIV or herpes virus make use of their lectins in order to fuse with the plasma membrane of the host cell and deliver the content of the viral particle into the cytosol. Alternatively, enveloped viruses like Influenza A (Ho et al., 2016) bind to the plasma membrane and are internalized via cellular endocytic pathways. The viral capsid of some non-enveloped viruses is composed of lectins assembled in lattices. A very well- studied example is the SV40 polynoma virus. The viral capsid of SV40 mainly consists of 72 Vp1 proteins, arranged in icosahedral particle. Vp1 is a pentavalent lectin specific to the ganglioside GM1. Ewers et al. (2010) rebuilt the uptake of SV40 in GUVs spiked with GM1. They showed that the viral capsid–GM1 interaction alone is sufficient for membrane tubule induction. Moreover, the application of soluble Vp1 protein molecules to the same GUV membranes also induced tubular invaginations, albeit less quickly than the viral particles. SV40 required only a few seconds for membrane tubule formation whereas soluble lectins (CtxB, StxB and also Vp1) required few minutes to induce a tubule. Recently, the Vp1 - GM1 interaction was characterized more precisely using molecular dynamic simulations (Kociurzynski et al., 2019). Multivalent binding of Vp1 to GM1 induces local curvature of the surrounding membrane, which further leads to tubule nucleation. Although, Vp1 proteins induce membrane tubules either being soluble or arranged as a lattice, these two processes are different. The Vp1 proteins assemble in aggregates on the membrane surface (similarly to StxB) and induce asymmetric stress in the membrane, whereas the viral capsid “imprints” its own curvature into the plasma

membrane via adhesion. The latter allows bending of the membrane with high tension that cannot be bent by multivalent lectins aggregation.

3.2.2. Glycan-mediated uptake of bacteria

Bacteria do not require the host cell machinery for replication. However, some bacteria (e.g. *Listeria, Shigella, etc…*) internalize into the intracellular environment, where they can stay protected from the immune system. Such pathogens can be taken up by phagocytic cells (macrophages, monocytes, dendritic cells etc.) together with extracellular fluid (pinocytosis). Furthermore, bacteria modify the intracellular environment in order to survive and proliferate (Eierhoff et al., 2012). The invasion of non-phagocytic cells by bacteria requires the pathogen to develop an additional machinery (Cossart, 2004). The two main mechanisms utilized by numerous bacteria for cell entry, are called "trigger" and "zipper" mechanisms. The trigger mechanism relies on type 3 secretion system (T3SS). T3SS forms a transient pore in the host cell membrane and is used by bacteria to inject their virulence factors directly into the host cell cytosol. The local plasma membrane environment is critical for the stability of thisa pore. It has been shown, that some bacteria that enter the host cell via "triggering" target specific membrane nanodomains, enriched in cholesterol and sphingolipids, for pore insertion. Virulence factors injected via T3SS, trigger an extensive actin polymerization within the host cell leading to bacterial engulfment. Typical representatives of bacteria that utilize the trigger mechanism are *Salmonella enterica*, *Shigella flexneri*, and *Pseudomonas aeruginosa* (Eierhoff et al., 2012; Pizarro-Cerdá and Cossart, 2006). As an alternative mechanism for bacterial internalization, the "zipper" mechanism requires a specific multivalent interaction of bacterial particles with cellular receptors. This interaction further activates cellular signaling cascades that induce the actin rearrangement for bacterial uptake. The modification of actin is, however, less severe in comparison to the "trigger" mechanism. Moreover, the interaction with multiple cellular receptors during the bacterial adhesion to the host cell seems to be the decisive event for the "zipper mechanism", as the wrapping of the bacteria with the host plasma membrane can also occur without actin polymerization. Typical representatives of bacteria that take advantage of the zipper mechanism are *Listeria monocytogenes* (targets the membrane glycoprotein E-cadherin), *Yersinia pseudotuberculosis* (targets the membrane protein β1 integrin), and *Pseudomonas aeruginosa* (targets the membrane glycolipid Gb3, integrins and asialo-gangliosides). Remarkably, their efficient adhesion to the target plasma membrane surface again relies on the local plasma membrane organization (Duncan et al., 2004; Zaas et al., 2005). Membrane domains enriched in sphingomyelin and cholesterol do not only enclose various plasma membrane receptors required for adhesion, but also serve as important platforms for the signal transduction required for actin polymerization (Eierhoff et al., 2014; Lafont and Van Der Goot, 2005).

3.3. The lectin LecA in the invasion of *P. aeruginosa*

Pseudomonas aeruginosa is an opportunistic, gram-negative, pathogenic bacterium (Emam et al., 2010). It is responsible for a high number of hospital-acquired infections and poses a high threat particularly for patients with cystic fibrosis or with a compromised immune system. The difficulties in treating *P. aeruginosa* arise from its versatile defense machinery. Among others, forming biofilms is a very efficient mechanism to protect individual bacteria from antibiotics and the host immune system (Johansson et al., 2008). Bacterial biofilms form by adhesion of bacteria to the surface of the host cell and their neighboring bacteria. Furthermore, bacteria secret hydrolytic enzymes and toxins to promote infection. Various compounds of the bacterial outer membrane are involved in efficient adhesion. Particularly important are bacterial lectins that are utilized to specifically target the host's cellular glycans. Adhesins (Eierhoff et al., 2012), specific to asialo-GM1 and -GM2 are of major importance for the bacterial adhesion. The bacterium *P. aeruginosa* expresses the two lectins, LecA and LecB (Chemani et al., 2009), that are particularly specific to α-galactose and l-fucose, respectively. Surprisingly, studies of bacterial infection of host cells that were depleted of glycosphingolipids (by blocking the biosynthesis of glucosylceramide) revealed that the glycosphingolipids are rather important for the bacterial internalization than for adhesion (Eierhoff et al., 2012; Emam et al., 2010). *P. aeruginosa* can invade a host cell following the "trigger" mechanism. Using the T3SS, the bacterium injects the effector proteins ExoT and ExoS, which promote actin rearrangement in the host cell, leading to the bacterial engulfment. Interestingly, Eierhoff et al. (2014) showed that *P. aeruginosa* is capable of invadinginvading host cells via the "zipper" mechanism as well. Here, however, the zipper is formed by multivalent lectin interactions with the host plasma membrane glycosphingolipid Gb3. Hence, this mechanism was coined "lipid zipper". Gb3 molecules are targeted by the *P. aeruginosa* lectin LecA that is enriched at the surface of the bacterium (figure 17 A). LecA (figure 17 B) is a homotetramer with four binding sites specific to α-galactosylated membrane components (e.g. Gb3 - figure 17 C). The two pairs of binding sites are oriented in opposite directions. Such an orientation of binding sites allows the protein to cross-link proximal lipid bilayers of GUVs functionalized with glycans (Villringer et al., 2018). Presumably, in a similar way, LecA mediates the adhesion of the bacterial outer membrane to the host cell surface (Novoa et al., 2014). This multivalent adhesion is a key event in the initialization of the lipid zipper. Remarkably, the adhesion to model GUVs leads to membrane deformation and bacterial engulfment even in the complete absence of actin (figure 17D). Furthermore, during the uptake of *P. aeruginosa* into H1299 lung epithelial cells, a pronounced co-localization of actin filaments with the internalized bacteria was not observed (figure 17E). The deletion of LecA decreases the internalization of the bacteria in host cells or GUVs drastically (more than 60 % (Eierhoff et al., 2014)). Moreover, blocking of LecA with a di-antennary galactose reduced the internalization of *P. aeruginosa* by more than 80% (Novoa et al., 2014). These findings prove that the lectin-GSL interaction is a decisive event in the bacterial invasion. However, the role of specific plasma membrane nanodomains (e.g. lipid rafts) in bacterial adhesion and internalization has to be further

explored. Recently, Song et al. (2019) demonstrated that the *P. aeruginosa* quorum sensing metabolites can induce a dissolution of ordered membrane domains. This effect was also reconstituted in model membranes – GUVs and SLBs. The role of the lectin-GSL ligation in fine-tuning membrane organization remains unclear. In particular, the implication of the multivalent LecA-Gb3 interaction requires further understanding.

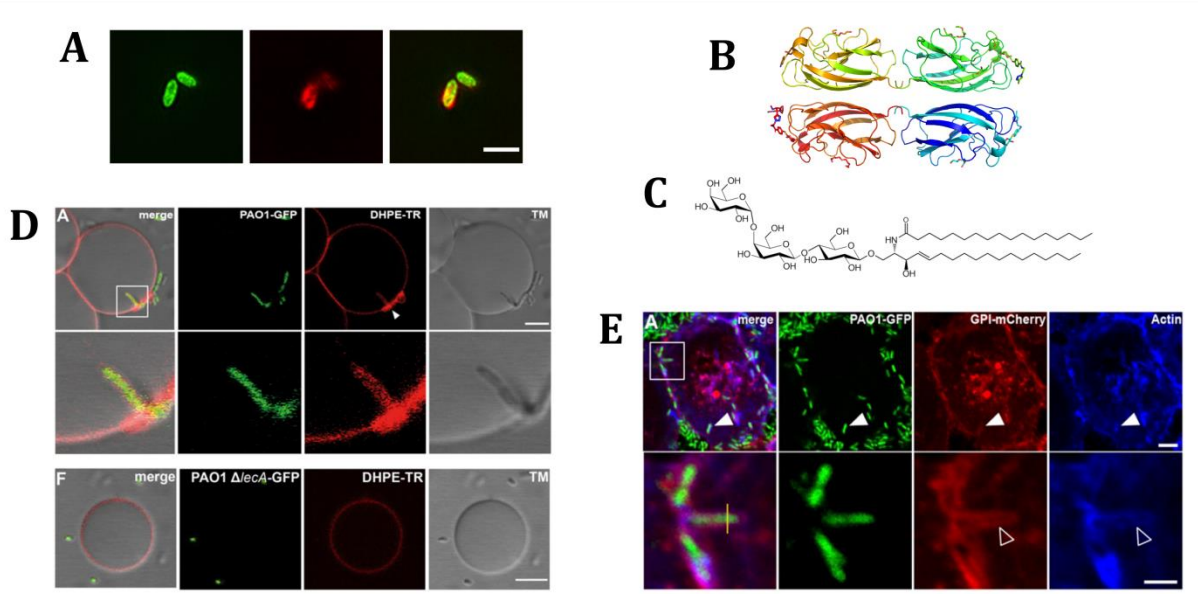

Figure 17| **The uptake of *P. aeruginosa* via a lipid zipper.** A) GFP-expressing *P. aeruginosa* (green) after surface staining of its lectin LecA with an anti-LecA antibody (Alexa 647, red); Scale bar – 2 µm. B) Ribbon diagram of LecA; C) Glycosphingolipid Gb3 – the cellular receptor targeted by LecA; D) The LecA-Gb3 interaction is sufficient for the lipid zipper formation and initiation of bacterial (GFP, green) internalization into GUVs composed of DOPC/chol/Gb3 (65/30/5) labeled with TexasRed (red). LecA deletion (D – bottom panel) inhibits the binding and internalization of the bacteria into GUVs (Eierhoff et al., 2014); Scale bars – 5 µm. E) Bacteria induce membrane invaginations in H1299 lung epithelia cells by a lipid zipper (Eierhoff et al., 2014). Actin co-localization with the newly formed invaginations induced by bacteria is negligible. This implies that the key process of bacterial uptake is the LecA-Gb3 interaction, whereas the involvement of actin is insignificant. Scale bars are 10 µm and 2.5 µm, respectively.

II Aims

LecA and StxB are both specific to the plasma membrane GSL globotriaosylceramide (Gb3). However, they are known to induce different signaling events (Zheng et al., 2017) and follow different pathways of intracellular trafficking (Müller et al., 2017). From the evidences, provided by the studies, reviewed in the introduction, we can hypothesize that these differences arise from a combination of two factors: First, LecA and StxB exhibit distinct binding preferences for Gb3 receptor molecules embedded in differently composed and organized membrane nanodomains. Second, the impact on spatial plasma membrane organization of LecA and StxB varies. Both these factors may determine the signaling and intracellular trafficking of LecA and StxB. Nevertheless, the questions of binding selectivity of LecA and StxB and the membrane reorganization induced by LecA and StxB were not properly addressed yet.

In this work, we propose to test our hypotheses by synthetically reconstituting the lectin-Gb3 interactions in model membranes. Collective effects of membrane lipids control the recognition of receptors by lectins (Lingwood et al., 2011). As a result, LecA and StxB may indeed target different membrane domains. The optimal strategy for investigating the binding preferences of lectins to membranes of different compositions is to employ synthetic membrane systems (e.g. GUVs). GUVs provide the ability to control the membrane composition and elucidate the role of specific components. Such cell-sized model membranes are frequently used in combination with fluorescence microscopy techniques for monitoring protein binding. However, usually fluorescence microscopy provides only qualitative information ("binding"/"no binding"). Methods for quantitative binding evaluation require further development. Hence, we aimed ***to develop a method for quantitative evaluation of lectin binding to GUVs based on fluorescence microscopy.*** Furthermore, in order to analyze sets of fluorescence microscopy images in a fast and unbiased manner, we aimed ***to develop software for fast automated image analysis.***

Furthermore, we used GUVs with ternary mixtures of DOPC, cholesterol and SM. By varying the ratios between these three lipids we were able to control the membrane order of the lipid bilayer. Moreover, GUVs exhibiting phase separation into Lo and Ld phase domains were produced. Furthermore, to elucidate the role of the Gb3 ceramide structure in lectin-Gb3 binding, we functionalized GUVs with Gb3 species having distinct fatty acyl chains (provided by our collaborators, the group of Prof. Daniel Werz, TU Braunschweig). In combination with the previously developed approach for quantitative evaluation of lectin binding, we aimed ***to analyze the binding preferences of StxB and LecA to the Gb3 receptor species incorporated in GUVs of different lipid compositions.***

In the last part of the thesis, we aimed to study the membrane reorganization induced by LecA and StxB. Rearrangement of plasma membrane nanodomains is necessary for various pathogens to promote infection. In particular, several bacteria utilize lectins to deform membranes and/or initiate downstream signaling events. In this context, we mimicked plasma membrane organization on the microscopic scale using phase-separated SLBs. We, then, applied lectins to such model membranes and visualized membrane rearrangements over time using fluorescence microscopy, with the aim ***to follow and characterize the impact of StxB and LecA on the membrane organization of phase-separated SLBs.***

Remarkably, we demonstrated that StxB and LecA have an opposite impact on SLB organization. StxB induced the formation of new Lo domains, whereas LecA dissolved Lo domains and induced complete membrane mixing. We hypothesized that membrane reorganization can originate from the geometry and valence of lectins. In order to understand the role of the specific binding sites of LecA, we used the commercially available lectin RPL α-Gal. This protein exists as a homodimer in aqueous solution and resembles a dimeric version of LecA with two Gb3-binding sites in total. Applying this lectin to the SLB, we aimed ***to elucidate the impact of LecA valence and geometry on the membrane reorganization.***

The LecA-Gb3 interaction is decisive for the *P. aeruginosa* adhesion to the host cell membrane. It was reported that *P. aeruginosa* induces rearrangements of the plasma membrane in order to facilitate the infection (Kierbel et al., 2007; Song et al., 2019). Here we aimed ***to investigate the role of LecA-Gb3 interaction in the membrane organization rearrangement induced by P. aeruginosa.*** We applied live *P. aeruginosa* to SLBs and followed the subsequent membrane reorganization. Remarkably, we found that LecA, coupled to the bacterial surface, in addition to allowing an efficient bacterial adhesion, also plays a key role in the Lo domain dissolution. In order to confirm the key role of LecA for the lipid bilayer rearrangement process, we also used a LecA-deficient mutant of *P. aeruginosa* (ΔLecA). In the absence of LecA, Lo domain dissolution did not occur.

III Results and discussion

1. Quantitative evaluation of lectin-Gb3 binding efficiency using confocal microscopy

(Sych et al., 2018b), for complete article see Chapter VII

Model membranes are widely used to evaluate the binding of proteins to membranes of different compositions. In particular, GUVs are often employed to address the question of lectin binding to the glycan moieties of glycolipids or glycoproteins incorporated into the GUV membrane. The binding of numerous lectins has been investigated with GUVs spiked with glycosylated components (Arnaud et al., 2013; Chinnapen et al., 2012; Römer et al., 2007; Villringer et al., 2018). GUVs are considered an ideal system for studying the binding of StxB and LecA to lipid bilayers of different compositions. Nevertheless, till now, binding studies with GUVs have been limited to qualitative information (binding/no binding). In order to provide quantitative results, we developed an approach for quantitative analysis of the lectin-Gb3 binding on GUVs imaged with confocal microscopy (Sych et al., 2018b). This approach enables comparative studies of lectin binding efficiencies to the GUVs of different lipid bilayer composition and organization. Furthermore, we developed a FIJI-based macro for fast and unbiased automated processing of GUV images (Sych et al., 2018b)

We tested the macro and validated the quantification approach using StxB binding to homogeneous or phase-separated GUVs of different lipid compositions. As expected, StxB binding to GUVs was allowed by introducing Gb3 receptor molecules (extracted from porcine brain, also referred to as "wild type" mixture, from now on – Gb3-mix) to the bilayer. In phase-separated GUVs (figure 18A), the Gb3-mix can be recognized by StxB exclusively in liquid-ordered (Lo) domains. The localization of StxB on GUVs can also be represented by circular profiles of fluorescence intensity (figure 18 B). The profiles confirm that Lo domains, in which the intensity of Bodipy is low, host StxB (red), whereas the binding of StxB to Ld domains enriched in Bodipy is negligible. Furthermore, from this image we extracted the mean fluorescence intensity of the protein bound to the GUV ($Bound\ protein$). Additionally, we extracted the mean fluorescence intensity of the protein that is freely dissolved in the solution outside of the GUV ($Free\ protein$). Based on these two values we evaluated the binding of the proteins to the GUV by the following expression:

$$\varepsilon = \frac{Bound\ protein - Free\ protein}{Free\ protein};$$

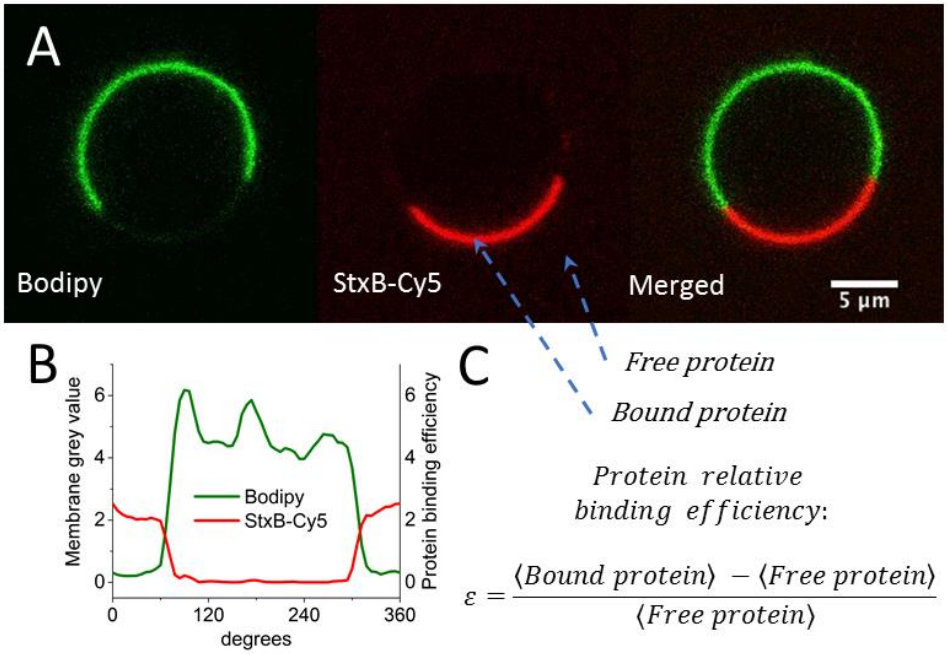

Figure 18 | StxB binding to **GUVs.** (A) StxB-Cy5 (red channel) binds to the Lo domains of a GUV composed of DOPC/chol/SM and the glycosphingolipid Gb3 (40/15/40/5). The Lo domains are not visible since the membrane probe Bodipy (green channel) preferentially localizes to Ld domains; (B) Circular profiles of the membrane marker Bodipy (green curve) and StxB-Cy5 (red curve). The units of the StxB-Cy5 circular profile (right Y axis) are quantified as shown in (C). (C) Calculation of the relative binding efficiency.

We named this value *relative binding efficiency.* It is "0" when no binding occurred. The positive values of the binding efficiency denote the extent of protein binding to the GUV. For example, in figure 18B, the circular profile of StxB shifts from 0 in the Ld domain (no binding) to 2.5 in the Lo domain. In fact, this value of 2.5 represents the fluorescence signal contrast of the bound protein over the free protein and, with proper calibration, can be converted into the actual number of protein molecules bound to the GUV (Weinberger et al., 2017). This approach can be used to compare the binding efficiency of the same protein to GUVs of different compositions.

We validated this approach using homogeneous GUVs spiked with different amounts of Gb3 receptors. We prepared GUVs containing 0, 2.5, 5 and 10 mol % of Gb3, and recorded their images with confocal microscopy (figure 19 A-D). As expected, the binding efficiency increased together with the amount of Gb3 in the membrane (figure 19E). The membrane without Gb3 was not recognized by StxB and the binding efficiency to such GUV was calculated as zero.

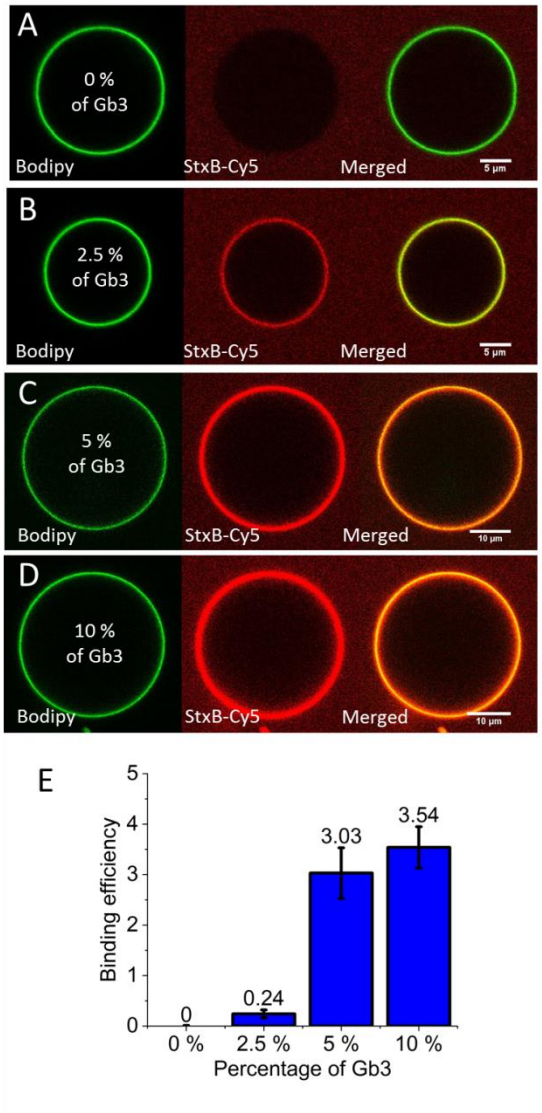

Figure 19 | StxB binding to GUVs containing different molar percentages of Gb3-mix. A-D) LSCM images of GUVs (in green) containing 0% (A), 2.5% (B), 5% (C) and 10% (D) of Gb3, which have been incubated with 100 nM of StxB-Cy5 (red). StxB-Cy5 intensities were all scaled equally so that the free protein signals are visible in all images. E) Binding efficiency ε values for StxB. Error bars represent standard deviation. Number of replicas for 0%, 2.5%, 5% and 10% Gb3-containing GUVs was 16, 12, 17 and 10, respectively.

Still, the method has a few limitations. Since it is based on the ratio between the bound protein and free protein in solution, the concentration of the protein in the solution must be kept the same for all experimental conditions used for comparison. The selection of an appropriate concentration is a very crucial task. If the concentration is selected too low, only a small amount of protein will be free, which will complicate the evaluation of the "free protein" value. On the other hand, a too high concentration of protein can create a problem with the binding detection, as the free protein in this case will produce a too high fluorescence signal. Furthermore, a quantitative comparison of different proteins is not possible. The method is not yet calibrated to be able to estimate the binding constants of the proteins for the membrane. Nevertheless, this method allows the comparison of lectin binding to GUVs of different lipid compositions. Moreover, protein binding to plasma membrane-derived liposomes (giant plasma membrane vesicles) or to spherical cells can also be examined. Moreover, one of the most important features of the macro is its capability to detect and separately process Lo and Ld domains in phase-separated vesicles.

2. Selective recognition of Gb3 species by StxB and LecA in model membranes of different membrane order

(Schubert T, Sych T et al., manuscript in preparation), for complete article see Chapter VII

LecA and StxB are both specific to the α-galactose residue of Gb3. However, we found that they segregate when applied simultaneously to the plasma membranes of live cells. They form spatially separated microdomains at the plasma membrane and inside the tubular invaginations of HeLa cells. Furthermore, in polarized epithelial cells (MDCK-II), LecA binds more efficiently to the basolateral (BL) membrane than to the apical (AP) whereas StxB prefers to bind the AP membrane. Remarkably, the primary cilium is targeted by StxB exclusively. Such selectivity may originate from the binding preferences of lectins to Gb3 incorporated in membrane domains of different composition and order. It is known that AP and BL membranes differ in lipid content and membrane order (Gerl et al., 2012; Ikenouchi et al., 2012). The AP membrane is more ordered and contains more sphingolipids, whereas the BL membrane is less ordered and enriched in phospholipids. Moreover, the structure of the Gb3 ceramide (namely its fatty acyl chain length and saturation degree) can alter the recognition of the carbohydrate moiety by lectins. In addition, the Gb3 species with different ceramides may sort selectively to AP or BL membranes which also can render the binding preferences of the lectins.

In this work, we reconstituted the binding of LecA and StxB to Gb3 in model membranes (GUVs) of different compositions. We used homogeneous and phase-separated GUVs spiked with Gb3 receptor molecules. Furthermore, we examined the influence of the Gb3 molecular structure on the binding preferences of StxB and LecA. The Gb3 species were synthesized and provided to us by our collaborators – the group of Prof. Daniel Werz, TU Braunschweig. We tested Gb3 species with lignoceric (Gb3-24:0) and nervonic (Gb3-24:1) fatty acyl chains. We also compared Gb3 species with distinct fatty acids to the Gb3-mix. Additionally, we used a synthetic function-spacer-lipid construct Gb3-FSL-DOPE (Gb3-FSL). This construct consists of the sugar moiety of Gb3 linked to the glycerophospholipid DOPE via a poly-ethylene glycol spacer (Blake et al., 2011). This construct is purely artificial; however, it gives an interesting insight into how the modification of the lipid backbone can alter the behavior of glycolipids in the lipid bilayer.

Initially, we used GUVs composed of a DOPC/chol/Gb3 mixture (65/30/5). We quantified the relative binding efficiency of either StxB or LecA to such GUVs. We compared the binding of LecA or StxB to different Gb3 species incorporated into DOPC/chol membranes. Though the concentration of Gb3 receptor molecules was always kept constant, the binding efficiencies of LecA and StxB were varying. Interestingly, the most efficient binding was observed with Gb3-FSL. This may be caused by the altered exposure of the Gb3-FSL carbohydrate due to the presence of the

linker. Otherwise, for both LecA and StxB, the binding efficiencies to Gb3-mix, Gb3-24:0 and Gb3-24:1 in DOPC/chol GUVs were similar (figure 20).

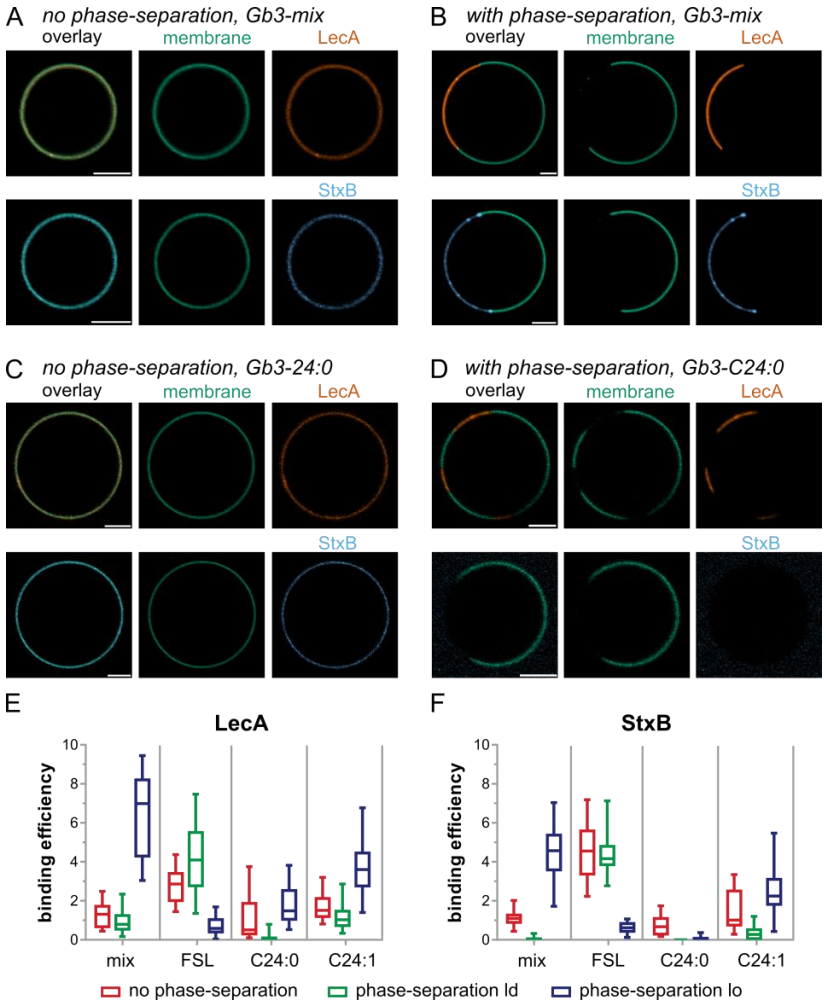

Figure 20 | The influence of Gb3 species and phase separation on LecA and StxB binding efficiencies. GUVs doped with 0.5 mol% of the membrane marker β-BODIPY-FL-C5-HPC (green) and 5 mol% Gb3-mix (A and B) or 5 mol% Gb3-C24:0 (C and D) were incubated with LecA-Cy5 (200 nM, orange) or StxB-Cy5 (200 nM, blue). Non-phase-separated GUVs (A and C) contained DOPC/cholesterol/Gb3 in the ratio 64.5/30/5 mol%, whereas phase-separated GUVs (B and D) consisted of DOPC/cholesterol/sphingomyelin/Gb3 in the ratio 42.5/14.5/42.5/5 mol%. The images A – D show equatorial sections through representative GUVs. Scale bars correspond to 5 µm. (E – F) Quantitative analysis of the binding efficiencies of LecA (E) and StxB (F) to non-phase-separated GUVs (red) or the Ld (green) or Lo (blue) phase of phase-separated GUVs containing 5 mol% of either Gb3-mix (mix), Gb3-C24:0 (C24:0), Gb3-C24:1 (C24:1), or Gb3-FSL (FSL). For each condition, the middle horizontal line represents the median, the boxes the 25th to 75th percentiles, and the whiskers the min and max values.

In homogeneous membranes a very important factor is neglected, namely the sorting of Gb3 receptor molecules. In the plasma membrane, GSLs are considered to associate with membrane nanodomains rich in sphingolipids and cholesterol (i.e. Lo-like domains). Although, we reconstituted Lo and Ld domains in separate GUVs, it is important to study the binding of lectins in phase-separated GUVs, where both Lo and Ld are present. We prepared phase-separated GUVs of a DOPC/SM/chol/Gb3

(37.5/37.5/20/5) composition. In such phase-separated liposomes, Ld domains are mostly composed of DOPC and Lo domains consist of a SM/chol mixture. First, we studied the lectins binding to the Gb3-mix (figure 20). Due to their association to SM and chol, the majority of the Gb3-mix molecules are known to incorporate into Lo domains. Hence, only Lo domains can be recognized by Gb3-binding lectins. Indeed, StxB–Gb3-mix binding, reconstituted in phase-separated GUVs, was exclusive to Lo domains, whereas the binding efficiency of StxB to the Ld membrane was zero. However, remarkably, LecA recognized some Gb3-mix receptor molecules in Ld domains with a binding efficiency between 1 and 2. This indicates that some Gb3 species can incorporate into Ld domains, but they cannot be recognized by StxB.

In contrast to the Gb3-mix, the artificial Gb3-FSL based on DOPE clearly demonstrated a preferential partition to Ld. Both LecA and StxB bound very efficiently to Ld domains spiked with Gb3-FSL. Nevertheless, some Gb3-FSL was present in Lo domains and recognized by both LecA and StxB.

Further, we compared the recognition of Gb3-24:0 and Gb3-24:1 species by LecA and StxB. The preferential partition of the Gb3 isoforms in phase-separated liposomes is unknown to date. Unfortunately, it is not possible to directly visualize the partition of such Gb3 species. Attempts were made to directly label the Gb3 molecules with a fluorophore (Patalag et al.), but the introduction of the fluorescent moiety clearly altered the incorporation preferences of Gb3.

Gb3-24:1 was recognized by both LecA and StxB in Ld and Lo domains. Hypothetically, Gb3-24:1 should preferentially incorporate into Ld domains due to its monounsaturated fatty acyl chain. However, binding of both lectins to the Lo domains was more efficient. This means that either the hypothesis of Gb3-24:1 preference to Ld is wrong or that Gb3-24:1 can be better recognized by lectins when incorporated iton Lo.

The Gb3-24:0 in phase-separated vesicles showed an even more interesting behavior. The binding of either LecA or StxB to Ld domains was negligible. Moreover, StxB could not recognize Gb3-24:0 in Lo domains, whereas LecA bound to Gb3-24:0 in Lo quite efficiently. Clearly, Lo domains contained Gb3-24:0 molecules. Whether Gb3-24:0 can incorporate into Ld or incorporates exclusively into Lo is yet unclear. Even more puzzling is the inability of StxB to recognize Gb3-24:0 in the Lo domains of phase-separated GUVs. Previously, we showed that StxB binds to Gb3-24:0 incorporated in GUVs composed of DOPC/chol. Interestingly, according to Schütte et al. (Schütte et al., 2015) and our observations presented in the supplementary information, StxB can bind to Gb3-24:0 in Lo phase domains of SLBs. The recognition of the Gb3-24:0 in the phase separated SLBs can be explained by the impact of the solid support is drastic enough to enable StxB binding, whereas in absence of the substrate, in phase-separated GUVs, Lo domains cannot be recognized. This observation again stresses the importance of the interleaflet coupling in the lipid bilayer.

We aimed to resolve the binding preferences of StxB and LecA to the AP and BL membranes of the epithelial cells. As the AP membrane is more ordered and enriched in SM and chol, we mimicked it with the GUVs composed of SM/chol (2/1). The less ordered BL membrane enriched in phospholipids we mimicked with pure DOPC. In fact, here we mimic AP and BL membranes with Lo and Ld – phase domains respectively.

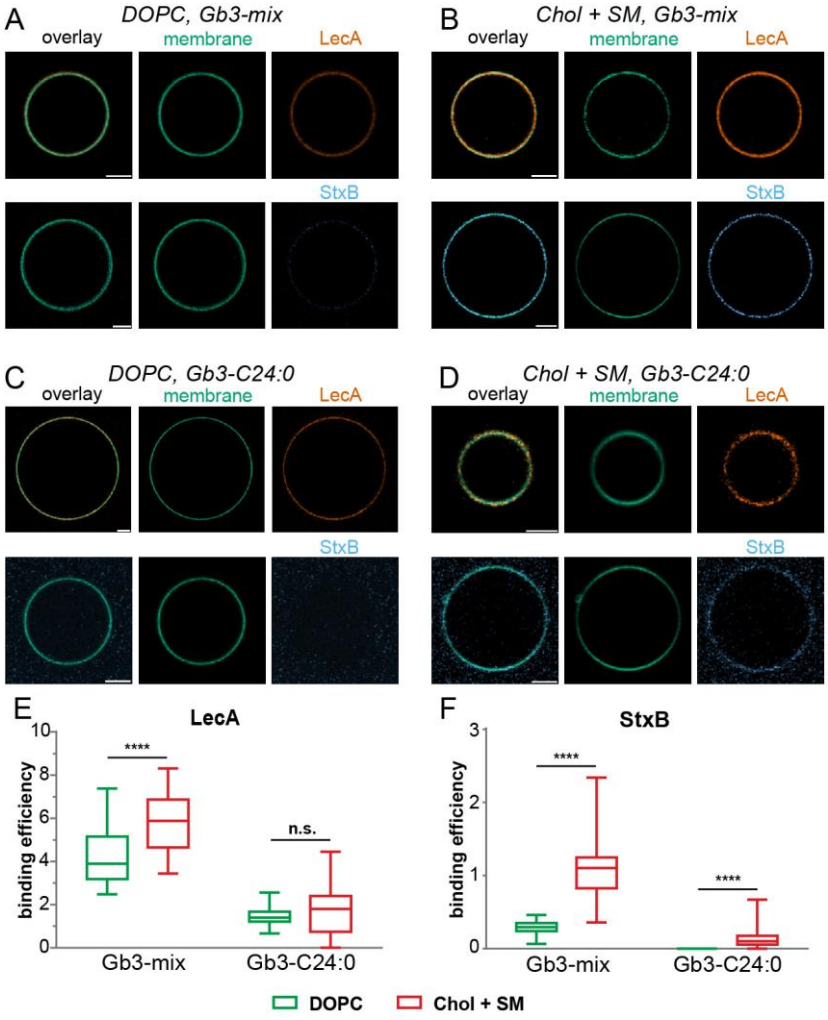

Figure 21 | The interplay between Gb3 species and cholesterol content influences LecA and StxB binding efficiencies. GUVs doped with 0.5 mol% of the membrane marker β-BODIPY-FL-C_5-HPC (green) and 5 mol% Gb3-mix (A and B) or 5 mol% Gb3-C24:0 (C and D) were incubated with LecA-Al647 (200 nM, orange) or StxB-Cy5 (200 nM, blue). GUVs approximating liquid-disordered membranes (DOPC, A and C) contained DOPC/Gb3 in the ratio 94.5/5 mol%, and GUVs resembling liquid-ordered membranes (Chol + SM, B and D) consisted of sphingomyelin/cholesterol/Gb3 in the ratio 64.5/30/5 mol%. The images A – D show equatorial sections through representative GUVs. Scale bars correspond to 5 µm. (E – F) Quantitative analysis of the binding efficiencies of LecA (E) and StxB (F) to DOPC GUVs (green) and Chol + SM GUVs (red) containing 5 mol% of either Gb3-mix, or Gb3-C24:0.

First, we explored the binding of LecA and StxB to of Gb3-mix (5 mol %) added to such GUVs. Remarkably, StxB clearly preferred binding to Gb3-mix incorporated in membranes rich in SM and chol, whereas the binding efficiency of StxB to DOPC/Gb3-mix vesicles is very low (figure 21). LecA is less selective and binds equally efficient to GUVs composed of DOPC/Gb3-mix and to GUVs composed of SM/chol/Gb3-mix. This effect is even more drastically pronounced when Gb3-mix is replaced by Gb3-24:0 : StxB did not bind at all to GUVs composed of DOPC/Gb3-24:0, whereas the binding of StxB to SM/chol/Gb3-24:0 was concluded. Again, LecA bound to both types of GUVs with equal efficiency (figure 21).

Clearly, the lectins have preferences to membrane domains of different order. StxB prefers highly ordered membrane domains (i.e. Lo). Cholesterol seems to be particularly important for the recognition of Gb3-24:0 by StxB, since StxB binds efficiently to the GUVs composed of DOPC/chol/Gb3-24:0. On the contrary, LecA is less selective and also binds efficiently to Gb3 species incorporated into less ordered membrane domains (i.e. Ld).

Thereafter, using our knowledge about the binding preferences of StxB and LecA, we succeeded to rebuild the spatial segregation of StxB and LecA on the membrane surface of synthetic GUVs. For that, we used phase-separated GUVs spiked with two Gb3 species: Gb3-24:0 and Gb3-FSL.

All in all, understanding the binding selectivity of StxB and LecA, we propose to use these two lectins in combination as a comparative plasma membrane stain to evaluate the plasma membrane order.

3. Impact of the binding of lectins to Gb3 on the membrane organization in Supported lipid bilayers

(Sych et al., manuscript in preparation), for complete article see Chapter VII

The direct visualization of the plasma membrane reorganization in live cells is a very challenging task. Even with the recent improvements in the spatio-temporal resolution of the fluorescence microscopy techniques, the imaging of membrane nanodomains in live cells is very complex. As the solution, the approach of reconstitution lipid nanodomains in model membranes has been successfully employed. It was applied to resolve the mechanisms of lipid and protein clustering in the lipid bilayer. In this work, we mimicked the plasma membrane organization with phase separated supported lipid bilayer (SLB).

Phase separation into liquid-disordered (Ld – composed of DOPC) and liquid-ordered (Lo, composed of SM and chol) resembles the heterogeneity of the plasma membrane on the microscopic scale. We spiked the lipid bilayer with 5 mol % of Gb3 receptor molecules and, furthermore, applying lectins to such lipid bilayer, followed the rearrangement of the lipid domains in the SLB.

We produced a SLB with DOPC/chol/SM/Gb3-mix (37.5/20/37.5/5) composition. The SLB exhibited phase separation at room temperature. We visualized the phase separation using the lipophilic membrane marker βBodipy – C_{12} – HPC (Bodipy) which localizes preferentially into Ld domains. Furthermore, we applied lectins and imaged the bilayer over time with wide field (HILO) fluorescence microscopy.

StxB, applied to the lipid bilayer, binds preferentially to the Lo domains (figure 21). This is perfectly in line with the observations on GUVs. However, during the first few minutes of incubation, StxB-rich clusters appear in the Ld domain (figure 21). Simultaneously, Bodipy-depleted microscopic membrane domains appear in Ld and co-localize with clusters of StxB.

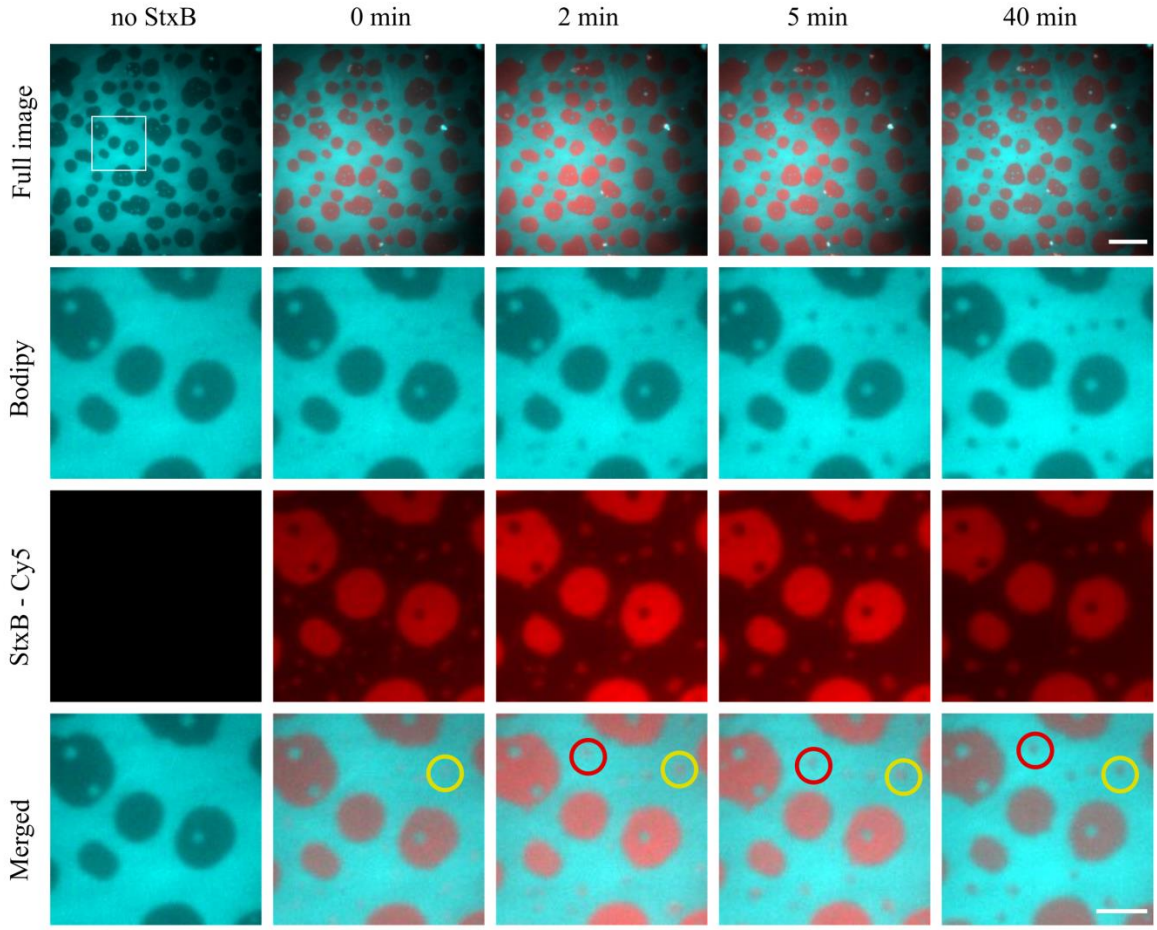

Figure 21| StxB-induced SLB reorganization. The SLB was composed of DOPC/chol/SM/Gb3 (37.5/20/37.5/5). The SLB was labeled by Bodipy-HPC that preferentially incorporates in Ld domains. StxB-Cy5 (200 nM) was applied. StxB binds almost exclusively to Lo domains. Moreover, it induces a formation of new Lo domains (red and yellow circles - Merged) by efficient clustering of the Gb3 molecules incorporated in the Ld phase. Scale bars – 10 and 5 μm respectively.

We suggest that these Bodipy-depleted domains are new Lo domains induced by efficient Gb3 clustering by StxB. Moreover, we suggest that together with Gb3, such clusters contain SM and chol (despite the phase separation, low concentrations of these

lipids are still present in Ld-domains). The StxB-induced membrane reorganization was studied in the context of StxB uptake initialization. In particular, Windschiegl et al. (Windschiegl et al., 2009) characterized the SLB reorganization induced by StxB using atomic force microscopy. According to their findings, StxB binding to SLB was shown to lead to efficient StxB cluster formation in homogeneous and phase-separated SLBs. Also, Safouane et al. (Safouane et al., 2010) showed the ability of StxB to induce phase separation in originally non-phase separated GUVs composed of DOPC/SM/chol/Gb3. These findings are perfectly in line with our observations suggesting that StxB acts as an efficient clustering agent.

LecA, also specific to Gb3 has different geometry and valence in comparison to StxB. It has only 4 binding sites. Its two pairs of binding sites are arranged to point in opposite directions. This enables LecA to cross-link membranes (Villringer et al., 2018). Moreover, LecA was found to highly accumulate at such interfaces. We applied 200 nM of LecA to phase-separated SLBs in order to study its impact on membrane organization. We used Bodipy-labeled SLBs of identical composition (DOPC/SM/chol/Gb3 -mix (37.5/20/37.5/5)) to the one used in the experiment with StxB.

At the earlier time points, LecA behaved similarly to StxB, as it bound preferentially to Lo domains enriched in Gb3 (figure 22a – black arrowhead). However, over time, no formation of new microscopic Lo domains was observed. On the contrary, Lo domains were decreasing in size and completely disappear (figure 22a – blue arrowhead). The total area of the Lo domains (figure 22b – blue curve) as well as the number of Lo domains and the size of the individual Lo domains decreased over time (figure 22c, d). Remarkably, after 20 min of incubation with LecA, almost all Lo domains are dissolved. In parallel, LecA forms large microscopic clusters (figure 22a – white arrowhead). Importantly, the fluorescence intensity in these newly formed clusters is much higher than the fluorescence intensity of LecA bound to Lo domains, suggesting a condensed enrichment of LecA. These LecA clusters co-localize with domains characterized by high intensity of Bodipy (figure 22a – purple arrowhead). These new domains form and grow simultaneously with the LecA clusters. We suggest that these new domains are composed of two or several lipid bilayers assembled in stacks with the LecA sandwiched in between the lipid bilayers. We named these structures – membrane multilayers. We suggest that LecA sequesters the lipids from the SLB in order to compose such multilayers. The formation of the multilayers depletes the SLB in lipid material and consequently the SLB breaks down and large membrane defects emerge (figure 22a – orange arrowhead). The area of the membrane defects increase over time and after 1 hour of incubation with LecA, the SLB is partially destroyed.

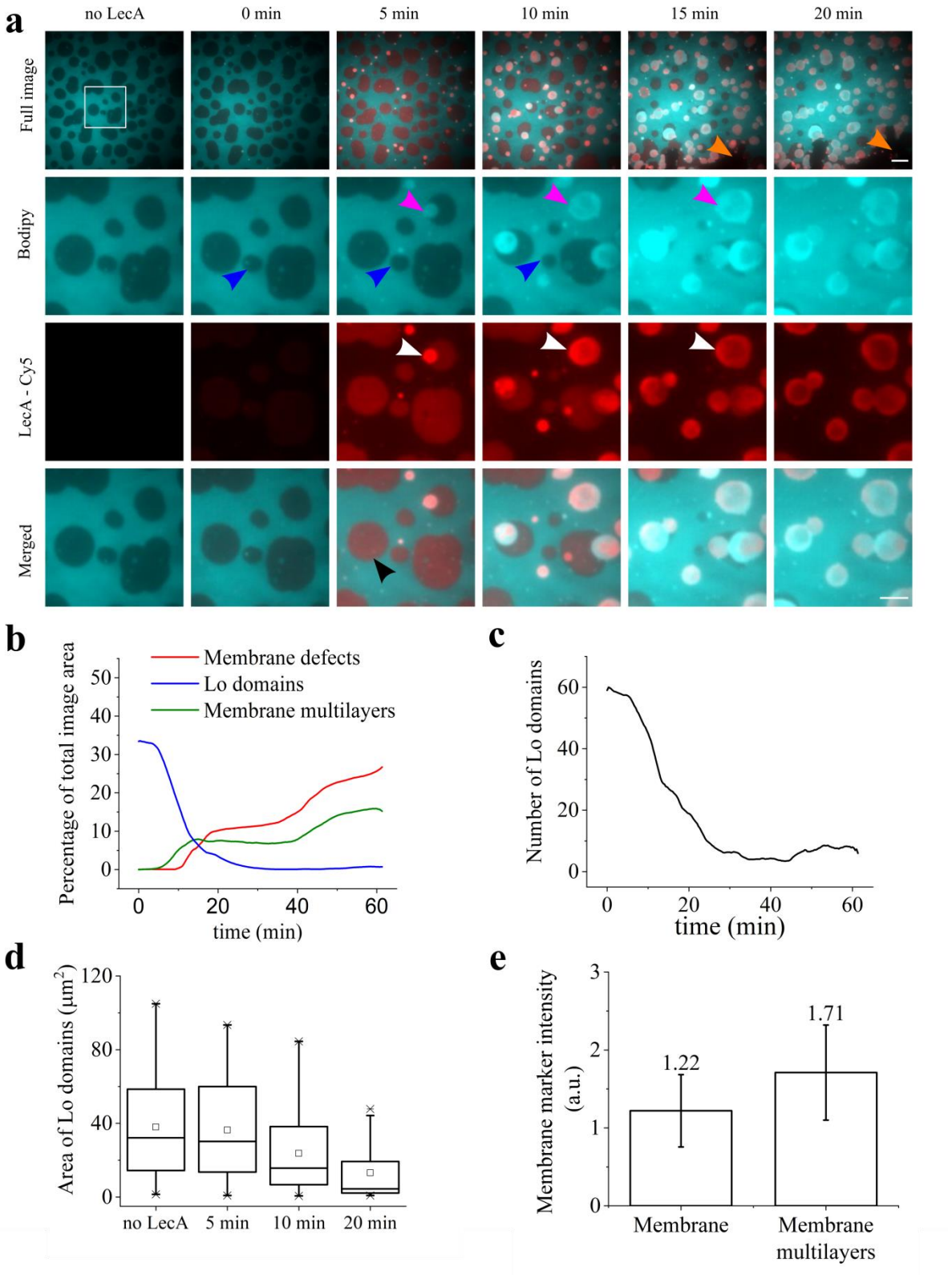
a
no LecA
0 min
5 min
10 min
15 min
20 min
Full image
Bodipy
LecA - Cy5
Merged
b
Membrane defects
Lo domains
Membrane multilayers
Percentage of total image area
time (min)
c
Number of Lo domains
time (min)
d
Area of Lo domains (μm²)
no LecA
5 min
10 min
20 min
e
Membrane marker intensity (a.u.)
1.22
1.71
Membrane
Membrane multilayers

Figure 22 | SLB reorganization induced by purified LecA. SLB is labeled by β Bodipy-C_{12}-FL-HPC that localizes in Ld domains (cyan). LecA ia labeled by Cy5 (red). Images are acquired with wide field microscopy (HILO). **a)** Time series of LecA interaction with phase-separated SLB (DOPC/chol/SM/Gb3-mix (37.5/20/37.5/5)). LecA induces Lo domains dissolution (blue arrowhead) and multilayer formation (purple arrowhead). Membrane multilayers co-localize with the bright LecA clusters (white arrow). At later time points, large membrane defects appear (orange arrowhead) **b)** The total area of the Lo domains, membrane defects and membrane multilayers changes over time. **c)** The total number of Lo domains decreases over time; **d)** The sizes of the individual Lo domains decrease over time; **e)** The mean fluorescence intensity signal in membrane multilayers is approximately 1.5 times higher than the intensity of the original, single bilayer membrane. Scale bars are 10 and 5 μm, respectively.

To further characterize the membrane multilayers, we quantified the fluorescence intensity of the membrane marker Bodipy in the multilayers and compared it to the fluorescence intensity of the Bodipy in Ld domains. A two-fold increase of Bodipy fluorescence intensity would indicate the formation of a membrane stack consisting of two lipid bilayers. However, we found that the membrane multilayers appear only approximately 1.5 times brighter than unilamellar Ld domains (figure 22e), which suggests that membrane multilayers have a distinct lipid organization that differs from the lipid organization in Ld or in Lo. Hence the amount of Bodipy in membrane multilayers is different. This question can be resolved by exploring the membrane order of SLBs at different time points of LecA-induced membrane reorganization.

We examined the membrane order using the environmentally sensitive lipophilic probe Nile Red 12 S (NR12S) in combination with the confocal ratiometric imaging. We found that membrane order of multilayers is indeed higher in comparison to the Ld domains, but lower than in Lo domains. This indicates that membrane multilayers are formed out of already mixed membrane, suggesting the importance of the Lo domains dissolution for the membrane multilayer formation.

In order to further understand the impact of LecA on membrane organization, we investigated the membrane multilayer formation and Lo domains dissolution, separately. At first, we applied LecA to non-phase separated SLB composed of DOPC/chol/Gb3-mix (65/30/5). Interestingly, in such SLB, the membrane multilayer formation together with complete membrane disintegration occurred very fast. Only after 15 min of incubation with 200 nM of LecA, the SLB was completely destroyed.

Separation of Lo domains dissolution from membrane multilayer formation is a more complicated task. We used the engineered protein RPL αGal (RPL). The monomer of this protein is similar to the monomer of LecA. However, it is stable as a dimer in solution. The application of this protein to SLB leads to a partial dissolution of the Lo domains without the formation of membrane multilayers. Based on these findings, we propose an interpretation for the roles of the different LecA binding sites in the lipid bilayer reorganization (Figure 23). For the dimeric LecA analogue, multilayers do not form

whereas the Lo domains dissolution occurs. This suggests that two binding sites pointing in one direction (as depicted on figure 23a – 1 and 2 or 3 and 4) are sufficient for Lo domains dissolution. In contrast, the complete tetrameric structure is required for the formation of membrane multilayers. The exact mechanism of phase mixing is not clear yet and may be resolved using SLBs of more specific composition (specific DOPC/SM/chol ratios and specific structures of Gb3 fatty acyl chains) combined with studies of line tension at the phase domains borders.

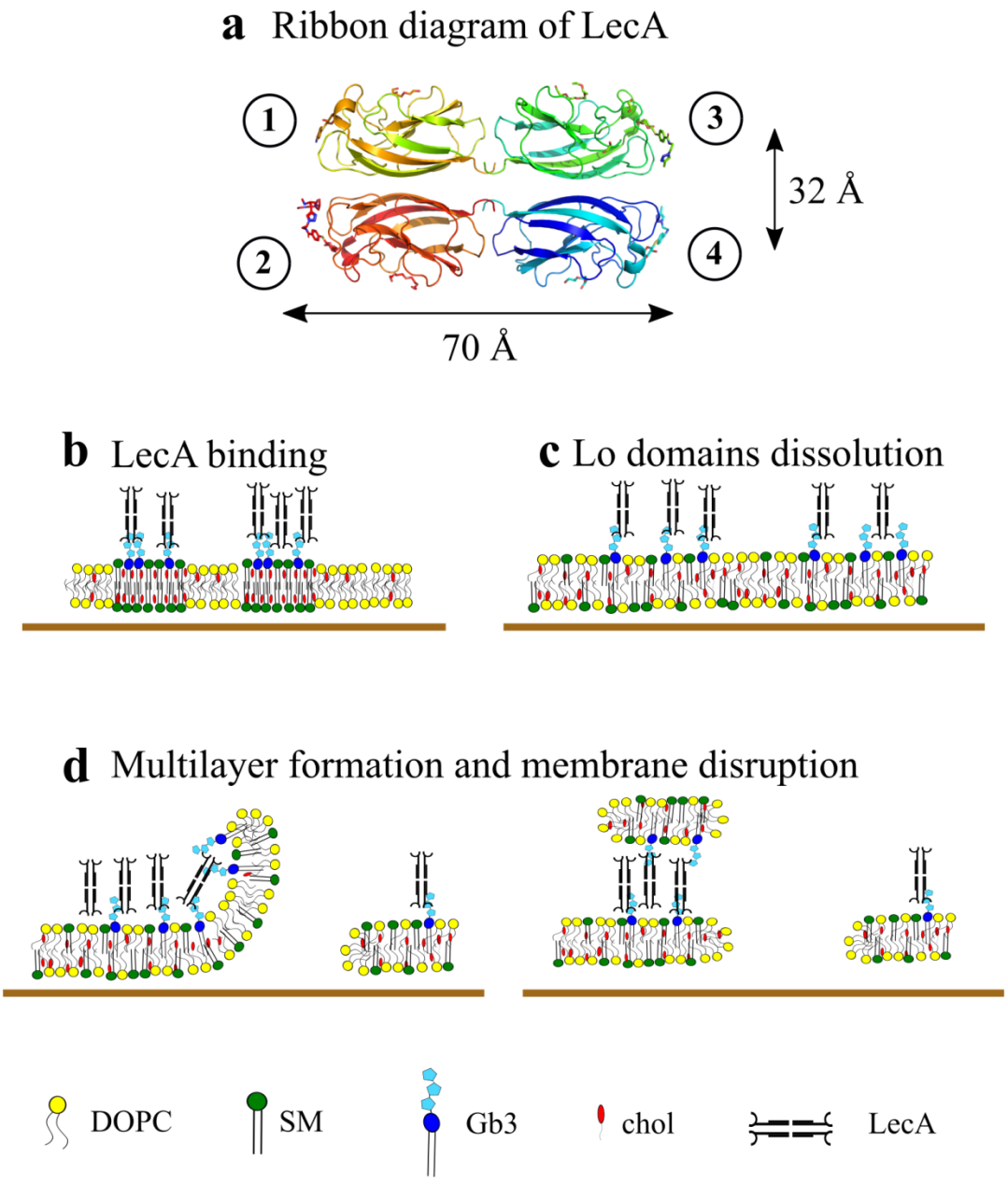

Figure 23| Schematic representation of the membrane reorganization induced by LecA. **a)** Ribbon diagram of LecA tetramer. Gb3-specific binding pockets are marked with numbers 1-4; **b)** LecA binding to a phase separated lipid bilayer; **c)** Lo domains dissolution; **d)** Membrane multilayer formation. LecA accumulates at the lipid bilayer interfaces.

4. Impact of *P. aeruginosa* on membrane organization studied in Supported lipid bilayers

(Sych et al., manuscript in preparation), for complete article see Chapter VII

LecA is the surface protein of *P. aeruginosa* and is of crucial importance for bacterial adhesion and internalization. In this work, we decipher the role of LecA in the membrane reorganization induced by *P. aeruginosa*. We investigated the membrane reorganization induced by two bacterial strains – *P. aeruginosa* strain PAO1 (wild type) and the *P. aeruginosa* strain deficient in LecA (ΔLecA). We reconstituted bacteria-membrane interactions in phase separated SLB of the same lipid composition as in the previous chapter (DOPC/SM/chol/Gb3 - (37.5/20/37.5/5)). However, since both bacterial strains were tagged with GFP, we changed the membrane marker. Here, we used Texas Red – DHPE that associates to the Ld domains.

Applied to the SLB, the wild type bacteria attach to the lipid bilayer and form aggregates (figure 24a – white arrowheads). These aggregates grow over time and accumulate more bacteria. On the contrary, ΔLecA strain bacteria do not form aggregates and the attachment of bacteria to the SLB is significantly reduced. Moreover, the ΔLecA bacteria can detach from the SLB (figure 24b – cyan arrowhead). The same reduction in attachment and absence of aggregation were observed when we applied both bacteria strains to SLB without Gb3 receptor (DOPC/chol/SM (37.5/20/37.5)). This clearly suggests that *P. aeruginosa* relies on the specific interaction of its proteins with the Gb3 membrane receptor for efficient adhesion and aggregation. Moreover, LecA is important for *P. aeruginosa* adhesion and requires the Gb3 receptor in the membrane.

We also examined the preferential locations of the bacterial attachment. Remarkably, bacteria exhibited a clear preference to the border of the Ld and Lo domains in phase separated SLB (figure 24a – purple arrowheads). Up to 60 % of the bacteria at the early time points were located at the Lo/Ld borders. Moreover, Ld domains were also attractive spots (approx.. 35 %) for bacterial adhesion, whereas Lo domains remained almost completely ignored by bacteria. Taking into account that the Gb3 is also present in Lo, we suggest that despite bacteria rely on a specific interaction of LecA to Gb3 for successful adhesion; additional mechanisms may amplify the Gb3 recognition incorporated in a more favorable environment (e.g. Ld domains, Lo/Ld boundaries). Importantly, at later time-points, bacteria prefer to join existing bacterial aggregates instead of adhesion to SLB area not yet occupied by bacteria.

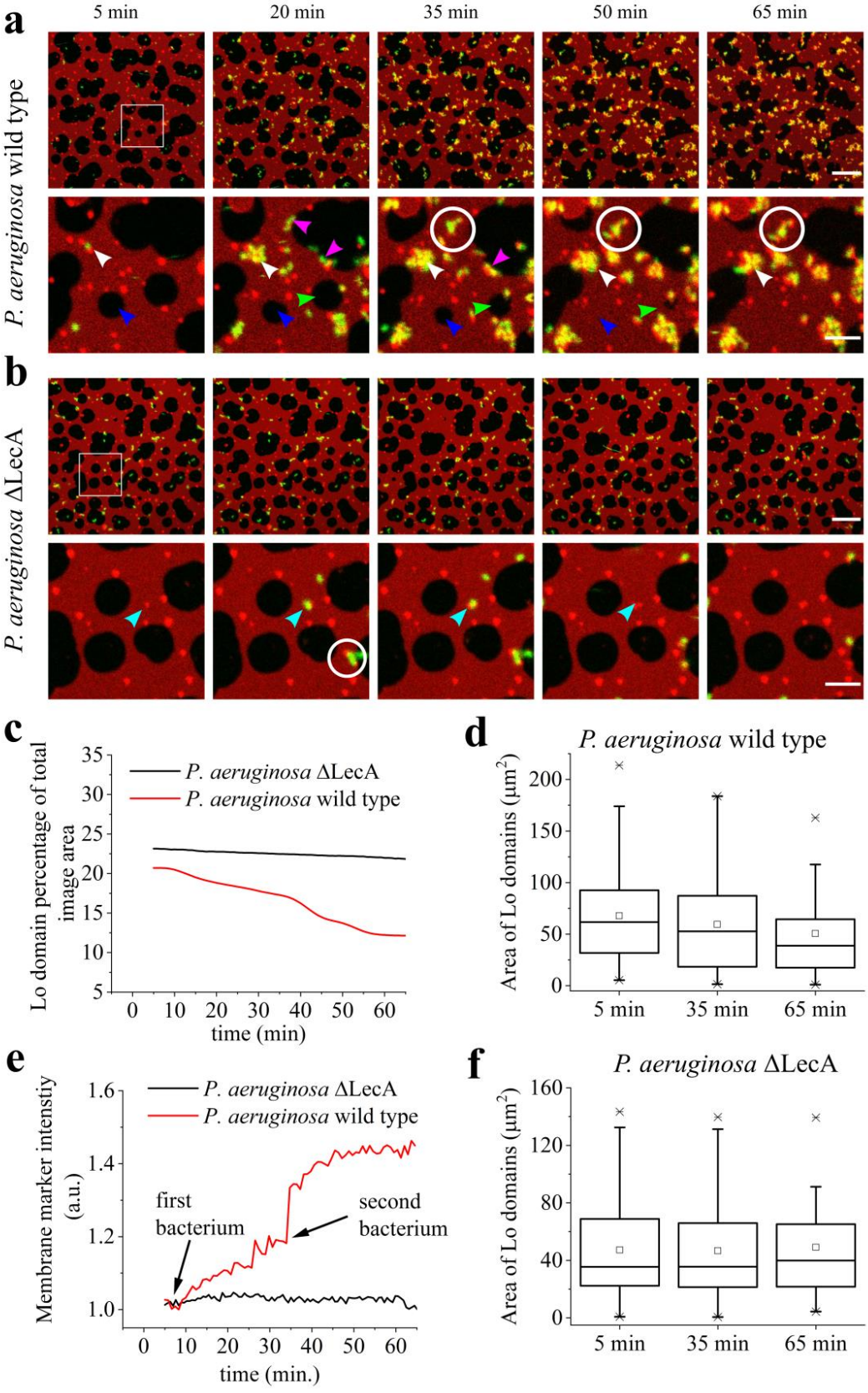
a
5 min
20 min
35 min
50 min
65 min
P. aeruginosa wild type
b
P. aeruginosa ΔLecA
c
Lo domain percentage of total image area
P. aeruginosa ΔLecA
P. aeruginosa wild type
time (min)
d
P. aeruginosa wild type
Area of Lo domains (μm²)
5 min
35 min
65 min
e
Membrane marker intenstiy (a.u.)
P. aeruginosa ΔLecA
P. aeruginosa wild type
first bacterium
second bacterium
time (min.)
f
P. aeruginosa ΔLecA
Area of Lo domains (μm²)
5 min
35 min
65 min

Figure 24 | SLB reorganization induced by P. aeruginosa. Bacteria labeled by GFP (green) are applied to phase separated SLBs composed of DOPC/chol/SM/Gb3 (37,5/20/37,5/5) and labeled by DHPE-TexasRed (red). Ld domains are enriched in DHPE-Texas Red, whereas the tightly packed Lo domains are depleted of the membrane marker and thus appear dark. Images are acquired with a laser scanning confocal microscope. **a)** The wild-type strain P. aeruginosa attaches to the SLB and forms bacterial clusters (white arrow). At the earlier time points, bacteria preferentially attach to the Lo/Ld domain boundaries (purple arrowhead). Furthermore, bacteria pull lipids out of the SLB to cover their surface with sequestered material (white circle). Additionally, P. aeruginosa alter the lipid organization of SLBs and dissolve the Lo domains (blue and green arrowheads). **b)** P. aeruginosa ΔLecA strain bacteria contact the lipid bilayer but do not remain stably attached to its surface (cyan arrowhead). Moreover, P. aeruginosa ΔLecA bacteria do not dissolve the Lo domains. **c)** In SLBs, P. aeruginosa wt induces the decrease of the total area of Lo domains over time (red curve) whereas P. aeruginosa ΔLecA does not. **d)** P. aeruginosa decreases the size of the individual Lo domains over time. **e)** P. aeruginosa wt (red curve) accumulates lipids from the SLB on the bacterial surface. The membrane marker intensity at the spot where bacterium is docked (a - white circle), increases over time. Two successive events of bacterial docking to the SLB are visible, indicating that two bacteria pull-out membrane material one after the other. In contrast, P. aeruginosa ΔLecA does not accumulate membrane material (black curve). The membrane marker intensity at the spot where bacterium is docked (b - white circle) does not increase over time. **f)** P. aeruginosa ΔLecA does not modify the size of the individual Lo domains. The scale bars are 10 and 5 μm, respectively.

Furthermore, we detected a local increase of the membrane marker signal at the spots of bacterial attachment (figure 24a – white circle, 24e). We suggest that bacteria sequester lipids out of the SLB to wrap themselves in membrane. This process seems to be analogous to the "lipid zipper" formation (Eierhoff et al., 2014) where bacteria by wrapping themselves with the membrane initialize their internalization. Here, however, the internalization is restricted by the SLB substrate, hence bacteria accumulate lipids on their surface. Importantly, LecA-Gb3 interaction is again crucial for this process. ΔLecA bacteria do not accumulate lipid material on their surface over time (figure 24b – white circle).

Most importantly, bacteria induce dissolution of the Lo domains. The Lo domains decrease in size over time and some of them disappear (figure 24a – blue and green arrowheads). In the absence of LecA-Gb3 interaction, the SLB organization remains stable. Previous studies with polarized epithelial cells by Kierbel et al (Kierbel et al., 2007) also showed an extensive membrane reorganization induced by *P. aeruginosa*. Furthermore, recent work of Song et al. (Song et al., 2019) suggested plasma membrane domains dissolution mediated by bacterial quorum sensing metabolites.

In our work, we observed that the Lo domains dissolution coincides with the bacterial aggregation mediated by bacteria-Gb3 interaction in absence of the cellular machinery. Moreover, we highlighted the importance of the lectin LecA in the dissolution of the Lo domains induced by bacteria.

IV Conclusions

Human pathogens are equipped with several independent mechanisms that ensure the successful binding and internalization into the host cell. Predominantly, pathogens initiate the uptake at the plasma membrane by specific targeting of various plasma membrane components. Particularly important are plasma membrane GSLs that can be recognized by lectins present in pathogens. Lectins bind to GSLs and induce membrane reorganization in order to promote infection. In this work, we explored the impact of bacterial lectins LecA and StxB on the membrane organization.

At first, we investigated the binding selectivity of StxB and LecA. Both proteins share a common receptor – globotriaosylceramide (Gb3). However, LecA and StxB exhibit preferences to Gb3 incorporated in membrane domains of different composition and organization. In the first part of my PhD project, we studied the binding preferences of LecA and StxB to Gb3 in model membranes (GUVs).

We developed a method for quantitative characterization of lectin binding to GUVs based on confocal fluorescence microscopy. In order to evaluate the binding, we calculate the mean fluorescence intensity of the bound proteins at the GUV rim and normalize it to the mean fluorescence intensity of the soluble protein. This provides a numerical evaluation of the imaging contrast which in turn represents the amount of proteins bound to the GUV. We named such value *relative binding efficiency*. Furthermore, in order to process numerous images with the GUVs in a fast and unbiased manner, we developed a FIJI-based macro for automated image processing. This approach is valid for the comparison of the binding efficiencies of the protein to GUVs of different compositions.

This high throughput method offers fast and unbiased analysis of the lectin binding to GUVs. However, it has several limitations. First, it does not provide the information on the binding affinity of the protein to the membrane. Furthermore, it allows direct quantifying of the amount of protein which is bound to the GUV only with proper calibration. Second, the value of relative binding efficiency depends on the concentration of the protein in the solution; the careful selection of the proper concentration is the responsibility of the user. Third, for now, the developed macro is limited to the GUVs or other round-shaped objects. Despite these limitations, the method was very successfully applied to explore the binding preferences of lectins to Gb3 incorporated in membranes of different organization.

In the second part of the project, we used GUVs for monitoring the LecA and StxB binding to Gb3. We controlled the membrane order of such GUVs by adjusting their composition. Also, we produced “phase separated” GUVs that contain spatially segregated domains of distinct membrane order. Moreover, we explored the lectin binding preferences to several Gb3 species, namely Gb3-24:0, Gb3-24:1 and to the artificial construct Gb3-FSL-DOPE. We found that StxB clearly prefers Gb3 receptor

molecules incorporated in liquid-ordered (Lo) domains composed of SM and chol. LecA demonstrated a less selective behavior. Though it binds preferentially to Lo domains, it also binds to less ordered domains (e.g. liquid-disordered, Ld). These binding preferences of StxB and LecA were especially pronounced for the Gb3 species with a 24:0 fatty acyl chain.

The synthetic membrane systems have proven to be a very useful tool for the characterization of lectin – Gb3 interactions. The investigation of the LecA and StxB binding to GUVs allows elucidating the influence of composition and organization of the lipid bilayer on the lectin binding. In particular, we determined that the content of cholesterol in the membrane can influence lectin binding drastically. Moreover, the length and the saturation degree of the Gb3 fatty acyl chain alters the recognition of the carbohydrate group by lectins. Most importantly, the lipid order of the membrane plays crucial role in the lectin recognition and binding.

Our studies of LecA and StxB binding to live cells also revealed differences in the lectin behavior. In polarized epithelial cells, StxB preferentially targets the more ordered apical membrane, whereas LecA binds more efficiently to the less-ordered basolateral membrane. Moreover, the primary cilium was exclusively targeted by StxB. Since the membrane order of the primary cilium is unknown yet, we suggest that it mainly harbors membrane ordered domains. Most importantly, we succeeded to reconstitute the spatial segregation and binding selectivity of LecA and StxB in phase-separated GUVs.

In the last part of the project we studied the membrane reorganization induced by both LecA and StxB. By binding to Gb3, lectins induce the rearrangement of membrane nanodomains. As the studies of such nanodomains in living membranes are a very complicated task, we reconstituted membrane domains on the microscopic scale using supported lipid bilayers (SLBs).

We prepared SLBs that exhibit phase separation into liquid-ordered (Lo) and liquid-disordered (Ld) domains. By application of lectins, we observed changes in the lateral organization of the Lo domains. We found, that StxB shrinks existing Lo domains, but also induces novel Lo domains. This confirms that StxB is an efficient clustering agent. On the contrary, LecA induces the complete dissolution of Lo domains. Moreover, LecA induces the formation of membrane multilayers with LecA clusters accumulated in between the lipid bilayers that assemble in stacks. Despite both of these processes occur simultaneously, we proved by a valence reduction of LecA that Lo domains dissolution can occur independently. Moreover, the analysis of membrane order in membrane multilayers showed that they are formed out of membrane of “intermediate order” between Lo and Ld which suggests that Lo dissolution is necessary for “multilayers” formation.

Furthermore, we studied Lo domains dissolution by bacterium *P. aeruginosa* that expresses LecA. We found that the bacteria bind to SLB and induce Lo domains

dissolution. Moreover, bacteria accumulate lipids from the SLB on their surface. Presumably, this is the analogue of lipid zipper formation but without the possibility to bend the membrane. We confirmed the importance of LecA for bacterium adhesion to SLB by using a LecA deficient strain. The ΔLecA bacteria do not bind well to SLBs and do not induce Lo domain dissolution. Lipid accumulation at the bacterial surface is not possible in the absence of LecA as well.

Supported lipid bilayers are very practical for the characterization of the lipid-lipid interactions on the large scale. Furthermore, the membrane deformation is constrained by the support; hence it is possible to study the lipid sorting and protein clustering explicitly. SLBs are widely used for the synthetic mimicry of the plasma membrane nanodomains (so-called lipid rafts). However, in these systems such domains are much bigger in size and temporally stable. Despite this, such system provides very interesting insights on how lectins and bacteria behave at the membranes of different composition and organization.

The impact of bacteria on the organization of the ordered domains is a very important observation. In native plasma membranes, the nanodomains of high order (lipid rafts) are implicated in various modes of signaling and initiation of endocytosis. Bacteria and viruses target lipid rafts and they exploit the machinery present in lipid rafts in order to promote infection. We believe that the Lo-domains dissolution, described in this work, may be common for numerous bacteria as a vital element of the host-pathogen interaction. Moreover, the Lo-domains dissolution driven by the interaction of the bacterial lectin with the plasma membrane GSL is reported for the first time.

V Outlook

In this work, we demonstrated several features of the interactions of the bacterial lectins with the GSL Gb3, reconstituted in model membranes. Although, some mechanisms of the StxB and LecA interactions with the membrane are now resolved, several open questions require further attention.

The sorting of the Gb3 species to the membrane domains of different composition and order is still elusive. Yet, we can recognize the presence of the Gb3 molecules in the lipid bilayer exclusively using the Gb3-binding lectins. However, lectins may induce the redistribution of the Gb3 in the membrane, hence the elucidation of the initial partition of the Gb3 species using lectins is challenging. The alternative strategies for the direct visualization of Gb3 molecules in the membrane must be employed. Our collaborators at TU Braunschweig (the group of Prof. Daniel Werz) developed the Bodipy-labeled synthetic Gb3 species. The unique feature of these constructs is that the fluorophore is attached to the sugar moiety; hence the introduction of such fluorophore should not influence drastically the incorporation of Gb3 in the lipid bilayer. However, the fluorophore coupled to the oligosaccharide group might interfere with the lectin recognition of Gb3. We aim to test in future the partition of such labeled Gb3 molecules in phase-separated model membranes, as well as the possibility to employ this constructs for the experiments with Gb3-binding lectins.

The membrane reorganization induced by LecA requires further characterization. The mechanism of the dissolution of the Lo domains is not yet resolved. The membrane reorganization studies in the SLBs that contain only single Gb3 species can give an interesting insight on how the specific interaction of LecA and Gb3 induces such extensive collective phenomenon in the lipid bilayer. Moreover, it can resolve the implications of different Gb3 species in the Lo domain dissolution induced by LecA. Furthermore, application of the Gb3 species tagged with the fluorophore can provide the information on the redistribution of Gb3 during the Lo dissolution. Also, the application of the molecular dynamic simulation can reveal very interesting details of this process. The formation of the membrane multilayers can be further characterized with the Atomic Force Microscopy. This method can provide information on the position of LecA at the lipid bilayer and inside the membrane multilayers as well as on the exact number of lipid bilayers in the multilayer.

The studies of the membrane order modifications by bacteria have to be further expanded to the investigation of the plasma membrane order during the bacterial uptake in live cells. The membrane order studies using the environmentally sensitive membrane markers can be employed. Using this techniques, the membrane order of the tubules formed by the “lipid zipper” in GUVs and live cells can be addressed.

VI References

Aigal, S., Claudinon, J., and Römer, W. (2015). Plasma membrane reorganization: A glycolipid gateway for microbes. Biochimica et Biophysica Acta (BBA) - Molecular Cell Research *1853*, 858–871.

Aktas, M., Danne, L., MÃ¶ller, P., and Narberhaus, F. (2014). Membrane lipids in Agrobacterium tumefaciens: biosynthetic pathways and importance for pathogenesis. Frontiers in Plant Science *5*.

Almeida, P.F. (2011). A Simple Thermodynamic Model of the Liquid-Ordered State and the Interactions between Phospholipids and Cholesterol. Biophysical Journal *100*, 420–429.

Almeida, R.F.M. de, Fedorov, A., and Prieto, M. (2003). Sphingomyelin/Phosphatidylcholine/Cholesterol Phase Diagram: Boundaries and Composition of Lipid Rafts. Biophysical Journal *85*, 2406–2416.

Ambrosi, M., Cameron, N.R., and Davis, B.G. (2005). Lectins: tools for the molecular understanding of the glycocode. Organic & Biomolecular Chemistry *3*, 1593.

Angelova, M.I., and Dimitrov, D.S. Liposome Electroformation. 13.

Antonietti, M., and Förster, S. (2003). Vesicles and Liposomes: A Self-Assembly Principle Beyond Lipids. Advanced Materials *15*, 1323–1333.

Arnaud, J., Claudinon, J., Tröndle, K., Trovaslet, M., Larson, G., Thomas, A., Varrot, A., Römer, W., Imberty, A., and Audfray, A. (2013). Reduction of Lectin Valency Drastically Changes Glycolipid Dynamics in Membranes but Not Surface Avidity. ACS Chemical Biology *8*, 1918–1924.

Arnaud, J., Tröndle, K., Claudinon, J., Audfray, A., Varrot, A., Römer, W., and Imberty, A. (2014). Membrane Deformation by Neolectins with Engineered Glycolipid Binding Sites. Angewandte Chemie International Edition *53*, 9267–9270.

Aufderhorst-Roberts, A., Chandra, U., and Connell, S.D. (2017). Three-Phase Coexistence in Lipid Membranes. Biophysical Journal *112*, 313–324.

Axelrod, D. (2001). Total Internal Reflection Fluorescence Microscopy in Cell Biology. Traffic *2*, 764–774.

Axelrod, D., Thompson, N.L., and Burghardt, T.P. (1983). Total internal reflection fluorescent microscopy. Journal of Microscopy *129*, 19–28.

Bacia, K., Schwille, P., and Kurzchalia, T. (2005). Sterol structure determines the separation of phases and the curvature of the liquid-ordered phase in model membranes. Proceedings of the National Academy of Sciences of the United States of America *102*, 3272–3277.

Barnett-Norris, J., Lynch, D., and Reggio, P.H. (2005). Lipids, lipid rafts and caveolae: Their importance for GPCR signaling and their centrality to the endocannabinoid system. Life Sciences *77*, 1625–1639.

Blake, D.A., Bovin, N.V., Bess, D., and Henry, S.M. (2011). FSL Constructs: A Simple Method for Modifying Cell/Virion Surfaces with a Range of Biological Markers Without Affecting their Viability. J Vis Exp.

Busto, J.V., García-Arribas, A.B., Sot, J., Torrecillas, A., Gómez-Fernández, J.C., Goñi, F.M., and Alonso, A. (2014). Lamellar Gel (Lβ) Phases of Ternary Lipid Composition Containing Ceramide and Cholesterol. Biophysical Journal *106*, 621–630.

Callan-Jones, A., Sorre, B., and Bassereau, P. (2011). Curvature-Driven Lipid Sorting in Biomembranes. Cold Spring Harbor Perspectives in Biology *3*, a004648–a004648.

Carravilla, P., Nieva, J.L., Goñi, F.M., Requejo-Isidro, J., and Huarte, N. (2015). Two-Photon Laurdan Studies of the Ternary Lipid Mixture DOPC:SM:Cholesterol Reveal a Single Liquid Phase at Sphingomyelin:Cholesterol Ratios Lower Than 1. Langmuir *31*, 2808–2817.

Carter, G.C., Bernstone, L., Sangani, D., Bee, J.W., Harder, T., and James, W. (2009). HIV entry in macrophages is dependent on intact lipid rafts. Virology *386*, 192–202.

Chemani, C., Imberty, A., Bentzmann, S. de, Pierre, M., Wimmerová, M., Guery, B.P., and Faure, K. (2009). Role of LecA and LecB Lectins in Pseudomonas aeruginosa-Induced Lung Injury and Effect of Carbohydrate Ligands. Infection and Immunity *77*, 2065–2075.

Chinnapen, D.J.-F., Hsieh, W.-T., te Welscher, Y.M., Saslowsky, D.E., Kaoutzani, L., Brandsma, E., D'Auria, L., Park, H., Wagner, J.S., Drake, K.R., et al. (2012). Lipid Sorting by Ceramide Structure from Plasma Membrane to ER for the Cholera Toxin Receptor Ganglioside GM1. Developmental Cell *23*, 573–586.

Collins, B.M., Davis, M.J., Hancock, J.F., and Parton, R.G. (2012). Structure-Based Reassessment of the Caveolin Signaling Model: Do Caveolae Regulate Signaling through Caveolin-Protein Interactions? Developmental Cell *23*, 11–20.

Cossart, P. (2004). Bacterial Invasion: The Paradigms of Enteroinvasive Pathogens. Science *304*, 242–248.

Coster, H.G.L. (2003). The Physics of Cell Membranes. Journal of Biological Physics *29*, 363–399.

Cox, D., Lee, D.J., Dale, B.M., Calafat, J., and Greenberg, S. (2000). A Rab11-containing rapidly recycling compartment in macrophages that promotes phagocytosis. PNAS *97*, 680–685.

Cremer, P.S., and Boxer, S.G. (1999). Formation and Spreading of Lipid Bilayers on Planar Glass Supports. The Journal of Physical Chemistry B *103*, 2554–2559.

Devaux, P.F. (1991). Static and dynamic lipid asymmetry in cell membranes. Biochemistry *30*, 1163–1173.

Devaux, P.F., and Morris, R. (2004). Transmembrane asymmetry and lateral domains in biological membranes. Traffic *5*, 241–246.

DeWitt, B.N., and Dunn, R.C. (2015). Interaction of Cholesterol in Ternary Lipid Mixtures Investigated Using Single-Molecule Fluorescence. Langmuir *31*, 995–1004.

Dezi, M., Cicco, A.D., Bassereau, P., and Lévy, D. (2013). Detergent-mediated incorporation of transmembrane proteins in giant unilamellar vesicles with controlled physiological contents. PNAS *110*, 7276–7281.

Dietrich, C., Bagatolli, L.A., Volovyk, Z.N., Thompson, N.L., Levi, M., Jacobson, K., and Gratton, E. (2001). Lipid Rafts Reconstituted in Model Membranes. Biophysical Journal *80*, 1417–1428.

Doherty, G.J., and McMahon, H.T. (2009). Mechanisms of Endocytosis. Annual Review of Biochemistry *78*, 857–902.

Duncan, R., and Richardson, S.C.W. (2012). Endocytosis and Intracellular Trafficking as Gateways for Nanomedicine Delivery: Opportunities and Challenges. Mol. Pharmaceutics *9*, 2380–2402.

Duncan, M.J., Li, G., Shin, J.-S., Carson, J.L., and Abraham, S.N. (2004). Bacterial Penetration of Bladder Epithelium through Lipid Rafts. Journal of Biological Chemistry *279*, 18944–18951.

Eierhoff, T., Stechmann, B., and Rmer, W. (2012). Pathogen and Toxin Entry - How Pathogens and Toxins Induce and Harness Endocytotic Mechanisms. In Molecular Regulation of Endocytosis, B. Ceresa, ed. (InTech), p.

Eierhoff, T., Bastian, B., Thuenauer, R., Madl, J., Audfray, A., Aigal, S., Juillot, S., Rydell, G.E., Müller, S., Bentzmann, S. de, et al. (2014). A lipid zipper triggers bacterial invasion. PNAS *111*, 12895–12900.

Emam, A., Carter, W.G., and Lingwood, C. (2010). Glycolipid-dependent, protease sensitive internalization of Pseudomonas aeruginosa into cultured human respiratory epithelial cells. Open Microbiology Journal *4*, 106–115.

Ewers, H., Römer, W., Smith, A.E., Bacia, K., Dmitrieff, S., Chai, W., Mancini, R., Kartenbeck, J., Chambon, V., Berland, L., et al. (2010). GM1 structure determines SV40-induced membrane invagination and infection. Nat Cell Biol *12*, 11–18.

Fahy, E., Subramaniam, S., Brown, H.A., Glass, C.K., Merrill, A.H., Murphy, R.C., Raetz, C.R.H., Russell, D.W., Seyama, Y., Shaw, W., et al. (2005). A comprehensive classification system for lipids. European Journal of Lipid Science and Technology *107*, 337–364.

Fan, H.Y., Das, D., and Heerklotz, H. (2016). “Staying Out” Rather than “Cracking In”: Asymmetric Membrane Insertion of 12:0 Lysophosphocholine. Langmuir.

Fan, J., Sammalkorpi, M., and Haataja, M. (2010). Formation and regulation of lipid microdomains in cell membranes: Theory, modeling, and speculation. FEBS Letters *584*, 1678–1684.

Fra, A.M., Williamson, E., Simons, K., and Parton, R.G. (1994). Detergent-insoluble glycolipid microdomains in lymphocytes in the absence of caveolae. J. Biol. Chem. *269*, 30745–30748.

Gennis, R.B. (2013). Biomembranes: Molecular Structure and Function (Springer Science & Business Media).

Gerl, M.J., Sampaio, J.L., Urban, S., Kalvodova, L., Verbavatz, J.-M., Binnington, B., Lindemann, D., Lingwood, C.A., Shevchenko, A., Schroeder, C., et al. (2012). Quantitative analysis of the lipidomes of the influenza virus envelope and MDCK cell apical membrane. The Journal of Cell Biology *196*, 213–221.

Gilbert, R.J.C., Serra, M.D., Froelich, C.J., Wallace, M.I., and Anderluh, G. (2014). Membrane pore formation at protein–lipid interfaces. Trends in Biochemical Sciences *39*, 510–516.

Glazier, R., and Salaita, K. Supported Lipid Bilayer Platforms to Probe Cell Mechanobiology. Biochimica et Biophysica Acta (BBA) - Biomembranes.

Gobbo, P., Patil, A.J., Li, M., Harniman, R., Briscoe, W.H., and Mann, S. (2018). Programmed assembly of synthetic protocells into thermoresponsive prototissues. Nature Materials *17*, 1145–1153.

Gracià, R.S., Bezlyepkina, N., Knorr, R.L., Lipowsky, R., and Dimova, R. (2010). Effect of cholesterol on the rigidity of saturated and unsaturated membranes: fluctuation and electrodeformation analysis of giant vesicles. Soft Matter *6*, 1472.

Haan, L. de, and Hirst, T.R. (2004). Cholera toxin: A paradigm for multi-functional engagement of cellular mechanisms (Review). Molecular Membrane Biology *21*, 77–92.

Hennesthal, C., and Steinem, C. (2000). Pore-Spanning Lipid Bilayers Visualized by Scanning Force Microscopy. J. Am. Chem. Soc. *122*, 8085–8086.

Hermann, E., Bleicken, S., Subburaj, Y., and Garcia-Saez, A.J. (2014). Automated analysis of giant unilamellar vesicles using circular Hough transformation. Bioinformatics *30*, 1747–1754.

Ho, C.S., Khadka, N.K., She, F., Cai, J., and Pan, J. (2016). Influenza M2 Transmembrane Domain Senses Membrane Heterogeneity and Enhances Membrane Curvature. Langmuir *32*, 6730–6738.

Ikenouchi, J., Suzuki, M., Umeda, K., Ikeda, K., Taguchi, R., Kobayashi, T., Sato, S.B., Kobayashi, T., Stolz, D.B., and Umeda, M. (2012). Lipid Polarity Is Maintained in Absence of Tight Junctions. Journal of Biological Chemistry *287*, 9525–9533.

Israelachvili, J.N. (2011). Intermolecular and surface forces (Amsterdam: Elsevier, Acad. Press).

Israelachvili, J.N., Mitchell, D.J., and Ninham, B.W. (1977). Theory of self-assembly of lipid bilayers and vesicles. Biochimica et Biophysica Acta (BBA)-Biomembranes *470*, 185–201.

Jäpelt, R.B., and Jakobsen, J. (2013). Vitamin D in plants: a review of occurrence, analysis, and biosynthesis. Front. Plant Sci. *4*.

Jing, Y., Trefna, H., Persson, M., Kasemo, B., and Svedhem, S. (2014). Formation of supported lipid bilayers on silica: relation to lipid phase transition temperature and liposome size. Soft Matter *10*, 187–195.

Joesaar, A., Yang, S., Bögels, B., van der Linden, A., Pieters, P., Kumar, B.V.V.S.P., Dalchau, N., Phillips, A., Mann, S., and de Greef, T.F.A. (2019). DNA-based communication in populations of synthetic protocells. Nature Nanotechnology.

Johannes, L., and Römer, W. (2010). Shiga toxins — from cell biology to biomedical applications. Nat Rev Micro *8*, 105–116.

Johannes, L., Wunder, C., and Bassereau, P. (2014). Bending “On the Rocks”--A Cocktail of Biophysical Modules to Build Endocytic Pathways. Cold Spring Harbor Perspectives in Biology *6*, a016741–a016741.

Johansson, E.M.V., Crusz, S.A., Kolomiets, E., Buts, L., Kadam, R.U., Cacciarini, M., Bartels, K.-M., Diggle, S.P., Cámara, M., Williams, P., et al. (2008). Inhibition and Dispersion of Pseudomonas aeruginosa Biofilms by Glycopeptide Dendrimers Targeting the Fucose-Specific Lectin LecB. Chemistry & Biology *15*, 1249–1257.

Jones, D.H., Lingwood, C.A., Barber, K.R., and Grant, C.W.M. (1997). Globoside as a Membrane Receptor: A Consideration of Oligosaccharide Communication with the Hydrophobic Domain. Biochemistry *36*, 8539–8547.

Jouhet, J. (2013). Importance of the hexagonal lipid phase in biological membrane organization. Front Plant Sci *4*.

Kadam, R.U., Bergmann, M., Hurley, M., Garg, D., Cacciarini, M., Swiderska, M.A., Nativi, C., Sattler, M., Smyth, A.R., Williams, P., et al. (2011). A Glycopeptide Dendrimer Inhibitor of the Galactose-Specific Lectin LecA and of Pseudomonas aeruginosa Biofilms. Angewandte Chemie International Edition *50*, 10631–10635.

Kaksonen, M., and Roux, A. (2018). Mechanisms of clathrin-mediated endocytosis. Nature Reviews Molecular Cell Biology *19*, 313–326.

Kierbel, A., Gassama-Diagne, A., Rocha, C., Radoshevich, L., Olson, J., Mostov, K., and Engel, J. (2007). Pseudomonas aeruginosa exploits a PIP3-dependent pathway to transform apical into basolateral membrane. The Journal of Cell Biology *177*, 21–27.

Klymchenko, A.S., and Kreder, R. (2014). Fluorescent Probes for Lipid Rafts: From Model Membranes to Living Cells. Chemistry & Biology *21*, 97–113.

Kociurzynski, R., Beck, S.D., Bouhon, J.-B., Römer, W., and Knecht, V. (2019). Binding of SV40's Viral Capsid Protein VP1 to Its Glycosphingolipid Receptor GM1 Induces Negative Membrane Curvature: A Molecular Dynamics Study. Langmuir *35*, 3534–3544.

Koldsø, H., Shorthouse, D., Hélie, J., and Sansom, M.S.P. (2014). Lipid Clustering Correlates with Membrane Curvature as Revealed by Molecular Simulations of Complex Lipid Bilayers. PLOS Computational Biology *10*, e1003911.

Kucherak, O.A., Oncul, S., Darwich, Z., Yushchenko, D.A., Arntz, Y., Didier, P., Mély, Y., and Klymchenko, A.S. (2010). Switchable Nile Red-Based Probe for Cholesterol and Lipid Order at the Outer Leaflet of Biomembranes. J. Am. Chem. Soc. *132*, 4907–4916.

Kühner, M., Tampé, R., and Sackmann, E. (1994). Lipid mono- and bilayer supported on polymer films: composite polymer-lipid films on solid substrates. Biophysical Journal *67*, 217–226.

Kwiatek, J.M., Hinde, E., and Gaus, K. (2014). Microscopy approaches to investigate protein dynamics and lipid organization. Molecular Membrane Biology *31*, 141–151.

Lafont, F., and Van Der Goot, F.G. (2005). Bacterial invasion via lipid rafts: Bacterial invasion via lipid rafts. Cellular Microbiology *7*, 613–620.

Lakowicz, J.R. (2006). Principles of fluorescence spectroscopy (New York: Springer).

Lee, A.G. (1977a). Lipid phase transitions and phase diagrams I. Lipid phase transitions. Biochimica et Biophysica Acta (BBA) - Reviews on Biomembranes *472*, 237–281.

Lee, A.G. (1977b). Lipid phase transitions and phase diagrams II. Mixtures involving lipids. Biochimica et Biophysica Acta (BBA) - Reviews on Biomembranes *472*, 285–344.

Leonenko, Z.V., Finot, E., Ma, H., Dahms, T.E.S., and Cramb, D.T. (2004). Investigation of Temperature-Induced Phase Transitions in DOPC and DPPC Phospholipid Bilayers Using Temperature-Controlled Scanning Force Microscopy. Biophysical Journal *86*, 3783–3793.

Lin, Q., and London, E. (2014). Preparation of artificial plasma membrane mimicking vesicles with lipid asymmetry. PLoS One *9*, e87903.

Lingwood, D., Binnington, B., Róg, T., Vattulainen, I., Grzybek, M., Coskun, Ü., Lingwood, C.A., and Simons, K. (2011). Cholesterol modulates glycolipid conformation and receptor activity. Nature Chemical Biology *7*, 260–262.

Lis, H., and Sharon, N. (1998). Lectins: carbohydrate-specific proteins that mediate cellular recognition. Chemical Reviews *98*, 637–674.

Mabrey, S., and Sturtevant, J.M. (1976). Investigation of phase transitions of lipids and lipid mixtures by sensitivity differential scanning calorimetry. PNAS *73*, 3862–3866.

Madl, J., Villringer, S., and Römer, W. (2017). Delving into Lipid-Driven Endocytic Mechanisms Using Biomimetic Membranes. In Chemical and Synthetic Approaches in Membrane Biology, A.K. Shukla, ed. (Springer New York), pp. 17–36.

Mahfoud, R., Manis, A., and Lingwood, C.A. (2009). Fatty acid-dependent globotriaosyl ceramide receptor function in detergent resistant model membranes. J. Lipid Res. *50*, 1744–1755.

Manna, M., Javanainen, M., Monne, H.M.-S., Gabius, H.-J., Rog, T., and Vattulainen, I. (2017). Long-chain GM1 gangliosides alter transmembrane domain registration through interdigitation. Biochimica et Biophysica Acta (BBA) - Biomembranes *1859*, 870–878.

Maxfield, F.R., and Tabas, I. (2005). Role of cholesterol and lipid organization in disease. Nature *438*, 612–621.

Meer, G. van (2002). The Different Hues of Lipid Rafts. Science *296*, 855–857.

van Meer, G., Voelker, D.R., and Feigenson, G.W. (2008). Membrane lipids: where they are and how they behave. Nat Rev Mol Cell Biol *9*, 112–124.

Méléard, P., Bagatolli, L.A., and Pott, T. (2009). Giant Unilamellar Vesicle Electroformation. In Methods in Enzymology, (Elsevier), pp. 161–176.

Mellander, L.J., Kurczy, M.E., Najafinobar, N., Dunevall, J., Ewing, A.G., and Cans, A.-S. (2014). Two modes of exocytosis in an artificial cell. Scientific Reports *4*, 3847.

Mingeot-Leclercq, M.-P., Deleu, M., Brasseur, R., and Dufrêne, Y.F. (2008). Atomic force microscopy of supported lipid bilayers. Nature Protocols *3*, 1654–1659.

Müller, S.K., Wilhelm, I., Schubert, T., Zittlau, K., Imberty, A., Madl, J., Eierhoff, T., Thuenauer, R., and Römer, W. (2017). Gb3-binding lectins as potential carriers for transcellular drug delivery. Expert Opinion on Drug Delivery *14*, 141–153.

Nicolson, G.L. (2014). The Fluid—Mosaic Model of Membrane Structure: Still relevant to understanding the structure, function and dynamics of biological membranes after more than 40years. Biochimica et Biophysica Acta (BBA) - Biomembranes *1838*, 1451–1466.

Novoa, A., Eierhoff, T., Topin, J., Varrot, A., Barluenga, S., Imberty, A., Römer, W., and Winssinger, N. (2014). A LecA Ligand Identified from a Galactoside-Conjugate Array Inhibits Host Cell Invasion by *Pseudomonas aeruginosa*. Angewandte Chemie International Edition *53*, 8885–8889.

Omidvar Ramin, and Römer Winfried (2019). Glycan-decorated protocells: novel features for rebuilding cellular processes. Interface Focus *9*, 20180084.

Ono, A., and Freed, E.O. (2001). Plasma membrane rafts play a critical role in HIV-1 assembly and release. PNAS *98*, 13925–13930.

Owen, D.M., Rentero, C., Magenau, A., Abu-Siniyeh, A., and Gaus, K. (2012). Quantitative imaging of membrane lipid order in cells and organisms. Nat. Protocols *7*, 24–35.

Pakkanen, K. (2009). From endosomes onwards: membranes, lysosomes and viral capsid interactions. Jyväskylä Studies in Biological and Environmental Science 203.

Parton, R.G., and del Pozo, M.A. (2013). Caveolae as plasma membrane sensors, protectors and organizers. Nature Reviews Molecular Cell Biology *14*, 98–112.

Parton, R.G., and Simons, K. (2007). The multiple faces of caveolae. Nat Rev Mol Cell Biol *8*, 185–194.

Patalag, L.J., Sibold, J., Schütte, O.M., Steinem, C., and Werz, D.B. Gb3 Glycosphingolipids with Fluorescent Oligoene Fatty Acids: Synthesis and Phase Behavior in Model Membranes. ChemBioChem *18*, 2171–2178.

Pawley, J. (2010). Handbook of Biological Confocal Microscopy (Springer Science & Business Media).

Pelkmans, L., and Helenius, A. (2002). Endocytosis Via Caveolae. Traffic *3*, 311–320.

Pezeshkian, W., G. Hansen, A., Johannes, L., Khandelia, H., C. Shillcock, J., S. Kumar, P.B., and H. Ipsen, J. (2016). Membrane invagination induced by Shiga toxin B-subunit: from molecular structure to tube formation. Soft Matter *12*, 5164–5171.

Pezeshkian, W., Gao, H., Arumugam, S., Becken, U., Bassereau, P., Florent, J.-C., Ipsen, J.H., Johannes, L., and Shillcock, J.C. (2017). Mechanism of Shiga Toxin Clustering on Membranes. ACS Nano *11*, 314–324.

Pinot, M., Vanni, S., Pagnotta, S., Lacas-Gervais, S., Payet, L.-A., Ferreira, T., Gautier, R., Goud, B., Antonny, B., and Barelli, H. (2014). Polyunsaturated phospholipids facilitate membrane deformation and fission by endocytic proteins. Science *345*, 693–697.

Pizarro-Cerdá, J., and Cossart, P. (2006). Bacterial Adhesion and Entry into Host Cells. Cell *124*, 715–727.

Quinn, P.J., and Wolf, C. (2009). The liquid-ordered phase in membranes. Biochimica et Biophysica Acta (BBA) - Biomembranes *1788*, 33–46.

Raghupathy, R., Anilkumar, A.A., Polley, A., Singh, P.P., Yadav, M., Johnson, C., Suryawanshi, S., Saikam, V., Sawant, S.D., Panda, A., et al. (2015). Transbilayer Lipid Interactions Mediate Nanoclustering of Lipid-Anchored Proteins. Cell *161*, 581–594.

Richter, R.P., and Brisson, A.R. (2005). Following the Formation of Supported Lipid Bilayers on Mica: A Study Combining AFM, QCM-D, and Ellipsometry. Biophys J *88*, 3422–3433.

Römer, W., and Steinem, C. (2004). Impedance analysis and single-channel recordings on nano-black lipid membranes based on porous alumina. Biophysical Journal *86*, 955–965.

Römer, W., Berland, L., Chambon, V., Gaus, K., Windschiegl, B., Tenza, D., Aly, M.R.E., Fraisier, V., Florent, J.-C., Perrais, D., et al. (2007). Shiga toxin induces tubular membrane invaginations for its uptake into cells. Nature *450*, 670–675.

Rothman, J.E., and Lenard, J. (1977). Membrane asymmetry. Science *195*, 743–753.

Roux, A., Cuvelier, D., Nassoy, P., Prost, J., Bassereau, P., and Goud, B. (2005). Role of curvature and phase transition in lipid sorting and fission of membrane tubules. The EMBO Journal *24*, 1537–1545.

Rydell, G.E., Svensson, L., Larson, G., Johannes, L., and Römer, W. (2013). Human GII.4 norovirus VLP induces membrane invaginations on giant unilamellar vesicles containing secretor gene dependent α1,2-fucosylated glycosphingolipids. Biochimica et Biophysica Acta (BBA) - Biomembranes *1828*, 1840–1845.

Safouane, M., Berland, L., Callan-Jones, A., Sorre, B., Römer, W., Johannes, L., Toombes, G.E.S., and Bassereau, P. (2010). Lipid Cosorting Mediated by Shiga Toxin Induced Tubulation. Traffic *11*, 1519–1529.

Sanchez, S.A., Tricerri, M.A., Gunther, G., Gratton, E., and others (2007). Laurdan generalized polarization: from cuvette to microscope. Modern Research and Educational Topics in Microscopy (Formatex) *2*, 1007–1014.

Sandvig, K. (2001). Shiga toxins. Toxicon *39*, 1629–1635.

Sasai, M., Tadokoro, S., and Hirashima, N. (2010). Artificial Exocytotic System That Secretes Intravesicular Contents upon Ca2+ Influx. Langmuir *26*, 14788–14792.

Schnaar, R.L., Suzuki, A., and Stanley, P. (2009). Glycosphingolipids. In Essentials of Glycobiology, A. Varki, R.D. Cummings, J.D. Esko, H.H. Freeze, P. Stanley, C.R. Bertozzi, G.W. Hart, and M.E. Etzler, eds. (Cold Spring Harbor (NY): Cold Spring Harbor Laboratory Press), p.

Schubert, T., and Römer, W. (2015). How synthetic membrane systems contribute to the understanding of lipid-driven endocytosis. Biochimica et Biophysica Acta (BBA) - Molecular Cell Research *1853*, 2992–3005.

Schütte, O.M., Ries, A., Orth, A., Patalag, L.J., Römer, W., Steinem, C., and Werz, D.B. (2014). Influence of Gb3 glycosphingolipids differing in their fatty acid chain on the phase behaviour of solid supported membranes: chemical syntheses and impact of Shiga toxin binding. Chemical Science *5*, 3104.

Schütte, O.M., Patalag, L.J., Weber, L.M.C., Ries, A., Römer, W., Werz, D.B., and Steinem, C. (2015). 2-Hydroxy Fatty Acid Enantiomers of Gb 3 Impact Shiga Toxin Binding and Membrane Organization. Biophysical Journal *108*, 2775–2778.

Seddon, A.M., Curnow, P., and Booth, P.J. (2004). Membrane proteins, lipids and detergents: not just a soap opera. Biochimica et Biophysica Acta (BBA) - Biomembranes *1666*, 105–117.

Sengupta, P., Seo, A.Y., Pasolli, H.A., Song, Y.E., Johnson, M.C., and Lippincott-Schwartz, J. (2019). A lipid-based partitioning mechanism for selective incorporation of proteins into membranes of HIV particles. Nature Cell Biology *21*, 452–461.

Sens, P., Johannes, L., and Bassereau, P. (2008). Biophysical approaches to protein-induced membrane deformations in trafficking. Current Opinion in Cell Biology *20*, 476–482.

Sezgin, E. (2017). Super-resolution optical microscopy for studying membrane structure and dynamics. J. Phys.: Condens. Matter.

Sezgin, E., Levental, I., Mayor, S., and Eggeling, C. (2017). The mystery of membrane organization: composition, regulation and roles of lipid rafts. Nature Reviews Molecular Cell Biology.

Shin, S.-H., Park, M.-H., Byeon, J.-J., Lee, B.I., Park, Y., Ko, A., Seong, M., Lee, S., Kim, M.R., Seo, J., et al. (2018). A Liquid Chromatography-Quadrupole-Time-of-Flight Mass Spectrometric Assay for the Quantification of Fabry Disease Biomarker Globotriaosylceramide (GB3) in Fabry Model Mouse. Pharmaceutics *10*, 69.

Shurer, C.R., Kuo, J.C.-H., Roberts, L.M., Gandhi, J.G., Colville, M.J., Enoki, T.A., Pan, H., Su, J., Noble, J.M., Hollander, M.J., et al. (2019). Physical Principles of Membrane Shape Regulation by the Glycocalyx. Cell.

Silvius, J. (1982). Thermotropic Phase Transitions of Pure Lipids in Model Membranes and Their Modifications by Membrane Proteins. In: Jost PC, Griffith OH, editors. Lipid-Protein Interactions.

Simons, K., and Gerl, M.J. (2010). Revitalizing membrane rafts: new tools and insights. Nature Reviews Molecular Cell Biology *11*, 688–699.

Simons, K., and Ikonen, E. (1997). Functional rafts in cell membranes. Nature *387*, 569.

Simons, K., and Toomre, D. (2000). Lipid rafts and signal transduction. Nat Rev Mol Cell Biol *1*, 31–39.

Simons, K., and Van Meer, G. (1988). Lipid sorting in epithelial cells. Biochemistry *27*, 6197–6202.

Singer, S.J., and Nicolson, G.L. (1972). The Fluid Mosaic Model of the Structure of Cell Membranes. Science *175*, 720–731.

Sinha, B., Köster, D., Ruez, R., Gonnord, P., Bastiani, M., Abankwa, D., Stan, R.V., Butler-Browne, G., Vedie, B., Johannes, L., et al. (2011). Cells Respond to Mechanical Stress by Rapid Disassembly of Caveolae. Cell *144*, 402–413.

Soltyk, A.M., MacKenzie, C.R., Wolski, V.M., Hirama, T., Kitov, P.I., Bundle, D.R., and Brunton, J.L. (2002). A Mutational Analysis of the Globotriaosylceramide-binding Sites of Verotoxin VT1. Journal of Biological Chemistry *277*, 5351–5359.

Song, D., Meng, J., Cheng, J., Fan, Z., Chen, P., Ruan, H., Tu, Z., Kang, N., Li, N., Xu, Y., et al. (2019). Pseudomonas aeruginosa quorum-sensing metabolite induces host immune cell death through cell surface lipid domain dissolution. Nature Microbiology *4*, 97–111.

Sorre, B., Callan-Jones, A., Manneville, J.-B., Nassoy, P., Joanny, J.-F., Prost, J., Goud, B., and Bassereau, P. (2009). Curvature-driven lipid sorting needs proximity to a demixing point and is aided by proteins. PNAS *106*, 5622–5626.

Sprong, H., van der Sluijs, P., and van Meer, G. (2001). How proteins move lipids and lipids move proteins. Nature Reviews. Molecular Cell Biology *2*, 504.

Svennerholm, L. (1964). The gangliosides. J. Lipid Res. *5*, 145–155.

Sych, T., Mély, Y., and Römer, W. (2018a). Lipid self-assembly and lectin-induced reorganization of the plasma membrane. Philosophical Transactions of the Royal Society B: Biological Sciences *373*, 20170117.

Sych, T., Schubert, T., Vauchelles, R., Madl, J., Omidvar, R., Thuenauer, R., Richert, L., Mély, Y., and Römer, W. (2018b). GUV-AP: multifunctional FIJI-based tool for quantitative image analysis of Giant Unilamellar Vesicles. Bioinformatics.

Tan, R.X., and Chen, J.H. (2003). The cerebrosides. Nat. Prod. Rep. *20*, 509–534.

Tareste, D., Shen, J., Melia, T.J., and Rothman, J.E. (2008). SNAREpin/Munc18 promotes adhesion and fusion of large vesicles to giant membranes. PNAS *105*, 2380–2385.

Tero, R. (2012). Substrate Effects on the Formation Process, Structure and Physicochemical Properties of Supported Lipid Bilayers. Materials *5*, 2658–2680.

Thuenauer, R., Müller, S.K., and Römer, W. (2017). Pathways of protein and lipid receptor-mediated transcytosis in drug delivery. Expert Opinion on Drug Delivery *14*, 341–351.

Tokunaga, M., Imamoto, N., and Sakata-Sogawa, K. (2008). Highly inclined thin illumination enables clear single-molecule imaging in cells. Nature Methods *5*, 159–161.

Tsien, R.Y. (1998). THE GREEN FLUORESCENT PROTEIN. Annual Review of Biochemistry *67*, 509–544.

Tuma, P.L., and Hubbard, A.L. (2003). Transcytosis: Crossing Cellular Barriers. Physiological Reviews *83*, 871–932.

Underhill, D.M., and Goodridge, H.S. (2012). Information processing during phagocytosis. Nat Rev Immunol *12*, 492–502.

Varki, A. (2017). Biological roles of glycans. Glycobiology *27*, 3–49.

Veatch, S.L., and Keller, S.L. (2005). Miscibility Phase Diagrams of Giant Vesicles Containing Sphingomyelin. Physical Review Letters *94*.

Villringer, S., Madl, J., Sych, T., Manner, C., Imberty, A., and Römer, W. (2018). Lectin-mediated protocell crosslinking to mimic cell-cell junctions and adhesion. Scientific Reports *8*.

Vogel, S.K., and Schwille, P. (2012). Minimal systems to study membrane–cytoskeleton interactions. Current Opinion in Biotechnology *23*, 758–765.

Wang, Y., Gkeka, P., Fuchs, J.E., Liedl, K.R., and Cournia, Z. (2016). DPPC-cholesterol phase diagram using coarse-grained Molecular Dynamics simulations. Biochimica et Biophysica Acta (BBA) - Biomembranes *1858*, 2846–2857.

Weinberger, A., Walter, V., MacEwan, S.R., Schmatko, T., Muller, P., Schroder, A.P., Chilkoti, A., and Marques, C.M. (2017). Cargo self-assembly rescues affinity of cell-penetrating peptides to lipid membranes. Scientific Reports *7*, 43963.

Windschiegl, B., Orth, A., Römer, W., Berland, L., Stechmann, B., Bassereau, P., Johannes, L., and Steinem, C. (2009). Lipid Reorganization Induced by Shiga Toxin Clustering on Planar Membranes. PLoS ONE *4*, e6238.

Witkowska, A., Jablonski, L., and Jahn, R. (2018). A convenient protocol for generating giant unilamellar vesicles containing SNARE proteins using electroformation. Scientific Reports *8*.

Xu, J., Sigworth, F.J., and LaVan, D.A. (2010). Synthetic Protocells to Mimic and Test Cell Function. Advanced Materials *22*, 120–127.

Xu, W., Nathwani, B., Lin, C., Wang, J., Karatekin, E., Pincet, F., Shih, W., and Rothman, J.E. (2016). A Programmable DNA Origami Platform to Organize SNAREs for Membrane Fusion. Journal of the American Chemical Society *138*, 4439–4447.

Yang, Y., Wang, J., Shigematsu, H., Xu, W., Shih, W.M., Rothman, J.E., and Lin, C. (2016). Self-assembly of size-controlled liposomes on DNA nanotemplates. Nat Chem *8*, 476–483.

Yilmaz, N., and Kobayashi, T. (2015). Visualization of Lipid Membrane Reorganization Induced by a Pore-Forming Toxin Using High-Speed Atomic Force Microscopy. ACS Nano *9*, 7960–7967.

Yoshida, A., Hayashi, H., Tanabe, K., and Fujita, A. Segregation of phosphatidylinositol 4-phosphate and phosphatidylinositol 4,5-bisphosphate into distinct microdomains on the endosome membrane. Biochimica et Biophysica Acta (BBA) - Biomembranes.

Zaas, D.W., Duncan, M., Rae Wright, J., and Abraham, S.N. (2005). The role of lipid rafts in the pathogenesis of bacterial infections. Biochimica et Biophysica Acta (BBA) - Molecular Cell Research *1746*, 305–313.

Zhang, Z., Yomo, D., and Gradinaru, C. (2017). Choosing the right fluorophore for single-molecule fluorescence studies in a lipid environment. Biochimica et Biophysica Acta (BBA) - Biomembranes *1859*, 1242–1253.

Zheng, S., Eierhoff, T., Aigal, S., Brandel, A., Thuenauer, R., de Bentzmann, S., Imberty, A., and Römer, W. The Pseudomonas aeruginosa lectin LecA triggers host cell signalling by glycosphingolipid-dependent phosphorylation of the adaptor protein CrkII. Biochimica et Biophysica Acta (BBA) - Molecular Cell Research.

VII Publications and manuscripts

In the following, all publications and manuscripts that I contributed to in the context of this thesis are listed and enclosed

First author publications and manuscripts

Sych, T., Mély, Y. and Römer, W., 2018. **Lipid self-assembly and lectin-induced reorganization of the plasma membrane.** *Philosophical Transactions of the Royal Society B: Biological Sciences*, *373*(1747), p.20170117.

Contribution: I contributed to the writing of the review and prepared the figures.

The accepted manuscript of the article is enclosed with permission of the publisher Royal Society.

Sych, T., Schubert, T., Vauchelles, R., Madl, J., Omidvar, R., Thuenauer, R., Richert, L., Mély, Y. and Römer, W., 2018. **GUV-AP: multifunctional FIJI-based tool for quantitative image analysis of Giant Unilamellar Vesicles.** Bioinformatics.

Contribution: I wrote the macro code, performed all experiments, prepared figures and wrote the manuscript.

The accepted manuscript of the article is enclosed with permission of the publisher Oxford Academic.

Sych, T., Schubert, T., Aigal. S., Thuenauer, R., Brandel, A., Omidvar, R., Eierhoff T., Richert, L., Mély, Y, Madl, J., and Römer, W. **The bacterium *Pseudomonas aeruginosa* perishes membrane organization by its lectin LecA** [*Manuscript in preparation*]

Contribution: I performed all experiments, prepared figures and wrote the manuscript.

The manuscript is enclosed.

Co - author manuscript

Schubert, T., Sych, T., Madl, J., Xu M., Brandel A., Omidvar R., Patalag L., Ries A., Kattelhoit K., Mely Y., Steinem C., Werz D., Thuenauer, R. and Römer, W. **Differential recognition of lipid domains by two Gb3-binding lectins** [*Manuscript in preparation*]

Contribution: I performed some experiments for the figures 2 and 4, I analyzed data and contributed to the writing of the manuscript.

The manuscript is enclosed

Other publications without context to this thesis

Villringer, S., Madl, J., Sych, T., Manner, C., Imberty, A. and Römer, W., 2018. **Lectin-mediated protocell crosslinking to mimic cell-cell junctions and adhesion.** *Scientific reports*, *8*(1), p.1932.

Zamotaiev, O.M., Shvadchak, V., Sych, T.P., Melnychuk, N.A., Yushchenko, D., Mely, Y. and Pivovarenko, V.G., 2016. **Environment-sensitive quinolone demonstrating long-lived fluorescence and unusually slow excited-state intramolecular proton transfer kinetics.** *Methods and applications in fluorescence*, *4*(3), p.034004.

Baaken, G., Zaitseva, E., Petersen, S., Sych, T., Stefan, K. and Behrends, J.C., 2019. **Array of Freestanding Planar Lipid Bilayers for Parallel Optical and Electrical Recordings.** *Biophysical Journal*, *116*(3), pp.294a-295a.

Lipid self-assembly and lectin-induced reorganisation of the plasma membrane

Taras Sych[1,2,3,4], Yves Mély[4] and Winfried Römer[1,2,3]

[1] Faculty of Biology, Albert-Ludwigs-University Freiburg, Schänzlestraße 1, 79104 Freiburg, Germany

[2] Centre for Biological Signalling Studies (BIOSS), Albert-Ludwigs-University Freiburg, Schänzlestraße 18, 79104 Freiburg, Germany

[3] Freiburg Center for Interactive Materials and Bioinspired Technology (FIT), Albert-Ludwigs-University Freiburg, Georges-Köhler-Allee 105, 79110 Freiburg, Germany

[4] Laboratoire de Bioimagerie et Pathologies, UMR 7021 CNRS, Faculté de Pharmacie Université de Strasbourg 67401 Illkirch Cedex France

Abstract

The plasma membrane represents an outstanding example of self-organisation in biology. It plays a vital role in protecting the integrity of the cell interior and regulates meticulously the import and export of diverse substances. Its major building blocks are proteins and lipids, which self-assemble to a fluid lipid bilayer driven mainly by hydrophobic forces. Even if the plasma membrane appears - globally spoken - homogeneous at physiological temperatures, the existence of specialised nano- to micrometer-sized domains of raft-type character within cellular and synthetic membrane systems has been reported. It is hypothesized that these domains are the origin of a plethora of cellular processes, such as signalling or vesicular trafficking.

This review intends to highlight the driving forces of lipid self-assembly into a bilayer membrane and the formation of small, transient domains within the plasma membrane. The mechanisms of self-assembly depend on several factors, such as the lipid composition of the membrane and the geometry of lipids. Moreover, the dynamics and organisation of glycosphingolipids into nanometer-sized clusters will be discussed, also in the context of multivalent lectins, which cluster several glycosphingolipid receptor molecules and thus create an asymmetric stress between the two membrane leaflets, leading to tubular plasma membrane invaginations.

1) The plasma membrane

The plasma membrane physically separates the cytoplasm of living cells from the extracellular environment and hence maintains the physical integrity of the cell. It acts as a barrier, which is selectively permeable to ions and organic molecules, and regulates transport processes into and out of the cell (1). The plasma membrane is involved in a multitude of cellular processes, such as signalling and adhesion, amongst others (2,3). It also helps to hold the cytoskeleton in place to preserve the cell shape (4). With respect to all these diverse functions, it sounds amazing that the plasma membrane represents a lipid matrix with a thickness of only 4-6 nm, with embedded integral and peripheral proteins (5,6). The principles how membrane lipids self-assemble into cell membranes and how lipid-lipid interactions lead to the formation of small, transient domains within the membrane will be outlined in the following.

2) Self-organisation of lipids in aqueous solutions

The plasma membrane consists of a complex mixture of components, among which lipids are the major building blocks. Plasma membranes contain a large number of different types of lipids that form a lipid bilayer with an inner (cytosolic) and an outer (extracellular) membrane leaflet (7). Lipids exhibit an impressive diversity of properties and can be classified by their geometry (8), as well as by the type of assembly they form in contact with water.

Since lipids contain a hydrophilic (polar head group) and a hydrophobic part (fatty acyl chain) they are considered as amphiphilic molecules. Exposed to water, lipids compact their hydrophobic parts in the energetically most favourable way, forming a hydrophobic core (9). This simple principle is underlying the self-organisation of lipids in an aqueous environment, e.g. in living cells as well as in artificial membrane systems.

As indicated by Israelachvili (10,11), the lipid behaviour in aqueous solution can be easily predicted by taking into consideration the geometrical parameters of its hydrophobic and hydrophilic parts. These are v, the volume of the nonpolar part, l, the length of the nonpolar part and a_0, the optimal surface area of the polar head group. The parameters v and l can be simply determined by the lipid size and shape (11,12). The determination of the parameter a_0 is less straightforward. The possible repulsive interactions between head groups and parameters of the aqueous environment (ionic strength, pH) have to be taken into account. This factor is particularly critical for charged lipids, e.g. phosphatidylserine (PS) or phosphatidylglycerol (PG), where the head groups have to be far enough from each other that Coulomb's repulsive forces are equilibrated by lipid-lipid interactions.

One of the potential assembly modes of lipid molecules in water is the formation of spherical micelles (Figure 1) (12). If a spherical micelle is built up of N lipid molecules, the total micelle surface area a_M and the volume of the micelle V_M can be determined as:

$$a_M = Na_0 = 4\pi R_m^2$$
$$V_M = Nv = 4/3\pi R_m^3$$

Hence, the radius of the micelle R_m can be expressed as:

$$R = 3v/a_0$$

Since $R_m \leq l$ for spherical micelles, the following equation accounts:

$$v/la_0 \leq 1/3$$

The expression of v/la_0 is called the *critical packing parameter*.

The interconnection between these three parameters determines the geometry of the lipid molecule and its behaviour in water. Using the same logic, the value of the *critical packing parameter* for a lipid bilayer can be obtained.

Lipids can be classified by their shapes into three major groups (Figure 1):

A) Inverted cone-shaped lipids ($v/la_0 < 1/2$), which form micellar phases with positive curvature in water. This group comprises mainly lipids with a single fatty acyl chain, such as lysophospholipids. To assemble as spherical micelles, the *critical packing parameter* of lipids has to be below 1/3, whereas lipids with $1/3 < v/la_0 < 1/2$ assemble as cylindrical micelles. The relevance of this type of lipids in native cell membranes is most obvious for pore formation (13) or vesicle budding (14).

B) Cone-shaped lipids ($v/la_0 > 1$), which self-organise in so-called hexagonal micellar phases of negative curvature (in acidic environment). This group of lipids includes mainly unsaturated lipids, which participate in uptake processes where the cell membrane is bended inwards (15).

C) Cylinder-shaped lipids ($1/2 < v/la_0 \leq 1$), which assemble into a lipid bilayer that forms a lamellar phase when assembled in stacks. These lipids that are characterized by two fatty acyl chains of different length and saturation degree represent probably the most important group of membrane lipids and form the fluid lipid matrix of the cell membrane. They can assemble into flexible lipid bilayers of liposomes ($1/2 < v/la_0 < 1$) as well as planar lipid bilayers ($v/la_0 \approx 1$).

In addition, factors such as the ion composition of aqueous solutions, pH or temperature can alter the lipid geometric parameters, and as a result, the assembly of lipids (11).

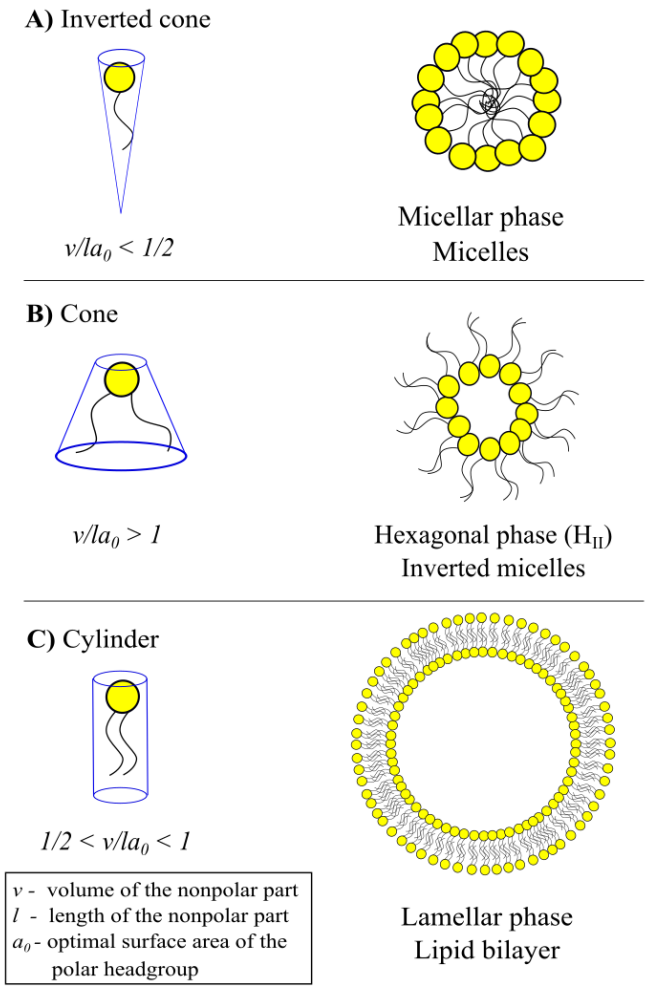

Figure 1: **Self-assembly of lipids in contact with water.** Lipids are characterised by their *critical packing parameter* v/la_0. **A)** Inverted cone-shaped lipids form micelles (micellar phase) of positive curvature. **B)** Cone-shaped lipids assemble into different structures of hexagonal (H_{II}) phase. **C)** Cylinder-shaped lipids form a lamellar phase.

A lipid bilayer can undergo solid-liquid phase transition , also referred to as main phase transition or chain-melting transition (16,17). Depending on the lipid, the main phase transition temperature varies from -17 ºC for unsaturated lipids, like dioleoylphosphatidylcholine (DOPC), up to 37 ºC for sphingomyelin (SM) with long saturated acyl chains (18). Glycolipids with sugar moieties have even higher solid-liquid phase transition temperatures (19). Lipid phase transitions have been intensively studied for already more than 50 years (20–22) using a large variety of techniques, such as X-ray diffraction (23), calorimetry (22), atomic force microscopy (AFM) (24) or fluorescence techniques on different membrane model systems (25,26). The length and saturation degree of the fatty acyl chain determines not only the temperature of the solid-liquid phase transition but also the degree of packing in the liquid phase. Quantitatively, this degree of packing can be described using the so-called acyl

chain order parameter. Lipids with a low value of order parameter form a bilayer phase of low order and high mobility, known as liquid-disordered (Ld) phase (7). Lipids that form Ld phases are mainly unsaturated phospholipids (Figure 2). In contrast, bilayers formed of long-chain saturated lipids, like sphingomyelin, adopt a solid-like phase of high order and low mobility. Addition of sterols, such as cholesterol, renders the solid-like membrane more mobile turning it into a liquid phase. This phase is called the liquid-ordered (Lo) phase as the order still remains high. Interestingly, addition of cholesterol enhances acyl chain order in Ld-membranes (7,27,28).

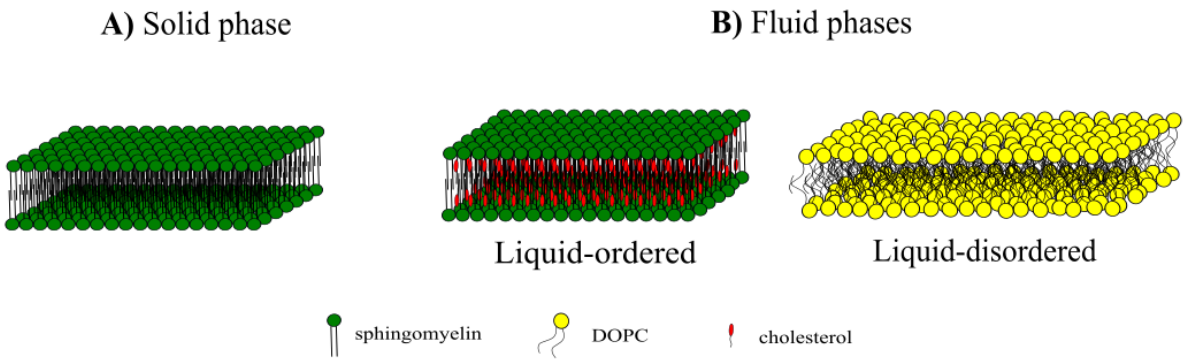

Figure 2: **Lipid bilayer phases.** Depending on the lipid composition, temperature and order parameters, the lamellar phase can adopt solid or fluid phases. **A)** Lipid bilayer of solid phase composed of sphingomyelin. **B)** Lipid bilayer of fluid phases can exist as liquid-ordered (composed of sphingomyelin and cholesterol) or liquid-disordered (composed of DOPC).

A lipid bilayer can contain spatially separated domains of different lipid phases. In binary mixtures composed of lipid species of low melting temperature (e.g. DOPC) and of high melting temperature (e.g. sphingomyelin), the bilayer exhibits spatial phase separation into solid and liquid-disordered phase domains. The temperature is the crucial factor for this process; phase separation can occur only at temperatures in between the main phase transition temperatures of the two lipids. Moreover, the coexistence of all three - Ld, Lo and solid phase - domains is possible by the addition of cholesterol (29). Remarkable is the preference of cholesterol to associate with sphingolipids and partition in sphingomyelin-containing Lo phases (30–32). Furthermore, phase separation can be reversed by increasing the lipid entropy (e.g. by increasing the temperature).

3) Higher-order organisation of lipids within the plasma membrane

To describe the structure of biological membranes, Singer and Nicolson introduced the fluid mosaic model in 1972 (33,34). According to this model, the cell membrane is considered as a two-dimensional liquid arranged as a lipid bilayer with homogeneously distributed proteins. Lipids in a

lipid bilayer are in continuous motion. In addition to translational diffusion (microseconds) and rotational movement (picoseconds - nanoseconds), they can flip from one leaflet to the other (milliseconds - seconds), or exhibit undulation movements (milliseconds - seconds), which are induced by transmembrane proteins or cytoskeleton (35–37). Further studies of biological membranes based on the use of detergents revealed the separation of the so-called detergent-resistant membrane (DRM) fractions, enriched in particular with sphingomyelin and cholesterol, from detergent-soluble membrane (DSM) fractions, enriched with rather unsaturated membrane phospholipids (38). Based on these and other important findings, the "lipid raft" theory was introduced by Simons and Ikonen in 1997 (39). According to this theory, the membrane is no longer a homogeneous fluid, where all components are randomly distributed, but contains highly ordered lipid (micro-) domains stabilized by sphingomyelin and cholesterol (Figure 3A). Lipid rafts are also enriched with (transmembrane) proteins and glycolipids, and are thought to play a key role in cell signalling, uptake and release (40–42). Further studies of membrane asymmetry revealed even more complicated structures of raft and non-raft membranes (43). Sphingomyelin-enriched rafts form mainly in the extracellular membrane leaflet while the cytosolic leaflet contains in total less than 10 % of all membrane sphingomyelin molecules (44–46). Consequently, the cytosolic leaflet is less viscous and does not sustain the formation of lipid rafts (47). In general, the cytosolic leaflet is enriched with lipids, such as phosphatidylinositol (PI), phosphatidylethanolamine (PE) and phosphatidylserine (PS). Remarkably, lipid raft-embedded GPI-anchored proteins in the extracellular leaflet interdigitate with PS clusters in the cytosolic membrane leaflet (48). Saturated PC lipids are found in the extracellular membrane leaflet.

The lipid raft theory is in line with data obtained from viral membranes. It was found that the HIV envelope is enriched in host cell sphingolipids and cholesterol, the typical lipid raft components (49). This suggested that the assembly of HIV Gag proteins at the cytosolic leaflet of the cell membrane induces the accumulation of lipid rafts on the extracellular leaflet, so that the HIV envelope consists mainly of raft-like membrane after virus release (50). This strengthens the significance of lipid rafts as important signalling platforms for diverse cellular processes (6,51).

The size and lifetime of lipid rafts are far below the spatial and temporal resolution of most conventional microscopy techniques, which makes a direct visualisation of these domains in cell membranes nearly impossible (52). Though impressive progress in fluorescence microscopy has been made with the development of advanced techniques that offer high temporal and spatial resolution (52–56), membrane nano-domains can hardly be visualised.

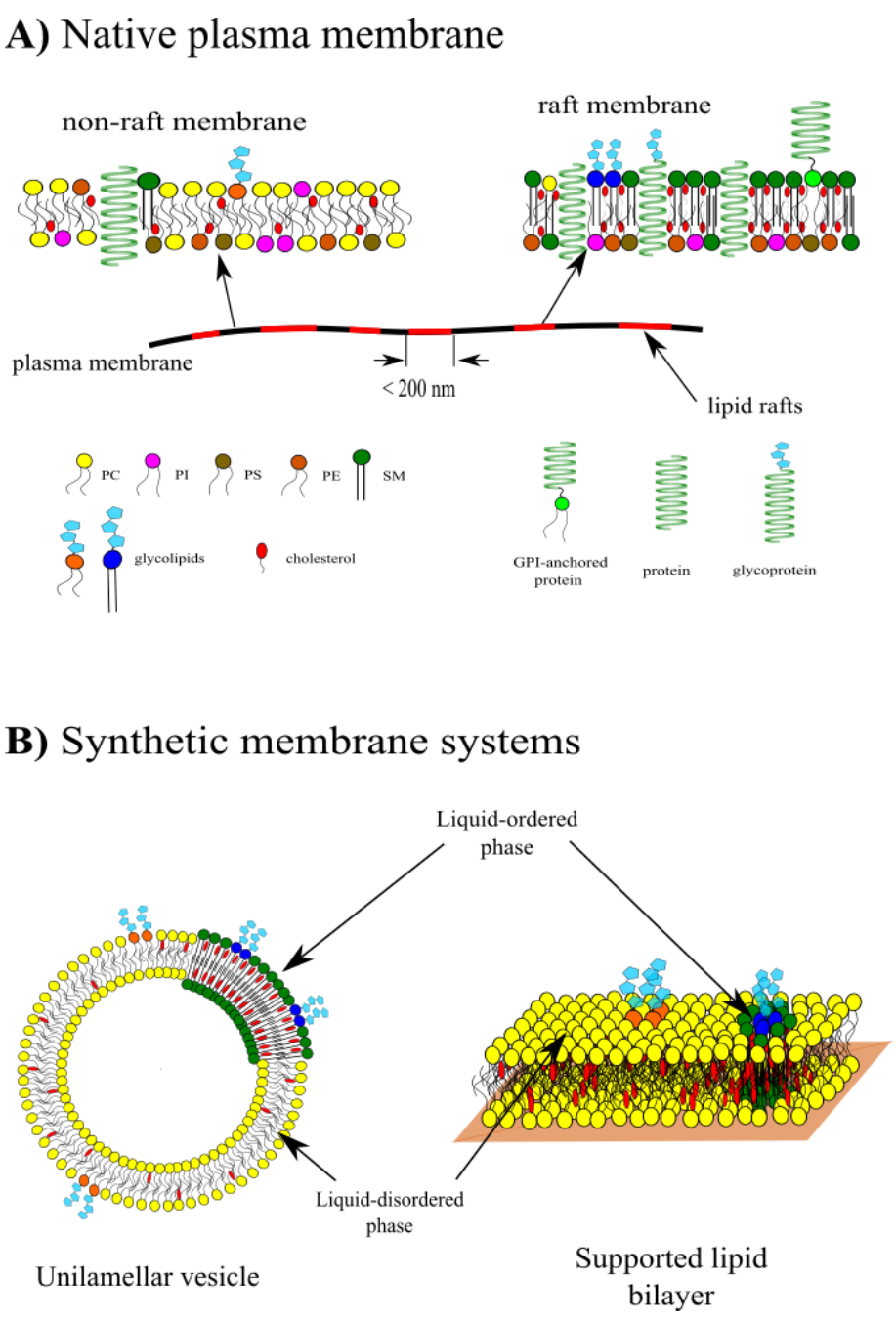

Figure 3: **From lipid rafts in native plasma membranes to liquid-ordered phases in synthetic membrane systems. A)** Composition of raft and non-raft types of native plasma membranes. The membrane is asymmetrical – the extracellular membrane leaflet is enriched with SM and saturated PC lipids, while PS, PI and PE lipids associate mainly to the cytosolic leaflet. **B)** Synthetic membrane systems composed of liquid membrane domains to mimic native membrane phases. The liquid-ordered domain mimics a lipid raft membrane and the liquid-disordered domain mimics a non-raft membrane. In synthetic membrane systems, lipids self-assemble into a lipid bilayer mainly in a symmetric manner. PC: phosphatidylcholine; PS: phosphatidylserine; PI: phosphatidylinositol; PE: phosphatidyl-ethanolamine; SM: sphingomyelin.

Plasma membrane organisation can be also explored in less dynamic systems with compositions close to native ones. This type of membrane systems, e.g. giant plasma membrane vesicles (57), plasma membrane spheres, or plasma membrane sheets (58) can be extracted from living cells by cell membrane disruption.

For elucidating the role of distinct membrane components, synthetic membrane systems (Figure 3B), such as unilamellar vesicles (59,60), supported (61) or pore-suspending (62) lipid bilayers, are employed. The main advantage of synthetic membrane systems is the possibility to adjust the lipid and/or protein content in order to prepare membranes of different properties. These systems are widely used to study the organisation of lipid bilayer phases (e.g. Lo and Ld) (63), membrane pore formation (64) and uptake processes (65). Reconstitution of Lo domains using lipids found in DRMs (e.g. sphingomyelin and cholesterol, in distinct ratios) enables mimicking some properties of lipid rafts at the microscopic scale. Various cellular processes (e.g. transport across the plasma membrane or induction of signalling events) require local reorganisation of the plasma membrane. For instance, extracellular (e.g. pore forming proteins (66–68) and cell penetrating peptides (69,70)) and cytosolic (e.g. actin (71,72), clathrin (73), BAR domains (74,75)) components can alter the lipid distribution within the lipid bilayer.

In this review, we focus on the membrane reorganisation driven by specific interactions of carbohydrate binding proteins (so-called lectins) with glycosphingolipids, their host cell receptors.

4) Glycosphingolipids self-organise in small clusters

Glycosphingolipids (GSLs) play crucial roles in intercellular communication and uptake processes, amongst others (76). The GSL content in cell membranes varies from 5% to more than 20% (77). GSLs are mainly found in the extracellular membrane leaflet – the hydrophobic ceramide backbone being embedded in the lipophilic part of the membrane and the carbohydrate moieties being exposed to the extracellular environment (78). The majority of GSLs is reported to be enriched in lipid rafts (5,39,79–81), where they associate with sphingomyelin and cholesterol. In addition, AFM studies as well as MD simulations have revealed the capability of GSLs to form separate clusters in lipid raft-like membranes (82–85). Variations in the length and saturation degree of the fatty acyl chain of the ceramide backbone affect the orientation and partitioning of GSLs in the lipid monolayer (86,87), and hence the exposure of the carbohydrate group rendering it partially inaccessible for ligands (88,89). GSL assemblies can modify locally membrane order and curvature, which is of high significance for various uptake processes. The long ceramide backbones of GSLs are also important elements for transbilayer coupling and communication since they interdigitate the two membrane leaflets (90).

5) Lectin-induced glycosphingolipid clustering re-organises the plasma membrane

Besides their natural functions, glycosphingolipids are hijacked by various pathogens (e.g. bacteria and viruses) (91–93) and pathogenic products (e.g. toxins, lectins) (94,95). Lectins (96) can either be soluble, prearranged as a viral capsid or attached to the outer bacterial membrane. They bind to the carbohydrate moieties of glycosphingolipids (97), either by targeting preformed glycosphingolipid domains or by inducing domains by local recruitment of receptor molecules underneath their oligomeric structures (94). Thereby, asymmetric stress between the extracellular and cytosolic membrane leaflets can lead to inward bending of the cell membrane and growth of tubular plasma membrane invaginations (94).

a) Toxins/ lectins act as clustering devices and generate membrane curvature

Based on cellular as well as synthetic membrane systems, it has been demonstrated that oligomeric toxins/ lectins bind to and cluster host cell glycosphingolipids, which leads to the formation of tubular plasma membrane invaginations as endocytic transport intermediates. For instance, the homopentameric B-subunit of Shiga toxin (StxB) from *Shigella dysenteriae* recognizes specifically the carbohydrate moieties of the GSL globotriaosylceramide (Gb3) on the extracellular membrane leaflet. Up to 15 Gb3 receptor molecules can interact with one toxin pentamer (98). This multivalent binding leads to Gb3 clustering and membrane reorganisation (99). Thus, the entropy of the system decreases together with lipid mobility (100), while the membrane order increases locally (85,101). StxB-induced Gb3 clustering modifies the area per lipid in the outer membrane leaflet. This creates asymmetric stress in the bilayer, and consequently a membrane tubule nucleates (102). Such a mechanism is probably in common for the cellular uptake of many oligomeric lectins (94,103,104). Nevertheless, the mechanism of lectin clustering on the extracellular membrane surface remains debated. Different reports claim that this process is either driven by capillary effect (105), by entropy modification of the lipid bilayer hydrophobic bulk (102,106) or by local lectin-induced curvature (107). However, Pezeshkian et al. (108) suggested that neither of these factors is critical and that multi-molecular lectin clustering is more likely related to membrane fluctuation-induced forces. Multiple carbohydrate binding sites of lectins ensure their efficient binding to GSLs and clustering on the membrane surface to induce cellular signalling and uptake processes. In order to explore the impact of lectin valency and binding site geometry on the induction of cellular processes, distinct carbohydrate binding sites of lectins have been modified by site-directed mutagenesis (94,99,103,109), and tailor-made neolectins have been designed (110). In comparison to the natural lectin RSL from *Ralstonia solanacearum*, which is trimeric and hexavalent, a divalent, monomeric neolectin, which is highly similar in structure, was sufficient to induce tubular membrane invaginations on giant unilamellar vesicles by binding to a fucosylated glycolipid receptor. Amazingly, only the divalent neolectin with two carbohydrate binding sites nearby was able to form membrane invaginations whereas divalent neolectins with more distant binding sites did not, even though their binding constants were quite similar (110).

b) Toxins/ lectins generate membrane curvature

Membrane curvature changes are the response to external or internal perturbations of the membrane, such as osmotic effects (111), membrane fusion (112), vesicle budding (113) or endocytosis (113–115). For instance, lectin-GSL interactions induce spontaneous curvature leading to tubular plasma membrane invaginations, which are energetically favourable. The efficiency of curvature induction and tubule formation depends on membrane rigidity and composition. In case of membranes with low rigidity, small protein clusters can initiate tubule nucleation, while in the case of membranes with higher rigidity larger protein clusters are required to bend the membrane (116,117). Once initiated, the endocytic membrane tubule grows and sequesters lectin molecules on its negatively bended surface. With increasing lectin concentrations inside the tubule, a highly curved bud forms (114) that finally undergoes scission. In living cells, bud formation and scission can be significantly facilitated by the assembly of clathrin, actin (115) or BAR proteins at the cytosolic leaflet of the membrane (75,118).

6) Lectin- and curvature-driven lipid sorting as membrane reorganisation process

Lipid sorting was reported for multicomponent lipid mixtures (119), where an interplay between membrane entropic forces and lipid-lipid interactions takes place. In such systems, like ternary mixtures close to phase separation (119,120), lipid sorting can be triggered by a change in temperature or lipid composition. When an oligomeric lectin binds to GSLs, it acts like a clustering device (Figure 4A, B) that can activate lipid sorting and induce phase separation in otherwise homogeneously mixed membranes (101,120–123). Local asymmetric stress imposed by lectin-GSL interactions, and subsequent membrane deformation can change locally the lipid organisation of the bilayer. Pinot et al. (124) highlighted the importance of polyunsaturated, cone-shaped phospholipids in those uptake processes. Such lipids can adapt their conformation to the membrane curvature and may support endocytosis (65,124). Besides, curvature-driven lipid sorting may trigger the redistribution of membrane lipids based on their molecular geometry. However, numerous studies (119,125–129) demonstrated that such curvature-driven lipid sorting is effective only in presence of membrane-bound or transmembrane proteins, otherwise entropy homogenises the lipid distribution even in highly curved membranes. The lipid composition of plasma membrane tubules is still elusive. Pulling a membrane tether from giant unilamellar vesicles using a micropipette (119,120,130) showed that tethers are enriched with unsaturated lipids, strongly arguing for their implication in tubule formation (130). However, as GSL clusters are associated with sphingomyelin, lectin-induced tubules may also contain saturated sphingolipids (101,130). Hence, successful tubule formation should involve an interplay between GSL clustering and attraction of saturated lipids (Figure 4C).

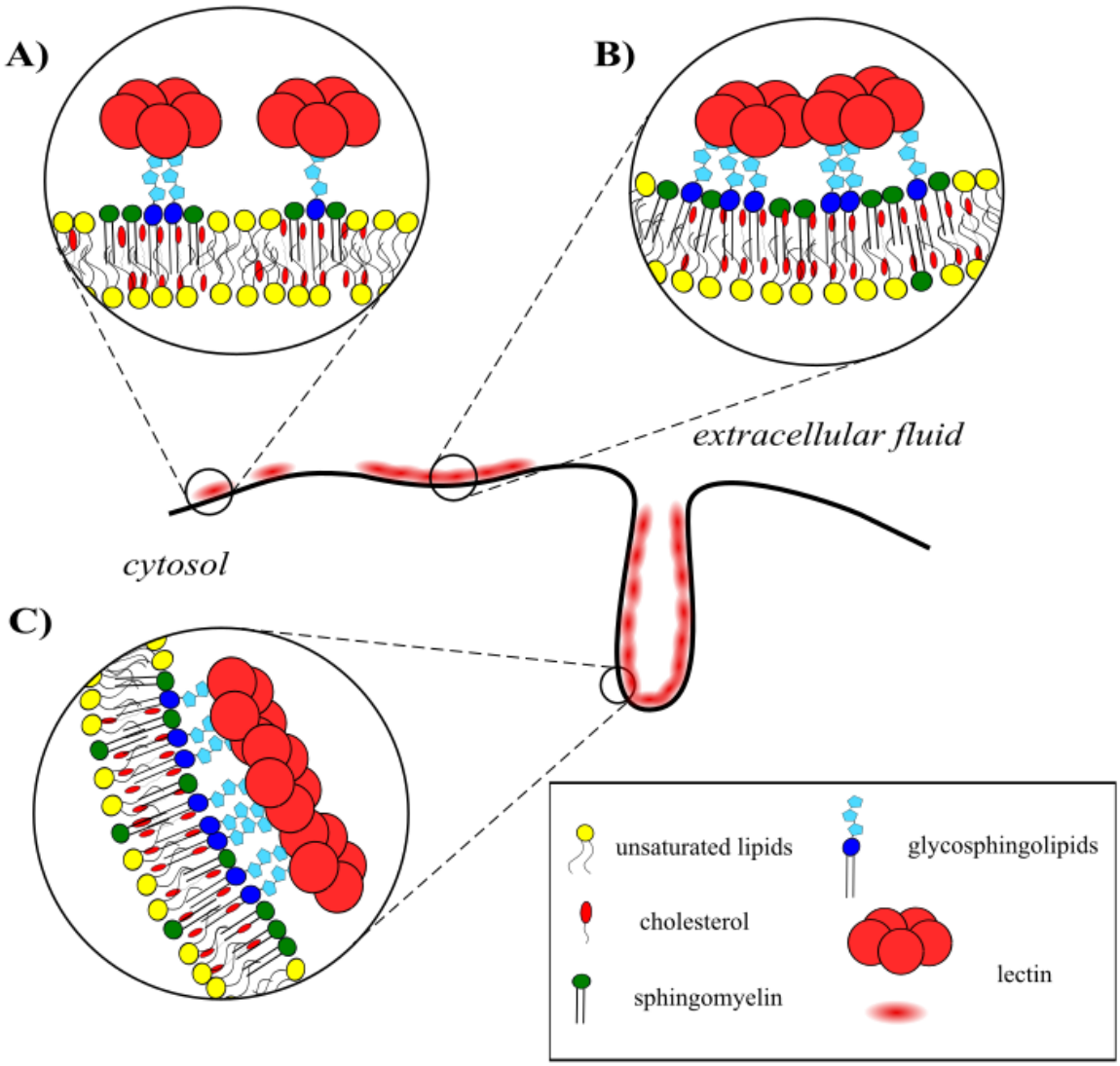

Figure 4: **Lectin- and curvature-driven lipid sorting. A)** Lectins recognise GSL receptors and bind to the membrane surface. **B)** Lectins crosslink the GSL-enriched clusters. These clusters induce an asymmetric stress in the membrane, which leads to tubule nucleation and plasma membrane invagination. **C)** Lectin-induced plasma membrane tubules are enriched with sphingolipids due to their association with GSL clusters.

7) Conclusions

The plasma membrane is an exciting example of self-organisation in nature. Although many discoveries have been made concerning lipid self-assembly into a bilayer and the organisation of distinct lipids into functional units within the plasma membrane, the exact membrane organisation and its dynamics are still ill-defined. Synthetic membrane models are helpful tools in mimicking, and hence understanding plasma membrane organisation and dynamics, but one should not forget that the

plasma membrane is a highly complex, asymmetric bilayer system consisting of a huge variety of lipid species that fulfil specific functions. Further improvements in microscopy techniques, in particular in super resolution live cell microscopy, as well as in the development of novel lipid labelling and detection methods are required to better decipher the principles of dynamic membrane organisation.

Acknowledgements

This work was supported by the Excellence Initiative of the German Research Foundation [EXC 294] and the German Research Foundation grant [IRTG 1642 - Soft Matter Science: Concepts for the design of functional materials]. TS acknowledges the support by the Franco-German University (PhD-track program "Polymer Sciences" and the program “Cotutelle de thèse”) and the Collège doctoral européen (Programme doctoral international). We are grateful to Toshihide Kobayashi for proof-reading of the manuscript.

References

1. Conner SD, Schmid SL. Regulated portals of entry into the cell. Nature. 2003 Mar 6;422(6927):37-44.
2. Hynes RO. Integrins: versatility, modulation, and signaling in cell adhesion. Cell. 1992 Apr 3;69(1):11-25.
3. Schlessinger J. Cell signaling by receptor tyrosine kinases. Cell. 2000 Oct 13;103(2):211-25.
4. Pollard TD, Cooper JA. Actin, a central player in cell shape and movement. Science. 2009 Nov 27;326(5957):1208-12.
5. Simons K, Toomre D. Lipid rafts and signal transduction. Nat. Rev. Mol. Cell Biol. 2001 Mar;2(216.10):1038.
6. Sezgin E, Levental I, Mayor S, Eggeling C. The mystery of membrane organization: composition, regulation and roles of lipid rafts. Nature Reviews Molecular Cell Biology. 2017 Mar 30.
7. Van Meer G, Voelker DR, Feigenson GW. Membrane lipids: where they are and how they behave. Nature reviews Molecular cell biology. 2008 Feb 1;9(2):112-24.
8. Cooke IR, Deserno M. Coupling between lipid shape and membrane curvature. Biophysical journal. 2006 Jul 15;91(2):487-95.
9. Tanford C. Theory of micelle formation in aqueous solutions. The Journal of Physical Chemistry. 1974 Nov;78(24):2469-79.
10. Israelachvili JN, Mitchell DJ, Ninham BW. Theory of self-assembly of lipid bilayers and vesicles. Biochimica et Biophysica Acta (BBA)-Biomembranes. 1977 Oct 17;470(2):185-201.
11. Israelachvili JN. Intermolecular and surface forces. Academic press; 2011 Jul 22.
12. Gennis RB, editor. Biomembranes: molecular structure and function. Springer Science & Business Media; 2013 Apr 17.
13. Reusch R. Biogenesis of ion channels. J. Biochem. Biophys. 2014;1:1-24.

14. Sprong H, van der Sluijs P, van Meer G. How proteins move lipids and lipids move proteins. Nature Reviews Molecular Cell Biology. 2001 Jul 1;2(7):504-13.
15. Jouhet J. Importance of the hexagonal lipid phase in biological membrane organization. Frontiers in plant science. 2013;4.
16. Reinert JC, Steim JM. Calorimetric detection of a membrane-lipid phase transition in living cells. Science. 1970 Jun 26;168(3939):1580-2.
17. Simons K, Vaz WL. Model systems, lipid rafts, and cell membranes. Annu. Rev. Biophys. Biomol. Struct.. 2004 Jun 9;33:269-95.
18. Caffrey M, Hogan J. LIPIDAT: A database of lipid phase transition temperatures and enthalpy changes. DMPC data subset analysis. Chemistry and physics of lipids. 1992 Mar 1;61(1):1-09.
19. Kociurzynski R, Pannuzzo M, Böckmann RA. Phase transition of glycolipid membranes studied by coarse-grained simulations. Langmuir. 2015 Aug 19;31(34):9379-87.
20. Lee AG. Lipid phase transitions and phase diagrams I. Lipid phase transitions. Biochimica et Biophysica Acta (BBA)-Reviews on Biomembranes. 1977 Aug 9;472(2):237-81.
21. Lee AG. Lipid phase transitions and phase diagrams II. Mixtures involving lipids. Biochimica et Biophysica Acta (BBA)-Reviews on Biomembranes. 1977 Nov 14;472(3-4):285-344.
22. Mabrey S, Sturtevant JM. Investigation of phase transitions of lipids and lipid mixtures by sensitivity differential scanning calorimetry. Proceedings of the National Academy of Sciences. 1976 Nov 1;73(11):3862-6.
23. Kjaer K, Als-Nielsen J, Helm CA, Laxhuber LA, Möhwald H. Ordering in lipid monolayers studied by synchrotron x-ray diffraction and fluorescence microscopy. Physical review letters. 1987 May 25;58(21):2224.
24. Leonenko ZV, Finot E, Ma H, Dahms TE, Cramb DT. Investigation of temperature-induced phase transitions in DOPC and DPPC phospholipid bilayers using temperature-controlled scanning force microscopy. Biophysical journal. 2004 Jun 30;86(6):3783-93.
25. Carravilla P, Nieva JL, Goñi FM, Requejo-Isidro J, Huarte N. Two-photon Laurdan studies of the ternary lipid mixture DOPC: SM: cholesterol reveal a single liquid phase at sphingomyelin: cholesterol ratios lower than 1. Langmuir. 2015 Feb 25;31(9):2808-17.
26. De Almeida RF, Fedorov A, Prieto M. Sphingomyelin/phosphatidylcholine/cholesterol phase diagram: boundaries and composition of lipid rafts. Biophysical journal. 2003 Oct 31;85(4):2406-16.
27. Veatch SL, Keller SL. Miscibility phase diagrams of giant vesicles containing sphingomyelin. Physical review letters. 2005 Apr 13;94(14):148101.
28. Maxfield FR, Tabas I. Role of cholesterol and lipid organization in disease. Nature. 2005 Dec 1;438(7068):612-21.
29. Aufderhorst-Roberts A, Chandra U, Connell SD. Three-Phase Coexistence in Lipid Membranes. Biophysical journal. 2017 Jan 24;112(2):313-24.
30. Busto JV, García-Arribas AB, Sot J, Torrecillas A, Gómez-Fernández JC, Goni FM, Alonso A. Lamellar gel (L β) phases of ternary lipid composition containing ceramide and cholesterol. Biophysical journal. 2014 Feb 4;106(3):621-30.
31. Sodt AJ, Sandar ML, Gawrisch K, Pastor RW, Lyman E. The molecular structure of the liquid-ordered phase of lipid bilayers. Journal of the American Chemical Society. 2014 Jan 3;136(2):725-32.
32. Brown DA, London E. Structure and origin of ordered lipid domains in biological membranes. Journal of Membrane Biology. 1998 Jul 24;164(2):103-14.

33. Singer SJ, Nicolson GL. The fluid mosaic model of the structure of cell membranes. Science. 1972 Feb 18;175(4023):720-31.
34. Nicolson GL. The Fluid—Mosaic Model of Membrane Structure: Still relevant to understanding the structure, function and dynamics of biological membranes after more than 40years. Biochimica et Biophysica Acta (BBA)-Biomembranes. 2014 Jun 30;1838(6):1451-66.
35. Vermeer LS, De Groot BL, Réat V, Milon A, Czaplicki J. Acyl chain order parameter profiles in phospholipid bilayers: computation from molecular dynamics simulations and comparison with 2H NMR experiments. European Biophysics Journal. 2007 Nov 1;36(8):919-31.
36. Gov N. Membrane undulations driven by force fluctuations of active proteins. Physical review letters. 2004 Dec 20;93(26):268104.
37. Sackmann E. Supported membranes: scientific and practical applications. Science-AAAS-Weekly Paper Edition. 1996 Jan 5;271(5245):43-8.
38. Seddon AM, Curnow P, Booth PJ. Membrane proteins, lipids and detergents: not just a soap opera. Biochimica et Biophysica Acta (BBA)-Biomembranes. 2004 Nov 3;1666(1):105-17.
39. Simons K, Ikonen E. Functional rafts in cell membranes. Nature. 1997 Jun 5;387(6633):569-72.
40. Simons K, Gerl MJ. Revitalizing membrane rafts: new tools and insights. Nature reviews Molecular cell biology. 2010 Oct 1;11(10):688-99.
41. Levental I, Grzybek M, Simons K. Raft domains of variable properties and compositions in plasma membrane vesicles. Proceedings of the National Academy of Sciences. 2011 Jul 12;108(28):11411-6.
42. Lingwood D, Simons K. Lipid rafts as a membrane-organizing principle. Science. 2010 Jan 1;327(5961):46-50.
43. van Meer G. The different hues of lipid rafts. Science. 2002 May 3;296(5569):855-7.
44. Rothman JE, Lenard J. Membrane asymmetry. Science. 1977 Feb 25;195(4280):743-53.
45. Devaux PF. Static and dynamic lipid asymmetry in cell membranes. Biochemistry. 1991 Feb;30(5):1163-73.
46. Ingólfsson HI, Melo MN, van Eerden FJ, Arnarez C, Lopez CA, Wassenaar TA, Periole X, de Vries AH, Tieleman DP, Marrink SJ. Lipid organization of the plasma membrane. Journal of the american chemical society. 2014 Oct 1;136(41):14554-9.
47. Devaux PF, Morris R. Transmembrane asymmetry and lateral domains in biological membranes. Traffic. 2004 Apr 1;5(4):241-6.
48. Raghupathy R, Anilkumar AA, Polley A, Singh PP, Yadav M, Johnson C, Suryawanshi S, Saikam V, Sawant SD, Panda A, Guo Z, Vishwakarma RA, Rao M, Mayor S. Transbilayer lipid interactions mediate nanoclustering of lipid-anchored proteins. Cell. 2015 Apr 23;161(3):581-94.
49. Ono A, Freed EO. Plasma membrane rafts play a critical role in HIV-1 assembly and release. Proceedings of the National Academy of Sciences. 2001 Nov 20;98(24):13925-30.
50. Vlach J, Saad JS. Structural and molecular determinants of HIV-1 Gag binding to the plasma membrane. Frontiers in microbiology. 2015;6.
51. Rajendran L, Simons K. Lipid rafts and membrane dynamics. Journal of cell science. 2005 Mar 15;118(6):1099-102.
52. Sezgin E. Super-resolution optical microscopy for studying membrane structure and dynamics. Journal of Physics: Condensed Matter. 2017 May 8.

53. Owen DM, Neil MA, French PM, Magee AI. Optical techniques for imaging membrane lipid microdomains in living cells. Seminars in cell & developmental biology 2007 Oct 31 (Vol. 18, No. 5, pp. 591-598). Academic Press.
54. Kwiatek JM, Hinde E, Gaus K. Microscopy approaches to investigate protein dynamics and lipid organization. Molecular membrane biology. 2014 Aug 1;31(5):141-51.
55. Klymchenko AS, Kreder R. Fluorescent probes for lipid rafts: from model membranes to living cells. Chemistry & biology. 2014 Jan 16;21(1):97-113.
56. Eggeling C, Ringemann C, Medda R, Schwarzmann G, Sandhoff K, Polyakova S, Belov VN, Hein B, von Middendorff C, Schönle A, Hell SW. Direct observation of the nanoscale dynamics of membrane lipids in a living cell. Nature. 2009 Feb 26;457(7233):1159-62.
57. Sezgin E, Kaiser HJ, Baumgart T, Schwille P, Simons K, Levental I. Elucidating membrane structure and protein behavior using giant plasma membrane vesicles. Nature protocols. 2012 Jun 1;7(6):1042-51.
58. Saka SK, Honigmann A, Eggeling C, Hell SW, Lang T, Rizzoli SO. Multi-protein assemblies underlie the mesoscale organization of the plasma membrane. Nature communications. 2014 Jul 25;5.
59. Hope MJ, Bally MB, Webb G, Cullis PR. Production of large unilamellar vesicles by a rapid extrusion procedure. Characterization of size distribution, trapped volume and ability to maintain a membrane potential. Biochimica et Biophysica Acta (BBA)-Biomembranes. 1985 Jan 10;812(1):55-65.
60. Madl J, Villringer S, Römer W. Delving into Lipid-Driven Endocytic Mechanisms Using Biomimetic Membranes. InChemical and Synthetic Approaches in Membrane Biology 2016 (pp. 17-36). Humana Press, New York, NY.
61. Mingeot-Leclercq MP, Deleu M, Brasseur R, Dufrêne YF. Atomic force microscopy of supported lipid bilayers. Nature protocols. 2008 Oct 1;3(10):1654-9.
62. Römer W, Steinem C. Impedance analysis and single-channel recordings on nano-black lipid membranes based on porous alumina. Biophysical journal. 2004 Feb 29;86(2):955-65.
63. Kaiser HJ, Lingwood D, Levental I, Sampaio JL, Kalvodova L, Rajendran L, Simons K. Order of lipid phases in model and plasma membranes. Proceedings of the National Academy of Sciences. 2009 Sep 29;106(39):16645-50.
64. Lee MT, Hung WC, Chen FY, Huang HW. Mechanism and kinetics of pore formation in membranes by water-soluble amphipathic peptides. Proceedings of the National Academy of Sciences. 2008 Apr 1;105(13):5087-92.
65. Schubert T, Römer W. How synthetic membrane systems contribute to the understanding of lipid-driven endocytosis. Biochimica et Biophysica Acta (BBA)-Molecular Cell Research. 2015 Nov 30;1853(11):2992-3005.
66. Phillips R, Ursell T, Wiggins P, Sens P. Emerging roles for lipids in shaping membrane-protein function. Nature. 2009 May 21;459(7245):379-85.
67. Yilmaz N, Kobayashi T. Visualization of lipid membrane reorganization induced by a pore-forming toxin using high-speed atomic force microscopy. ACS nano. 2015 Aug 6;9(8):7960-7.
68. Gilbert RJ, Dalla Serra M, Froelich CJ, Wallace MI, Anderluh G. Membrane pore formation at protein–lipid interfaces. Trends in biochemical sciences. 2014 Nov 30;39(11):510-6.
69. Sodt AJ, Pastor RW. Molecular modeling of lipid membrane curvature induction by a peptide: more than simply shape. Biophysical journal. 2014 May 6;106(9):1958-69.

70. Maniti O, Piao HR, Ayala-Sanmartin J. Basic cell penetrating peptides induce plasma membrane positive curvature, lipid domain separation and protein redistribution. The international journal of biochemistry & cell biology. 2014 May 31;50:73-81.
71. Römer W, Pontani LL, Sorre B, Rentero C, Berland L, Chambon V, Lamaze C, Bassereau P, Sykes C, Gaus K, Johannes L. Actin dynamics drive membrane reorganization and scission in clathrin-independent endocytosis. Cell. 2010 Feb 19;140(4):540-53.
72. Head BP, Patel HH, Insel PA. Interaction of membrane/lipid rafts with the cytoskeleton: impact on signaling and function: membrane/lipid rafts, mediators of cytoskeletal arrangement and cell signaling. Biochimica et Biophysica Acta (BBA)-Biomembranes. 2014 Feb 28;1838(2):532-45.
73. Saleem M, Morlot S, Hohendahl A, Manzi J, Lenz M, Roux A. A balance between membrane elasticity and polymerization energy sets the shape of spherical clathrin coats. Nature communications. 2015 Feb 19;6.
74. Itoh T, Takenawa T. Mechanisms of membrane deformation by lipid-binding domains. Progress in lipid research. 2009 Sep 30;48(5):298-305.
75. Johannes L, Parton RG, Bassereau P, Mayor S. Building endocytic pits without clathrin. Nature Reviews Molecular Cell Biology. 2015 May 1;16(5):311-21.
76. Johannes L, Wunder C, Shafaq-Zadah M. Glycolipids and Lectins in Endocytic Uptake Processes. Journal of molecular biology. 2016 Dec 4;428(24):4792-818.
77. Varki A, Cummings RD, Esko JD, Freeze HH, Stanley P, Bertozzi CR, Hart GW, Etzler ME. Essentials of Glycobiology, Cold Spring Harbour; New York, 2nd edn, 2009.
78. Manna M, Róg T, Vattulainen I. The challenges of understanding glycolipid functions: an open outlook based on molecular simulations. Biochimica et Biophysica Acta (BBA)-Molecular and Cell Biology of Lipids. 2014 Aug 31;1841(8):1130-45.
79. López CA, Sovova Z, van Eerden FJ, de Vries AH, Marrink SJ. Martini force field parameters for glycolipids. Journal of chemical theory and computation. 2013 Feb 5;9(3):1694-708.
80. Fra AM, Williamson E, Simons K, Parton RG. Detergent-insoluble glycolipid microdomains in lymphocytes in the absence of caveolae. Journal of Biological Chemistry. 1994 Dec 9;269(49):30745-8.
81. Hooper NM. Detergent-insoluble glycosphingolipid/cholesterol-rich membrane domains, lipid rafts and caveolae. Molecular membrane biology. 1999 Jan 1;16(2):145-56.
82. Shi J, Yang T, Kataoka S, Zhang Y, Diaz AJ, Cremer PS. GM1 clustering inhibits cholera toxin binding in supported phospholipid membranes. Journal of the American Chemical Society. 2007 May 9;129(18):5954-61.
83. Mondal S, Mukhopadhyay C. Molecular level investigation of organization in ternary lipid bilayer: a computational approach. Langmuir. 2008 Aug 20;24(18):10298-305.
84. Koldsø H, Shorthouse D, Hélie J, Sansom MS. Lipid clustering correlates with membrane curvature as revealed by molecular simulations of complex lipid bilayers. PLoS computational biology. 2014 Oct 23;10(10):e1003911.
85. Solovyeva V, Johannes L, Simonsen AC. Shiga toxin induces membrane reorganization and formation of long range lipid order. Soft matter. 2015;11(1):186-92.
86. Chinnapen DJ, Hsieh WT, te Welscher YM, Saslowsky DE, Kaoutzani L, Brandsma E, D'Auria L, Park H, Wagner JS, Drake KR, Kang M, Benjamin T, Ullman MD, Costello CE, Kenworthy AK, Baumgart T, Massol RH, Lencer WI. Lipid sorting by ceramide structure from plasma membrane to ER for the cholera toxin receptor ganglioside GM1. Developmental cell. 2012 Sep 11;23(3):573-86.

87. Schütte OM, Ries A, Orth A, Patalag LJ, Römer W, Steinem C, Werz DB. Influence of Gb 3 glycosphingolipids differing in their fatty acid chain on the phase behaviour of solid supported membranes: chemical syntheses and impact of Shiga toxin binding. Chemical Science. 2014;5(8):3104-14.
88. Mahfoud R, Manis A, Lingwood CA. Fatty acid-dependent globotriaosyl ceramide receptor function in detergent resistant model membranes. Journal of lipid research. 2009 Sep 1;50(9):1744-55.
89. Schütte OM, Patalag LJ, Weber LM, Ries A, Römer W, Werz DB, Steinem C. 2-Hydroxy fatty acid enantiomers of Gb 3 impact Shiga toxin binding and membrane organization. Biophysical journal. 2015 Jun 16;108(12):2775-8.
90. Manna M, Javanainen M, Monne HM, Gabius HJ, Rog T, Vattulainen I. Long-chain GM1 gangliosides alter transmembrane domain registration through interdigitation. Biochimica et Biophysica Acta (BBA)-Biomembranes. 2017 May 31;1859(5):870-8.
91. Rydell GE, Svensson L, Larson G, Johannes L, Römer W. Human GII. 4 norovirus VLP induces membrane invaginations on giant unilamellar vesicles containing secretor gene dependent α1, 2-fucosylated glycosphingolipids. Biochimica et Biophysica Acta (BBA)-Biomembranes. 2013 Aug 31;1828(8):1840-5.
92. Ewers H, Römer W, Smith AE, Bacia K, Dmitrieff S, Chai W, Mancini R, Kartenbeck J, Chambon V, Berland L, Oppenheim A, Schwarzman G, Feizi T, Schwille P, Sens P, Helenius A, Johannes L. GM1 structure determines SV40-induced membrane invagination and infection. Nature cell biology. 2010 Jan 1;12(1):11-8.
93. Eierhoff T, Bastian B, Thuenauer R, Madl J, Audfray A, Aigal S, Juillot S, Rydell GE, Müller S, de Bentzmann S, Imberty A, Fleck C, Römer W. A lipid zipper triggers bacterial invasion. Proceedings of the National Academy of Sciences. 2014 Sep 2;111(35):12895-900.
94. Römer W, Berland L, Chambon V, Gaus K, Windschiegl B, Tenza D, Aly MR, Fraisier V, Florent JC, Perrais D, Lamaze C, Raposo G, Steinem C, Sens P, Basserau P, Johannes L. Shiga toxin induces tubular membrane invaginations for its uptake into cells. Nature. 2007 Nov 29;450(7170):670-5.
95. Zheng S, Eierhoff T, Aigal S, Brandel A, Thuenauer R, de Bentzmann S, Imberty A, Römer W. The Pseudomonas aeruginosa lectin LecA triggers host cell signalling by glycosphingolipid-dependent phosphorylation of the adaptor protein CrkII. Biochimica et Biophysica Acta (BBA)-Molecular Cell Research. 2017 Jul 31;1864(7):1236-45.
96. Sharon N. Lectins: carbohydrate-specific reagents and biological recognition molecules. Journal of Biological Chemistry. 2007 Feb 2;282(5):2753-64.
97. Aigal S, Claudinon J, Römer W. Plasma membrane reorganization: A glycolipid gateway for microbes. Biochimica et Biophysica Acta (BBA)-Molecular Cell Research. 2015 Apr 30;1853(4):858-71.
98. Johannes L, Römer W. Shiga toxins—from cell biology to biomedical applications. Nature Reviews Microbiology. 2010 Feb 1;8(2):105-16.
99. Windschiegl B, Orth A, Römer W, Berland L, Stechmann B, Bassereau P, Johannes L, Steinem C. Lipid reorganization induced by Shiga toxin clustering on planar membranes. PLoS One. 2009 Jul 16;4(7):e6238.
100. Johannes L, Mayor S. Induced domain formation in endocytic invagination, lipid sorting, and scission. Cell. 2010 Aug 20;142(4):507-10.
101. Safouane M, Berland L, Callan-Jones A, Sorre B, Römer W, Johannes L, Toombes GE, Bassereau P. Lipid cosorting mediated by shiga toxin induced tubulation. Traffic. 2010 Dec 1;11(12):1519-29.

102. Pezeshkian W, Hansen AG, Johannes L, Khandelia H, Shillcock JC, Kumar PS, Ipsen JH. Membrane invagination induced by Shiga toxin B-subunit: from molecular structure to tube formation. Soft matter. 2016;12(23):5164-71.
103. Arnaud J, Claudinon J, Tröndle K, Trovaslet M, Larson G, Thomas A, Varrot A, Römer W, Imberty A, Audfray A. Reduction of lectin valency drastically changes glycolipid dynamics in membranes but not surface avidity. ACS chemical biology. 2013 Jul 23;8(9):1918-24.
104. Lakshminarayan R, Wunder C, Becken U, Howes MT, Benzing C, Arumugam S, Sales S, Ariotti N, Chambon V, Lamaze C, Loew D,Shevchenko A, Gaus K, Parton RG, Johannes L. Galectin-3 drives glycosphingolipid-dependent biogenesis of clathrin-independent carriers. Nature cell biology. 2014 Jun 1;16(6):592-603.
105. Gil T, Ipsen JH. Capillary condensation between disks in two dimensions. Physical Review E. 1997 Feb 1;55(2):1713.
106. Pezeshkian W, Chaban VV, Johannes L, Shillcock J, Ipsen JH, Khandelia H. The effects of globotriaosylceramide tail saturation level on bilayer phases. Soft Matter. 2015;11(7):1352-61.
107. Reynwar BJ, Illya G, Harmandaris VA, Müller MM, Kremer K, Deserno M. Aggregation and vesiculation of membrane proteins by curvature-mediated interactions. Nature. 2007 May 24;447(7143):461-4.
108. Pezeshkian W, Gao H, Arumugam S, Becken U, Bassereau P, Florent JC, Ipsen JH, Johannes L, Shillcock JC. Mechanism of Shiga Toxin Clustering on Membranes. ACS nano. 2016 Dec 16;11(1):314-24.
109. Bast DJ, Banerjee L, Clark C, Read RJ, Brunton JL. The identification of three biologically relevant globotriaosyl ceramide receptor binding sites on the Verotoxin 1 B subunit. Molecular microbiology. 1999 Jun 1;32(5):953-60.
110. Arnaud J, Tröndle K, Claudinon J, Audfray A, Varrot A, Römer W, Imberty A. Membrane deformation by neolectins with engineered glycolipid binding sites. Angewandte Chemie International Edition. 2014 Aug 25;53(35):9267-70.
111. Shibly SU, Ghatak C, Karal MA, Moniruzzaman M, Yamazaki M. Experimental estimation of membrane tension induced by osmotic pressure. Biophysical journal. 2016 Nov 15;111(10):2190-201.
112. Kozlov MM, Chernomordik LV. Membrane tension and membrane fusion. Current opinion in structural biology. 2015 Aug 31;33:61-7.
113. Sens P, Turner MS. Budded membrane microdomains as tension regulators. Physical Review E. 2006 Mar 20;73(3):031918.
114. Liu J, Kaksonen M, Drubin DG, Oster G. Endocytic vesicle scission by lipid phase boundary forces. Proceedings of the National Academy of Sciences. 2006 Jul 5;103(27):10277-82.
115. Hassinger JE, Oster G, Drubin DG, Rangamani P. Design principles for robust vesiculation in clathrin-mediated endocytosis. Proceedings oft he National Academy of Sciences. 2017 Feb 14;114(7):E1118-27.
116. Johannes L, Wunder C, Bassereau P. Bending "on the rocks"—a cocktail of biophysical modules to build endocytic pathways. Cold Spring Harbor perspectives in biology. 2014 Jan 1;6(1):a016741.
117. Sens P, Johannes L, Bassereau P. Biophysical approaches to protein-induced membrane deformations in trafficking. Current opinion in cell biology. 2008 Aug 31;20(4):476-82.
118. Simunovic M, Manneville JB, Renard HF, Evergren E, Raghunathan K, Bhatia D, Kenworthy AK, Voth GA, Prost J, McMahon HT, Johannes L, Basserau P, Callan-Jones A.

Friction mediates scission of tubular membranes scaffolded by BAR proteins. Cell. 2017 Jun 29;170(1):172-84.
119. Roux A, Cuvelier D, Nassoy P, Prost J, Bassereau P, Goud B. Role of curvature and phase transition in lipid sorting and fission of membrane tubules. The EMBO journal. 2005 Apr 20;24(8):1537-45.
120. Sorre B, Callan-Jones A, Manneville JB, Nassoy P, Joanny JF, Prost J, Goud B, Bassereau P. Curvature-driven lipid sorting needs proximity to a demixing point and is aided by proteins. Proceedings of the National Academy of Sciences. 2009 Apr 7;106(14):5622-6.
121. Hammond AT, Heberle FA, Baumgart T, Holowka D, Baird B, Feigenson GW. Crosslinking a lipid raft component triggers liquid ordered-liquid disordered phase separation in model plasma membranes. Proceedings of the National Academy of Sciences of the United States of America. 2005 May 3;102(18):6320-5.
122. Lingwood D, Ries J, Schwille P, Simons K. Plasma membranes are poised for activation of raft phase coalescence at physiological temperature. Proceedings of the National Academy of Sciences. 2008 Jul 22;105(29):10005-10.
123. Bacia K, Schwille P, Kurzchalia T. Sterol structure determines the separation of phases and the curvature of the liquid-ordered phase in model membranes. Proceedings of the National Academy of Sciences of the United States of America. 2005 Mar 1;102(9):3272-7.
124. Pinot M, Vanni S, Pagnotta S, Lacas-Gervais S, Payet LA, Ferreira T, Gautier R, Goud B, Antonny B, Barelli H. Polyunsaturated phospholipids facilitate membrane deformation and fission by endocytic proteins. Science. 2014 Aug 8;345(6197):693-7.
125. Kamal MM, Mills D, Grzybek M, Howard J. Measurement of the membrane curvature preference of phospholipids reveals only weak coupling between lipid shape and leaflet curvature. Proceedings of the National Academy of Sciences. 2009 Dec 29;106(52):22245-50.
126. Tian A, Baumgart T. Sorting of lipids and proteins in membrane curvature gradients. Biophysical journal. 2009 Apr 8;96(7):2676-88.
127. Auth T, Gompper G. Budding and vesiculation induced by conical membrane inclusions. Physical Review E. 2009 Sep 3;80(3):031901.
128. Tsafrir I, Sagi D, Arzi T, Guedeau-Boudeville MA, Frette V, Kandel D, Stavans J. Pearling instabilities of membrane tubes with anchored polymers. Physical review letters. 2001 Feb 5;86(6):1138.
129. Campelo F, McMahon HT, Kozlov MM. The hydrophobic insertion mechanism of membrane curvature generation by proteins. Biophysical journal. 2008 Sep 1;95(5):2325-39.
130. Callan-Jones A, Sorre B, Bassereau P. Curvature-driven lipid sorting in biomembranes. Cold Spring Harbor perspectives in biology. 2011 Feb 1;3(2):a004648.

Bioinformatics, 2018, 1–3
doi: 10.1093/bioinformatics/xxxxx
Advance Access Publication Date: DD Month YYYY
Manuscript Category

Bioimage informatics

GUV-AP: multifunctional FIJI-based tool for quantitative image analysis of Giant Unilamellar Vesicles

Taras Sych[1,2,§], Thomas Schubert[1,3,§], Romain Vauchelles[2], Josef Madl[1,#], Ramin Omidvar[1], Roland Thuenauer[1], Ludovic Richert[2], Yves Mély[2,*] and Winfried Römer [1,*]

[1]Faculty of Biology, Centre for Biological Signalling Studies (BIOSS), Freiburg Center for Interactive Materials and Bioinspired Technology (FIT), Albert-Ludwigs-University Freiburg, Germany; [2]Laboratoire de Bioimagerie et Pathologies, UMR 7021 CNRS, Faculté de Pharmacie, Université de Strasbourg, France; [3]Toolbox Imaging Platform, Centre for Biological Signalling Studies (BIOSS), Albert-Ludwigs-University Freiburg, Germany; [§]Contributed equally, # present address: Institute for Experimental Cardiovascular Medicine, University Heart Center Freiburg - Bad Krozingen, Medical Faculty of the University of Freiburg, Germany; *To whom correspondence should be addressed;

Associate Editor: Robert Murphy

Received on June 10, 2018; revised on November 19, 2018; accepted on November 23, 2018

Abstract

Motivation: Giant Unilamellar Vesicles (GUVs) are widely used synthetic membrane systems that mimic native membranes and cellular processes. Various fluorescence imaging techniques can be employed for their characterization. In order to guarantee a fast and unbiased analysis of imaging data, the development of automated recognition and processing steps is required.

Results: We developed a fast and versatile Fiji-based macro for the analysis of digital microscopy images of GUVs. This macro was designed to investigate membrane dye incorporation and protein binding to membranes. Moreover, we propose a fluorescence intensity-based method to quantitatively assess protein binding.

Availability: The ImageJ distribution package FIJI is freely available online: https://imagej.net/Fiji. The macro file GUV-AP.ijm is available at https://github.com/AG-Roemer/GUV-AP

Contact: winfried.roemer@bioss.uni-freiburg.de and yves.mely@unistra.fr

Supplementary information: Supplementary data are available at Bioinformatics online.

1 Introduction

Giant Unilamellar Vesicles (GUVs) represent cell-sized (tens of micrometers in diameter) spherical lipid bilayers. In combination with fluorescence microscopy techniques, GUVs became a frequently used approach to study cellular processes such as membrane permeabilization (Hermann et al., 2014), adhesion (Villringer et al., 2018) and endocytosis (reviewed in (Schubert and Römer, 2015)). GUVs with a spatial phase-separation in liquid disordered (Ld) and liquid ordered (Lo) domains are of particular interest to mimic the heterogeneity of the plasma membrane including lipid rafts (reviewed in (Sych et al., 2018)). Acquired fluorescence microscopy data requires processing of a large number of data sets, especially if a quantitative description is requested. As manual image analysis is biased and highly time consuming, the use of high throughput methods implemented in automated software can significantly speed up the analysis and reduce biases. Current automated software packages for GUV analysis based on 3-D micrographs (Husen et al., 2012; Sendra et al., 2015) or GUV contour (Hermann et al., 2014) require commercial software licences, are not compatible with different microscope output formats, or lack effective high throughput analysis capabilities. In this application note, we introduce a novel, powerful FIJI-based macro for fast and versatile analysis of multiple GUVs per image.

2 Presented macro

We have developed a macro using the ImageJ (FIJI) environment (Rueden et al., 2017; Schindelin et al., 2012), an open source microscopy image processing software. It has multiple built-in functionalities and most importantly it is compatible with the majority of microscopy data output formats thanks to the BioFormats plug-in (Linkert et al., 2010). Briefly, the macro detects circular particles (e.g. GUVs, supplementary figure 1) in the microscopy image and determines their centers and radii. The algorithm is explained in detail and step by step in the Manual.

3 GUV processing, validation and application

When GUVs are detected, various processing approaches can be applied. Here, we demonstrate a selection. We tested the performance of GUV-AP based on laser scanning confocal microscopy images of GUVs. These GUVs were composed of DOPC, sphingomyelin and cholesterol

in different ratios and labeled by various fluorescent probes (supplementary information – materials and methods).

3.1 Characterization of fluorescent membrane probes

We show in figure 1 as well as in the supplementary figures S2 and S3 that our macro can be applied to decipher the fluorescence properties (intensity, lifetime) of a membrane dye incorporated in the lipid bilayer as well as its preference to distinct lipid phases and its orientation in the lipid bilayer (Klymchenko and Kreder, 2014). For instance, the lipophilic membrane probe ß-Bodipy FL C5-HPC (Bodipy) is known to have preferences for the Ld phase (Figure 1A), whereas it is almost completely excluded from the Lo phase. Furthermore, the GUV analysis macro can also be used to display the circular profile that visualizes the variations of fluorescence intensity along the GUV contour as a 2D plot (figure 1B).

3.2 Quantification of protein binding to GUVs

In order to highlight the performance of our macro for the observation and quantification of protein binding, we imaged phase-separated GUVs containing the neutral glycosphingolipid globotriaosylceramide (Gb3; also known as CD77 or Pk blood group antigen) (reviewed in (Johannes and Römer, 2010)). Gb3 is the receptor for the galactose-binding B-subunit of Shiga toxin (StxB) from *Shigella dysenteriae* (Römer et al., 2007). In phase-separated GUVs (figure 1A), Cy5-labeled StxB preferentially binds to Lo domains. This binding can be more accurately displayed using the circular profiles of Bodipy (figure 1B - green) and StxB-Cy5 (figure 1B - red).

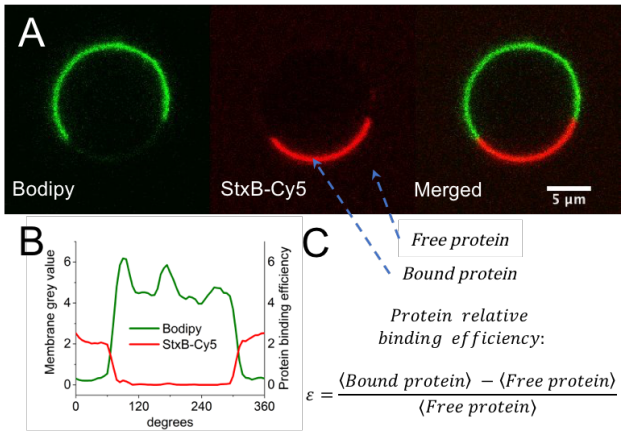

Figure 1: GUV processing. A) StxB-Cy5 (red channel) binds to the Lo domain of a GUV composed of DOPC/chol/SM and the glycosphingolipid Gb3 (40/15/40/5). The Lo domains are not visible since the membrane probe Bodipy (green channel) preferentially localizes to Ld domains. B) Circular profiles of the membrane marker Bodipy (green curve) and StxB-Cy5 (red curve). The units of StxB-Cy5 circular profile (right Y axis) are quantified as shown in (C). C) Calculation of the relative binding efficiency.

To quantitatively evaluate the protein binding, we calculated the relative binding efficiency ε as shown in Figure 1C. ⟨Bound protein⟩ is the mean fluorescence intensity signal from the protein located on the vesicle contour and ⟨Free protein⟩ is the mean fluorescence intensity signal from the free protein in solution, extracted from the area of the image, which surrounds the GUV (Figure 1C). In absence of protein binding, the ⟨Bound protein⟩ value is equal to the ⟨Free protein⟩ value, so that the relative binding efficiency is ≈ 0. If ε is above 0, binding occurs. This binding efficiency value depends on the number of protein molecules bound to the membrane. Moreover, as shown by Weinberger et al. (Weinberger et al., 2017) it is possible to link such fluorescence intensity quantifications to the actual number of protein molecules bound to the membrane using proper calibration. The robustness of the method was validated by analyzing StxB binding to GUVs differing in their Gb3 content. As expected, the binding efficiency of StxB to GUVs increased with the amount of Gb3 molecules in the membrane (supplementary figure S4).

Conclusion

We developed a script for the recognition and analysis of circular segments of GUVs in order to study the partition of membrane probes as well as protein binding to membranes. In addition, we proposed a quantitative analysis to compare the binding efficiency of proteins to membranes of different compositions and biophysical properties. Our script is not limited to the analysis of GUVs, but can also process other spherical membranes like native giant plasma membrane vesicles, or any circular object. The script can be combined with time-frame analysis to study dynamics of binding processes and, with a tracking algorithm, to monitor GUV motions.

Acknowledgements

Funding: This work has been supported by the German Research Foundation (EXC 294, RO 4341/2-1, RO 4341/3-1 and IRTG 1642). Taras Sych acknowledges the support by the Franco-German University (programs "Polymer Sciences" and "Cotutelle de thèse") and the Collège Doctoral Européen (PDI). We are grateful to Andrey Klymchenko for providing the lipophilic membrane probes. *Conflict of Interest:* The authors declare no conflict of interest.

References

Hermann, E. *et al*. (2014). Automated analysis of giant unilamellar vesicles using circular Hough transformation. Bioinformatics *30*, 1747–1754.

Husen, P. *et al*. (2012). Morphometric Image Analysis of Giant Vesicles: A New Tool for Quantitative Thermodynamics Studies of Phase Separation in Lipid Membranes. Biophysical Journal *103*, 2304–2310.

Johannes, L., and Römer, W. (2010). Shiga toxins — from cell biology to biomedical applications. Nat Rev Micro *8*, 105–116.

Klymchenko, A.S., and Kreder, R. (2014). Fluorescent Probes for Lipid Rafts: From Model Membranes to Living Cells. Chemistry & Biology *21*, 97–113.

Linkert, M. *et al*. (2010). Metadata matters: access to image data in the real world. The Journal of Cell Biology *189*, 777–782.

Römer, W. *et al*. (2007). Shiga toxin induces tubular membrane invaginations for its uptake into cells. Nature *450*, 670–675.

Rueden, C.T. *et al*. (2017). ImageJ2: ImageJ for the next generation of scientific image data. BMC Bioinformatics *18*, 529.

Schindelin, J. *et al*. (2012). Fiji - an Open Source platform for biological image analysis. Nat Methods *9*.

Schubert, T., and Römer, W. (2015). How synthetic membrane systems contribute to the understanding of lipid-driven endocytosis. BBA - Molecular Cell Research *1853*, 2992–3005.

Sendra, G.H. *et al*. (2015). 2D map projections for visualization and quantitative analysis of 3D fluorescence micrographs. Scientific Reports *5*.

Sych, T., Mély, Y., and Römer, W. (2018). Lipid self-assembly and lectin-induced reorganization of the plasma membrane. Phil. Trans. R. Soc. B *373*, 20170117.

Villringer S. *et al*. (2018). Lectin-mediated protocell crosslinking to mimic cell-cell junctions and adhesion. Scientific Reports *8(1)*,1932.

Weinberger, A. *et al*. (2017). Cargo self-assembly rescues affinity of cell-penetrating peptides to lipid membranes. Scientific Reports *7*, 43963.

Supplementary figures

GUV-AP: multifunctional FIJI-based tool for quantitative image analysis of Giant Unilamellar Vesicles

Taras Sych[1,2,§], Thomas Schubert[1,§], Romain Vauchelles[2], Josef Madl[1], Ramin Omidvar[1], Roland Thuenauer[1], Ludovic Richert[2], Yves Mély[2,*] and Winfried Römer [1,*]

[1]Faculty of Biology, Centre for Biological Signalling Studies (BIOSS), Freiburg Center for Interactive Materials and Bioinspired Technology (FIT), Albert-Ludwigs-University Freiburg, Germany; [2]Laboratoire de Bioimagerie et Pathologies, UMR 7021 CNRS, Faculté de Pharmacie, Université de Strasbourg, France; [3]Toolbox Imaging Platform, Centre for Biological Signalling Studies (BIOSS), Albert-Ludwigs-University Freiburg, Germany; [§]Contributed equally, # present address: Institute for Experimental Cardiovascular Medicine, University Heart Center Freiburg - Bad Krozingen, Medical Faculty of the University of Freiburg, Germany; *To whom correspondence should be addressed;

Winfried Römer: winfried.roemer@bioss.uni-freiburg.de

Yves Mély: yves.mely@unistra.fr

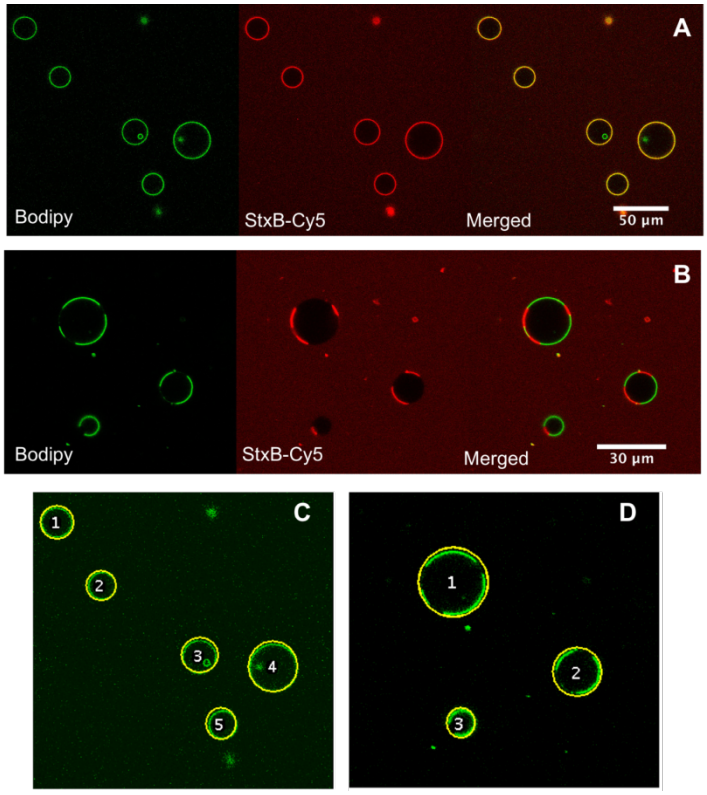

Fig. S1. GUV detection. Representative laser scanning confocal microscopy (LSCM) raw images illustrating StxB binding to GUVs. A) Cy5-labeled StxB (StxB-Cy5) binding (red channel) to homogeneous (DOPC/chol/Gb3 – 65/30/5) GUVs labeled by ß-Bodipy FL C5-HPC (Bodipy, green channel). B) Selective binding of StxB to the Lo phase of phase-separated (DOPC/chol/SM/Gb3 – 40/15/40/5) GUVs. C) Homogeneous (DOPC/chol/Gb3 – 65/30/5) GUVs are detected as full circles. D) Phase-separated (DOPC/chol/SM/Gb3 – 40/15/40/5) GUVs are detected from series of unconnected circular segments from the membrane channel of B (green) using the method described in the Manual.

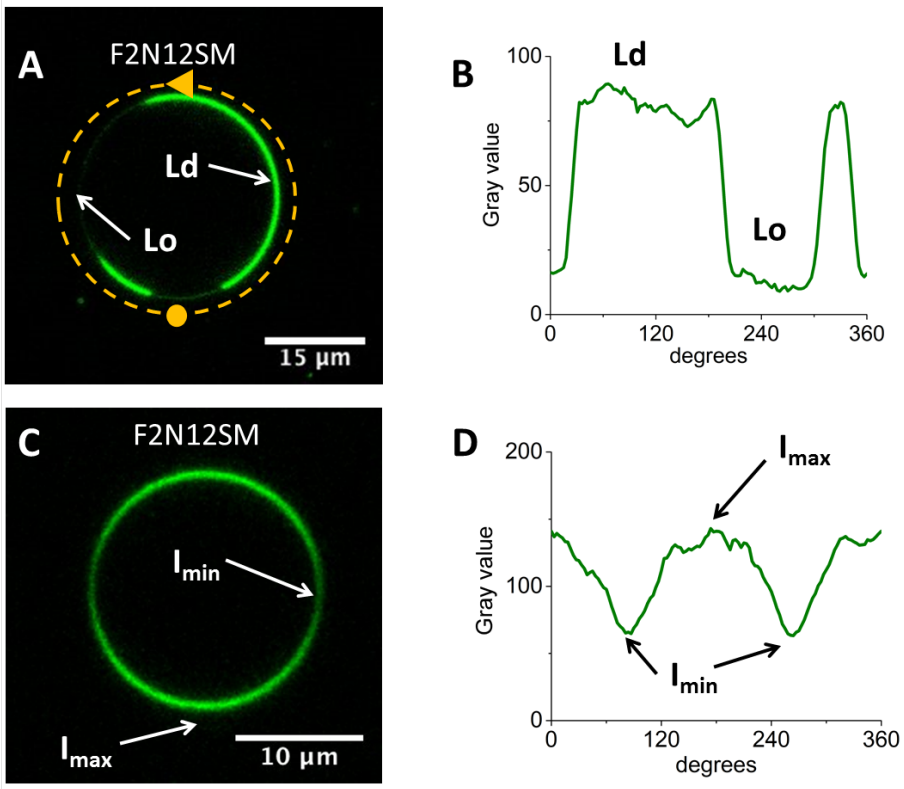

Fig. S2. Membrane partitioning of the membrane probe F2N12SM. A and B) Partitioning of the F2N12SM probe into Ld and Lo phases. A) Phase-separated GUV composed of DOPC/chol/SM (40/15/40) labeled by F2N12SM (Kreder et al., 2015). The yellow dot and the dashed arrow respectively indicate the starting point and the direction used to extract the circular profile given in (B). This circular profile shows that the F2N12SM intensity is high in Ld phase and negligible in Lo phase. C) and D) show the polarization effect (Haluska et al., 2008), which results in the variation of the fluorescence intensity of the probe in the bilayer along the GUV contour. I_{max} is the fluorescence intensity where the molecules of the probe have parallel orientation to the excitation laser polarization. At I_{min} probes are oriented perpendicular to the laser polarization. This effect can be used to determine the orientation of the probe in the bilayer; C) GUV composed of SM/chol (70/30) labeled by F2N12SM. The fluorescence intensity of F2N12SM varies along the GUV contour, as a result of the orientation of the dye in the membrane. D) Circular profile of the GUV in (C).

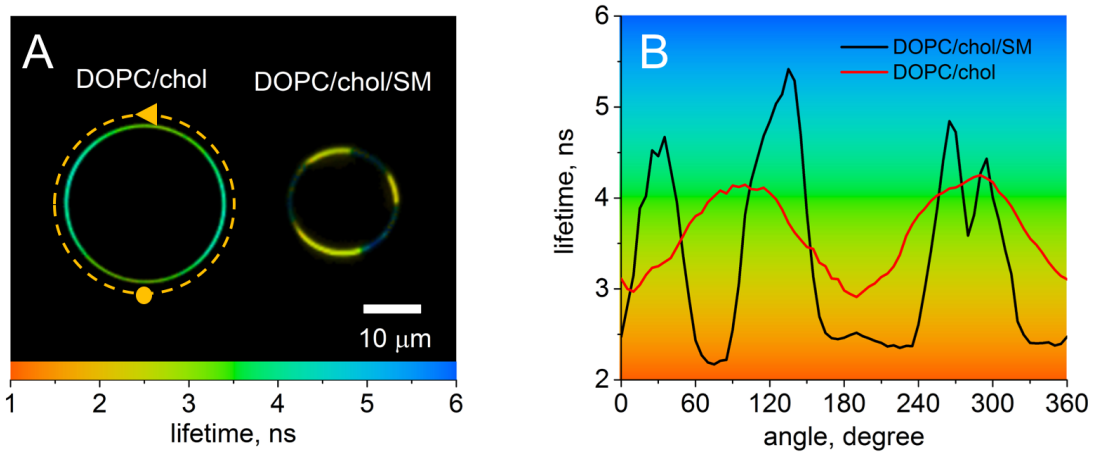

Fig. S3. Circular profile extraction of fluorescence lifetime imaging microscopy (FLIM) images. A) Color-coded FLIM images of a non-phase-separated GUV (left) composed of DOPC/cholesterol (chol) (65/30) and a phase-separated GUV (right) composed of DOPC/chol/Sphingomyelin– 40/15/40). Both GUVs are labeled with the environmentally sensitive probe F2N12S (Kilin et al., 2015). The colors of the pixels represent the lifetime values according to the color scale on the X-axis. The yellow dot and the dashed arrow, respectively, indicate the starting point and the direction of the circular profile extraction. B) Circular profile of GUVs presented in A. The variation of the apparent lifetime in the GUV composed of DOPC/chol is due to the polarization effect (Haluska et al., 2008).

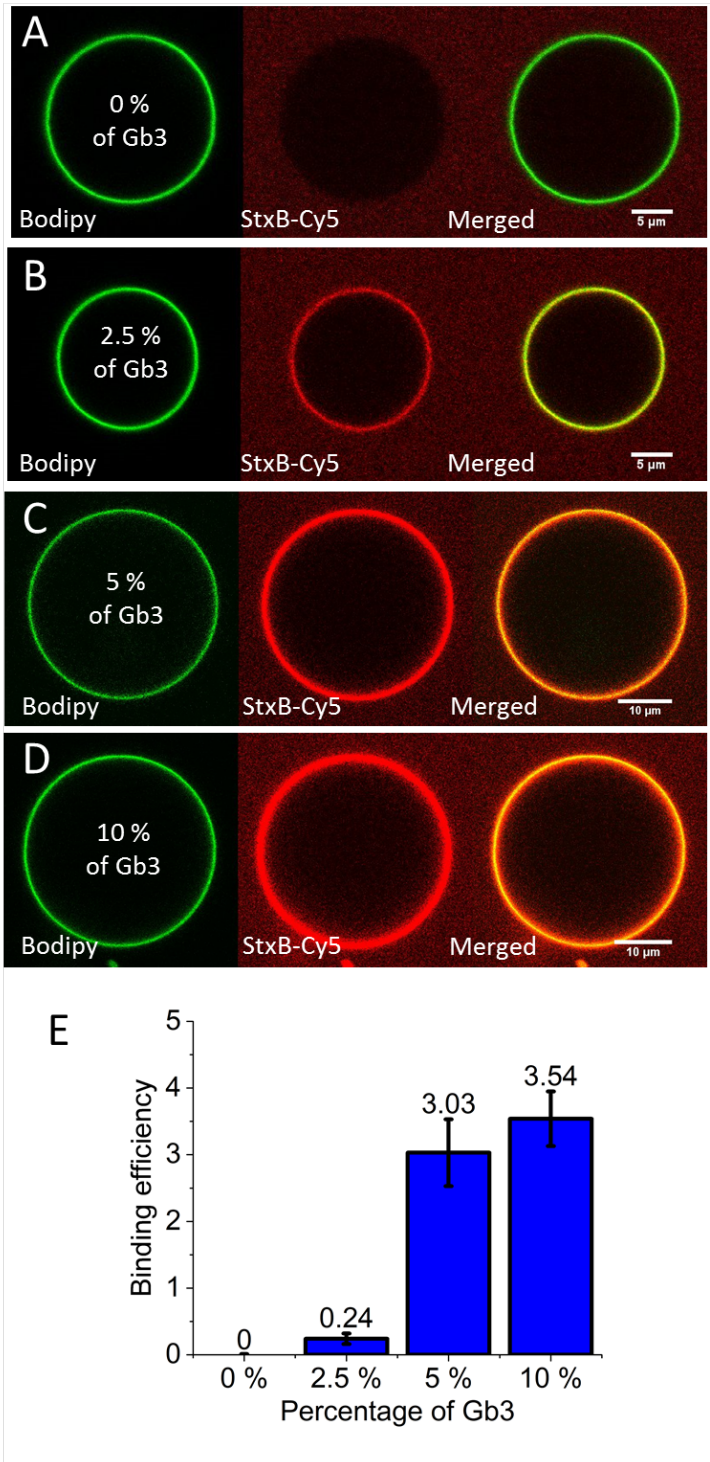

Fig. S4. StxB binding to GUVs containing different molar percentages of Gb3. A-D) LSCM images of GUVs (in green) containing 0% (A), 2.5% (B), 5% (C) and 10% (D) of Gb3, which have been incubated with 100 nM of StxB-Cy5 (red). StxB-Cy5 intensities were all scaled equally so that the free protein signals are visible in all images. E) Binding efficiency ε values for StxB. Error bars represent standard deviation. Number of replicas for 0%, 2.5%, 5% and 10% Gb3-containing GUVs was 16, 12, 17 and 10, respectively.

Table S1. Macro execution time. The macro was run on the Mac OS X El Capitan version 10.11.6, processor 2.9 GHz Intel Core i5, memory 8 GB 1867 MHz DDR3.

Type of GUVs	Batch mode	Channels	Circularity check	GUV stitching	Number of images processed	Number of GUVs processed	Total execution time	Time per image	Time per GUV
phase-separated	no	2	no	yes	25	108	13 min 46 s	33 s	7.7 s
	yes	-	-	-	-	-	-	-	-
homogeneous	no	2	yes	no	80	90	10 min 55 s	8.2 s	7.3 s
	yes	2	yes	no	80	90	7 min 58 s	6 s	5.3 s

Materials and methods

GUV preparation

1,2-dioleoyl-sn-glycero-3-phosphocholine (DOPC), brain sphingomyelin (SM) and cholesterol (chol) were purchased from Avanti Polar Lipids. Globotriaosylceramide (Gb3) isolated from porcine brain was from Matreya. ß-Bodipy FL C_5-HPC and di-4-ANEPPDHQ were from ThermoFisher Scientific. F2N12S and F2N12SM were provided by Dr. Andrey Klymchenko. GUVs were prepared as described in (Madl et al., 2016). In brief, solutions of lipids were prepared in chloroform. For phase-separated GUV preparation, a DOPC/chol/BSM/Bodipy (40/15/40/5/0.5) mixture was used. Three types of homogeneous GUVs differing in Gb3 content (0, 2.5, 5 and 10 mol %) were prepared using DOPC/chol/Bodipy (65/30/0.5), DOPC/chol/Gb3/Bodipy (65/30/2.5/0.5), DOPC/chol/Gb3/Bodipy (65/30/5/0.5) and DOPC/chol/Gb3/Bodipy (65/30/10/0.5) mixtures, respectively. The lipid solutions in chloroform were spread on the conducting surfaces of two Indium tin oxide (ITO) slides, and then chloroform was removed by drying under vacuum for 1 h. After chloroform was completely removed, GUVs were prepared by electroformation in a 300 µM sucrose solution for 3 h.

Protein labeling

StxB (Sigma-Aldrich) was labeled with Cy5 mono-reactive dye from GE Healthcare Life Sciences according to the amine-reactive probe labeling protocol from ThermoFisher Scientific. Briefly, 1 µl of a 10 mg/ml solution of the amino-reactive probe in DMSO was added to 100 µl of a 1 mg/ml protein solution supplemented with 100 µM $NaHCO_3$. The mixture was incubated for 1 h at room temperature with continuous shaking. The labeled protein was purified using Zeba Spin Desalating Columns, 0.5 ml, from ThermoFisher Scientific.

Microscopy techniques

The fluorescence intensity measurements of GUVs (Figure 1, Figures S1, S2, S4) were performed on a confocal fluorescence microscope (Nikon Eclipse Ti-E with A1R confocal laser scanner, 60x oil objective, N.A. 1.49). For fluorescence excitation, 405 nm (F2N12SM), 488 nm (ß-Bodipy FL C_5-HPC and Di-4ANEPPDHQ) and 642 nm (StxB-Cy5) lasers were used. The emission of ß-Bodipy FL C_5-HPC and F2N12SM, as well as the green part of the emission di-4ANEPPDHQ were recorded using a 525/50 BP filter. The emission of the red part of di-4ANEPPDHQ emission and the emission of StxB-Cy5 were detected using a 700/75 BP filter.

Fluorescence lifetime imaging microscopy (FLIM – Figure S3) was performed using a home built two photon laser scanning setup based on an Olympus IX70 inverted microscope with an Olympus 60x water immersion objective (N.A. 1.2) (Kilin et al, 2015). Two-photon excitation was provided by an Insight Deep see laser (Spectra Physics)). The typical excitation power was ~2.5 mW (λ = 830 nm) at the sample. Photons were detected using an avalanche photodiode (SPCM-AQR-14-FC; Perkin Elmer) coupled to an HQ 585/40 bandpass filter and a single-photon-counting TCSPC module (SPC830; Becker & Hickl). FLIM data were analyzed with a binning of one using the SPCImage V4.6 software (Becker & Hickl), which uses an iterative reconvolution method to recover the lifetimes from the fluorescence decays.

References

Haluska, C.K., Schröder, A.P., Didier, P., Heissler, D., Duportail, G., Mély, Y., and Marques, C.M. (2008). Combining Fluorescence Lifetime and Polarization Microscopy to Discriminate Phase Separated Domains in Giant Unilamellar Vesicles. Biophys. J. *95*, 5737–5747.

Kilin, V., Glushonkov, O., Herdly, L., Klymchenko, A., Richert, L., and Mely, Y. (2015). Fluorescence Lifetime Imaging of Membrane Lipid Order with a Ratiometric Fluorescent Probe. Biophys. J. *108*, 2521–2531.

Kreder, R., Oncul, S., Kucherak, O.A., Pyrshev, K.A., Real, E., Mély, Y., and Klymchenko, A.S. (2015). Blue fluorogenic probes for cell plasma membranes fill the gap in multicolour imaging. RSC Adv. *5*, 22899–22905.

Madl, J., Villringer, S., and Römer, W. (2016). Delving into Lipid-Driven Endocytic Mechanisms Using Biomimetic Membranes. (Humana Press, New York, NY), pp. 17–36.

Differential recognition of lipid domains by two Gb3-binding lectins

Thomas Schubert[a,b,c], Taras Sych[a,b,d], Josef Madl[a,b], Maokai Xu[a,b], Ramin Omidvar[a,b], Lukas J. Patalag[e], Annika Ries[f], Katharina Kettelhoit[e],Yves Mely[c], Claudia Steinem[f], Daniel B. Werz[e], Roland Thuenauer[a,b,g,1], Winfried Römer[a,b,1]

[a] Faculty of Biology, Albert-Ludwigs-University Freiburg, Freiburg, Germany
[b] Synthetic Biology of Signalling Processes, Signalling Research Centres BIOSS and CIBSS, Albert-Ludwigs-University Freiburg, Freiburg, Germany
[c] Toolbox, BIOSS Centre for Biological Signalling Studies, Albert-Ludwigs-University Freiburg, Freiburg, Germany
[d] Laboratory of Bioimaging and Pathologies, UMR 7021 CNRS, Faculty of Pharmacy, University of Strasbourg, France
[e] Institut für Organische Chemie, TU Braunschweig, Braunschweig, Germany
[f] Institut für Organische und Biomolekulare Chemie, Georg-August-Universität Göttingen, Göttingen, Germany.
[g] Advanced Light and Fluorescence Microscopy Facility, Centre for Structural Systems Biology (CSSB) and University of Hamburg, Hamburg, Germany

[1] To whom correspondence should be addressed. Email: roland.thuenauer@cssb-hamburg.de (RT), winfried.roemer@bioss.uni-freiburg.de (WR)

Abstract

The two lectins LecA from *Pseudomonas aeruginosa* and the B-subunit of Shiga toxin from *Shigella dysenteriae* (StxB) share the glycosphingolipid globotriaosylceramide (Gb3) as receptor. Counterintuitively, we found that LecA and StxB segregated into different domains after recognizing Gb3 at the plasma membrane of cells. Based on this observation, we proposed the hypothesis that how Gb3 is embedded in the lipid bilayer and thus how the carbohydrate head group of Gb3 is oriented, differentially influences Gb3 binding by LecA and StxB. To test this hypothesis, we reconstituted lectin-Gb3 interaction using giant unilamellar vesicles and supported lipid bilayers. Also in these model systems we were able to rebuild LecA and StxB segregation. Furthermore, the structure of the fatty acyl chain of Gb3 and the local membrane environment, which both control Gb3 membrane embedding, distinctively modulated Gb3 recognition by LecA and StxB. Specifically, StxB preferred more ordered membranes in comparison to LecA.

Based on these findings, we propose comparing staining patterns of LecA and StxB as an alternative method to assess membrane order in cells. To verify our novel approach, we re-established that the apical plasma membrane of epithelial cells is more ordered than the basolateral plasma membrane. Additionally, we found that StxB was able to recognize Gb3 at the primary cilium and at the surrounding periciliary membrane, whereas LecA was only able to bind periciliary Gb3. This suggests that the membrane of the primary cilium is of higher order than the surrounding periciliary membrane.

Significance statement

Lipid order crucially mediates the function of plasma membrane components. Sensing membrane order in cells is challenging and currently available order-sensitive fluorescent probes can cause side effects by their incorporation in the lipid bilayer. Here, we introduce the use of the lectins, LecA and StxB, which both recognize the glycosphingolipid Gb3, as alternative. The binding of the two lectins to Gb3 varied differentially in dependence of the lipid environment. In particular, StxB showed a much stronger preference for more ordered domains

than LecA did. Hence, comparative staining with StxB and LecA can be applied to monitor local differences of membrane order in cells.

Keywords

Shiga toxin, LecA, primary cilium, plasma membrane, membrane order, lipid-mediated endocytosis, *Pseudomonas aeruginosa*, giant unilamellar vesicles

Introduction

The plasma membrane controls the movement of substances between the interior and the outside of a cell. It is based on a lipid bilayer matrix that consists of lipids with diverse head groups and fatty acyl chains. The different membrane lipids are inhomogenously distributed in the plasma membrane: First, the inner and the outer leaflets of the lipid bilayer are composed of different lipid classes and this asymmetry is actively maintained by the cell (1–4). Second, the plasma membrane is also heterogeneous along each leaflet: lipid domains of specific composition are formed (5–7) that serve as platforms for various cellular processes such as endocytosis (8) and signal transduction (9–11) and manifest in locally altered membrane order (12–14).

Detecting and following lipid domains in cells has turned out to be a challenging endeavor (15, 16). Direct fluorescent labeling of a lipid is casting doubt on its natural behavior and phase partitioning properties (17–19). As alternative, environmentally sensitive probes that intercalate in the lipid bilayer and change their fluorescence spectra in dependence of the membrane order have been extensively used (19). However, such probes often show cytotoxic effects, can require technically advanced equipment, and can cause side effects by altering membrane order (20). An alternative approach is based on carbohydrate-binding proteins, so called lectins, which specifically recognize the carbohydrate-moieties of glycosphingolipids (21). For example, the B-subunit of cholera toxin (CtxB) targets the ganglioside monosialotetrahexosylganglioside (GM1). It has become a frequently used marker for highly ordered membrane domains termed as 'lipid rafts' (22–25).

Here, we report that the lectins LecA from *Pseudomonas aeruginosa* (26–28) and the B-subunit of Shiga toxin (StxB) from *Shigella dysenteriae* (29–31), which recognize the same glycosphingolipid, the globotriaosylceramide (Gb3, also referred to as P^K blood group antigen and CD77 (32)), segregate into different domains at the plasma membrane of cells. Furthermore, we were able to successfully rebuild LecA and StxB spatial segregation in synthetic lipid bilayer systems - giant unilamellar vesicles (GUVs) and supported lipid bilayers (SLBs). Such artificially prepared membranes with controlled lipid composition are

extensively employed for studying lipid organization and function (14, 33, 34). They allow to choose conditions to achieve lateral lipid segregation (5, 35, 36), resulting in the formation of liquid disordered (ld) and liquid ordered (lo) phases, which resembles lateral cellular plasma membrane heterogeneities. Experiments with GUVs and SLBs enabled us to identify the interplay between the molecular structure of Gb3 (i.e. which Gb3 species it is) and the membrane environment, which both determine Gb3 membrane embedding and head group orientation (37), as critical parameters causing differential Gb3 recognition by LecA and StxB. In particular, we revealed that StxB has a preference for more ordered domains in comparison to LecA.

Based on these results we suggest that comparing the staining patterns of LecA and StxB yields a novel approach for evaluating membrane order in cells. To demonstrate the feasibility of this approach, we used epithelial cells. The apical plasma membranes of epithelial cells are known to be more ordered than basolateral plasma membranes (2, 38). As expected from this order difference, StxB showed a stronger preference for the apical plasma membrane in comparison to LecA. In addition, we found that StxB, but not LecA, was able to recognize the primary cilium. This surprising finding suggests that the membrane of the primary cilium contains a lipid domain that has a higher order than the surrounding apical plasma membrane.

Results

LecA and StxB recognize different lipid domains on cells

The two lectins LecA and StxB share the same receptor, the globoside Gb3 (30, 39). Upon application of LecA and StxB to either the apical or basolateral side of polarized Madin-Darby canine kidney (MDCK) strain II cells stably expressing Gb3 synthase (9), both lectins were found at higher concentration at apical cell membranes than at basolateral cell membranes (Fig. 1A). However, StxB showed a significantly stronger preference for the apical plasma membrane than LecA did (apical to basolateral signal intensity ratio for StxB 6.96 ± 1.04 versus 2.70 ± 0.47 for LecA). Furthermore, we found that StxB was able to bind the primary cilium (Fig. 1B), which confirms that Gb3 lipids are also found in this cellular organelle that shares a continuous lipid bilayer with the apical plasma membrane. Strikingly however, no LecA binding was detected at the cilium, even at relatively high LecA concentrations (Fig. 1B). Since the cilium represents only a tiny fraction of the area of the apical plasma membrane, StxB binding to the primary cilium cannot fully explain the higher apical to basolateral binding ratio for StxB in comparison to LecA. But measuring the total amount of bound lectin at the apical and basolateral plasma membrane provides only a global view and neglects any potential segregation of the two lectins at the plasma membrane on a smaller scale. Indeed, a closer look on Fig. 1B shows that at the (non-ciliary) apical plasma membrane LecA and StxB displayed only partially overlapping binding patterns. In agreement, previous studies found a partial segregation of the two lectins during early stages of their endocytosis (9), thus suggesting that the segregation between LecA and StxB occurs already at the plasma membrane.

To independently confirm these findings, we used HeLa cells, which endogenously express Gb3 (41). We applied energy-depletion (8) in order to inhibit energy-dependent scission of endocytic buds. This results in the formation of fairly stable tubular invaginations at the plasma membrane (8). The super-resolution microscopy technique TIRF-SIM revealed that LecA and StxB clearly segregate into different domains at the plasma membrane (Fig. 1C).

These findings demonstrate that - despite sharing the same receptor - LecA and StxB show different binding patterns on cells.

LecA and StxB also segregate on GUVs containing a mixture of Gb3 species

In order to identify the mechanism causing LecA and StxB spatial segregation, we applied model systems based on artificial lipid bilayers. To mimic the behavior and embedding of Gb3 in the cellular plasma membrane, we chose GUVs as model system. We produced GUVs containing 5 mol-% of a natural mixture of Gb3 species extracted from porcine brain (Gb3-mix) and applied both lectins (Fig. 2). Under certain conditions, StxB can induce tubular invaginations on GUVs (8, 42). Hence, to rule out secondary effects, we imaged at time points before the lectins were able to induce tubules. With these settings LecA and StxB showed spatially separated binding patterns on the surface of phases-separated GUVs (Fig. 2A). In these experiment we included the ld phase marker β-BODIPY-FL-C_5-HPC (17). This revealed that both lectins preferred the lo phase, but LecA and StxB only partially overlapped within the lo phase. In contrast, in non-phase-separated GUVs no segregation between LecA and StxB was observed (Fig. 2B).

To rule out unspecific effects, we carried out several control experiments. First, we established that GUVs lacking Gb3 were not able to bind LecA or StxB (Fig. S1). Second, only negligible spectral crosstalk occurred between the membrane marker channel (β-BODIPY-FL-C_5-HPC) and the channels used for the fluorescent labels of the lectins (Cy3 and Cy5) (Fig. S2).

These results demonstrate that the different binding patterns between LecA and StxB, which were observed in cells, could be successfully rebuilt in a model system of controlled composition based on GUVs. In such synthetic systems, in absence of the active cellular machinery, only the lectin-Gb3 interaction and the membrane environment can drive the spatial segregation between LecA and StxB .

Analysis of LecA and StxB preference for Gb3 species and membrane order

Based on previously reported observations with a specific class of Gb3-binding lectins, pentameric vero toxins (43–48), we hypothesized that LecA and StxB prefer to recognize differently exposed carbohydrate head groups of Gb3. The exposure of the head group of a glycolipid is predominantly determined by the way it is embedded in the lipid bilayer (47, 49). The embedding itself is influenced by (i) the length and saturation degree of its fatty acyl chain and (ii) the constitution of the surrounding lipid environment. To test how the structure of the fatty acyl chains influences LecA and StxB binding, we produced GUVs containing only Gb3 molecules with defined fatty acyl chains (Gb3-C24:0, Gb3-C24:1, and Gb3-FSL) and Gb3-mix as a control. Hereby, Gb3-FSL is a synthetic lipid that contains the Gb3 head group linked via a spacer ($O(CH_2)_3NH$) to a dioleoylphosphatidylethanolamine (DOPE) backbone (50). Furthermore, to investigate how the lipid environment influences LecA and StxB binding, we prepared non-phase-separated and phase-separated GUVs. To measure the binding of the two lectins in a quantitative manner, we used the recently developed FIJI macro GUV-AP that determines protein binding efficiency to GUVs and enables analysis of large datasets (51). For quantifying the binding efficiency, we determined the ratio between the signal of the lectin at the rim of the GUV and the free lectin in the solution (51). Such ratio represents quantitatively the contrast between the bound and free lectin. If the lectin cannot bind to the GUV, the contrast and thus the binding efficiency equals to 0. Furthermore, we included a feature in the macro to discriminate protein binding to ld and lo phases in phase-separated GUVs.

In non-phase-separated GUVs containing Gb3-mix, separately applied LecA and StxB were able to bind homogenously (Fig. 3A) and with comparable binding efficiency (Figs. 3E-F and Tables S1-S2). Introducing phase-separation to GUVs containing Gb3-mix showed that both, LecA and StxB, preferentially bound lo phases (Fig. 3B) as it has already been shown before (Fig. 2A). Interestingly, LecA recognized Gb3-mix in the lo phase much better than StxB.

In non-phase-separated GUVs containing Gb3-C24:0, LecA and StxB were able to bind with similar efficiency (Fig. 3C). But in phase-separated GUVs containing Gb3-C24:0, clear differences became apparent: Only LecA detectably bound to lo phases, whereas StxB hardly bound lo phases (Figs. 3D-F). In GUVs containing

Gb3-C24:1 both lectins showed similar binding patterns (Fig. S3A and Figs. 3E-F).

In general, for Gb3-mix and all single Gb3 species tested so far, both lectins preferred the lo phase over the ld phase in phase-separated GUVs. However, Gb3-FSL demonstrated the opposite behavior: In phase-separated GUVs containing Gb3-FSL, LecA and StxB bound better to the ld phase (Fig. S3B and Figs. 3E-F). In addition, whereas LecA displayed higher binding efficiencies than StxB in non-phase-separated GUVs containing Gb3-C24:0 and Gb3-C24:1, the opposite was true for non-phase-separated GUVs containing Gb3-FSL (Fig. S3B and Figs. 3E-F).

These results demonstrate that by altering the incorporation of Gb3 in the lipid bilayer, different binding behavior of LecA *versus* StxB can be achieved.

The most obvious difference was seen for Gb3-C24:0, where LecA was able to recognize lo phase-localized Gb3, but StxB hardly bound. This difference could be caused by the lipid order of the lo phase domains that is dependent on cholesterol and sphingomyelin (5, 35, 52). Thus, to test the impact of cholesterol and sphingomyelin directly, we prepared 'pure phase' GUVs that did not contain cholesterol and sphingomyelin and approximate ld phases ('DOPC' in Fig. 4) and GUVs that did contain cholesterol and sphingomyelin approximating lo phases ('Chol + SM' in Fig. 4). Chol + SM-GUVs bound both lectins significantly better than DOPC-GUVs (Figs. 4A-B and 4E-F), but the relative differences between Chol + SM-GUVs and DOPC-GUVs were more pronounced for StxB. This effect was enhanced for GUVs containing only Gb3-C24:0. In this case, LecA equally bound to DOPC-GUVs and Chol + SM-GUVs, but StxB was only able to recognize Chol + SM-GUVs (Figs. 4C-F and Tables S3-S4).

Taken together, using GUVs as model system enabled us to reveal that the two parameters 'Gb3 fatty acyl chain structure' and 'lipid environment' can cause conditions leading to preferential binding of either LecA or StxB. Both parameters influence Gb3 embedding in the lipid bilayer, which determines the orientation of the Gb3 head group (43, 47, 49). The head group conformation is

known to affect the binding efficiency of lectins to glycosphingolipids (37). Our analysis demonstrated that both parameters have to be considered to explain the different binding behavior of LecA and StxB.

Redesign of LecA and StxB segregation using a minimal system with pure Gb3 species

If the hypothesis is correct that the combination of Gb3 fatty acyl chain structure and membrane environment differentially determines the binding preferences of LecA and StxB, it should be possible to rebuild LecA and StxB segregation on the same GUV using minimal set of distinct Gb3 species. Since we observed the starkest differences between StxB and LecA for Gb3-C24:0 and Gb3-FSL, we chose to test LecA and StxB segregation in phase-separated GUVs containing 5 mol-% of each of these two Gb3 species. Indeed, this was sufficient to achieve different, but partially overlapping, staining patterns of LecA and StxB (Fig. 5) that resembled the patterns observed on cells (Figs. 1B-C) and on phase-separated GUVs containing Gb3 mix (Fig. 2A). In particular, in GUVs containing only Gb3-C24:0 and Gb3-FSL, StxB was only able to bind the ld phase, whereas LecA showed a preference for the lo phase.

Moreover, we investigated whether such segregation can also be seen in phase-separated SLBs containing 5 mol-% of Gb3-C24:0 and 5 mol-% of Gb3-FSL (Fig. S4A). Single microscopic images of flat SLBs provide a larger overview along the lateral direction of the lipid bilayer than images of GUVs. Therefore, in the images of SLBs multiple StxB clusters with distinct binding efficiencies for StxB within the ld phase became apparent. LecA bound in a pattern inverse to the StxB binding pattern and preferentially recognized lo phases. To gain more insights into LecA and StxB binding behavior on SLBs, we carried out experiments with SLBs containing only single Gb3 species. In SLBs containing Gb3-FSL, LecA formed clusters in the ld phase (Fig. S4B) and StxB homogeneously bound ld phases in SLBs containing Gb3-FSL (Fig. S4C). SLBs containing only Gb3-C24:0 showed preferential binding of LecA to lo phases (Fig. S4D). Surprisingly, in these SLBs StxB also bound lo phases (Fig. S4E) as also previously reported (53). However, this is in contrast to the results obtained with phase-separated GUVs containing Gb3-C24:0, where StxB was not able to

bind significantly (Fig. 3D). This observations suggest that an additional parameter, such as altered inter-leaflet coupling in SLBs caused by the interaction of one leaflet with the underlying mica substrate, results in changes in Gb3 head group exposure that can be sensed by StxB.

Taken together, our results demonstrate that a minimal system containing only two selected Gb3 species is sufficient to replicate different binding patterns of LecA and StxB.

Discussion

The concept of LecA and StxB as sensors for membrane environment

LecA and StxB bind both to the glycosphingolipid Gb3 (30, 39). However, we found that LecA and StxB spatially segregated at the plasma membrane of cells. By using GUVs, which combine the advantages of (i) being artificial membrane systems with well-defined lipid composition and phases with (ii) mimicking the incorporation of Gb3 in cellular plasma membranes, we were able to redesign the segregation between LecA and StxB. This proves that the different binding behavior of LecA and StxB is based on the direct interaction between the lectins and Gb3. Moreover, we identified two interdependent parameters that control the efficiency of LecA and StxB binding to Gb3: the structure of the fatty acyl chain of Gb3 (i.e. Gb3 species) and the order of the membrane environment. Both parameters determine how a single Gb3 molecule is embedded in the lipid bilayer, and hence, how the Gb3 head group is oriented. Thus, in accordance with previous studies (5, 37, 47), we propose that the conformation of the carbohydrate head group of Gb3 is the critical factor that alters binding efficiencies for LecA and StxB. Importantly, we demonstrated here that the specific binding preferences of LecA and StxB are different. This enables utilizing the comparison of staining patterns of the two lectins as readout for the local membrane environment.

The primary cilium harbors a unique lipid domain

The formation of distinct LecA and StxB domains on cells occurred on various scales. Even complete cellular organelles, like the primary cilium, were not recognized by LecA, while they were bound by StxB. The primary cilium membrane and the apical plasma membrane are continuous and there are no apparent obstacles that could directly block lipid movement along the outer plasma membrane leaflet (54). Nevertheless, our surprising finding suggests that the primary cilium membrane contains a distinct lipid domain of higher order that does not extend to the surrounding apical plasma membrane. Support for this hypothesis can be found in literature. Primary cilia were found to be cholesterol-rich (55) (56). The gangliosides GM1 and GM3 (57), and the

Forssman glycolipid (58), which are all considered as lipid raft markers, localize to the primary cilium of mammalian cells. Furthermore, *Trypanosoma brucei* flagellar membranes, which resemble primary cilia, are enriched in lipid raft components (59).

Influence of membrane order on LecA and StxB binding

It is well established that the lipid composition and overall membrane order differ between the apical and basolateral plasma membrane of epithelial cells (2, 38, 60), with the apical plasma membrane displaying a higher order and containing more cholesterol and sphingolipids relative to the basolateral plasma membrane (61). LecA and StxB were also able to recognize these differences, with StxB showing a significantly stronger binding preference for the apical plasma membrane than LecA. This fits to the observations from our studies with artificial membranes, which revealed that, overall, LecA more tolerantly recognized different Gb3 species and membrane environments than StxB. By using GUVs, we were able to demonstrate in Fig. 4 that the apical preference of StxB can be explained by higher membrane order induced by cholesterol and sphingomyelin: For GUVs containing Gb3-mix, both LecA and StxB preferred the more ordered GUVs, but the preference was more pronounced for StxB, as it was for the apical to basolateral binding ratio on cells (Fig 1A). When using GUVs containing only the single Gb3 species Gb3-C24:0, the effect became drastically enhanced. LecA demonstrated equal binding to GUVs with and without cholesterol and sphingomyelin, whereas StxB only bound to GUVs with cholesterol or sphingomyelin.

Interplay between Gb3 species and membrane environment

Not only the total binding efficiencies of LecA and StxB at the apical and basolateral plasma membrane were different, but also on smaller scales distinct binding differences were seen: At the plasma membrane of energy depleted cells, LecA and StxB segregated into only partially overlapping nano-domains (Fig. 1C). This suggests that LecA and StxB segregation promptly develop after binding and most likely continue during endocytosis (9), which provides an explanation for the different intracellular trafficking of LecA and StxB we reported before (9).

Importantly, we were able to rebuild such a domain separation between LecA and StxB in GUVs containing Gb3-mix and also in GUVs containing only the two Gb3 species Gb3-C24:0 and Gb3-FSL.

The reasons why Gb3-C24:0 and Gb3-FSL are minimally sufficient for reconstituting LecA and StxB segregation can be deduced from our experiments with single Gb3 species and illustrate how the interplay between Gb3 species and membrane environment governs different LecA and StxB binding: In phase-separated GUVs containing Gb3-FSL, both lectins preferred the ld phase over the lo phase. This was in stark contrast to the results obtained with phase-separated GUVs containing Gb3-mix and single non-FSL Gb3 species in which both lectins preferred the lo phase over the ld phase. Most likely, this is caused by a preferential integration of Gb3-FSL into the ld phase, since lectins bound to Gb3-FSL always co-localized with the ld marker β-BODIPY-FL-C5-HPC (17) (Figure S3B). As already described above, our GUV experiments with Gb3-C24:0 illustrate that for StxB Gb3 is best exposed in lo environments and the membrane composition alone is able to block or mask the binding of StxB.

The results from SLBs are in line with findings from GUVs in case of LecA, but for StxB divergent outcomes were observed: In phase-separated GUVs StxB hardly bound lo and ld phases, while on phase-separated SLBs binding of StxB to lo and ld phases occurred. This demonstrates that the system has a high sensitivity: Additional parameters that lead to subtle changes in the lipid bilayer and hence cause different Gb3 head group exposure, such as altered inter-leaflet coupling induced by the substrate of SLBs, can significantly shift the binding ability of StxB.

Conclusion and outlook

Taken together, our data revealed that the two Gb3-binding lectins LecA and StxB segregate into different domains at the plasma membrane of cells. We were able to reconstitute these effects in synthetic systems demonstrating that the driving force for segregation is controlled by parameters that determine the conformation of the Gb3 head group. These parameters, Gb3 fatty acyl chain structure and membrane environment, are interdependent, and enable LecA and StxB to act as sensors for membrane order on native cells with StxB indicating

more ordered membranes. Thus, comparing LecA with StxB staining patterns could be used in future as a sensitive read out for determining membrane order during cellular processes.

Materials and Methods

Cell lines and cell culture

Madin-Darby canine kidney (MDCK) strain II cells and HeLa cells were maintained at 37°C and 5% CO_2 in Dulbecco's modified Eagle's medium (DMEM) supplemented with 5% (for MDCK) and 10% (for HeLa) fetal calf serum. MDCK cells stably expressing Gb3 were established by stable overexpression of Gb3 synthase as described earlier (9, 42). For generating polarized monolayers, MDCK cells were confluently seeded to transwell filters (Corning, 0.4 µm pore size, polycarbonate membrane) and cultured for 4 d.

Lipids and preparation of lipid mixtures

1,2-dioleoyl-sn-glycero-3-phosphocholine (DOPC), cholesterol (Chol) and sphingomyelin (SM) were purchased from Avanti Polar Lipids, whereas Gb3-FSL was purchased from Sigma Aldrich. Gb3-mix was from Matreya, consisting of a mixture of Gb3 species extracted from porcine brain. The Gb3-species Gb3-C24:0 and Gb3-C24:1 were synthesized as described earlier (53). The fluorescent lipid 2-(4,4-difluoro-5,7-dimethyl-4-bora-3a,4a-diaza-s-indacene-3-pentanoyl)-1-hexadecanoyl-sn-glycero-3-phosphocholine (β-BODIPY-FL-C5-HPC) was from Invitrogen. All lipids were dissolved in chloroform, only Gb3-mix and Gb3-species were dissolved in a 2:1 chloroform/methanol mixture. Dissolved lipids were stored with an argon layer on top at -20°C. Lipid mixtures were prepared with a concentration of 0.5 mg of total lipid mass per 1 mL organic solvent or aqueous environment or buffers. The lipid ratios of each composition were calculated in molar percentages.

Preparation of GUVs

GUVs were produced utilizing electro-swelling (62). Briefly, lipid mixtures were spread on each side of an indium-tin oxidized (ITO) glass slide (Sigma Aldrich) with a Hamilton syringe (Hamilton) and evaporated overnight. Electro-swelling was done in phosphate buffered saline (PBS, Carl Roth) supplemented with 1 mg/mL sucrose (Carl Roth) for 3 h at room temperature for non-phase-

separated GUVs or for 3 h at 55°C for phase-separated GUVs. The imaging buffer for GUVs was adjusted to the same osmolarity as the PBS/sucrose solution.

Preparation of SLBs

Supported lipid membranes were prepared using vesicle fusion (63). Briefly, lipid films were resuspended in low-Ca buffer (20 mM TRIS/HCl, 100 mM NaCl, and 1 mM $CaCl_2$, pH 7.5) at 55°C for 35 min. Small vesicles were created using an extruder with a 50 nm cut-off polycarbonate membrane (Avestin) and directly transferred to the sample chamber. The sample chamber was home-built using mica, either grade V1 or V3 (Plano GmbH), which was fixed with optical adhesive (NOA 61, Norland Products) to a glass bottom dish (35 mm, #1.5 glass, World Precision Instruments). To induce vesicle fusion, a high-Ca buffer (20 mM TRIS/HCl, 100 mM NaCl, and 10 mM $CaCl_2$, pH 7.5) was added to increase the $CaCl_2$ concentration and bilayers were heated to 55°C for 1 h, followed by gentle cooling to room temperature. To remove non-fused vesicles and other debris, samples were rinsed with low-Ca buffer.

Lectin production and labeling

Recombinant LecA was produced from *Escherichia coli* following previously published procedures (39). The StxB used was the B-subunit of Shiga toxin 1 produced in *Escherichia coli* (Sigma Aldrich). Lectins were dissolved at 1 mg/mL in PBS (for StxB) or in PBS supplemented with 100 mg/mL $MgCl_2$ and 100 mg/mL $CaCl_2$ (for LecA), sterile filtered, and stored at 4°C prior usage.

For fluorescent labeling, NHS-ester conjugated Alexa488 (Thermo Fisher), Cy3, and Cy5 (GE Healthcare Life Science) was used. Dyes were dissolved at 1 mg/mL in water-free DMSO (Carl Roth), aliquoted, and stored at -20°C before usage. To set up the labeling reaction, 200 µL of lectin (1 mg/mL) was supplemented with 25 µL of a 1 M $NaHCO_3$ (pH 9) solution. The molar ratio between dye and lectin was set to 5:1. The labeling mix was incubated at room temperature for 50 min and uncoupled dyes separated using Zeba Spin desalting columns (7k MWCO, 0.5 mL, Thermo Fischer). Labeled lectins were aliquoted into working stocks and stored at -80°C until usage.

Microscopy

MDCK cells grown on transwell filters were fixed with 4% formaldehyde and mounted as described before (9).

GUVs and MDCK cell samples were imaged using a laser scanning confocal microscope system from Nikon (A1R), equipped with a 60x oil immersion objective with a numerical aperture (*NA*) of 1.49, and laser lines at 488 nm, 561 nm, and 647 nm. Image acquisition and processing was done using the software NIS-Elements (built version 4.5, Nikon).

SLBs were imaged with a Nikon Eclipse Ti-E inverted microscope, equipped with a TIRF-illuminator, a 100x oil immersion objective (*NA* 1.49) and an EM-CCD camera (Andor Ixon DU-879). Images were acquired using a highly inclined laser beam (HILO-configuration) (64). Image acquisition and processing was done using the software NIS-Elements (built version 4.5, Nikon).

TIRF-SIM imaging was done using a Nikon-N-SIM microscope equipped with laser lines at 488 nm, 561 nm, and 647 nm, and a CFI apochromatic TIRF 100x oil objective (*NA* 1.49).

Image analysis

Quantification of lectin binding to MDCK cells was done by measuring fluorescent intensities in single cells that were not surrounded by labeled cells using a custom-written Matlab program as described before (40).

Quantification of lectin binding efficiencies to GUVs was done using the ImageJ-macro GUV-AP (51). Furthermore, we included a feature in the macro to enable the independent assessment of binding to ld and lo phases in phase-separated GUVs. To this end we modified the macro with a procedure that recognizes and stores the locations of ld and lo domains from β-BODIPY-FL-C5-HPC staining patterns separately for all GUVs in a given image. The macro source code including the modifications is available at: https://github.com/AG-Roemer/GUV-AP/releases/tag/v2.0

Energy depletion

HeLa cells were energy depleted by incubation for 20 minutes at 37°C with PBS supplemented with 10 mM 2-deoxy-D-glucose (DOG) and 10 mM NaN_3. The compounds were kept present during all incubation steps at 37°C.

References

1. van Meer G, Voelker DR, Feigenson GW (2008) Membrane lipids: where they are and how they behave. *Nat Rev Mol Cell Biol* 9:112–124.
2. Simons K, van Meer G (1988) Lipid sorting in epithelial cells. *Biochemistry* 27:6197–6202.
3. Pomorski T, Hrafnsdóttir S, Devaux PF, van Meer G (2001) Lipid distribution and transport across cellular membranes. *Seminars in cell & developmental biology* 12:139–148.
4. Sharom FJ (2011) Flipping and flopping--lipids on the move. *IUBMB life* 63:736–746.
5. Lingwood D, Simons K (2010) Lipid rafts as a membrane-organizing principle. *Science* 327:46–50.
6. Hancock JF (2006) Lipid rafts: contentious only from simplistic standpoints. *Nat Rev Mol Cell Biol* 7:456–462.
7. Munro S (2003) Lipid rafts: elusive or illusive? *Cell* 115:377–388.
8. Romer W *et al. (*2007) Shiga toxin induces tubular membrane invaginations for its uptake into cells. *Nature* 450:670–675.
9. Müller SK *et al. (*2017) Gb3-binding lectins as potential carriers for transcellular drug delivery. *Expert opinion on drug delivery* 14:141–153.
10. Chinnapen DJ-F *et al. (*2012) Lipid sorting by ceramide structure from plasma membrane to ER for the cholera toxin receptor ganglioside GM1. *Developmental Cell* 23:573–586.
11. Simons K, Toomre D (2000) Lipid rafts and signal transduction. *Nat Rev Mol Cell Biol* 1:31–39.
12. Windschiegl B *et al. (*2009) Lipid Reorganization Induced by Shiga Toxin Clustering on Planar Membranes. *PLoS ONE* 4:e6238.
13. Vereb G *et al. (*2003) Dynamic, yet structured: The cell membrane three decades after the Singer-Nicolson model. *Proc Natl Acad Sci U S A* 100:8053–8058.
14. Schubert T, Römer W (2015) How synthetic membrane systems contribute to the understanding of lipid-driven endocytosis. *Biochimica et biophysica acta* 1853:2992–3005.
15. Pike LJ (2008) The challenge of lipid rafts. *The Journal of Lipid Research* 50:S323-S328.
16. Mayor S, Rao M (2004) Rafts: scale-dependent, active lipid organization at the cell surface. *Traffic* 5:231–240.
17. Baumgart T, Hunt G, Farkas ER, Webb WW, Feigenson GW (2007) Fluorescence probe partitioning between Lo/Ld phases in lipid membranes. *Biochimica et biophysica acta* 1768:2182–2194.
18. Sengupta P, Hammond A, Holowka D, Baird B (2008) Structural determinants for partitioning of lipids and proteins between coexisting fluid phases in giant plasma membrane vesicles. *Biochimica et biophysica acta* 1778:20–32.
19. Klymchenko AS, Kreder R (2014) Fluorescent probes for lipid rafts: from model membranes to living cells. *Chemistry & biology* 21:97–113.
20. Sezgin E, Sadowski T, Simons K (2014) Measuring lipid packing of model and cellular membranes with environment sensitive probes. *Langmuir : the ACS journal of surfaces and colloids* 30:8160–8166.
21. Lingwood CA (2011) Glycosphingolipid functions. *Cold Spring Harb Perspect Biol* 3.

22. Sezgin E *et al. (*2012) Partitioning, diffusion, and ligand binding of raft lipid analogs in model and cellular plasma membranes. *Biochim Biophys Acta* 1818:1777–1784.
23. Baumgart T *et al. (*2007) Large-scale fluid/fluid phase separation of proteins and lipids in giant plasma membrane vesicles. *Proceedings of the National Academy of Sciences of the United States of America* 104:3165–3170.
24. Blank N *et al. (*2007) Cholera toxin binds to lipid rafts but has a limited specificity for ganglioside GM1. *Immunology and cell biology* 85:378–382.
25. Raghunathan K *et al. (*2016) Glycolipid Crosslinking Is Required for Cholera Toxin to Partition Into and Stabilize Ordered Domains. *Biophys. J.* 111:2547–2550.
26. Cioci G *et al. (*2003) Structural basis of calcium and galactose recognition by the lectin PA-IL of Pseudomonas aeruginosa. *FEBS Lett* 555:297–301.
27. Kirkeby S, Hansen AK, d'Apice A, Moe D (2006) The galactophilic lectin (PA-IL, gene LecA) from Pseudomonas aeruginosa. Its binding requirements and the localization of lectin receptors in various mouse tissues. *Microbial pathogenesis* 40:191–197.
28. Chen CP, Song SC, Gilboa-Garber N, Chang KS, Wu AM (1998) Studies on the binding site of the galactose-specific agglutinin PA-IL from Pseudomonas aeruginosa. *Glycobiology* 8:7–16.
29. Pina DG, Johannes L (2005) Cholera and Shiga toxin B-subunits: thermodynamic and structural considerations for function and biomedical applications. *Toxicon* 45:389–393.
30. Pina DG, Johannes L, Castanho, Miguel A R B (2007) Shiga toxin B-subunit sequential binding to its natural receptor in lipid membranes. *Biochim Biophys Acta* 1768:628–636.
31. St. Hilaire, Phaedria M., Boyd MK, Toone EJ (1994) Interaction of the Shiga-like Toxin Type 1 B-Subunit with Its Carbohydrate Receptor. *Biochemistry* 33:14452–14463.
32. Johannes L, Romer W (2010) Shiga toxins--from cell biology to biomedical applications. *Nat Rev Microbiol* 8:105–116.
33. Dietrich C *et al. (*2001) Lipid Rafts Reconstituted in Model Membranes. *Biophysical Journal* 80:1417–1428.
34. Sych T, Mély Y, Römer W (2018) Lipid self-assembly and lectin-induced reorganization of the plasma membrane. *Philosophical transactions of the Royal Society of London. Series B, Biological sciences* 373.
35. Simons K, Sampaio JL (2011) Membrane organization and lipid rafts. *Cold Spring Harbor perspectives in biology* 3:a004697.
36. Simons K, Gerl MJ (2010) Revitalizing membrane rafts: new tools and insights. *Nat Rev Mol Cell Biol* 11:688–699.
37. Lingwood D *et al. (*2011) Cholesterol modulates glycolipid conformation and receptor activity. *Nat. Chem. Biol.* 7:260–262.
38. Simons K, van Meer G (1988) Lipid sorting in epithelial cells. *Biochemistry* 27:6197–6202.
39. Blanchard B *et al. (*2008) Structural Basis of the Preferential Binding for Globo-Series Glycosphingolipids Displayed by Pseudomonas aeruginosa Lectin I. *Journal of Molecular Biology* 383:837–853.

40. Thuenauer R *et al. (*2014) Four-dimensional live imaging of apical biosynthetic trafficking reveals a post-Golgi sorting role of apical endosomal intermediates. *Proc Natl Acad Sci U S A* 111:4127–4132.
41. Jacewicz M (1986) Pathogenesis of shigella diarrhea. XI. Isolation of a shigella toxin- binding glycolipid from rabbit jejunum and HeLa cells and its identification as globotriaosylceramide. *Journal of Experimental Medicine* 163:1391–1404.
42. Eierhoff T *et al. (*2014) A lipid zipper triggers bacterial invasion. *Proceedings of the National Academy of Sciences of the United States of America* 111:12895–12900.
43. Arab S, Lingwood CA (1996) Influence of phospholipid chain length on verotoxin/globotriaosyl ceramide binding in model membranes: comparison of a supported bilayer film and liposomes. *Glycoconj J* 13:159–166.
44. Binnington B, Lingwood D, Nutikka A, Lingwood CA (2002) Effect of globotriaosyl ceramide fatty acid alpha-hydroxylation on the binding by verotoxin 1 and verotoxin 2. *Neurochem. Res.* 27:807–813.
45. Kiarash A, Boyd B, Lingwood CA (1994) Glycosphingolipid receptor function is modified by fatty acid content. Verotoxin 1 and verotoxin 2c preferentially recognize different globotriaosyl ceramide fatty acid homologues. *Journal of Biological Chemistry* 269:11138–11146.
46. Lingwood C (1996) Role of verotoxin receptors in pathogenesis. *Trends in Microbiology* 4:147–153.
47. Lingwood CA *et al. (*2010) New aspects of the regulation of glycosphingolipid receptor function. *Chem. Phys. Lipids* 163:27–35.
48. Pellizzari A, Pang H, Lingwood CA (1992) Binding of verocytotoxin 1 to its receptor is influenced by differences in receptor fatty acid content. *Biochemistry* 31:1363–1370.
49. Lingwood CA, Binnington B, Manis A, Branch DR (2010) Globotriaosyl ceramide receptor function - where membrane structure and pathology intersect. *FEBS Letters* 584:1879–1886.
50. Blake DA, Bovin NV, Bess D, Henry SM (2011) FSL constructs: a simple method for modifying cell/virion surfaces with a range of biological markers without affecting their viability. *Journal of visualized experiments : JoVE*.
51. Sych T *et al. (*2018) GUV-AP: multifunctional FIJI-based tool for quantitative image analysis of Giant Unilamellar Vesicles. *Bioinformatics (Oxford, England)*.
52. Simons K, Vaz, Winchil L C (2004) Model systems, lipid rafts, and cell membranes. *Annu Rev Biophys Biomol Struct* 33:269–295.
53. Schütte OM *et al. (*2014) Influence of Gb3 glycosphingolipids differing in their fatty acid chain on the phase behaviour of solid supported membranes: chemical syntheses and impact of Shiga toxin binding. *Chem. Sci.* 5:3104.
54. Reiter JF, Blacque OE, Leroux MR (2012) The base of the cilium: roles for transition fibres and the transition zone in ciliary formation, maintenance and compartmentalization. *EMBO Reports* 13:608–618.
55. Ott C, Lippincott-Schwartz J (2012) Visualization of live primary cilia dynamics using fluorescence microscopy. *Current protocols in cell biology* Chapter 4:Unit 4.26.
56. Cuevas P, Gutierrez Diaz JA (1985) Absence of filipin-sterol complexes from the ciliary necklace of ependymal cells. *Anatomy and embryology* 172:97–99.

57. Janich P, Corbeil D (2007) GM1 and GM3 gangliosides highlight distinct lipid microdomains within the apical domain of epithelial cells. *FEBS Lett* 581:1783–1787.
58. Vieira OV *et al. (*2006) FAPP2, cilium formation, and compartmentalization of the apical membrane in polarized Madin-Darby canine kidney (MDCK) cells. *Proc Natl Acad Sci U S A* 103:18556–18561.
59. Tyler KM *et al. (*2009) Flagellar membrane localization via association with lipid rafts. *Journal of Cell Science* 122:859–866.
60. Owen DM, Magenau A, Majumdar A, Gaus K (2010) Imaging membrane lipid order in whole, living vertebrate organisms. *Biophys. J.* 99:L7-9.
61. Maxfield FR, Wüstner D (2002) Intracellular cholesterol transport. *The Journal of clinical investigation* 110:891–898.
62. Madl J, Villringer S, Römer W (2017) in *Chemical and synthetic approaches in membrane biology*, ed Shukla AK. (Humana Press, New York, NY), pp 17–36.
63. Tamm LK, McConnell HM (1985) Supported phospholipid bilayers. *Biophysical Journal* 47:105–113.
64. Tokunaga M, Imamoto N, Sakata-Sogawa K (2008) Highly inclined thin illumination enables clear single-molecule imaging in cells. *Nature methods* 5:159–161.

Acknowledgements

This work was supported by the German Research Foundation [EXC 294, RO 4341/2-1, RO 4341/3-1, IRTG 1642, RTG 2202, SFB 803], the Ministry of Science, Research and the Arts of Baden-Württemberg [Az: 33-7532.20] and a starting grant from the European Research Council [Programme "Ideas," ERC-2011-StG 282105]. Ta.S. acknowledges support by the Franco-German University (programs 'Polymer Sciences' and 'Cotutelle de thèse') and the Collège Doctoral Européen (PDI).

Contributions

W.R. conceived the project. Th.S., Ta.S., R.T., and W.R. designed and carried out experiments. M.X., A.B. carried out experiments. Th.S., Ta.S., and R.T. analyzed data. L.J.P., A.R., K.K., and D.B.W. produced Gb3-24:0 and Gb3-24:1. J.M., R.O., C.S., and Y.M. contributed to method development. Th.S. and R.T. wrote the paper involving the comments and corrections of all authors.

Figures

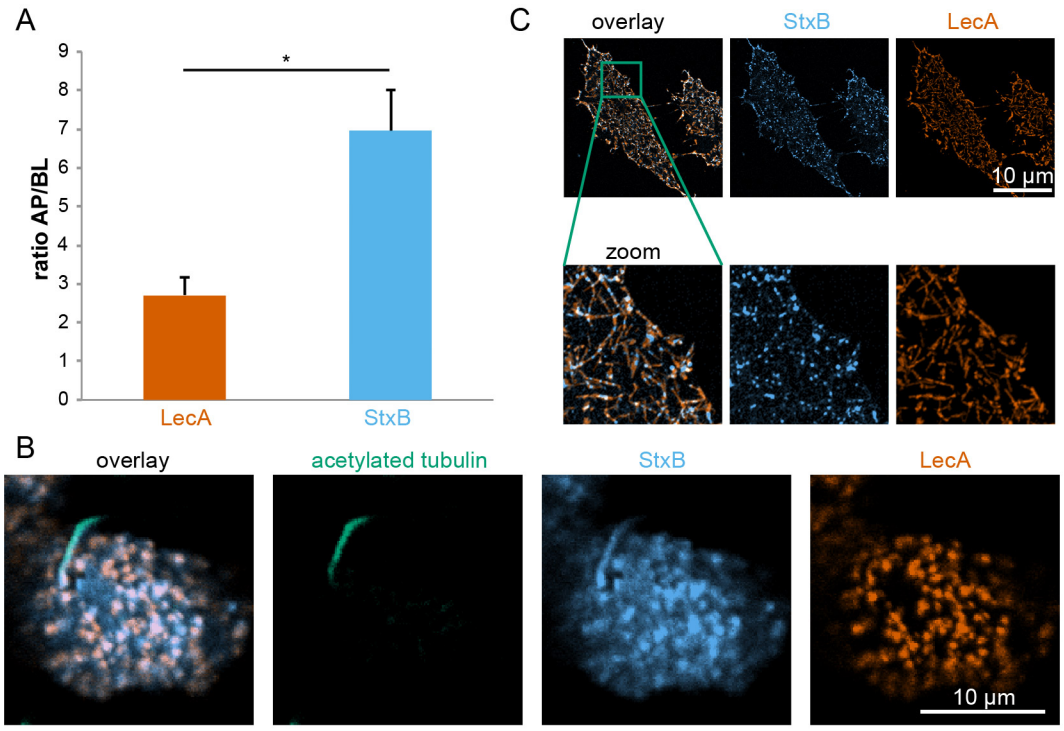

Figure 1: LecA and StxB show different binding patterns on cells

(A) MDCK cells stably expressing Gb3 synthase were mixed with wild type MDCK cells 1:10, seeded on transwell filters, and cultured for 4 d to form polarized monolayers. LecA-Alexa488 (117 nM) or StxB-Cy3 (106 nM) were applied only to the apical (AP) or basolateral (BL) side of the cells and incubated for 30 min at 4°C. After washout, samples were fixed, mounted, and the intensities of AP or BL bound LecA or StxB were determined in single cells by measuring LecA-Alexa488 and StxB-Cy3 intensities from image stacks recorded with a confocal microscope. Then the AP to BL signal intensities were calculated from the mean values from n > 50 cells per condition. The graphs display the mean values from 3 independent experiments, the error bars represent the standard error mean. Statistical significance was assayed with a paired two-tailed t-test, * indicates $p < 0.05$. (B) Polarized MDCK cells stably expressing Gb3 synthase were incubated apically with LecA-Alexa488 (196 nM, orange) and StxB-Cy3 (13 nM, blue) for 30 min at 37°C. After washout of unbound lectin, cells were fixed and primary cilia were stained using an antibody recognizing acetylated tubulin (green). The images show confocal sections at the height of the apical plasma membrane. (C) HeLa cells were energy-depleted and then incubated with LecA-Alexa488 (98 nM) or

StxB-Cy3 (106 nM) for 15 min at 37°C. After fixation, cells were imaged with a TIRF-SIM microscope.

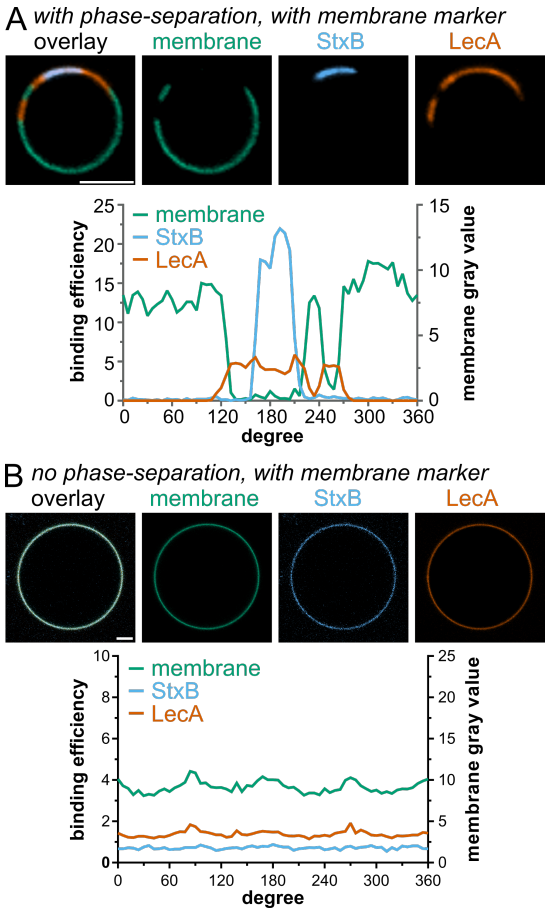

Figure 2: Segregation between LecA and StxB can be reconstituted in GUVs containing a natural mixture of Gb3 species

GUVs containing 5 mol-% Gb3-mix were incubated with LecA-Al647 (200 nM, orange) and StxB-Cy3 (600 nM in A and 200 nM in B, blue) (A and B). The images show equatorial sections through representative GUVs with a diagram displaying the corresponding circular intensity profiles underneath. Phase-separated GUV (A) contained DOPC/sphingomyelin/cholesterol/ Gb3-mix in the ratio 42.5/14,5/42.5/5 mol-%, whereas non-phase-separated GUV (B) contained DOPC/cholesterol/Gb3-mix in the ratio 64.5/30/5 mol-%. GUVs in A and B were additionally spiked with 0.5 mol-% of the membrane marker β-BODIPY-FL-C_5-HPC (green). Scale bars correspond to 5 µm.

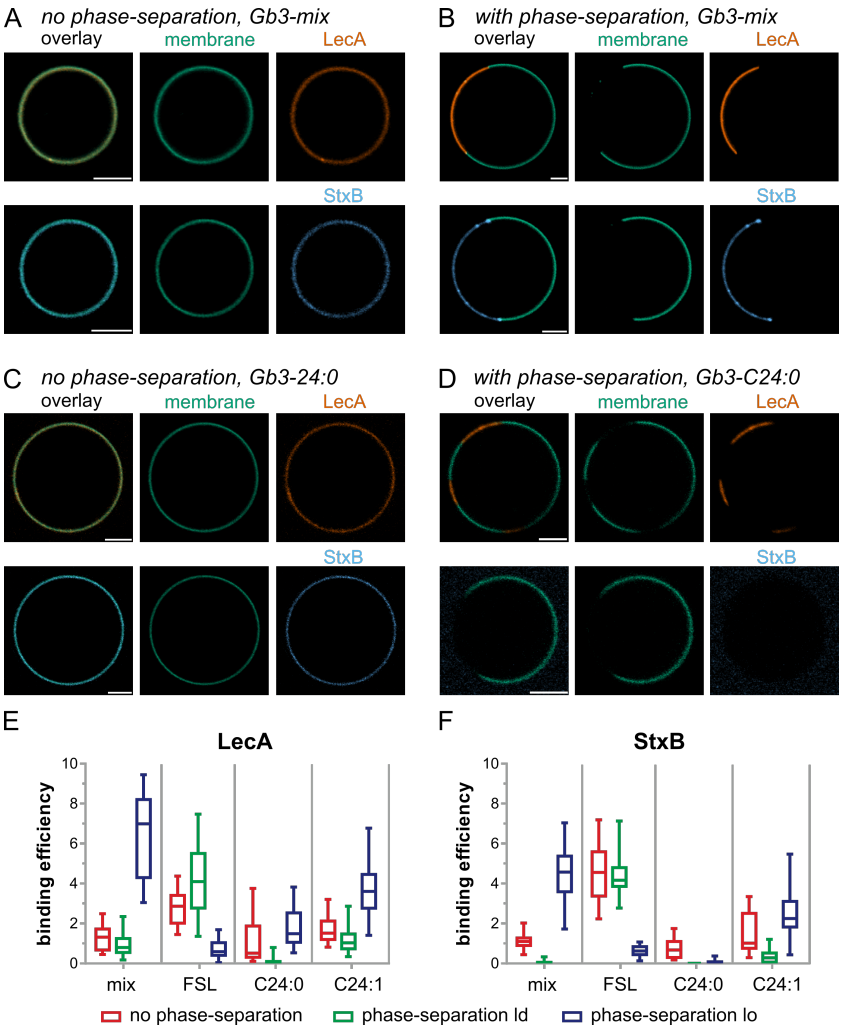

Figure 3: Investigation how Gb3 species and phase separation influence LecA and StxB binding efficiencies

GUVs doped with 0.5 mol-% of the membrane marker β-BODIPY-FL-C_5-HPC (green) and 5 mol-% Gb3-mix (A and B) or 5 mol-% Gb3-C24:0 (C and D) were incubated with LecA-Cy5 (200 nM, orange) or StxB-Cy5 (200 nM, blue). Non-phase-separated GUVs (A and C) contained DOPC/cholesterol/Gb3 in the ratio 64.5/30/5 mol-%, whereas phase-separated GUVs (B and D) consisted of DOPC/cholesterol/sphingomyelin/Gb3 in the ratio 42.5/14.5/42.5/5 mol-%. The images A – D show equatorial sections through representative GUVs. Scale bars correspond to 5 µm. (E – F) Quantitative analysis of the binding efficiencies of LecA (E) and StxB (F) to non-phase-separated GUVs (red) or the ld (green) or lo (blue) phase of phase-separated GUVs containing 5 mol-% of either Gb3-mix (mix), Gb3-C24:0 (C24:0), Gb3-C24:1 (C24:1), or Gb3-FSL (FSL). For each condition, the middle horizontal line represents the median, the boxes the 25th to 75th percentiles, and the whiskers the min and max values. In Table S1 the

descriptive statistics of the data is summarized and Table S2 contains the data from a significance analysis.

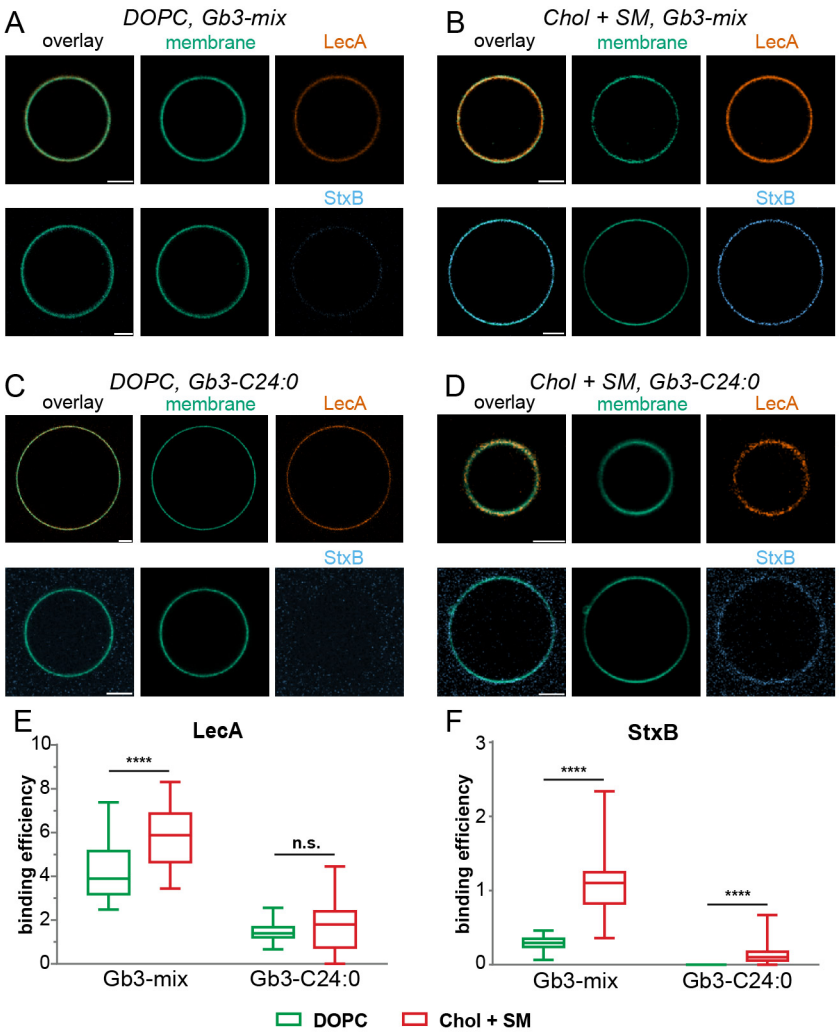

Figure 4: The interplay between Gb3 species and cholesterol content influences LecA and StxB binding efficiencies

GUVs doped with 0.5 mol-% of the membrane marker β-BODIPY-FL-C_5-HPC (green) and 5 mol-% Gb3-mix (A and B) or 5 mol-% Gb3-C24:0 (C and D) were incubated with LecA-Al647 (200 nM, orange) or StxB-Cy5 (200 nM, blue). GUVs approximating liquid-disordered membranes (DOPC, A and C) contained DOPC/Gb3 in the ratio 94.5/5 mol-%, and GUVs resembling liquid-ordered membranes (Chol + SM, B and D) consisted of sphingomyelin/cholesterol/Gb3 in the ratio 64.5/30/5 mol-%. The images A – D show equatorial sections through representative GUVs. Scale bars correspond to 5 µm. (E – F) Quantitative analysis

of the binding efficiencies of LecA (E) and StxB (F) to DOPC GUVs (green) and Chol + SM GUVs (red) containing 5 mol-% of either Gb3-mix, or Gb3-C24:0. For each condition, the middle horizontal line represents the median, the boxes the 25th to 75th percentiles, and the whiskers the min and max values. In Table S3 the descriptive statistics of the data is summarized, and Table S4 contains the complete data from the significance analysis.

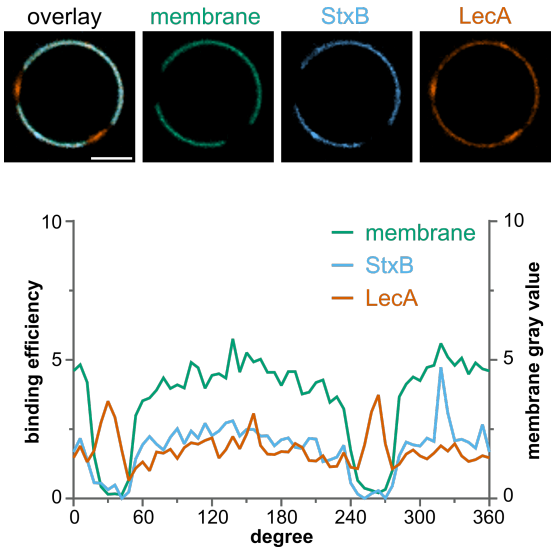

Figure 5: Reconstituting LecA and StxB segregation in minimal systems

(A) Phase-separated GUVs composed of DOPC/cholesterol/sphingomyelin/ β-BODIPY-FL-C_5-HPC (green)/Gb3-FSL/Gb3-C24:0 in the ratio 40/14.5/40/0.5/5/5 mol-%) were incubated with LecA-Al647 (200 nM, orange) and StxB-Cy3 (600 nM, blue). Equatorial sections through a representative GUV are shown and the corresponding circular intensity profiles are displayed underneath. Scale bar corresponds to 5 µm.

Supplementary Materials

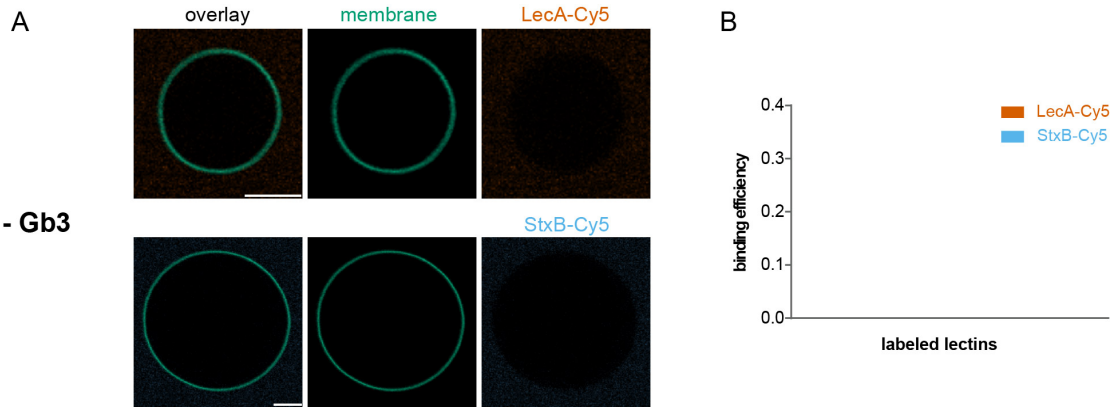

Figure S1: GUVs lacking Gb3 do not bind LecA or StxB

(A) GUVs composed of DOPC/cholesterol/β-BODIPY-FL-C_5-HPC (green) in the ratio 69.5/30/ 0.5 mol-% were incubated with either LecA-Cy5 (orange, 200 nM, top row) or with StxB-Cy5 (blue, 200 nM, bottom row). Represented equatorial cross sections were acquired with identical microscope settings as for the quantitative binding studies. Scale bars correspond to 5 µm. (B) Quantification of the binding efficiencies, showing that no binding occurs in GUVs without Gb3.

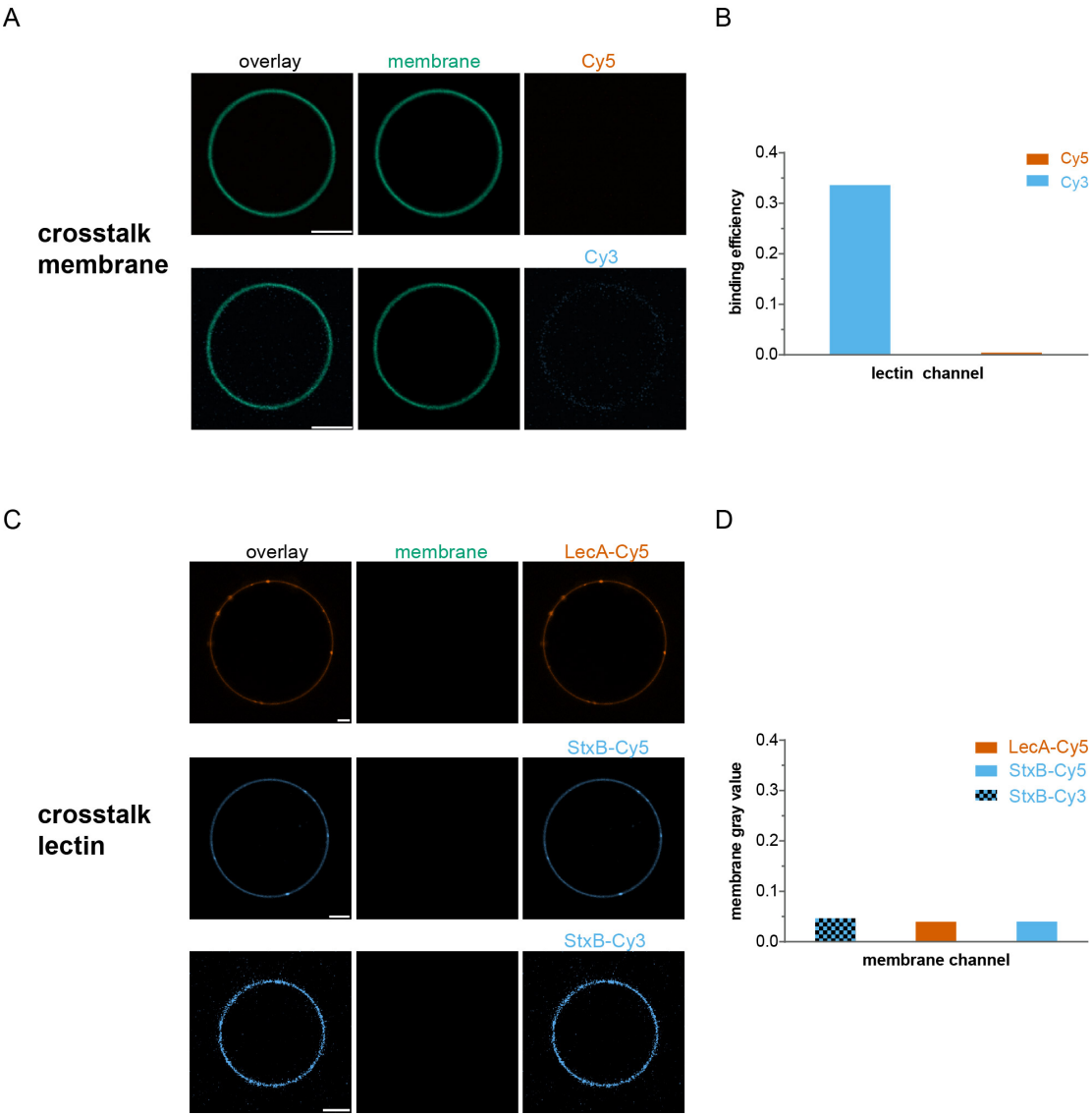

Figure S2: Controls for spectral crosstalk between the used channels

(A) GUVs composed of DOPC/cholesterol/β-BODIPY-FL-C_5-HPC (green)/Gb3-mix in the ratio 64.5/30/0.5/5 mol-%, but without added lectins, were imaged using the same microscope settings as for the quantitative binding studies. Thus, the images for the Cy5 (orange) and Cy3 (blue) channels represent crosstalk signals. Scale bars correspond to 5 µm. (B) Quantification of the apparent binding efficiencies for the GUVs displayed in (A) as estimate of the crosstalk. (C) GUVs consisting of DOPC/cholesterol/Gb3-mix in the ratio 65/30/5 mol-% were incubated with either LecA-Cy5 (orange, 200 nM, top row), StxB-Cy5 (blue, 200 nM, middle row), or with StxB-Cy3 (blue, 200 nM, bottom row) and were imaged using the same microscope settings as for the quantitative binding studies. Thus, the images for the membrane channel (green) represent crosstalk signals. Scale

bars correspond to 5 µm. (D) Quantification of the apparent membrane signal intensities for the GUVs displayed in (C) as estimate of the crosstalk.

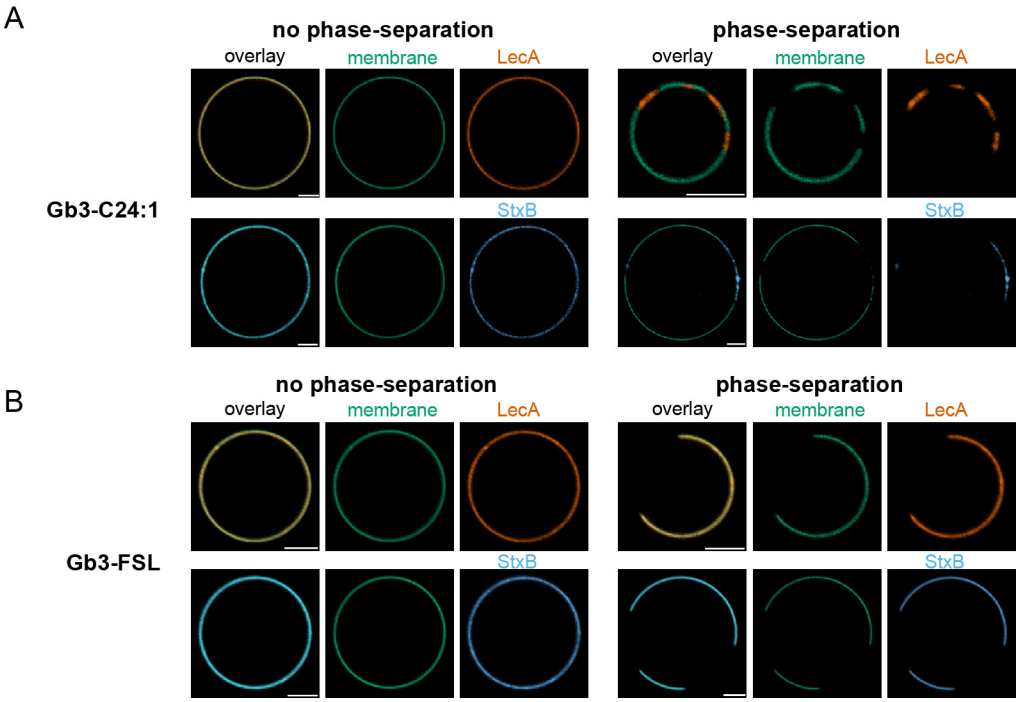

Figure S3: Control experiments related to Figure 3

GUVs doped with 0.5 mol-% of the membrane marker β-BODIPY-FL-C_5-HPC (green) and 5 mol-% Gb3-C24:1 (A), or 5 mol-% Gb3-FSL (B) were incubated with LecA-Cy5 (200 nM, orange) or StxB-Cy5 (200 nM, blue). Non-phase-separated GUVs (left panels) contained DOPC/cholesterol/Gb3 in the ratio 64.5/30/5 mol-%, whereas phase-separated GUVs (right panels) consisted of DOPC/cholesterol/sphingomyelin/Gb3 in the ratio 42.5/14.5/42.5/5 mol-%. Scale bars correspond to 5 µm.

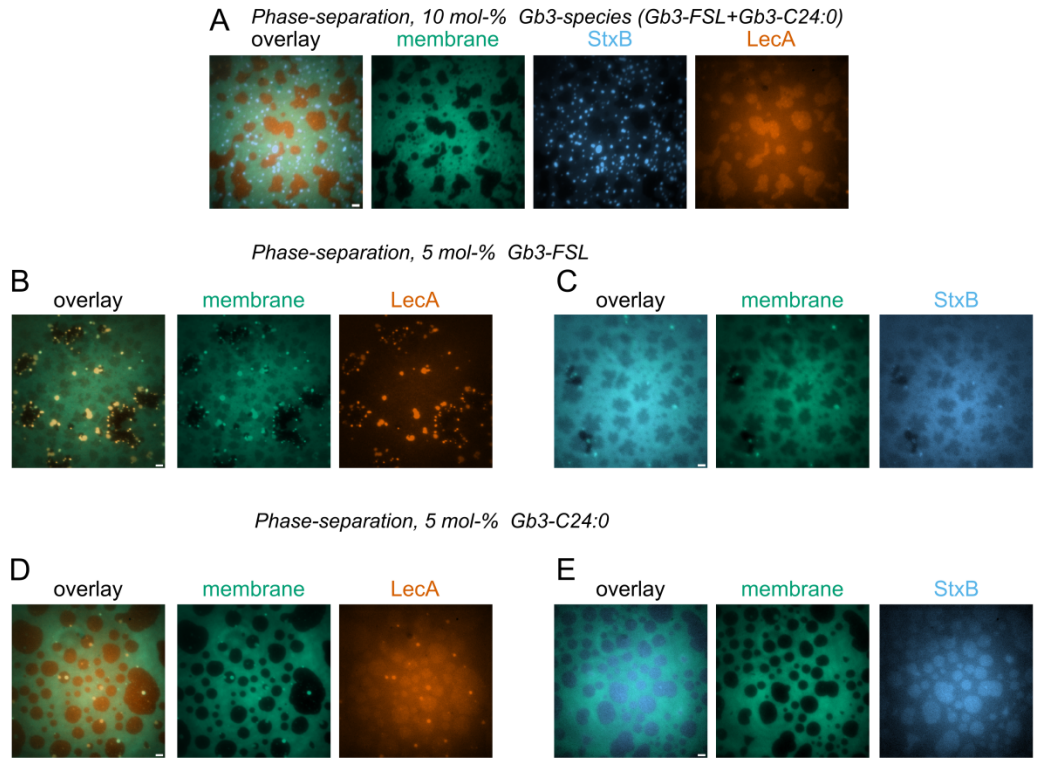

Figure S4: Investigating LecA and StxB binding on SLBs containing single Gb3 species

(A) Phase-separated SLBs consisting of DOPC/cholesterol/sphingomyelin/β-BODIPY-FL-C_5-HPC (green)/Gb3-FSL/Gb3-C24:0 in the ratio 40/14.9/40/0.1/5/5 mol-%) were incubated with StxB-Cy3 (100 nM, blue) and LecA-Cy5 (100 nM, orange). (B-E) Phase-separated SLBs consisting of DOPC/cholesterol/sphingomyelin/β-BODIPY-FL-C_5-HPC (green) in the ratio 37.4/20/37.5/0.1 mol-% and either 5 mol-% of Gb3-FSL (B, C) or 5 mol-% of Gb3-C24:0 (D, E) were incubated with either 200 nM LecA-Cy5 (200 nM, orange, C and D) or StxB-Cy5 (200 nM, blue, D and E). Scale bars correspond to 5 µm.

Table S1: Descriptive statistics of the data displayed in Figs. 3E-F

	Minimum		Maximum		Mean		Std. Deviation		Number of replicates	
	LecA	StxB	LecA	StxB	LecA	StxB	LecA	StxB	LecA	StxB
1 Gb3-mix No Phase	0,443	0,436	2,487	2,020	1,279	1,095	0,586	0,336	36	39
2 Gb3-mix Phase Ld	0,169	0	2,349	0,329	0,921	0,054	0,517	0,096	33	27
3 Gb3-mix Phase Lo	3,044	1,722	9,446	7,038	6,570	4,520	2,007	1,452	33	27
4 Gb3-FSL No Phase	1,450	2,226	4,368	7,192	2,822	4,505	0,837	1,287	37	46
5 Gb3-FSL Phase Ld	1,356	2,769	7,471	7,128	4,144	4,317	1,600	0,915	17	22
6 Gb3-FSL Phase Lo	0,041	0,125	1,685	1,069	0,728	0,619	0,464	0,251	17	22
7 Gb3-C24:0 No Phase	0,103	0,172	3,758	1,744	1,089	0,742	1,019	0,460	44	41
8 Gb3-C24:0 Phase Ld	0	0	0,798	0	0,106	0	0,171	0	41	51
9 Gb3-C24:0 Phase Lo	0,525	0	3,819	0,370	1,728	0,045	0,909	0,077	41	51
10 Gb3-C24:1 No Phase	0,810	0,288	3,203	3,345	1,671	1,400	0,586	0,915	50	39
11 Gb3-C24:1 Phase Ld	0,338	0	2,862	1,203	1,110	0,334	0,563	0,285	35	27
12 Gb3-C24:1 Phase Lo	1,408	0,425	6,770	5,473	3,777	2,448	1,300	1,060	35	27

Table S2: Statistical analysis of the data from Figs. 3E-F

Statistical analysis was carried out with GraphPad Prism (Version 6.0) with a two-way ANOVA Tukey´s multiple comparisons test. The significance level was set to 0.05.

		LecA			StxB		
Condition (I)	**Condition (J)**	**Mean Difference (I-J)**	**95% CI of diff.**	**Significant**	**Mean Difference (I-J)**	**95% CI of diff.**	**Significant**
1 Gb3-mix No Phase	**2** Gb3-mix Phase Ld	0,357	-0,4111 to 1,126	No	1,041	0,4296 to 1,653	Yes****
	3 Gb3-mix Phase Lo	-5,291	-6,059 to -4,523	Yes****	-3,425	-4,037 to -2,814	Yes****
	4 Gb3-FSL No Phase	-1,544	-2,290 to -0,7973	Yes****	-3,411	-3,942 to -2,879	Yes****
	5 Gb3-FSL Phase Ld	-2,865	-3,803 to -1,927	Yes****	-3,222	-3,874 to -2,571	Yes****
	6 Gb3-FSL Phase Lo	0,550	-0,3879 to 1,489	No	0,476	-0,1751 to 1,127	No
	7 Gb3-C24:0 No Phase	0,190	-0,5266 to 0,9066	No	0,353	-0,1936 to 0,8990	No
	8 Gb3-C24:0 Phase Ld	1,173	0,4444 to 1,901	Yes****	1,095	0,5753 to 1,614	Yes****
	9 Gb3-C24:0 Phase Lo	-0,449	-1,178 to 0,2785	No	1,050	0,5302 to 1,569	Yes****
	10 Gb3-C24:1 No Phase	-0,393	-1,090 to 0,3043	No	-0,305	-0,8579 to 0,2483	No
	11 Gb3-C24:1 Phase Ld	0,169	-0,5882 to 0,9256	No	0,761	0,1493 to 1,372	Yes**
	12 Gb3-C24:1 Phase Lo	-2,498	-3,255 to -1,742	Yes****	-1,353	-1,965 to -0,7420	Yes****
2 Gb3-mix Phase Ld	**3** Gb3-mix Phase Lo	-5,648	-6,433 to -4,863	Yes****	-4,466	-5,131 to -3,802	Yes****
	4 Gb3-FSL No Phase	-1,901	-2,665 to -1,138	Yes****	-4,452	-5,044 to -3,860	Yes****
	5 Gb3-FSL Phase Ld	-3,222	-4,174 to -2,270	Yes****	-4,263	-4,965 to -3,562	Yes****
	6 Gb3-FSL Phase Lo	0,193	-0,7589 to 1,145	No	-0,565	-1,266 to 0,1365	No
	7 Gb3-C24:0 No Phase	-0,167	-0,9017 to 0,5669	No	-0,688	-1,294 to -0,08309	Yes*
	8 Gb3-C24:0 Phase Ld	0,815	0,06957 to 1,561	Yes*	0,054	-0,5276 to 0,6350	No
	9 Gb3-C24:0 Phase Lo	-0,807	-1,553 to -0,06141	Yes*	0,009	-0,5726 to 0,5899	No
	10 Gb3-C24:1 No Phase	-0,750	-1,465 to -0,03490	Yes*	-1,346	-1,957 to -0,7344	Yes****
	11 Gb3-C24:1 Phase Ld	-0,188	-0,9624 to 0,5850	No	-0,280	-0,9451 to 0,3844	No
	12 Gb3-C24:1 Phase Lo	-2,856	-3,630 to -2,082	Yes****	-2,395	-3,059 to -1,730	Yes****
3 Gb3-mix Phase Lo	**4** Gb3-FSL No Phase	3,747	2,984 to 4,511	Yes****	0,015	-0,5775 to 0,6068	No
	5 Gb3-FSL Phase Ld	2,426	1,474 to 3,378	Yes****	0,203	-0,4986 to 0,9043	No
	6 Gb3-FSL Phase Lo	5,841	4,889 to 6,793	Yes****	3,901	3,200 to 4,603	Yes****
	7 Gb3-C24:0 No Phase	5,481	4,747 to 6,215	Yes****	3,778	3,173 to 4,383	Yes****
	8 Gb3-C24:0 Phase Ld	6,464	5,718 to 7,209	Yes****	4,520	3,939 to 5,101	Yes****
	9 Gb3-C24:0 Phase Lo	4,841	4,096 to 5,587	Yes****	4,475	3,894 to 5,056	Yes****
	10 Gb3-C24:1 No Phase	4,898	4,183 to 5,613	Yes****	3,120	2,509 to 3,732	Yes****
	11 Gb3-C24:1 Phase Ld	5,460	4,686 to 6,233	Yes****	4,186	3,521 to 4,851	Yes****
	12 Gb3-C24:1 Phase Lo	2,793	2,019 to 3,566	Yes****	2,072	1,407 to 2,736	Yes****
4 Gb3-FSL No Phase	**5** Gb3-FSL Phase Ld	-1,321	-2,255 to -0,3869	Yes***	0,188	-0,4449 to 0,8213	No
	6 Gb3-FSL Phase Lo	2,094	1,160 to 3,028	Yes****	3,887	3,254 to 4,520	Yes****
	7 Gb3-C24:0 No Phase	1,734	1,023 to 2,445	Yes****	3,763	3,239 to 4,288	Yes****
	8 Gb3-C24:0 Phase Ld	2,716	1,993 to 3,439	Yes****	4,505	4,009 to 5,002	Yes****
	9 Gb3-C24:0 Phase Lo	1,094	0,3710 to 1,817	Yes****	4,460	3,964 to 4,957	Yes****
	10 Gb3-C24:1 No Phase	1,151	0,4596 to 1,843	Yes****	3,106	2,574 to 3,637	Yes****
	11 Gb3-C24:1 Phase Ld	1,712	0,9606 to 2,464	Yes****	4,171	3,579 to 4,763	Yes****
	12 Gb3-C24:1 Phase Lo	-0,954	-1,707 to -0,2028	Yes**	2,057	1,465 to 2,649	Yes****
5 Gb3-FSL Phase Ld	**6** Gb3-FSL Phase Lo	3,415	2,322 to 4,509	Yes****	3,698	2,962 to 4,435	Yes****
	7 Gb3-C24:0 No Phase	3,055	2,144 to 3,966	Yes****	3,575	2,930 to 4,221	Yes****
	8 Gb3-C24:0 Phase Ld	4,038	3,118 to 4,957	Yes****	4,317	3,694 to 4,940	Yes****
	9 Gb3-C24:0 Phase Lo	2,415	1,495 to 3,335	Yes****	4,272	3,649 to 4,895	Yes****
	10 Gb3-C24:1 No Phase	2,472	1,577 to 3,368	Yes****	2,918	2,266 to 3,569	Yes****
	11 Gb3-C24:1 Phase Ld	3,034	2,091 to 3,976	Yes****	3,983	3,282 to 4,685	Yes****
	12 Gb3-C24:1 Phase Lo	0,366	-0,5761 to 1,309	No	1,869	1,167 to 2,570	Yes****
6 Gb3-FSL Phase Lo	**7** Gb3-C24:0 No Phase	-0,361	-1,271 to 0,5501	No	-0,123	-0,7689 to 0,5220	No
	8 Gb3-C24:0 Phase Ld	0,622	-0,2976 to 1,542	No	0,619	-0,004255 to 1,242	No
	9 Gb3-C24:0 Phase Lo	-1	-1,920 to -0,08038	Yes*	0,574	-0,04934 to 1,197	No
	10 Gb3-C24:1 No Phase	-0,943	-1,838 to -0,04791	Yes*	-0,781	-1,432 to -0,1297	Yes**
	11 Gb3-C24:1 Phase Ld	-0,382	-1,324 to 0,5609	No	0,285	-0,4168 to 0,9861	No
	12 Gb3-C24:1 Phase Lo	-3,049	-3,992 to -2,106	Yes****	-1,830	-2,531 to -1,128	Yes****
7 Gb3-C24:0 No Phase	**8** Gb3-C24:0 Phase Ld	0,983	0,2905 to 1,675	Yes***	0,742	0,2298 to 1,254	Yes***
	9 Gb3-C24:0 Phase Lo	-0,639	-1,332 to 0,05240	No	0,697	0,1848 to 1,209	Yes***
	10 Gb3-C24:1 No Phase	-0,583	-1,242 to 0,07644	No	-0,658	-1,204 to -0,1112	Yes**
	11 Gb3-C24:1 Phase Ld	-0,021	-0,7435 to 0,7009	No	0,408	-0,1973 to 1,013	No
	12 Gb3-C24:1 Phase Lo	-2,688	-3,411 to -1,966	Yes****	-1,706	-2,311 to -1,101	Yes****
8 Gb3-C24:0 Phase Ld	**9** Gb3-C24:0 Phase Lo	-1,622	-2,327 to -0,9182	Yes****	-0,045	-0,5287 to 0,4386	No
	10 Gb3-C24:1 No Phase	-1,565	-2,237 to -0,8935	Yes****	-1,400	-1,919 to -0,8801	Yes****
	11 Gb3-C24:1 Phase Ld	-1,004	-1,738 to -0,2702	Yes***	-0,334	-0,9154 to 0,2472	No
	12 Gb3-C24:1 Phase Lo	-3,671	-4,405 to -2,937	Yes****	-2,448	-3,030 to -1,867	Yes****
9 Gb3-C24:0 Phase Lo	**10** Gb3-C24:1 No Phase	0,057	-0,6147 to 0,7289	No	-1,355	-1,874 to -0,8350	Yes****
	11 Gb3-C24:1 Phase Ld	0,618	-0,1154 to 1,352	No	-0,289	-0,8703 to 0,2923	No
	12 Gb3-C24:1 Phase Lo	-2,049	-2,783 to -1,315	Yes****	-2,403	-2,985 to -1,822	Yes****
10 Gb3-C24:1 No Phase	**11** Gb3-C24:1 Phase Ld	0,561	-0,1414 to 1,264	No	1,066	0,4541 to 1,677	Yes****
	12 Gb3-C24:1 Phase Lo	-2,106	-2,809 to -1,403	Yes****	-1,049	-1,660 to -0,4372	Yes****
11 Gb3-C24:1 Phase Ld	**12** Gb3-C24:1 Phase Lo	-2,667	-3,429 to -1,905	Yes****	-2,114	-2,779 to -1,449	Yes****

Table S3: Descriptive statistics of the data displayed in Figs. 4E-F

	Minimum		Maximum		Mean		Std. Deviation		Number of replicates	
	LecA	StxB	LecA	StxB	LecA	StxB	LecA	StxB	LecA	StxB
1 Gb3-mix + DOPC	2.478	0.064	7.385	0.461	4.205	0.295	1.329	0.074	13	38
2 Gb3-mix + Chol + SM	3.445	0.358	8.309	2.345	5.774	1.104	1.311	0.369	27	39
3 Gb3-C24:0 + DOPC	0.666	0	2.561	0	1.436	0	0.423	0	39	36
4 Gb3-C24:0 + Chol + SM	0	0	4.451	0.674	1.692	0.141	1.044	0.134	36	51

Table S4: Statistical analysis of the data from Figs. 4E-F

Statistical analysis was carried out with GraphPad Prism (Version 6.0) with a two-way ANOVA Tukey´s multiple comparisons test. The significance level was set to 0.05.

		LecA			StxB		
Condition (I)	**Condition (J)**	**Mean Difference (I-J)**	**95% CI of diff.**	**Significant**	**Mean Difference (I-J)**	**95% CI of diff.**	**Significant**
1 Gb3-mix + DOPC	**2** Gb3-mix + Chol + SM	-1.568	-2.448 to -0.688	Yes****	-0.807	-0.925 to -0.690	Yes****
	3 Gb3-C24:0 + DOPC	2.77	1.935 to 3.605	Yes****	0.295	0.176 to 0.415	Yes****
	4 Gb3-C24:0 + Chol + SM	2.513	1.670 to 3.357	Yes****	0.153	0.043 to 0.264	Yes**
2 Gb3-mix + Chol + SM	**3** Gb3-C24:0 + DOPC	4.338	3.686 to 4.991	Yes****	1.104	0.984 to 1.223	Yes****
	4 Gb3-C24:0 + Chol + SM	4.082	3.418 to 4.745	Yes****	0.961	0.852 to 1.071	Yes****
3 Gb3-C24:0 + DOPC	**4** Gb3-C24:0 + Chol + SM	-0.256	-0.858 to 0.345	N o	-0.141	-0.254 to -0.029	Yes**

The bacterium *Pseudomonas aeruginosa* perishes membrane organization by its lectin LecA

Taras Sych [1,2,3,4], Thomas Schubert [1,2,3], Sahaja Aigal [1,2,5], Roland Thuenauer[1,2], Annette Brandel[1,2], Ramin Omidvar [1,2,3], Thorsten Eierhoff [6], Ludovic Richert [4], Yves Mely [4,*], Josef Madl [1,2,3*] and Winfried Römer [1,2,3,5*]

[1] Faculty of Biology, Albert-Ludwigs-University Freiburg, Schänzlestraße 1, 79104 Freiburg, Germany

[2] Signalling Research Centres BIOSS and CIBSS, Albert-Ludwigs-University Freiburg, Schänzlestraße 18, 79104 Freiburg, Germany

[3] Freiburg Center for Interactive Materials and Bioinspired Technology (FIT), Albert-Ludwigs-University Freiburg, Georges-Köhler-Allee 105, 79110 Freiburg, Germany

[4] Laboratoire de Bioimagerie et Pathologies, UMR 7021 CNRS, Faculté de Pharmacie, Université de Strasbourg, 67401 Illkirch Cedex, France

[5] International Max Planck Research School for Molecular and Cellular Biology, Max Planck Institute of Immunobiology and Epigenetics, Stübeweg 51, 79108 Freiburg, Germany

[6] Klinik für Vaskuläre und Endovaskuläre Chirurgie, Albert-Schweitzer-Campus 1, 48149, Münster, Germany

* corresponding authors

Correspondence to:

Winfried Römer – winfried.roemer@bioss.uni-freiburg.de

Josef Madl – josef.madl@universitaets-herzzentrum.de

Yves Mely – yves.mely@unistra.fr

Abstract

The bacterial invasion of *P. aeruginosa* strongly depends on the specific interactions with the plasma membrane lipids and proteins. In the former work of our group we demonstrated that the interaction of bacterial surface lectin LecA with host cell glycosphingolipid Gb3 is the key event for *P. aeruginosa* internalization. In plasma membrane, Gb3 molecules are enriched in highly ordered membrane nanodomains ("lipid rafts"). Nevertheless, the role of lipid rafts in the bacterial invasion is still elusive. In this work, we reconstituted lipid rafts in SLBs at the microscopic scale as the liquid-ordered (Lo) domains. Bacteria, applied to such SLBs induce the dissolution of these Lo domains. We found that LecA-Gb3 interaction is crucial for this process. We confirmed this finding by application of the purified LecA to SLB. We suggest that the dissolution of the ordered membrane domains is required by *P. aeruginosa* for promoting infection.

Introduction

Host cell invasion is a strategy exploited by many bacteria to escape the host's immune defenses and to fulfill nutritive and metabolic requirements [1–3]. Commonly, invasion strongly relies on tight host-pathogen interactions, and the interplay of bacterial factors and the host cell machinery [4]. The bacterial uptake is mostly induced at the cell surface by binding to a wide range of plasma membrane molecules. These initial interactions can trigger diverse signaling events leading to actin polymerization, which is described as a major driving force for bacterial engulfment. Recently, we have introduced the concept of the "lipid zipper", a membrane invagination process that also leads to wrapping of the plasma membrane around the bacterium, but in a fully different way [1]. We have reported that the interaction of the bacterial surface lectin LecA[6,7] with the host cell glycosphingolipid Gb3 was fully sufficient for membrane bending and engulfment of the bacterium *P. aeruginosa* in the absence of actin polymerization. Remarkably, reconstitution of bacterium-Gb3 interactions in synthetic membrane systems (e.g. giant unilamellar vesicles) as well as theoretical modeling contributed largely to the understanding of the mechanism of LecA-

triggered lipid zippering. We found that interfering with LecA-Gb3 interactions by LecA deletion or blocking, and Gb3 depletion led to a significant (more than 60%) reduction in invasiveness of *P. aeruginosa* [1]. Based on the crucial role of LecA-Gb3 interactions for bacterial uptake, divalent LecA binders have been designed, which reduced cellular invasiveness of *P. aeruginosa* more than 80% when applied in a concentration of 50 nM [8].

Glycosphingolipids [9], such as Gb3, are enriched in so-called lipid rafts, which play key roles as signaling platforms for the internalization of many bacteria [10,11]. Lipid rafts are highly ordered, dynamic membrane domains, mainly composed of sphingomyelin, cholesterol[12–14] and a large variety of plasma membrane lipids and proteins important for cell signaling and internalization.

For bacterial entry, the impact of the tetravalent, galactose-binding lectin LecA on plasma membrane organization and dynamics, in particular on lipid rafts, is elusive. In this work, we mimicked the cell membrane organization by using phase-separated supported lipid bilayers (SLBs) as minimal synthetic membrane system. SLBs were prepared using a ternary mixture of the phospholipid DOPC, sphingomyelin (SM) and cholesterol (chol), supplemented with the glycosphingolipid Gb3. They exhibited phase-separation at room temperature and formed two distinct phases – liquid-disordered (Ld, mainly composed of DOPC) and liquid-ordered (Lo, mainly composed of SM/chol). The Lo domains in such SLBs can be considered as a minimalistic model of lipid rafts at the microscopic scale.

Furthermore, we explored the impact of *P. aeruginosa* and especially of its lectin LecA on the lipid organization of phase-separated SLBs. We found that the *P. aeruginosa* strain PAO1 adheres to SLBs, forms aggregates and dissolves Lo domains. We demonstrated that LecA-Gb3 interactions are the driving forces for these processes by using wild-type and LecA-deficient strains. Moreover, the dissolution of Lo domains was also induced by purified, tetravalent LecA and an engineered divalent LecA variant. The dissolution mechanism was investigated in more detail to decipher the crucial role of protein structure and valence for this process.

Results

Aggregation of *P. aeruginosa* at the membrane and partial dissolution of ordered domains.

Planar SLBs with lateral phase separation, which represent a widely used synthetic membrane system to mimic cellular lipid rafts, were prepared on mica surface using a lipid composition of DOPC, chol, SM and the glycosphingolipid Gb3 (37.5/20/37.5/5). To monitor the membrane organization, the lipophilic probe Texas Red-DHPE was used. This probe preferentially associates to the less tightly packed Ld domains, whereas the more tightly packed Lo domains appear dark (figure 1a).

We applied 250 μL of a suspension of the *P. aeruginosa* wild type strain PAO1[1] (15×10^6 cells/mL) to SLBs at room temperature. By fluorescence microscopy, we observed the interactions of fluorescent bacteria (green) with the membrane (red, figure 1a and supplementary movie 1). First, individual bacteria adhere to the membrane. Interestingly, bacteria are not uniformly distributed. They localize predominantly (around 60%) at the boundaries of Ld and Lo domains (purple arrowheads), approximately 35% associate with Ld domains, and only 5% of bacteria with Lo domains (figure 1a and corresponding quantifications in figure S3a). After about 10 min of incubation, bacteria start to form aggregates with newly attaching bacteria, which grow in size over time (figure 1a and S3b).

Simultaneously with the formation of bacterial aggregates, SLBs get drastically reorganized (figure 1a): Over time, the shape and size of Lo domains change: The total area of Lo domains (figure 1c) as well as the areas of individual Lo domains (figure 1d) decrease. Remarkably, several Lo domains disappear completely (figure 1a, blue and green arrowhead). In parallel to the dissolution of Lo domains, the fluorescence intensity of the membrane marker Texas Red-DHPE increases around bacteria, indicating a local enrichment of lipid membranes. One selected event describing the subsequent adhesion of two bacteria (figure 1a) was quantitatively analyzed (figure 1e). At this point, we speculate that *P. aeruginosa* tries to cover its surface by recruiting lipid membrane from the SLB. By this means, bacteria seem to have an effect on the collective organization of the membrane since

Lo domains that have not encountered any bacterium in close proximity, also dissolve (figure 1a, blue arrowhead).

As Eierhoff et al. highlighted the crucial role of the interaction of the *P. aeruginosa* lectin LecA with the host cell glycosphingolipid Gb3 for host cell invasion[1], we wanted to elucidate the impact of LecA on membrane organization. Therefore, we studied the effects of the LecA-deficient PAO1 strain (PAO1-ΔLecA) on membrane organization of SLBs (figure 1b and supplementary movie 2). In the absence of specific LecA-Gb3 interactions, the number of PAO1-ΔLecA adhering to a Gb3-containing lipid bilayer was reduced (approx. 4 fold – figure S3) and detachment of bacteria away from the lipid bilayer was recorded (figure 1b, cyan arrowhead).

As the PAO1 wild type strain, the PAO1-ΔLecA strain preferentially targets the Lo/Ld domain boundaries (59% ± 6%). Furthermore, 44% ± 6 % of LecA-deficient bacteria adhere to Ld domains, and Lo domains are rather neglected (5% ± 2%) (figure 1b and corresponding quantifications in figure S3a). In addition, there was no formation of bacterial aggregates (figure S3c), indicating thatthe bacterial adhesion to and the aggregation at the membrane is mediated by LecA-Gb3 interactions. Importantly, the PAO1-ΔLecA strain does not induce the dissolution of Lo domains (figure 1b). The total area of Lo domains remains largely constant over the incubation time (figure 1c) and the individual areas of Lo domains do not decrease (figure 1f). Furthermore, we did not observe the accumulation of membrane lipids around LecA-deficient bacteria (figure 1b – white circle and figure 1e).

As control experiments, we applied the *P. aeruginosa* wild type and ΔLecA strains to SLBs devoid of Gb3 consisting of DOPC, chol and SM (37.5/20/37.5). In comparison to Gb3-containg SLBs, the adhesion of both bacterial strains to Gb3-negative SLBs was strongly reduced (5.5 fold for PAO1 wt and 60 fold for PAO1 ΔLecA – figure S4).

All these findings confirm the key importance of the LecA-Gb3 interactions not only for the adhesion of *P. aeruginosa* to the membrane, but also for the dissolution of Lo domains.

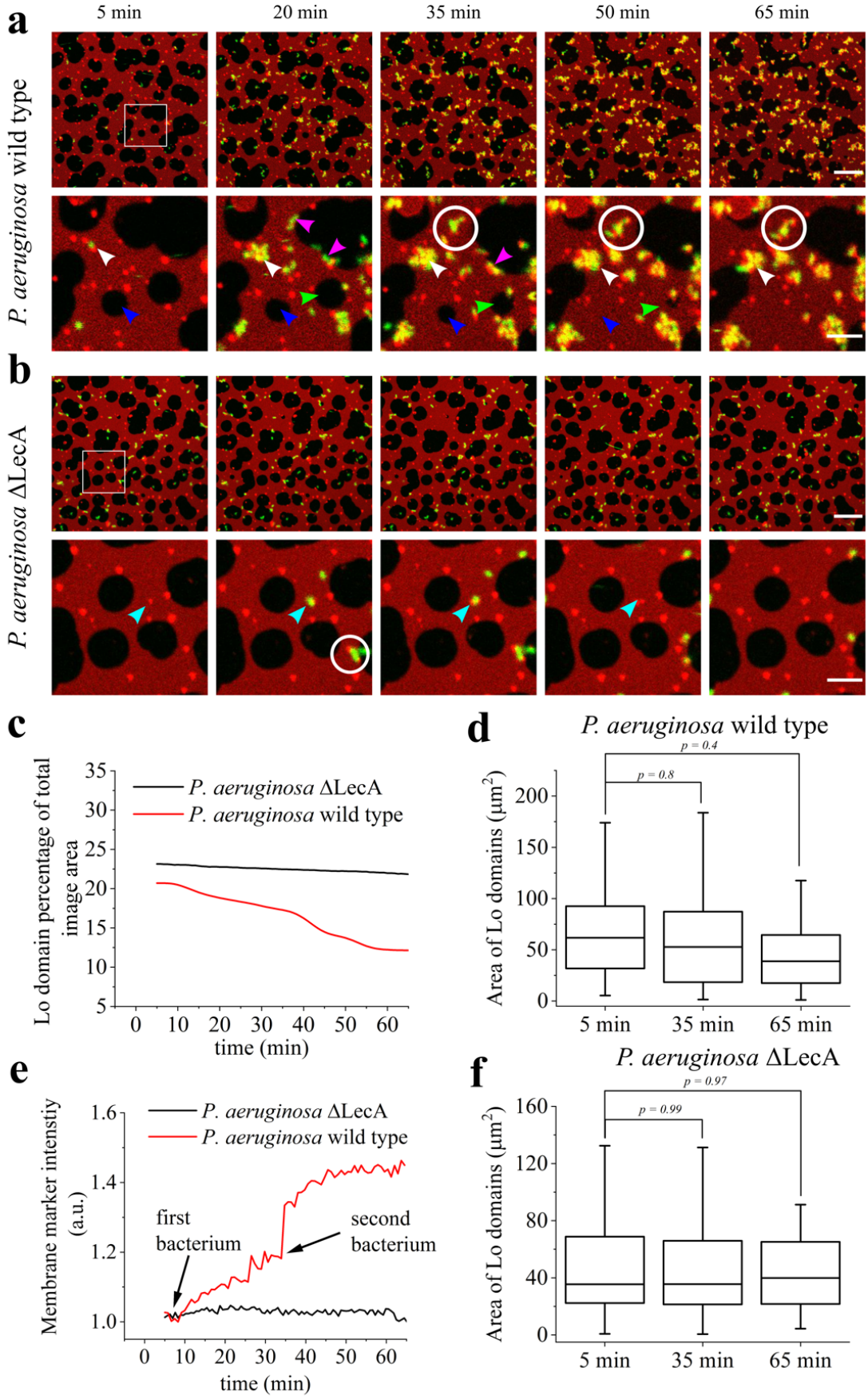
a
5 min
20 min
35 min
50 min
65 min
P. aeruginosa wild type
b
P. aeruginosa ΔLecA
c
Lo domain percentage of total image area
P. aeruginosa ΔLecA
P. aeruginosa wild type
time (min)
d
P. aeruginosa wild type
p = 0.4
p = 0.8
Area of Lo domains (μm²)
5 min
35 min
65 min
e
Membrane marker intenstiy (a.u.)
P. aeruginosa ΔLecA
P. aeruginosa wild type
first bacterium
second bacterium
time (min)
f
P. aeruginosa ΔLecA
p = 0.97
p = 0.99
Area of Lo domains (μm²)
5 min
35 min
65 min

Figure 1 | **SLB reorganization induced by *P. aeruginosa*.** Bacteria expressing GFP (green) were applied to phase-separated SLBs composed of DOPC/chol/SM/Gb3 (37.5/20/37.5/5) and labeled by Texas Red-DHPE (red). **a)** At the earlier time points bacteria prefer to attach to the Lo/Ld domain boundaries (purple arrowhead). Furthermore, the *P. aeruginosa* wild type strain forms bacterial clusters (white arrow). Bacteria accumulate membrane from the SLB at the spots of bacterial attachment (white circle). *P. aeruginosa* dissolves Lo domains (blue and green arrowheads). **b)** *P. aeruginosa* ΔLecA strain contact the lipid bilayer but do not remain stably attached to its surface (cyan arrowhead). Moreover, *P. aeruginosa* ΔLecA do not induce the disappearance of Lo domains. Bacteria do not accumulate membrane from SLB. **c)** In SLBs, *P. aeruginosa* wild type strain induces the decrease of the total area of Lo domains over time (red curve) whereas *P. aeruginosa* ΔLecA do not (black curve). **d)** *P. aeruginosa* wild type strain decreases the size of the individual Lo domains over time. **e)** *P. aeruginosa* wild type (red curve) accumulates membrane from the SLB on the bacterial surface. The membrane marker intensity at the spot where bacterium is attached (a - white circle), increases over time. Two successive events of bacterial docking to the SLB are visible, indicating that two bacteria accumulate membrane material one after the other. In contrast, *P. aeruginosa* ΔLecA do not accumulate membrane material (black curve, b - white circle). **f)** *P. aeruginosa* ΔLecA do not modify the size of the individual Lo domains. The scale bars are 10 and 5 μm, respectively. The complete time sequence for a and b are available online as the supplementary movies 1 and 2.

LecA dissolves Lo domains and forms membrane multilayers.

Since our results showed clear evidence that LecA plays a key role in adhesion of *P. aeruginosa* to membranes and in dissolution of Lo domains, we directly investigated the impact of purified LecA on the membrane organization. LecA in a concentration of 200 nM (recombinantly expressed in *E. coli* [7]) was incubated with SLBs of identical lipid compositions as used for bacterial studies. To facilitate two-color microscopy with LecA (fluorescently labeled with Cy5), the membrane marker Texas Red-DHPE was replaced by β-Bodipy FL C12-HPC (Bodipy). This dye also labels preferentially the Ld domains (figure 2a – cyan color) whereas the Lo domains appear dark.

Purified LecA (presented in red color) binds mainly to Gb3 molecules in Lo domains (figure 2a – 0 min and supplementary movie 3). Over time, LecA induces the dissolution of the Lo domains (figure 2a – blue arrowhead traces one of many events). The total area of the Lo domains decreases, and after about 40 min of incubation with LecA the Lo domains disappear completely (blue curve in figure 2b). A more detailed description of the dynamics of Lo domain dissolution reveals a simultaneous reduction of the number of Lo domains (figure 2c) and the area of

individual Lo domains (figure 2d). This is in line with our previous observations of altered membrane organization induced by LecA-expressing *P. aeruginosa*.

Roughly 5 min after application of LecA, more intense LecA clusters emerge (figure 2a). These clusters grow over time to micrometer size. Interestingly, this LecA clustering coincides with the appearance of areas characterized by enhanced Bodipy fluorescence intensity (figure 2a). As published recently [15], LecA has the ability to crosslink opposing lipid membranes upon which it strongly accumulates at membrane interfaces. Accordingly we presume that these novel areas represent membrane-LecA-membrane sandwiches, i.e a double or even multilayer of bilayer membrane crosslinked by LecA. Furthermore, after 15 min, large defects in the SLB start to appear (figure 2a and supplementary movie 3). The total area of the membrane defects increases over time (figure 2b, figure S5) with the increasing area of membrane multilayers (figure 2b). However, the membrane multilayer formation precedes the membrane destruction (green curve in figure 2b). Hence, we suggest that the formation of multilayers depletes the initial SLB in lipids, which results in extensive membrane defects. Later on, we will use a dimeric LecA variant to elucidate the dynamics of Lo domain dissolution in absence of multilayer formation.

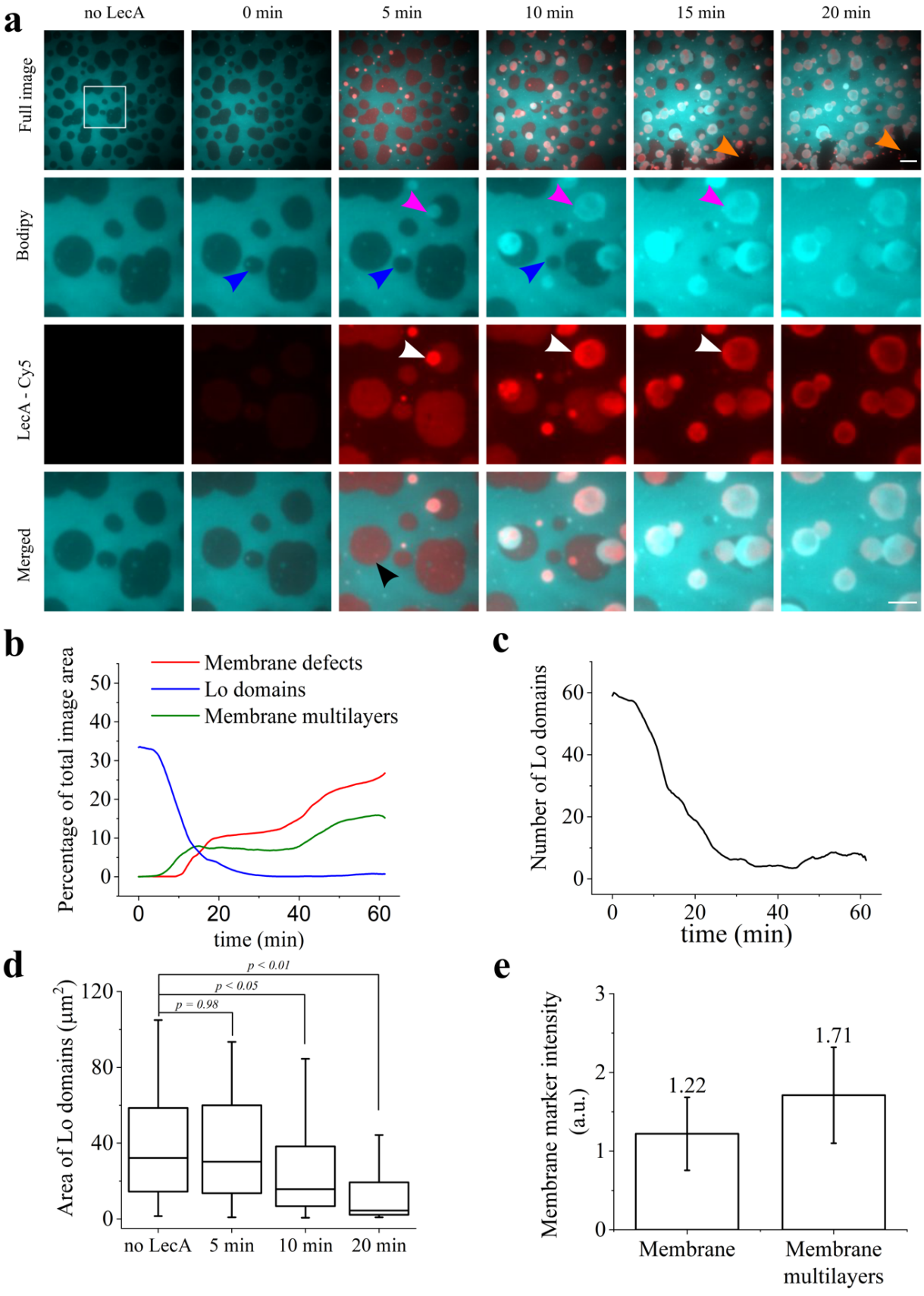
a
no LecA
0 min
5 min
10 min
15 min
20 min
Full image
Bodipy
LecA - Cy5
Merged
b
Membrane defects
Lo domains
Membrane multilayers
Percentage of total image area
time (min)
c
Number of Lo domains
time (min)
d
p < 0.01
p < 0.05
p = 0.98
Area of Lo domains (μm²)
no LecA
5 min
10 min
20 min
e
Membrane marker intensity (a.u.)
1.22
1.71
Membrane
Membrane multilayers

Figure 2 | **SLB reorganization induced by purified LecA.** SLB is labeled by β Bodipy-C_{12}-FL-HPC that localizes to Ld domains (cyan). LecA is labeled with Cy5 (red). Images are acquired with wide field microscopy (HILO). **a)** Time series of LecA interaction with phase-separated SLB (DOPC/chol/SM/Gb3 (37.5/20/37.5/5)). LecA induces Lo domains dissolution (blue arrowhead). Simultaneously, LecA clusters at the SLB (white arrowhead). LecA clusters induce the formation of membrane multilayers (purple arrowhead). At the later time points, large membrane defects appear (arrowhead) **b)** The total area of the Lo domains, membrane defects and membrane multilayers changes over time. **c)** The total number of Lo domains decreases over time; **d)** The sizes of the individual Lo domains decrease over time; **e)** The mean fluorescence intensity signal in membrane multilayers is approximately 1.5 times higher than the intensity of the original, single bilayer membrane. Scale bars are 10 and 5 µm, respectively. The later timepoints are presented in figure S5. The complete time sequence is available online as the supplementary movie 3.

To further characterize the membrane multilayers, we quantified the fluorescence intensity signal of Bodipy of membrane multilayers and compared it to the Bodipy signal of initial Ld membrane domains. A two-fold increase of Bodipy fluorescence intensity indicates the formation of a membrane stack consisting of two lipid bilayers on top of each other. However, we found that the membrane multilayers appear approximately 1.5 times brighter than unilamellar Ld domains (figure 2e), which suggests that the membrane multilayers have a distinct lipid organization. To explain this, we explored the membrane order of SLBs at different time points of LecA-induced membrane reorganization.

LecA drastically alters membrane order.

Lo domains enriched in SM and chol exhibit a highly-ordered lipid organization, whereas the surrounding membrane environment is low-ordered (also called disordered). However, after LecA-induced Lo domain dissolution, SM and chol are still present in the membrane; they are redistributed and very likely modify the membrane order. Various techniques provide the possibility to sense the local membrane order of the lipid bilayer[35,36]. In this work, we employed fluorescence–based ratiometric imaging using the environmental sensitive membrane marker Nile Red 12 S (NR12S)[37]. This probe is sensitive to the membrane hydration and exhibits a drastic red-shift in polar environments (i.e. in Ld domains). The general polarization (GP) value of NR12S represents the local membrane order. The GP value can vary

from -1 to 1. Low values correspond to low membrane order whereas higher GP values indicate a higher membrane order. NR12S was added to phase-separated SLBs (DOPC/chol/SM/Gb3 (37.5/20/37.5/5)). We reconstructed the GP image to map the membrane order of the SLB (figure 3a).

In absence of LecA, the GP image displays a clear distinction between Lo domains (green, with a GP value of approximately -0.2) and Ld domains (blue, with a GP value of around -0.7). Here, the GP histogram shows two distinct populations that correspond to Lo and Ld domains (figure 3b – black curve). After the application of 200 nM of LecA, Lo domain dissolution, formation of multilayers and membrane disintegration were observed (figure 3a and S6), as described above. In brief, Lo domains shrink, rearrange and disappear (figure 3a – red arrowhead). Since the total area of Lo domains is reduced at 20 min of LecA incubation (figure S6), the Lo population of the GP histogram is reduced accordingly, whereas the Ld population is increased (figure 3b – red curve). At 40 min, the Lo domains are almost completely dissolved (figure 3a). Here, the GP histogram shows only one distinct population (figure 3b – blue curve). This population is still located in the GP value range of low-ordered membranes (i.e. Ld domains), but exhibits a slight shift towards higher GP values. This indicates the redistribution of SM and cholesterol in this novel “mixed” membrane.

Concurrent with Lo domain dissolution, membrane multilayers grow (figure 3a – all circles). Using raw confocal images (figure S6) we located multilayers for further quantification of membrane order (figure 3a – 40 min, all circles). Interestingly, we observed that the upper bilayer can grow on the top of an existing Lo domain, apparently blocking its dissolution (figure 3a – gray circles). We excluded this multilayer from our quantifications. As a result, the membrane order of multilayers is higher (figure 3c) than the order of Ld domains and lower than the order of Lo domains of the original lipid bilayer.

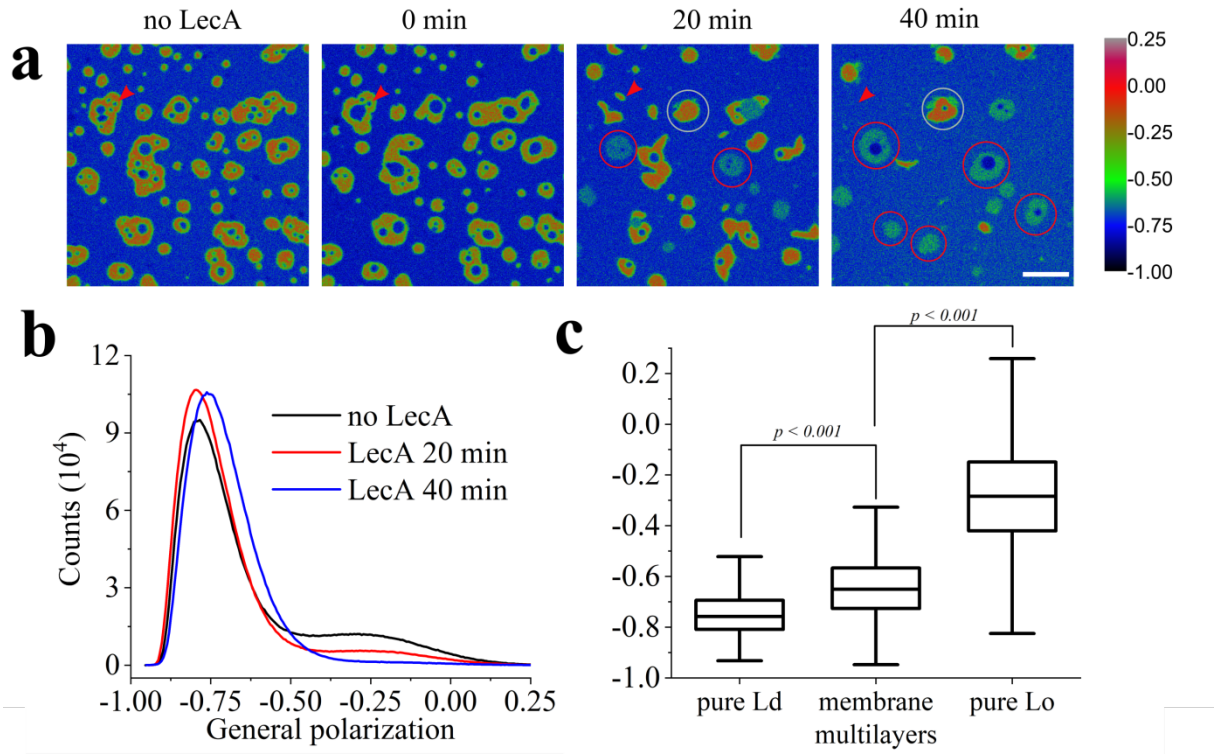

Figure 3| **Membrane order modifications of SLB induced by LecA.** The two-color imaging was performed using confocal microscopy. The time sequence in two color channels is presented in figure S6. **a)** GP images of the SLB before and at several time points after LecA application. The GP values are according to the color code on the right panel. Phase dissolution occurs in the same way as in figure 2 (red arrowhead). The membrane multilayers are highlighted by circles. **b)** GP histograms of the SLB before (black curve) and 20 min (red curve) and 40 min (blue curve) after LecA application. **c)** Membrane order of the Lo domains, Ld domains and membrane multilayers. Scale bar 10 µm.

This intermediate membrane order is the consequence of the lipid redistribution in the membranes caused by the dissolution of Lo domains. We suggest that Lo dissolution is a prerequisite for multilayer formation. For a better understanding of the dynamics of these processes, it would be advantageous to analyze both separately from each other (figure 2b and figure S6b). To focus on multilayer formation, we used homogeneous SLBs consisting of DOPC/chol/Gb3 (65/30/5), where classical phase-separation does not exist, and accordingly Lo domains cannot be dissolved. In this system, LecA (200 nM) induces multilayer formation and membrane disintegration (figure S7). Moreover, in this case (i.e. in the absence of phase separation) the membrane disintegration occurs very fast; the membrane is completely destroyed within 15 min after LecA application.

To study the dissolution of Lo domains separately, membrane multilayer formation has to be constrained. For that, the engineered homodimeric LecA variant RPL α-Gal (RPL) was used.

Dimeric LecA variant dissolves Lo domains without forming membrane multilayers. The amino acid sequence of RPL monomer is similar to the LecA monomer but the N-terminus of the protein is modified with a 6xHis-tag. This minor modification guarantees the stability of the protein as a dimer in aqueous solution and does not affect its specificity to the α-galactose moiety of glycoconjugates (e.g. Gb3). The crystal structure of this lectin is not resolved yet, but, presumably, the geometry of the dimeric form is arranged as presented in figure S1. Applied to phase-separated SLBs, RPL (200 nM) recognizes preferentially Lo domains (figure 4a) and the SLB reorganization is triggered immediately after RPL addition. Lo domains fuse and decrease in size over the first 15 min (figure 4a-c). At this point, the re-shaping of Lo domains stops. Nevertheless, the fluorescence intensity ratio between Ld and Lo domains (I_{Ld}/I_{Lo}) indicates a two-fold drop over the next 45 min (figure 4 a, d, e). This can be explained by asymmetric Lo domain dissolution. We hypothesize that in the upper membrane leaflet, which is directly exposed to RPL, Lo domains dissolve, whereas in the lower leaflet, which is in direct contact with the mica substrate, the dissolution of Lo domains is constrained.

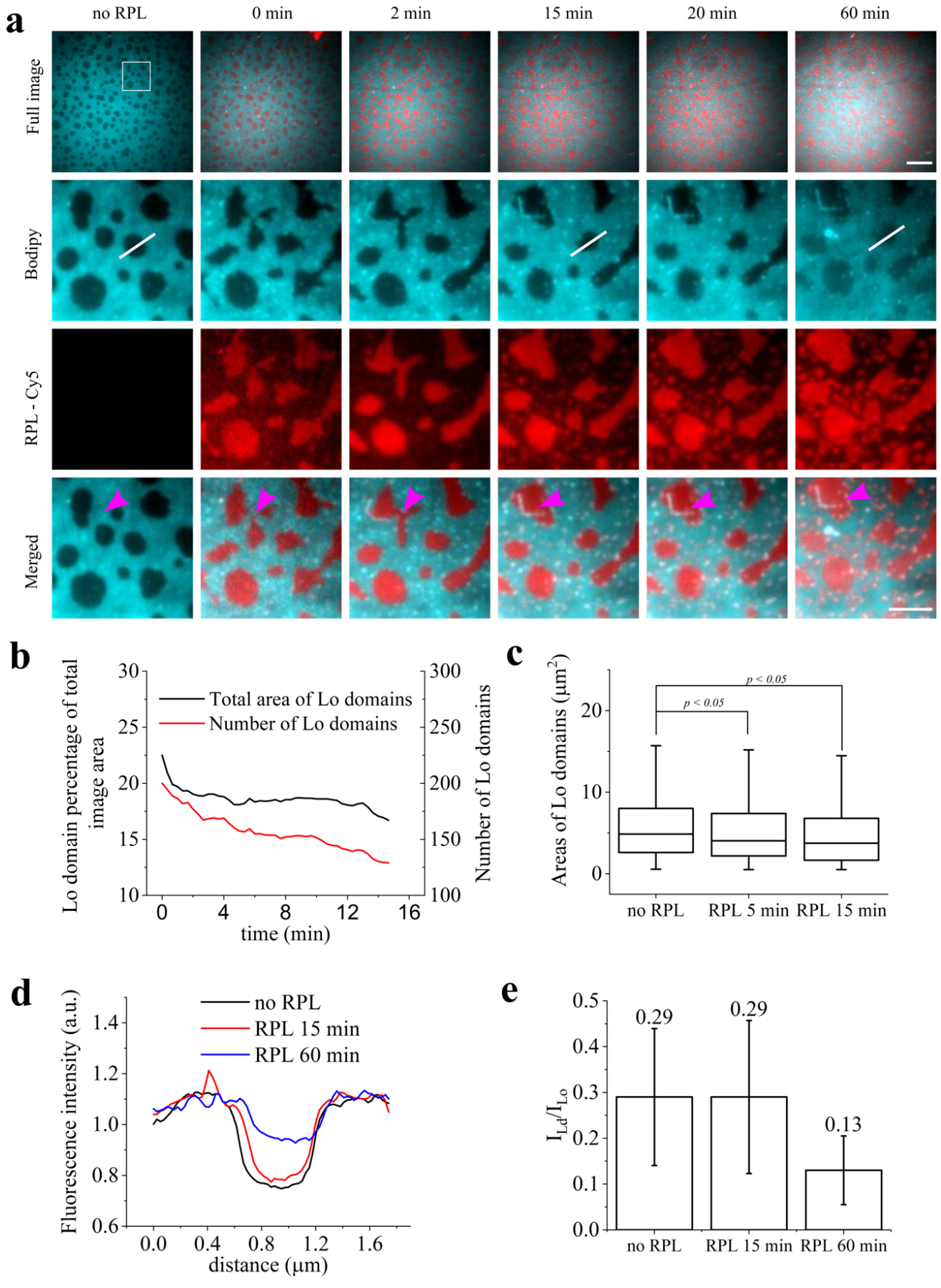
a
no RPL
0 min
2 min
15 min
20 min
60 min
Full image
Bodipy
RPL - Cy5
Merged
b
Lo domain percentage of total image area
Number of Lo domains
Total area of Lo domains
Number of Lo domains
time (min)
c
Areas of Lo domains (μm²)
p < 0.05
p < 0.05
no RPL
RPL 5 min
RPL 15 min
d
Fluorescence intensity (a.u.)
no RPL
RPL 15 min
RPL 60 min
distance (μm)
e
I_Ld/I_Lo
0.29
0.29
0.13
no RPL
RPL 15 min
RPL 60 min

Figure 4| **SLB reorganization induced by the dimeric LecA variant RPL αGal.** SLB is labeled by β Bodipy-C_{12}-FL-HPC that localizes to Ld domains (cyan). RPL is labeled by Cy5 (red). Images are acquired with wide field microscopy (HILO). **a)** The time series of the RPL interaction with phase separated SLB (DOPC/chol/SM/Gb3 (37.5/20/37.5/5)). RPL binds preferentially to the Lo domains. RPL induces fusion and a decrease in size of the Lo domains (purple arrowhead). **b)** The total area and the number of Lo domains decreases over time; **c)** The sizes of the individual Lo domains slightly decrease over time; **d,e)** The contrast of the fluorescence signal between the Ld and Lo domains at different time points. **d)** The Bodipy fluorescence intensity profile along the white line displayed in (a) at different time points. **e)** The intensity contrast (ratio between the fluorescence intensity signals of Bodipy in Ld and Lo domains) value at different time points for all Lo domains. After 1 hour, the contrast dropped to about half of the initial value. The scale bars are 10 and 5 μm respectively. The complete time sequence is available online as the supplementary movie 4.

Membrane multilayer formation was not observed in these experiments. Clearly, the membrane dissolution process is not a collective effect induced by multilayer formation, but rather an independent process.

Discussion

Multiple works suggested the crucial implication of the lipid rafts in the *P. aeruginosa* infection. Lipid rafts harbor big variety of components that can be targeted by *P. aeruginosa* in order to promote infection. Song et al. [20] demonstrated the ability of quorum-sensing metabolites, secreted by *P. aeruginosa* to induce the apoptosis of the immune cells via the dissolution of plasma membrane ordered nanodomains. Lipid rafts are also highly involved in the bacterial internalization. In particular, such important lipid raft-associated plasma membrane components as ceramides[21,22] and cholesterol [23] are known to play crucial role in the *P. aeruginosa* uptake in the host cell. In polarized epithelial cells, the bacterial entry from the apical site requires the enrichment of PIP3[24] at the cytosolic plasma membrane leaflet and PIP3 is also raft-associated membrane component[25]. The cholesterol rich membrane domains are required for the type 3 secretion system of the *P. aeruginosa* to initiate the trigger uptake mechanism[26]. Also, the glycosphingolipids, enriched in lipid rafts, such as asialo-gangliosides GM1 and GM2 or globoside Gb3 are the membrane receptors that mediate the bacterial adhesion to the host cell membrane [1,27]. Moreover, the interaction of the *P. aeruginosa* with glycosphigolipid Gb3 can initiate the bacterial

invasion through the lipid zipper[1]. The interaction of the *P. aeruginosa* with the Gb3 is granted by its surface lectin LecA. This galactose specific lectin mediates the *P. aeruginosa* adhesion and bacterial impact on the lipid rafts.

In this work, we demonstrated that *P. aeruginosa* can drastically alter the lipid organization in the model membranes. Namely, *P. aeruginosa* dissolves the ordered membrane domains. We observed this process in the SLBs – model membranes on the solid substrate. The Lo domains in such SLBs mimic the nanodomains (lipid rafts) of the plasma membranes of living cells at the microscopic scale. Clearly, the native membrane nanodomains are smaller in size and highly dynamic, whereas the Lo domains in SLBs are large and stable over time (figure S8). Nevertheless, the principles that underlie the constitution of such ordered nanodomains can be elucidated from the SLBs. Moreover, the reorganization of the Lo domains in SLBs induced by various factors can be visualized and analyzed.

We applied bacteria to the SLBs and observed its binding and clustering (figure 1). The interactions of the bacteria with the SLBs induced the decrease of the areas of the Lo domains, several Lo domains completely disappeared. We suggest that the rupture of membrane order is required for the *P. aeruginosa* to promote infection. We demonstrated, that the specific LecA-Gb3 interaction is responsible for the Lo domains dissolution in the SLB induced by *P. aeruginosa*. LecA-deficient strain showed the reduced binding to the SLB and also it was not able to rearrange the Lo domains. The similar situation was observed when both wild type and LecA-deficient strains were applied to the SLBs without Gb3.

Interestingly, we observed the accumulation of the SLB membrane at the bacterial surface. This process seems to be the analogue of the bacterial wrapping with the membrane via “lipid zipper”. Clearly, this “wrapping” cannot induce the bacterial internalization as the membrane bending is constrained by SLB substrate. Hence, bacteria, wrapped in membrane remain at the support. Also, in absence of the LecA-Gb3 interaction, the bacterial “wrapping” with membrane was not observed.

The role of LecA and Gb3 for plasma membrane reorganization during *P. aeruginosa* adhesion was validated by the studies of the impact on the organization of SLBs induced by soluble purified LecA (recombined in *E. coli*). Interestingly, LecA prefers to bind to Lo domains, whereas bacteria prefer Lo/Ld boundaries. Furthermore, LecA

induces Lo domains dissolution. Simultaneously, LecA forms micrometer-sized clusters at the SLB. These clusters sequester the lipids from the initial lipid bilayer in order to form membrane multilayers. This effect induces depletion of the SLB in lipids and as a result, it becomes disintegrated.

The impact of purified LecA is not a common feature for the Gb3-specific lectins. The reorganization of membrane supplemented by Gb3 was formerly studied in context of cellular uptake of the B subunit of Shiga toxin from *S. dysenteriae.* The studies on synthetic membrane systems (GUVs[28] and SLBs[29]) showed the specific preference of StxB to the Gb3 incorporated in Lo domains as well as efficient clustering of the Gb3 molecules induced by the multivalent binding of the StxB. Moreover, StxB shrinks Lo domains and induces the formation of novel Lo domains in supported lipid bilayers (figure S9, also demonstrated by Windschiegl et al. [29]). Efficient Gb3 clustering by StxB is granted by the number, position and orientation of binding pockets (all 15 of them are pointing in one direction). Unlike StxB, LecA contains only 4 Gb3-specific binding sites and, in addition, the distance between them is larger than in case of StxB (ref). Despite, as well as StxB, LecA binds initially also to Lo domains, we did not observe new Lo domains formation as in case of StxB. On the contrary, LecA induces the dissolution of the Lo domains homogenizing the membrane. Moreover, LecA – Gb3 interaction is strong enough to detach the membrane from the solid support and to either wrap it around bacterium or to form multilayers with LecA sandwiched in between the membrane layers. Indeed, as we also observed for GUV membranes [15] , the preferential location for LecA is in the membrane interfaces.

In order to resolve the composition of the membrane multilayers, we compared the membrane order in multilayers to the membrane order in Ld and Lo. We found that the multilayers exhibit the intermediate membrane order in between the Ld and Lo domains. This suggests that membrane multilayers are composed out of the mixed content of former Ld and Lo domains. Hence, we assume that the Lo domains dissolution is required for the membrane multilayers formation.

Interestingly, for the membrane dissolution the whole tetravalent form of LecA is not necessarily required. Divalent LecA variant (α-galactose specific RPL α Gal) induces

Lo domains dissolution, but the membrane multilayers are not formed. Hence, clearly, the complete tetrameric form is required for the multilayer formation.

Multiple bacteria exploit cellular machinery through interaction with lipid rafts in order to promote infection[10,11,31,32]. In this work, on the example of *P. aeruginosa*, we demonstrated that bacteria are capable of the induction of the extensive reaarangement of the membrane ordered domains: Lipid raft-like domains, reconstituted in synthetic SLBs were targeted by bacteria and dissolved. We suggest that the rearrangement of the ordered domains in the membrane might be required by bacteria for successful adhesion and/or internalization into the host cell. We also highlight the crucial importance of the host cell glycosphingolipids and bacterial lectins in this process.

Methods (3 000 words)

Materials. Lipids (1,2-dioleoyl-sn-glycero-3-phosphocholine(DOPC), sphingomyelin and cholesterol) were from Avanti Polar Lipids. Gb3 “wild type” (ceramide trihexosides) was from Matreya. The lipophilic membrane probe β-BODIPY C12-HPC (2-(4,4-Difluoro-5-Methyl-4-Bora-3a,4a-Diaza-s-Indacene-3-Dodecanoyl)-1-Hexadecanoyl-sn-Glycero-3-Phosphocholine) and DHPE-TexasRed were from ThermoFisher Scientific. The environmental sensitive membrane marker NR12S was provided by Dr. Andrey Klymchenko (University of Strasbourg). Shiga toxin B subunit was from Sigma Aldrich. Recombinant LecA was produced from *Escherichia coli* following previously published procedures[7]. Recombinant RPL αGal was from Glycoselect. The marker for lectin labeling (Cy-5 monoreactive NHS esther) was from GE Healthcare. PBS (-/-) buffer was from Gibco.

Bacterial culture. GFP-tagged *P. aeruginosa* PAO1 wild type and PAO1 ΔLecA were constructed according to the previously published procedure[1].

Lectin labeling. Lectins were labeled with Cy5 mono-reactive dye from GE Healthcare Life Sciences according to the amine-reactive probe labeling protocol from ThermoFisher Scientific. Briefly, 1 μl of a 10 mg/ml solution of the amino-

reactive probe in DMSO was added to 100 μl of a 1 mg/ml protein solution supplemented with 100 μM NaHCO3. The mixture was incubated for 1 h at room temperature with continuous shaking. The labeled protein was purified using Zeba Spin Desalating Columns, 0.5 ml, from ThermoFisher Scientific.

Solid supported lipid bilayer preparation. The lipid mixtures of DOPC/chol/SM/Gb3 with the molar ratio of 37.5/20/37.5/5 were prepared in chloroform. SLBs were labeled adding 0.1 mol % of Bodipy or TexasRed to the lipid mixture in chloroform. Chloroform was further removed by evaporation first under nitrogen atmosphere and under vacuum (10 -15 mBar). Lipids were resuspended in ultrapure water at 55 ºC with extensive vortexing in order to form large multilamellar vesicles. Furthermore, the vesicle suspension was extruded using the LiposoFast-Basic extruder (Avestin) with 50 nm pore size filter (55 ºC, 50 passages). The thin freshly cleaved layer of mica (PLANO) was attached to the microscopy glass coverslip (Menzel Gläser) using UV-curing glue (Norland optical adhesive). The extruded small unilamellar vesicles (SUV) suspension (50 μl) was applied to the mica together with 150 microliters of high (10 mM) $CaCl_2$ solution in pure water. The coverslips were incubated 30 min at 55 ºC in order to form the non-phase separated lipid bilayer. Thereafter, SLBs were washed with warm (55 ºC) PBS (-/-) to remove the lipids not attached to mica. Finally, SLBs were cooled down very slowly (1 -1.5 hours) to room temperature in order to induce the lipid phase separation on microscopic scale. For membrane order studies, lipid bilayers were prepared unlabeled and then NR12S (2 μl of 0.1 mM NR12S in DMSO) was added to the SLBs when the bilayer formation has already been completed. After 1-2 min of incubation, the lipid bilayer was washed mildly with PBS. Each individual SLB-containing well plate was further mounted on the microscopy holding dish for further imaging. Bacteria or lectins were further applied to the assembled well-plate.

The imaging of the LecA at the surface of bacteria with Structured Illumination Microscopy. An overnight culture of *P. aeruginosa* strains PAO1-GFP wild type and PAO1-GFP ΔLecA were centrifuged at 6000 rpm and resuspended in 500 μl of PBS (-/-) . 1:1000 dilution of the bacterial stock was pelleted and used for the staining

procedure. The bacteria were fixed with 4% PFA at RT for 20 min. After fixation, both strains were spun down and excess PFA was removed by NH4Cl quenching. After blocking with 3% BSA, bacteria were stained with anti-LecA antibody 1:200 for 45 min. This was followed by 3X washes with PBS (-/-). Bacteria were then incubated with secondary antibody (1:300) for 30 min. The stained bacteria were washed three times with PBS and the pellet was mixed with mowiol, spotted on a cover slip and mounted onto a glass slide**.** Imaging was performed with an N-SIM microscope system (Eclipse Ti-E with 100x oil objective, N.A. 1.49) with ORCA-Flash 4.0 sCMOS camera (Hamamatsu Photonics K.K.). The images were acquired and reconstructed using the reconstruction slice system from NIS-Elements software (Nikon).

Imaging of SLB reorganization induced by bacteria with the confocal microscopy. Overnight cultures of bacteria were pelleted and resuspended in PBS (-/-). Bacteria were applied to SLBs at room temperature and examined on the inverted confocal fluorescence microscope. Of note, due to the safety reasons (the imaging chamber must be tightly sealed before it can be mounted on the microscope), it was possible to start the imaging of live bacteria applied to SLBs only starting from the time point 5 min after bacterial application. The two color imaging was performed on a confocal fluorescence microscope (Nikon Eclipse Ti-E with A1R confocal laser scanner, 60x oil objective, N.A. 1.49). For imaging of GFP-tagged bacteria, 488 nm laser for excitation and the emission filter 525/50 BP were used. Simultaneously, the SLB was imaged using 561 nm laser excitation and 585/40 BP emission filter.

HILO – illumination microscopy. SLBs are often imaged using TIRF microscopy[33] . However, in our case, the specific design of the SLB support doesn't allow to achieve the total internal reflection of the laser beam at the mica/SLB interface. Therefore, we used HILO – highly inclined thin layer illumination below the angle of total internal reflection[34]. This method provides a high signal to background ratio decreasing the illumination of the non-bound lectins in the solution.

HILO-illumination imaging was performed on a (Nikon Eclipse Ti-E with 100x oil objective, N.A. 1.49 and iXon 897 EMCCD camera (Andor Technology)). The 488 nm and 647 nm lasers were used to excite Bodipy and Cy-5 respectfully. After lectin application several areas of each SLB was imaged with exposure time of 30 – 50ms and interval of 20 seconds between frames.

Time lapse data analysis. The resulting time-frame images of the SLBs were analyzed using the FIJI-based home-made macro. First the bleaching and laser-profile corrections were applied. Then, the total area of the membrane defects, Lo domains, Ld membrane and membrane multilayers for each frame was calculated. In addition, the sizes of the individual Lo domains were extracted.

Confocal ratiometric microscopy. The two color ratiometric imaging was performed on a confocal fluorescence microscope (Nikon Eclipse Ti-E with A1R confocal laser scanner, 60x oil objective, N.A. 1.49). For fluorescence excitation, 488 nm laser was used. The emission of NR12S was simultaneously recorded in two color channels – green (using 525/50 BP filter) and far red (700/75 BP filter). The two-color-channel raw image was analyzed using home-made FIJI-based macro in order to produce the general polarization (GP) value of NR12S spectrum for each pixel of the image using the formula:

$$GP = \frac{I_{green} - I_{red}}{I_{green} + I_{red}}$$

where I_{green} is the gray value of the pixel in green color channel and I_{red} is the gray value of the pixel in red color channel. The resulting GP image contained GP values for each pixel of the image. The GP histogram was extracted from the resulting GP image.

Statistical data analysis and representation. Statistical data is visualized using box-whiskers plots, where the middle horizontal line represents the median, the boxes the 25th to 75th percentiles, and the whiskers - the standard deviation. For the plots in figure S1 also the outliers are indicated with dots. The statistical significance was analyzed with one-way ANOVA. The p-values are indicated at the plots.

Acknowledgments

This study was supported by the German Research Foundation (DFG) under Germany's Excellence Strategy (CIBSS – EXC-2189 – Project ID 390939984, BIOSS – EXC 294), by DFG grants RO 4341/2-1, RO 4341/3-1, RTG 2202 and IRTG 1642, by the Ministry of Science, Research and the Arts of Baden-Württemberg (Az: 33-7532.20), by the German Federal Ministry of Education and Research (BMBF) in the framework of the EU ERASynBio project SynGlycTis, and by a starting grant from the European Research Council (Programme "Ideas," ERC-2011-StG 282105). T.S. acknowledges support by the Franco-German University (programs 'Polymer Sciences' and 'Cotutelle de thèse') and the Collège Doctoral Européen (PDI). We are grateful to Andrey Klymchenko for providing the lipophilic membrane probes. S.A. acknowledges support from the International Max Planck Research School for Molecular and Cellular Biology.

References

1. Eierhoff, T. *et al.* A lipid zipper triggers bacterial invasion. *PNAS* **111**, 12895–12900 (2014).
2. Cossart, P. Bacterial Invasion: The Paradigms of Enteroinvasive Pathogens. *Science* **304**, 242–248 (2004).
3. Eierhoff, T., Stechmann, B. & Rmer, W. Pathogen and Toxin Entry - How Pathogens and Toxins Induce and Harness Endocytotic Mechanisms. in *Molecular Regulation of Endocytosis* (ed. Ceresa, B.) (InTech, 2012).
4. Aigal, S., Claudinon, J. & Römer, W. Plasma membrane reorganization: A glycolipid gateway for microbes. *Biochimica et Biophysica Acta (BBA) - Molecular Cell Research* **1853**, 858–871 (2015).
5. Poole, J., Day, C. J., von Itzstein, M., Paton, J. C. & Jennings, M. P. Glycointeractions in bacterial pathogenesis. *Nature Reviews Microbiology* **16**, 440–452 (2018).
6. Chemani, C. *et al.* Role of LecA and LecB Lectins in Pseudomonas aeruginosa-Induced Lung Injury and Effect of Carbohydrate Ligands. *Infection and Immunity* **77**, 2065–2075 (2009).

7. Blanchard, B. *et al.* Structural Basis of the Preferential Binding for Globo-Series Glycosphingolipids Displayed by Pseudomonas aeruginosa Lectin I. *Journal of Molecular Biology* **383**, 837–853 (2008).
8. Novoa, A. *et al.* A LecA Ligand Identified from a Galactoside-Conjugate Array Inhibits Host Cell Invasion by *Pseudomonas aeruginosa*. *Angewandte Chemie International Edition* **53**, 8885–8889 (2014).
9. Johannes, L., Wunder, C. & Shafaq-Zadah, M. Glycolipids and Lectins in Endocytic Uptake Processes. *Journal of Molecular Biology* **428**, 4792–4818 (2016).
10. Lafont, F. & Van Der Goot, F. G. Bacterial invasion via lipid rafts: Bacterial invasion via lipid rafts. *Cellular Microbiology* **7**, 613–620 (2005).
11. Zaas, D. W., Duncan, M., Rae Wright, J. & Abraham, S. N. The role of lipid rafts in the pathogenesis of bacterial infections. *Biochimica et Biophysica Acta (BBA) - Molecular Cell Research* **1746**, 305–313 (2005).
12. Simons, K. & Ikonen, E. Functional rafts in cell membranes. *Nature* **387**, 569 (1997).
13. Lingwood, D. & Simons, K. Lipid Rafts As a Membrane-Organizing Principle. *Science* **327**, 46–50 (2010).
14. Sezgin, E., Levental, I., Mayor, S. & Eggeling, C. The mystery of membrane organization: composition, regulation and roles of lipid rafts. *Nature Reviews Molecular Cell Biology* (2017). doi:10.1038/nrm.2017.16
15. Villringer, S. *et al.* Lectin-mediated protocell crosslinking to mimic cell-cell junctions and adhesion. *Scientific Reports* **8**, (2018).
16. Kreder, R. *et al.* Blue fluorogenic probes for cell plasma membranes fill the gap in multicolour imaging. *RSC Adv.* **5**, 22899–22905 (2015).
17. Kwiatek, J. M., Hinde, E. & Gaus, K. Microscopy approaches to investigate protein dynamics and lipid organization. *Molecular Membrane Biology* **31**, 141–151 (2014).
18. Kucherak, O. A. *et al.* Switchable Nile Red-Based Probe for Cholesterol and Lipid Order at the Outer Leaflet of Biomembranes. *J. Am. Chem. Soc.* **132**, 4907–4916 (2010).

19. Keogh, D. *et al.* Generating novel recombinant prokaryotic lectins with altered carbohydrate binding properties through mutagenesis of the PA-IL protein from Pseudomonas aeruginosa. *Biochimica et Biophysica Acta (BBA) - General Subjects* **1840**, 2091–2104 (2014).
20. Song, D. *et al.* Pseudomonas aeruginosa quorum-sensing metabolite induces host immune cell death through cell surface lipid domain dissolution. *Nature Microbiology* **4**, 97–111 (2019).
21. Becker, K. A., Grassmé, H., Zhang, Y. & Gulbins, E. Ceramide in *Pseudomonas aeruginosa* Infections and Cystic Fibrosis. *Cellular Physiology and Biochemistry* **26**, 57–66 (2010).
22. Grassmé, H. *et al.* Host defense against Pseudomonas aeruginosa requires ceramide-rich membrane rafts. *Nature Medicine* **9**, 322–330 (2003).
23. Kannan, S., Audet, A., Huang, H., Chen, L. -j. & Wu, M. Cholesterol-Rich Membrane Rafts and Lyn Are Involved in Phagocytosis during Pseudomonas aeruginosa Infection. *The Journal of Immunology* **180**, 2396–2408 (2008).
24. Kierbel, A. *et al.* Pseudomonas aeruginosa exploits a PIP3-dependent pathway to transform apical into basolateral membrane. *The Journal of Cell Biology* **177**, 21–27 (2007).
25. Wang, J. & Richards, D. A. Segregation of PIP2 and PIP3 into distinct nanoscale regions within the plasma membrane. *Biol Open* **1**, 857–862 (2012).
26. Schoehn, G. *et al.* Oligomerization of type III secretion proteins PopB and PopD precedes pore formation in Pseudomonas. *The EMBO Journal* **22**, 4957–4967 (2003).
27. Krivan, H. C., Ginsburg, V. & Roberts, D. D. Pseudomonas aeruginosa and Pseudomonas cepacia isolated from cystic fibrosis patients bind specifically to gangliotetraosylceramide (asialo GM1) and gangliotriaosylceramide (asialo GM2). *Archives of Biochemistry and Biophysics* **260**, 493–496 (1988).
28. Safouane, M. *et al.* Lipid Cosorting Mediated by Shiga Toxin Induced Tubulation. *Traffic* **11**, 1519–1529 (2010).
29. Windschiegl, B. *et al.* Lipid Reorganization Induced by Shiga Toxin Clustering on Planar Membranes. *PLoS ONE* **4**, e6238 (2009).
30. Schubert, T. & Römer, W. How synthetic membrane systems contribute to the understanding of lipid-driven endocytosis. *Biochimica et Biophysica Acta (BBA) - Molecular Cell Research* **1853**, 2992–3005 (2015).

31. Duncan, M. J., Li, G., Shin, J.-S., Carson, J. L. & Abraham, S. N. Bacterial Penetration of Bladder Epithelium through Lipid Rafts. *Journal of Biological Chemistry* **279**, 18944–18951 (2004).
32. Tsuda, K. *et al.* Functional Analysis of α5β1 Integrin and Lipid Rafts in Invasion of Epithelial Cells by Porphyromonas gingivalis using Fluorescent Beads Coated with Bacterial Membrane Vesicles. *Cell Structure and Function* **33**, 123–132 (2008).
33. Dietrich, C. *et al.* Lipid Rafts Reconstituted in Model Membranes. *Biophysical Journal* **80**, 1417–1428 (2001).
34. Tokunaga, M., Imamoto, N. & Sakata-Sogawa, K. Highly inclined thin illumination enables clear single-molecule imaging in cells. *Nature Methods* **5**, 159–161 (2008).

Supplementary figures

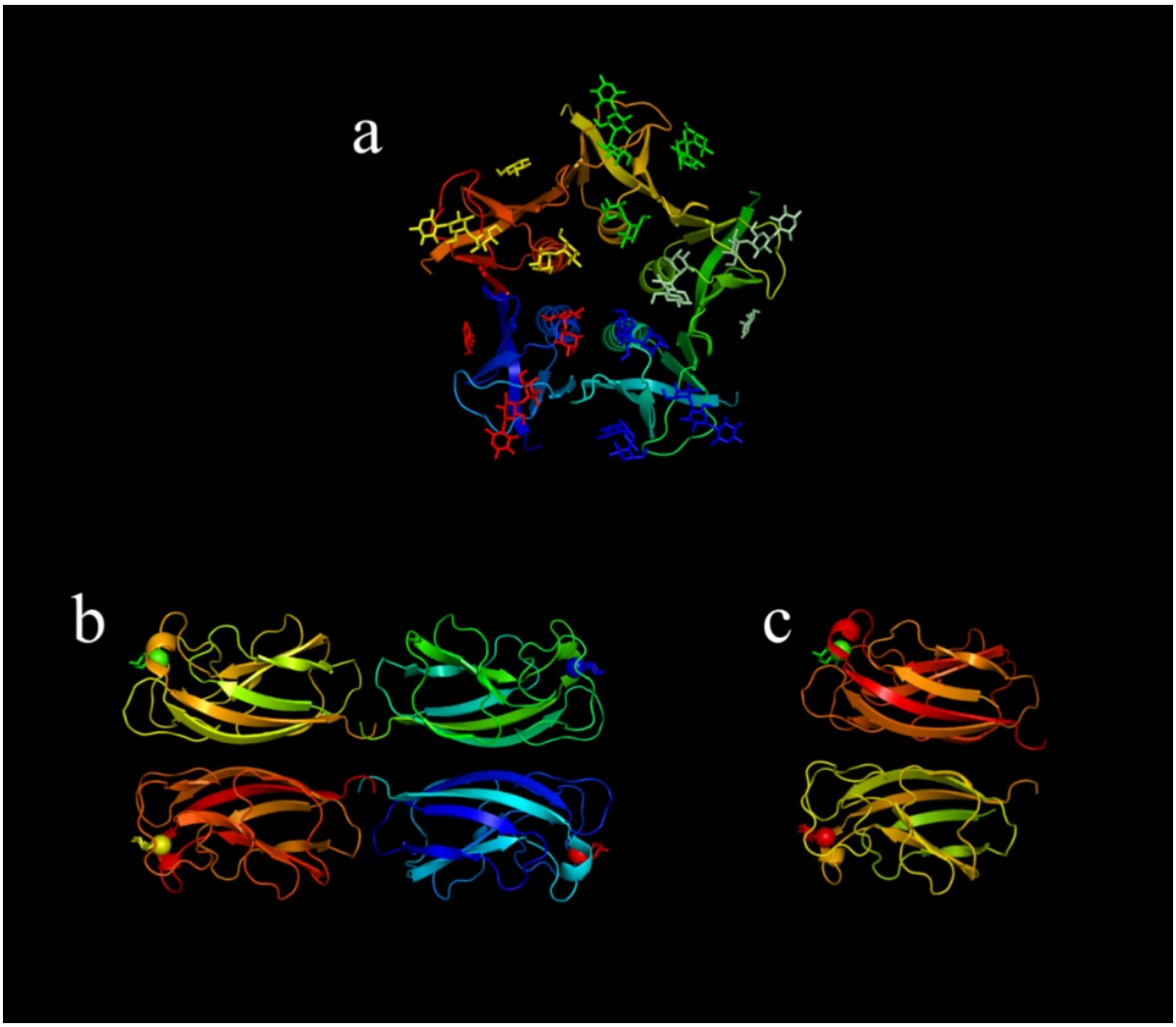

Figure S1|**Ribbon diagrams of lectins.** The Gb3 binding sites are marked by the carbohydrates and Ca^{2+} ions. **a)** Shiga toxin B subunit (StxB) from *S. dysenteriae*; **b)** LecA from *P. aeruginosa*; **c)** Recombinant prokaryotic lectin α Gal (RPL). The structures in a and b were provided by RCSB Protein Data Bank and visualized by Pymol software. The ribbon diagram in c is presumptive.

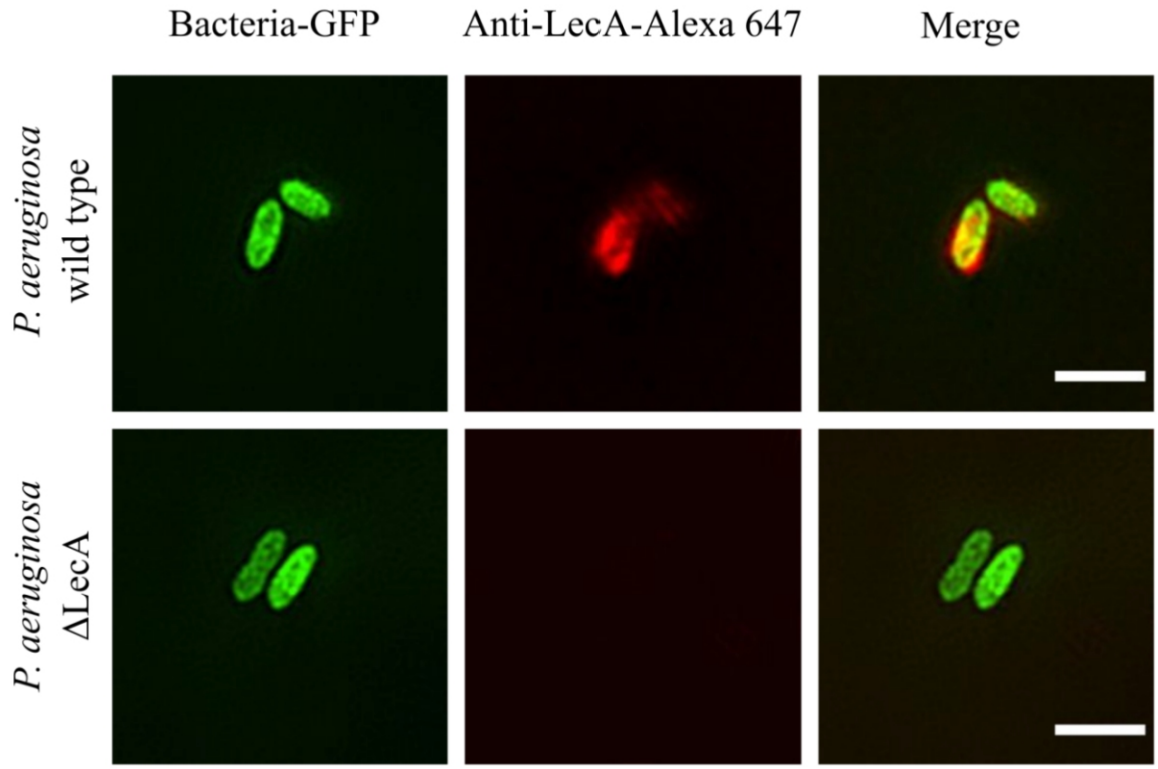

Figure S2| **LecA on the surface of *P. aeruginosa*.** Surface of *P. aeruginosa* wild type and *P. aeruginosa* ΔLecA was stained with an antiLecA antibody. Bacteria are labeled by GFP (green). Anti-LecA (red) is labeled by Alexa 647. Images were obtained with Structured Illumination Microscopy. Scale bars – 2 µm.

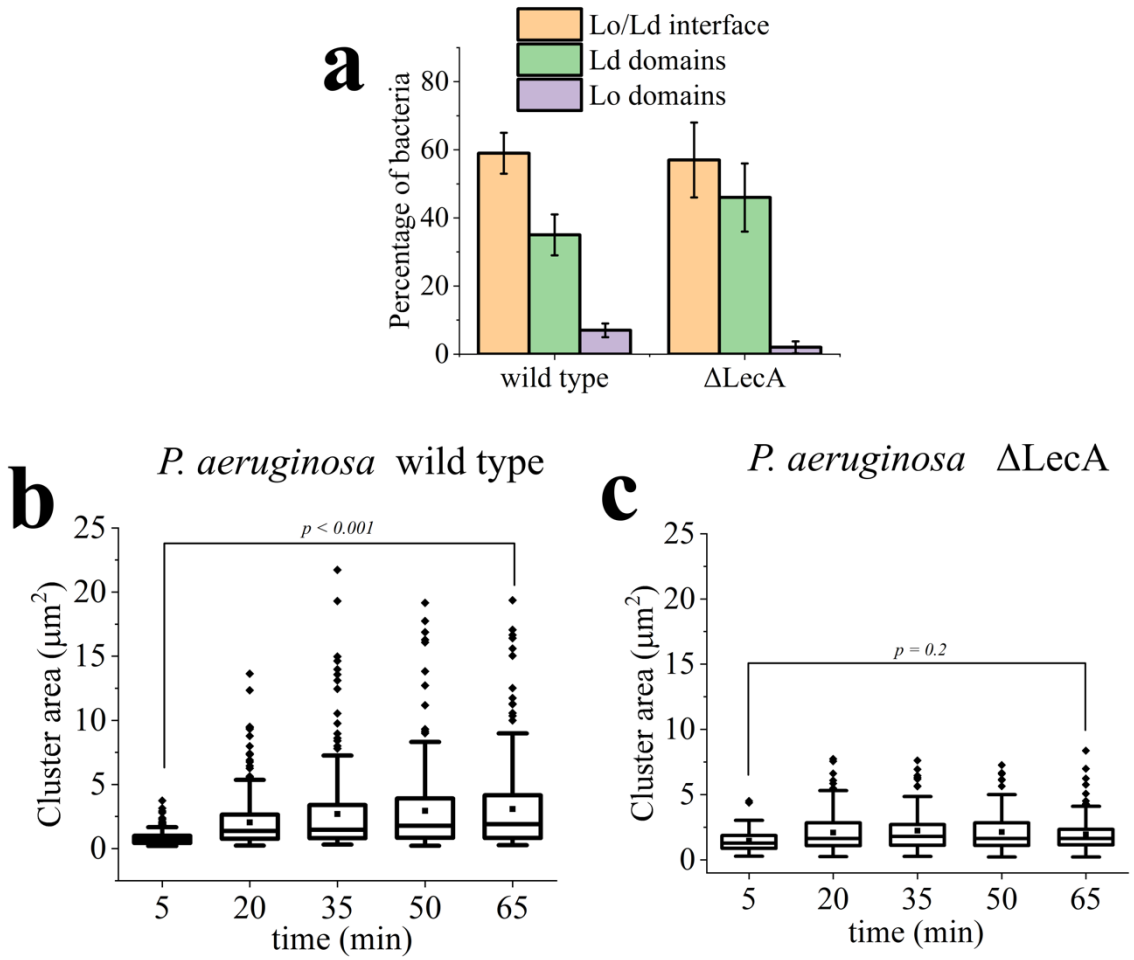

Figure S3| **Binding and clustering of *P. aeruginosa* on the supported lipid bilayer** displayed in Figure 1**.** The composition of the lipid bilayer is DOPC/chol/SM/Gb3 (37.5/20/37.5/5). **a)** The bacteria bind preferentially to the boundary of the Lo and Ld phase domains. Ld phase domains host a lower amount of bacteria, whereas the amount of bacteria docked to the Lo domain is very small. The majority of *P. aeruginosa* ΔLecA bacteria also bind to the Ld phase domains and Lo/Ld phase domains boundaries with a slight preference for the latter. Data for the quantification was extracted from the images obtained during the first 10 min after bacteria application. Numbers of bacteria detected: *P. aeruginosa* wild type – 915 *P. aeruginosa* ΔLecA - 217 **(b, c)** Formation of clusters. While wild-type *P. aeruginosa* clusters grow in size significantly **(b)**, *P. aeruginosa* ΔLecA do not show significant clustering **(c)**. The sizes of bacterial clusters are measured from the confocal images. The area of each cluster is extracted using a home-made FIJI macro. The middle horizontal line represents the median, the boxes represent the 25th to 75th percentiles, and the whiskers – the standard deviation. The statistical significance was analyzed with one-way ANOVA;

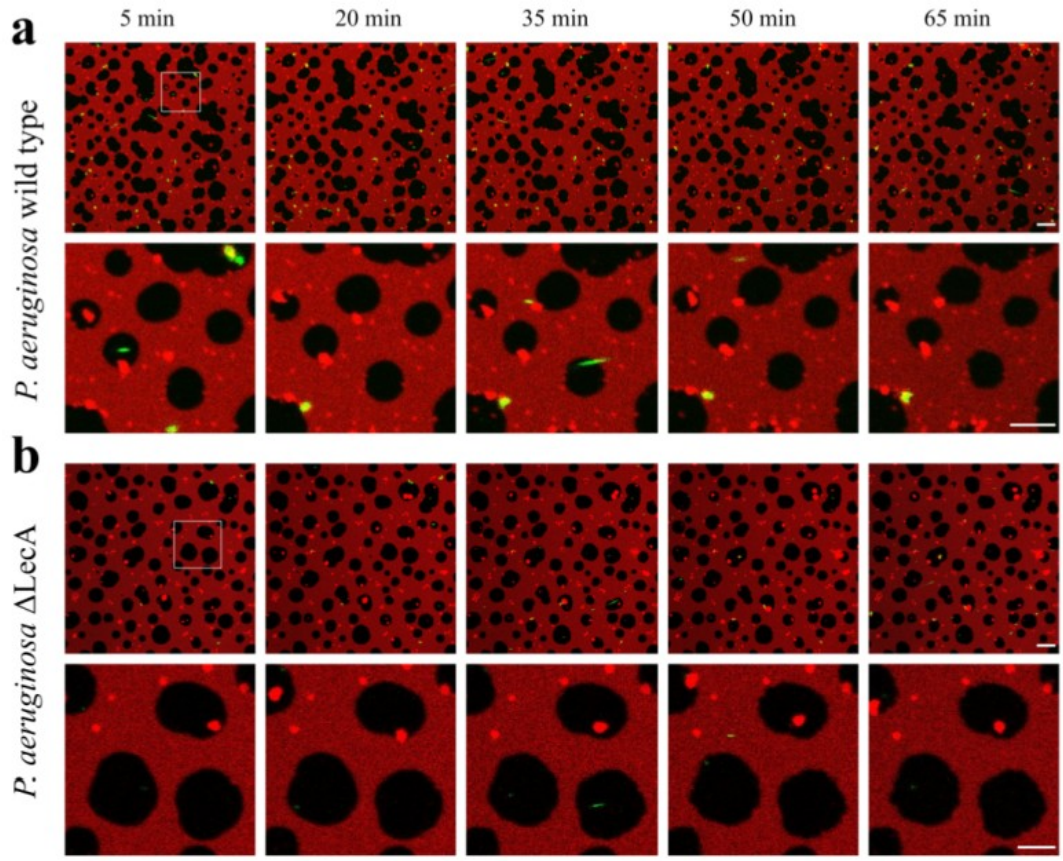

Figure S4| **Binding and clustering of *P. aeruginosa* on Gb3-free SLBs.** Lipid bilayer (DOPC/chol/SM (2/1/2)) is labeled with DHPE - Texas Red; Bacterial concentration – 15×10^6 mL^{-1}. Bacteria do not bind specifically to such lipid bilayer. However, some bacteria still precipitate to the lipid bilayer surface (a,b). The total number of bacteria, bound to SLBs is strongly reduced. Numbers of bacteria detected: *P. aeruginosa* wild type – 164, *P. aeruginosa* ΔLecA – 30. Scale bars – 10 and 5 µm, respectively.

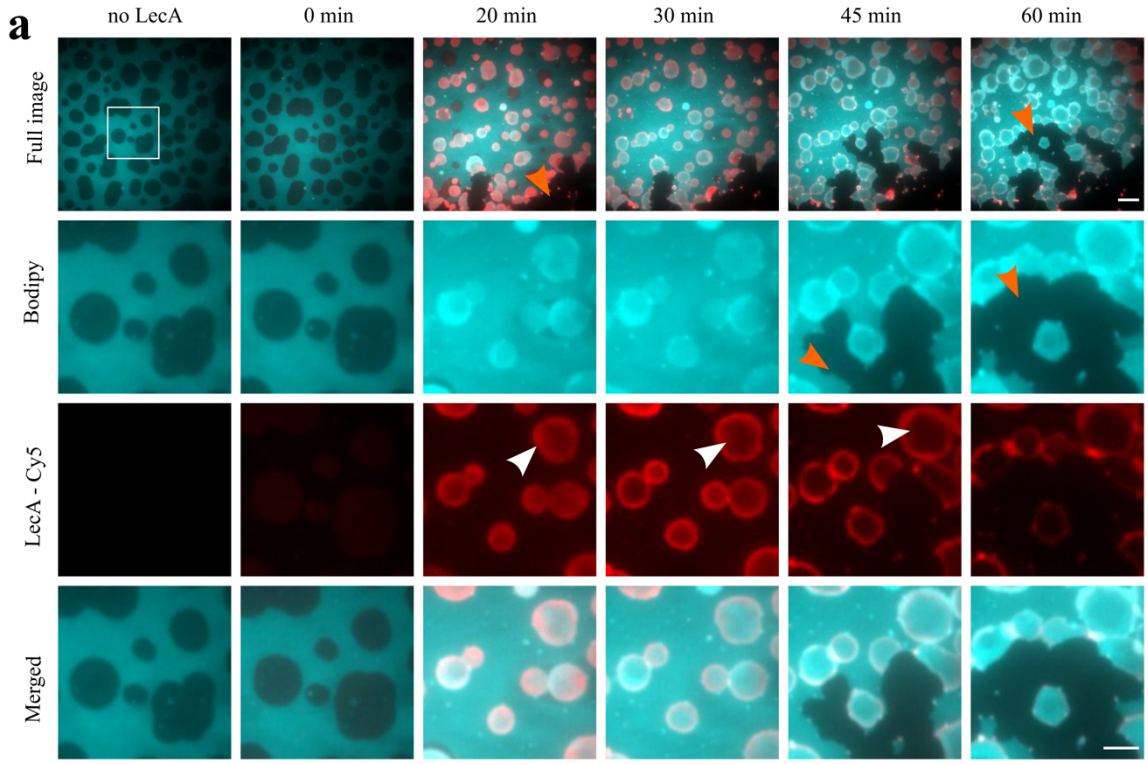

Figure S5| **Membrane defects induced by LecA.** a) Membrane reorganization induced by LecA. The images correspond to the same experiments as in Figure 2, but at longer time points. Membrane defects grow over time and the SLB becomes partially disintegrated (orange arrow). The fluorescent LecA clusters accumulated in membrane multilayers fade over time. Most likely, it is due to the bleaching of the Cy 5 label. Scale bars – 10 and 5 µm respectively.

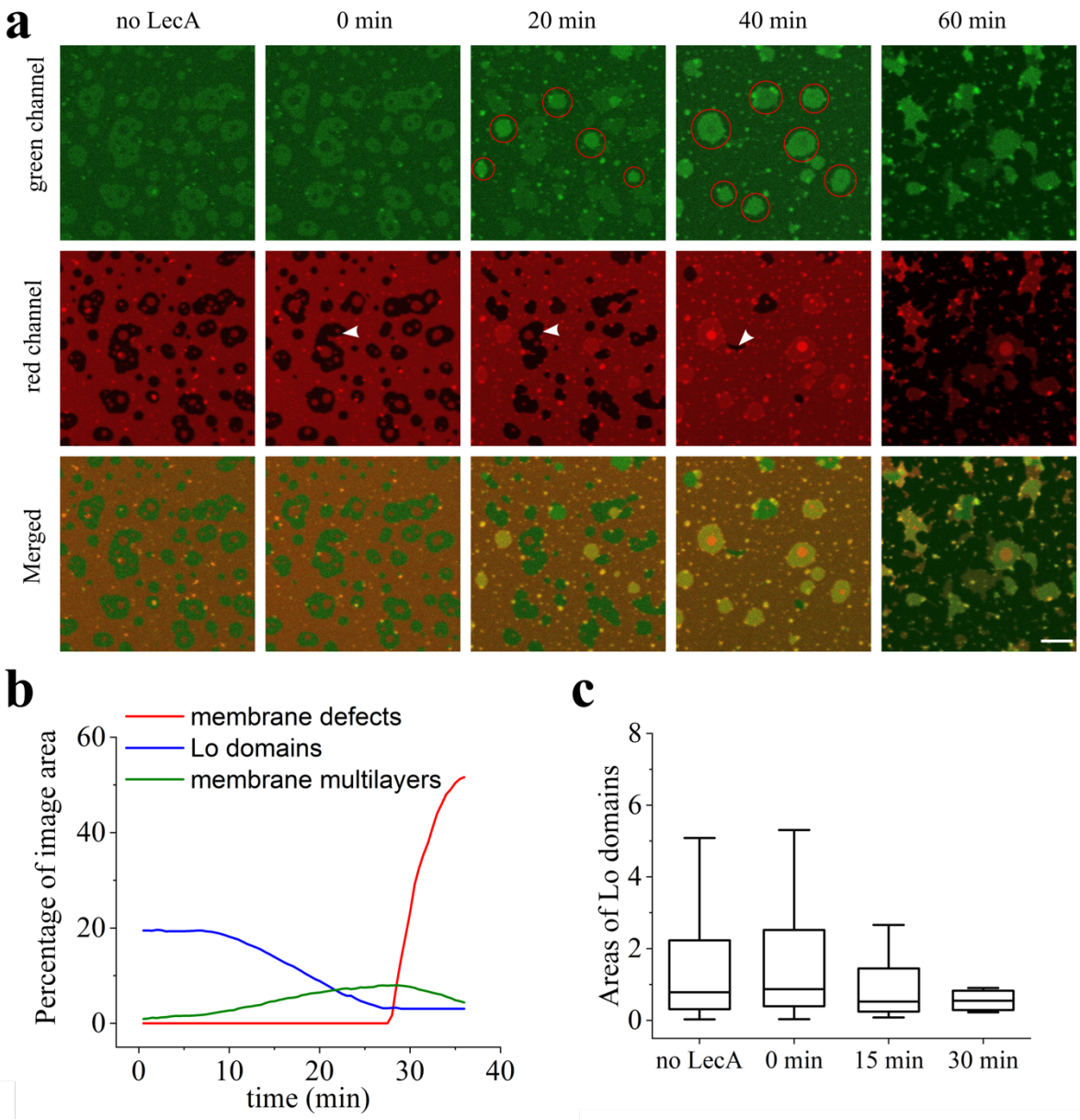

Figure S6|**Time series of the two-color imaging for membrane order mapping.** SLB is labeled by NR12S. LecA is unlabeled. Green channel is acquired using the 525/50 BP emission filter, red channel is acquired using 700/75 BP emission filter. **a)** The dynamics of the membrane reorganization are in line with the observations presented in main figure 2. Lo domains decrease in size and finally disappear. Membrane multilayers form (highlighted with red circles on the 20 min and 40 min frame of green channel). **b)** Total areas of membrane defects, Lo domains, Ld domains and membrane multilayers over time. **c)** Lo domains decrease in size after 20 min of incubation with LecA. Scale bar – 10 µm. The middle horizontal line represents the median, the boxes represent the 25th to 75th percentiles, and the whiskers – the standard deviation.

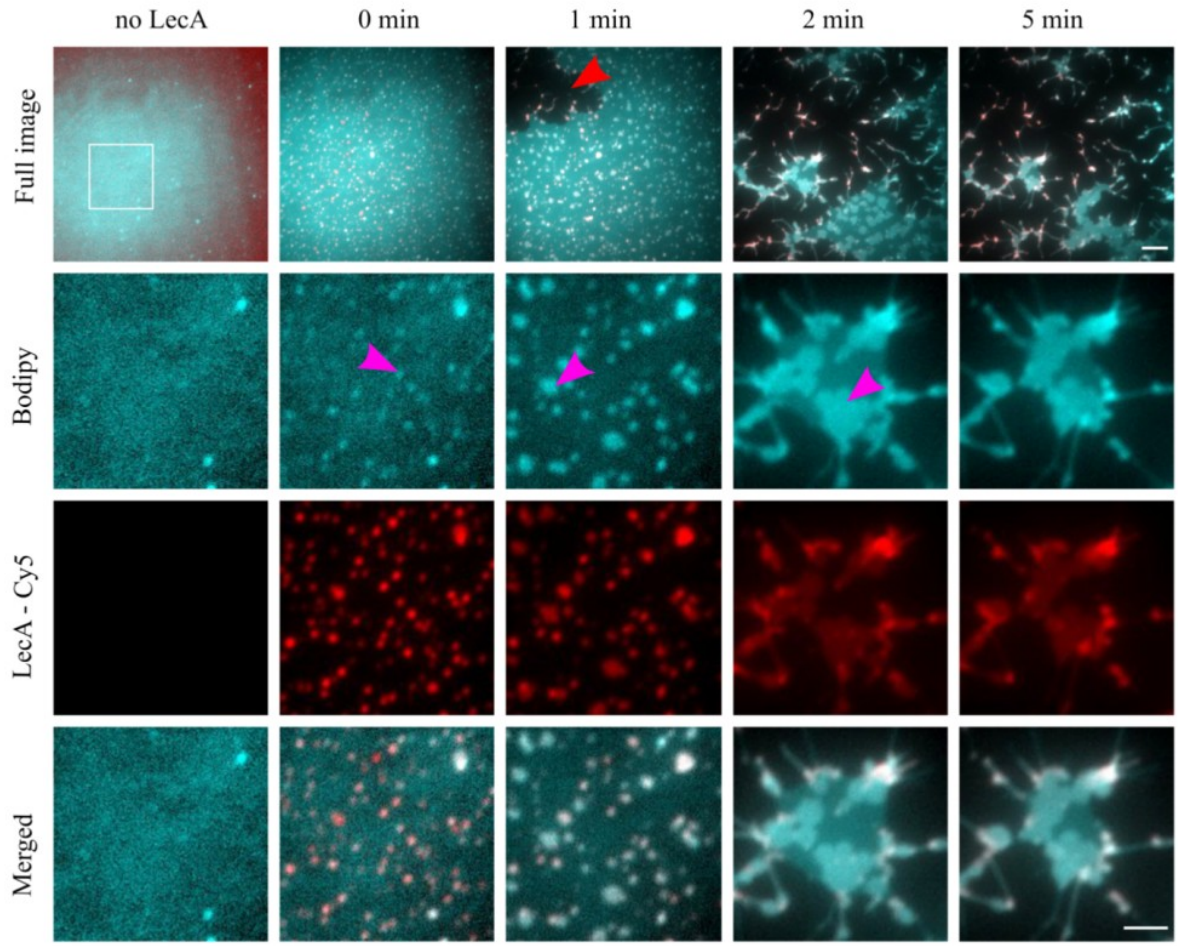

Figure S7 | **LecA-induced membrane reorganization of homogeneous SLB.** The SLB was prepared from a non-phase separating lipid mixture (DOPC/chol/Gb3 (65/30/5). Membrane marker – HPC-Bodipy). Since such lipid bilayers do not exhibit phase separation, the membrane fluorescence signal (cyan) appears homogeneous. Application of LecA labeled with Cy5 (red) induces membrane multilayers formation (magenta arrows) and fast membrane disintegration (membrane defect is highlighted with red arrow). Scale bars – 10 and 5 µm respectively.

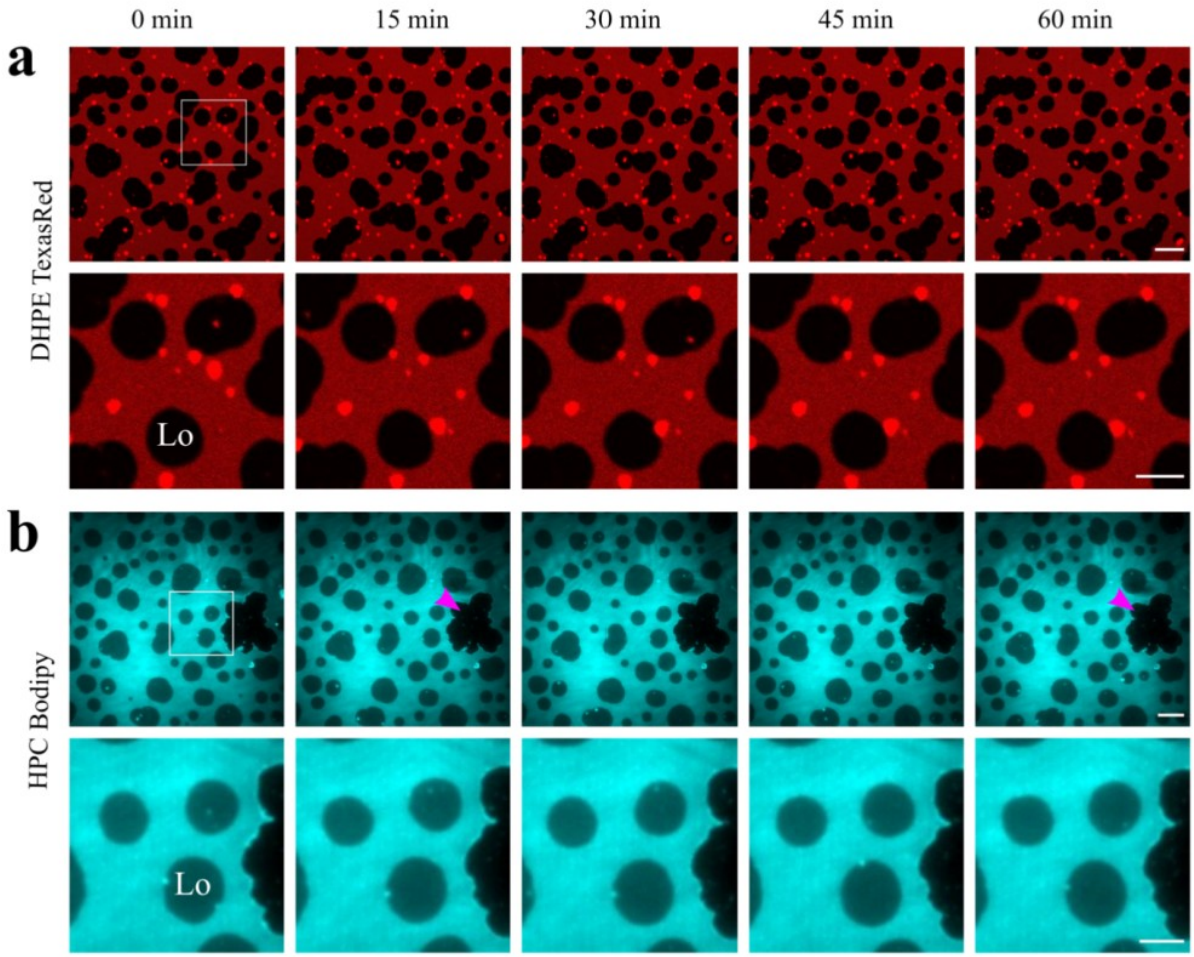

Figure S8| **Negative control.** Phase separated SLBs labeled by DHPE-Texas Red (a) and HPC-Bodipy (b) were imaged during one hour using confocal (a) and widefield (b labeling). The Lo domains and their lateral distribution are stable during one hour of acquisition for both types of labeling and acquisition. A membrane defect (HPC-Bodipy – magenta arrow) that formed during SLB preparation is stable and neither expands or shrinks during the acquisition. Scale bars – 10 and 5 µm respectively.

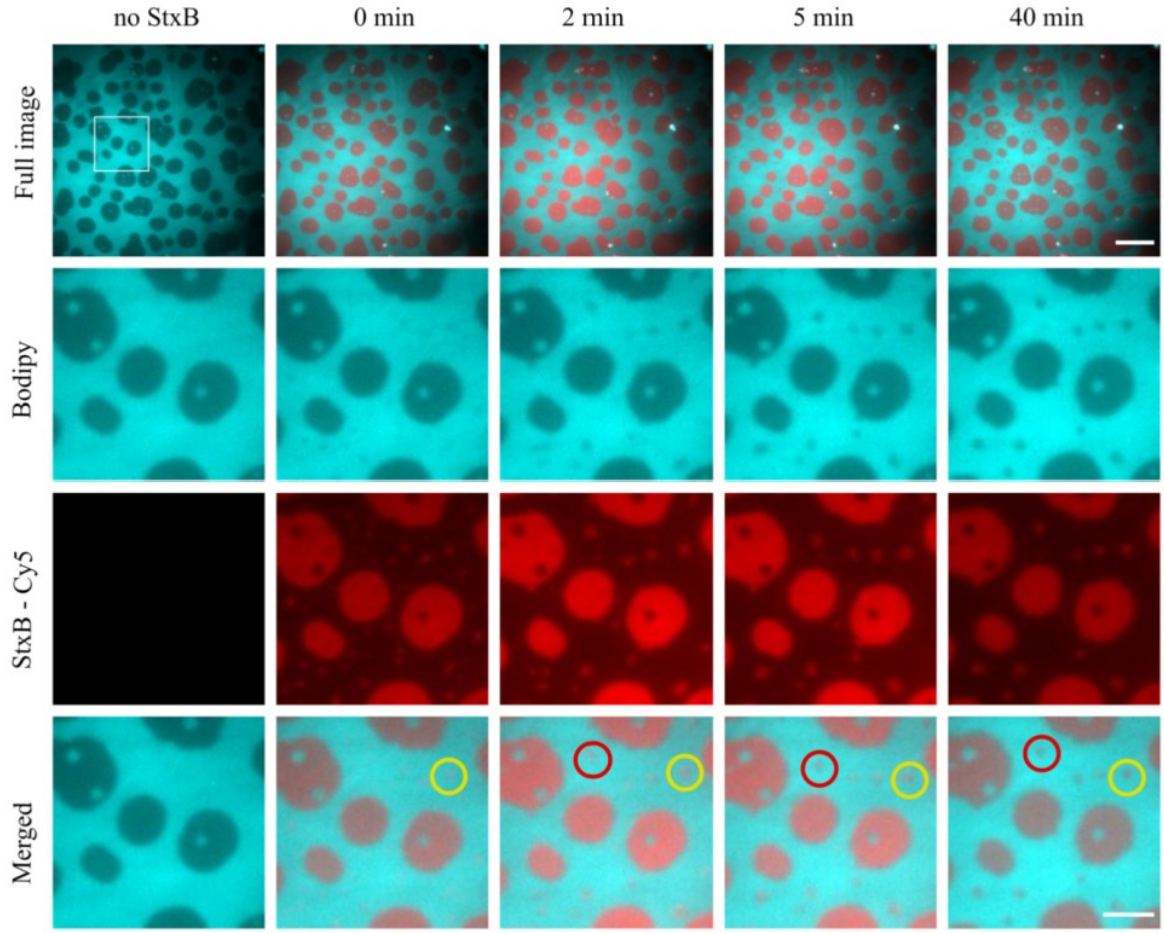

Figure S9| StxB-induced SLB reorganization. The SLB was composed of DOPC/chol/SM/Gb3 (37.5/20/37.5/5). The SLB was labeled by Bodipy-HPC that preferentially incorporates in Ld domains. StxB-Cy5 (200 nM) was applied. StxB binds almost exclusively to Lo domains. Moreover, it induces a formation of new Lo domains (red and yellow circles - Merged) by efficient clustering of the Gb3 molecules incorporated in the Ld phase. Scale bars – 10 and 5 µm respectively.

Supplementary video 1| *P. aeruginosa* wild type induce reorganization of the SLB. The complete time sequence of the experiment, presented in figure 1a. Bacteria bind to the SLB and cluster (white arrowhead). Lo domains decrease in size, some of them disappear completely (white arrowhead).

Supplementary video 2| *P. aeruginosa* ΔLecA does not induce reorganization of the SLB. The complete time sequence of the experiment, presented in figure 1b. Bacteria still can unspecifically attach to the SLB, but some of them detach with the time (white arrowhead).

Supplementary video 3| Purified LecA induces reorganization of the SLB. The complete time sequence of the experiment, presented in figure 2a. LecA binds to the Lo domains and dissolves them (purple arrowheads). The membrane multilayers, induced by LecA are depicted with the white arrowheads.

Supplementary video 4| Divalent RPL α Gal induces reorganization of the SLB. The complete time sequence of the experiment, presented in figure 4a. RPL binds to the Lo domains and induces their partial dissolution (white arrowheads). Thereafter, the re-shaping of the Lo domains stops, but they are dissolved asymmetrically (white circles).

Université de Strasbourg

Taras SYCH

École Doctorale des Sciences de la Vie et de la Santé STRASBOURG

Rôles et mécanismes des Lectines à Gb3 et de *P. aeruginosa* sur la réorganisation de la membrane plasmique

Résumé

L'interaction des glycosphingolipides de la membrane plasmique avec les protéines de liaison aux glucides (lectines) est d'une importance vitale pour l'infection de la cellule hôte par divers virus et bactéries. Dans ce travail, nous avons exploré l'interaction des lectines LecA de la bactérie *P. aeruginosa* et de la sous-unité B de la toxine Shiga (StxB) de *S. dysenteriae* avec son récepteur à membrane plasmatique, le globotriaosylcéramide (Gb3). De plus, nous avons étudié l'interaction de la bactérie complète *P. aeruginosa* avec Gb3. Afin de déchiffrer l'interaction lectine-Gb3 en l'absence d'autres composants cellulaires, nous avons utilisé les systèmes de membrane artificielle - vésicules unilamellaires géantes (GUV) et bicouches lipidiques supportées (SLB). Nous avons observé la liaison de la lectine en utilisant différents modes de microscopie à fluorescence (confocal, TIRF, etc.). Nous examinons la liaison des deux lectines aux domaines membranaires de différents ordres et compositions. Nous avons constaté que StxB préfère des domaines membranaires plus ordonnés alors que LecA est moins préférentiel. De plus, les deux lectines induisent la réorganisation des domaines membranaires: StxB stabilise les domaines ordonnés, les réduit et induit la formation des nouveaux domaines ordonnés. D'autre part, LecA ainsi que la bactérie *P. aeruginosa* induisent la dissolution des domaines ordonnés. Nous pensons que ces processus de réorganisation membranaire sont cruciaux pour l'infection bactérienne.

Mots de clés: Membrane plasmique, Invasion bactérienne, Lectines, Glycosphingolipides

Résumé en anglais

The interaction of plasma membrane glycosphingolipids with the carbohydrate binding proteins (lectins) is of vital importance for the infection of the host cell by various viruses and bacteria. In this work, we explored the interaction of the lectins LecA from the bacterium *P. aeruginosa* and B subunit of Shiga toxin (StxB) from *S. dysenteriae* with its plasma membrane receptor globotriaosylceramide (Gb3). Moreover, we studied the interaction of the complete bacterium *P. aeruginosa* with Gb3. In order to decipher the lectin-Gb3 interaction in absence of other cellular components we employed the artificial membrane systems – Giant unilamellar vesicles (GUVs) and Supported lipid bilayers (SLBs). We observed the lectin binding using different modes of fluorescence microscopy (confocal, TIRF, etc…). We examine the binding of both lectins to the membrane domains of different ordere and composition. We found that StxB prefers more ordered membrane domains whereas LecA is less preferential. Moreover, both lectins induce the reorganization of the membrane domains: StxB stabilizes ordered domains, shrinks them and induces the formation of the novel ordered domains. On the other hand LecA, as well as the bacterium P. aeruginosa induce the dissolution of the ordered domains. We believe, these membrane reorganization processes are crucial for the bacterial infection.

Keywords: Plasma membrane, Bacterial invasion, Lectins, Glycosphingolipids